UNIVERSITY OF LEEDS

Mechanisms of Olfactory Perception and Learning

Mark William Conway

Submitted in accordance with the requirements for the degree of Doctor of Philosophy

University of Leeds
School of Biomedical Sciences

April, 2024

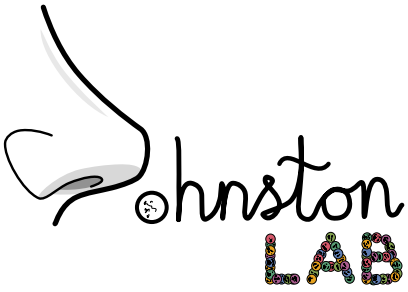

I confirm that the work submitted is my own, except where work which has formed part of jointly authored publications has been included. My contribution and the other authors to this work has been explicitly indicated below. I confirm that appropriate credit has been given within the thesis where reference has been made to the work of others.

Results Chapters 4 and 5 contain work published in the following pre-print: 'Perceptual constancy for an odour is acquired through changes in primary sensory neurons', Mark Conway, Merve Oncul, Kate Allen, Jamie Johnston, bioRxiv (2023). My contributions include writing the majority of the text, conducting behavioural perception tests (Figure 1A & B), performing craniotomies and *in vivo* two-photon Ca^{2+} imaging (Figures 2,3 & 5), and executing olfactory learning experiments (Figure 5). I also analysed the datasets and created Figures 1A, 2, 3 & 5. Merve Oncul conducted the head-fixed perception tests (Figure 1C-E) and wrote the methods for these tests. Kate Allen performed the majority of 'strong' food-finding tests (Figure 5A) and contributed data for *in vivo* Ca^{2+} imaging from the associated cohort (Figure 5C, E & F). Jamie Johnston proofread all content and revised most of the text and figures. Additionally, Jamie developed the olfactory receptor neuron model (Figure 4), produced Figures 1B-E, 4 & 5A, and assisted with analysis.

Acknowledgements

This research has been carried out by a team which has included Jamie Johnston, Merve Oncul, Kate Allen and Emma Smith. My own contributions, fully and explicitly indicated in the thesis, have included performing craniotomies and *in vivo* two-photon Ca^{2+} imaging, executing olfactory learning experiments and behavioural perception tests, and data analysis. The other members of the group and their contributions have been as follows: Head-fixed perception tests and the associated surgeries were performed by Merve Oncul. Most of the 'strong' food-finding tests were executed by Kate Allen, who also performed a portion of craniotomies and *in vivo* Ca^{2+} imaging with the associative learning cohort of mice. Jamie Johnston implemented the olfactory receptor neuron model, built the two-photon microscope and behavioural boxes, and developed the head-fixed perception tests. Additionally, he provided key assistance with data analysis.

I acknowledge the use of ChatGPT-4 in the proof-reading of the thesis before submission. I confirm that the proof-reading undertaken by ChatGPT-4 was in accordance with the Postgraduate Researcher Proof-reading Policy.

Firstly, I would like to thank the School of Biomedical Sciences for funding my studies and the Medical Research Council for funding my research. There are many people at the University who have made my experience a joy—more than I can reasonably list—including (in no particular order) Jim, Sue, Emma, Emily, Ben, Andreea, Marilyn, Natalie, Varinder, Merve, Cédric, Kate, and Zhang. I would like to especially acknowledge Andreea and Cédric for their invaluable tutelage. Finally, special thanks to Jamie, not only for giving me the opportunity to do a PhD in his lab, but also for truly mentoring me over the past four and a half years.

Abstract

Odours are complex blends of volatile chemicals, each of which can give rise to a distinct smell. The path these odours take is often influenced by irregular and unpredictable air currents, which can alter the trajectory and concentration of the odour molecules before they arrive at the nose. Despite the turbulent nature of airflow, and changes in our proximity to the source, we can reliably identify the same smells. This ability to consistently recognise an object, regardless of variability in sensory input, is termed perceptual constancy. Perceptual constancy is not innate, rather it develops early in life and is likely shaped by experience (*1*, *2*). The underlying neural mechanisms that facilitate the development of this phenomenon remain largely elusive. We leveraged the olfactory system of mice in a controlled laboratory setting where exposure to odours is inherently limited, allowing us to analyse how perception changes with experience. We demonstrate that naïve mice experience a perceptual shift with increasing concentrations of an odour, which coincides with a rapid decline in activity within a single olfactory receptor channel that is exquisitely sensitive to the odour. This sharp reduction in activity stems from a mismatch between the sensitivity of the olfactory receptor neurons within the nose to the odour, rather than interactions within the olfactory bulb. Furthermore, we show that exposure to the odour in association with food modifies the sensitivity of the receptor channel, aligning it with the odour's characteristics. This adjustment prevents transmission failure and promotes perceptual stability. These data indicate that plasticity within the nose underpins the development of perceptual constancy.

Table of Contents

Chapter 1: Introduction 1

1.1 :The Olfactory System.....1

1.1.1 Overview 1

1.1.2 The Nasal Cavity 3

1.1.3 Olfactory Receptors 5

1.1.4 The Main Olfactory Epithelium 8

1.1.4.1 Organisation 8

1.1.4.2 Odour Transduction.....10

1.1.5 The Olfactory Bulb 12

1.1.5.1 Organisation 12

1.1.5.2 Top-Down Feedback 16

1.2 :Odour Encoding 20

1.2.1 Overview 20

1.2.2 Combinatorial Coding 20

1.2.2.1 Combinatorial Receptor Codes.....20

1.2.2.2 Odourant-Receptor Interactions 23

1.2.3 Phase Coding.....26

1.2.4 Primacy Coding.....29

1.3 :Odour Adaptation.....32

1.3.1 Overview 32

1.3.2 Receptor Desensitisation 32

1.3.3 Adaptation of the Transduction Machinery 35

1.3.4 Response Termination....38

1.3.5 Stimulus-Induced Depression....41

1.4 :Olfactory Learning....44

1.4.1 Overview....44

1.4.2 Passive Experience....45

1.4.2.1 Changes at the Periphery....46

1.4.2.2 Modulation of Olfactory Bulb Output....46

1.4.2.3 A Role for Inhibition....47

1.4.2.4 Bulbar Dynamics During Sensory Deprivation....49

1.4.3 Associative Learning....50

1.4.3.1 Reward-Based Classical Conditioning....50

1.4.3.2 Fear-Based Classical Conditioning....52

1.4.3.3 Operant Conditioning....53

1.5 :Aims....55

Chapter 2: Methods....56

2.1 :Animals....56

2.2 :Olfactometry....57

2.3 :Behaviour....58

2.3.1 Cross-Habituation Test....58

2.3.2 Odour Learning Protocols....59

2.3.2.1 Odour Exposure....59

2.3.2.2 Food-Odour Association....60

2.3.2.3 Food Preference Test....61

2.3.2.4 Food- and Odour-Finding Tests 61

2.4 :*In Vivo* Imaging 62

2.4.1 Surgery 62

2.4.2 2-Photon Ca^{2+} Imaging 63

2.4.3 Head-Fixed Perception Tests 64

2.4.4 Pharmacology 65

2.5 :Data Analysis 66

2.5.1 Image Segmentation of Glomeruli 66

2.5.2 Defining Glomerular Responses 67

2.5.3 Response Integral 68

2.5.4 Jaccard Index 68

2.5.5 Adaptation Index 68

2.5.6 Response Maps 69

2.5.7 Support Vector Machine (SVM) Classification 69

2.5.8 Ranking Glomerular Activation Times 70

2.5.9 Glomerular Size Measurements 70

2.5.10 Statistical Analysis 71

2.6 :Depolarising Block Model 71

Chapter 3: Odour Adaptation in the Olfactory Bulb 74

3.1 :Odour Sensitivity Varies Widely Across Glomeruli 74

3.2 :Relative Odour Strength and Stimulus Duration Influence Adaptation 79

3.3 :Recovery is Delayed in Adapted Neurons 87

Chapter 4: Transmission Failure to a Single Glomerulus Culminates in

Odour Constancy Break Down 91

4.1 :Odour Concentration Generates Perceptual Shifts 91

4.2 :A Sparse Code Underlies Odour Percepts 95

4.3 :Rapid Adaptation is Consistent with Depolarising Block in Olfactory Receptor Neurons 102

Chapter 5: Adaptations in Primary Sensory Neurons Facilitate Perceptual Constancy for an Odour.....108

5.1 :Associative Learning Establishes Perceptual Constancy 108

5.2 :Perceptual Constancy Emerges from Dynamic Range Matching in the Primary Glomerulus 112

5.3 :Odour Learning Shifts Sensitivity in Dual-Responsive Glomeruli for Unconditioned Odours 117

Chapter 6: Discussion 127

6.1 :Temporal Dynamics in Odour Encoding.....127

6.2 :Signal Failure and Sensory Adjustment 129

6.3 :Input Strength and Adaptation.....130

6.4 :High-Affinity Glomeruli 132

6.5 :Olfactory Learning as a Modifier of Odour Sensitivity 133

6.6 :A Model for Odour Identity.....134

6.7 :Conclusion & Future Directions.....137

Bibliography.....139

Figure 1.1: The Olfactory System.....3

Figure 1.2: Olfactory System Anatomy 4

Figure 1.3: Olfactory Receptors 7

Figure 1.4: The Main Olfactory Epithelium 9

Figure 1.5: Odour Transduction.....12

Figure 1.6: The Olfactory Bulb 16

Figure 1.7: Olfactory Bulb Projection and Top-Down Feedback.....19

Figure 1.8: Combinatorial Receptor Code for Odourants 22

Figure 1.9: Odourant-Receptor Interactions in Odour Encoding 25

Figure 1.10: Phase Coding Model of Odour Identity.....29

Figure 1.11: Primacy Model for Encoding Odour Identity.....31

Figure 1.12: Olfactory Receptor Desensitisation.....34

Figure 1.13: Mechanisms of Ca^{2+}-Mediated Adaptation in Olfactory Receptor Neurons 37

Figure 1.14: Proposed Mechanisms of Response Termination in Olfactory Receptor Neurons.....41

Figure 1.15: Stimulus-Induced Depression in an Olfactory Receptor Neuron 43

Figure 1.16: Odour Exposure-Induced Plasticity 48

Figure 1.17: Olfactory Associative Learning Paradigms 51

Figure 2.1: Genetically Engineered Mouse Lines 56

Figure 2.2: Odour Delivery Protocol 58

Figure 2.3: Cross-Habituation Test.....59

Figure 2.4: Odour Exposure Setup.....60

Figure 2.5: Food-Odour Association Setup 60

Figure 2.6: Food Preference Test 61

Figure 2.7: Food- and Odour-Finding Test Setup 62

Figure 2.8: Surgery and 2-Photon Ca^{2+} Imaging 64

Figure 2.9: Head-Fixed Perception Tests 65

Figure 2.10: Pharmacology 66

Figure 2.11: Image Segmentation of Glomeruli 67

Figure 2.12: Adaptation Index 69

Figure 3.1: Visualising Neural Activity in the Olfactory Bulb 75

Figure 3.2: Odour Sensitivity Varies Widely Across Olfactory Receptor Neurons 77

Figure 3.3: Odour Sensitivity Varies Widely Across Mitral and Tufted Cells 79

Figure 3.4: The Extent and Rate of Adaptation Vary with Relative Odour Strength..80

Figure 3.5: Glomeruli Most Sensitive for an Odour Rapidly Adapt at High Concentrations 83

Figure 3.6: Stimulus Duration and Odour Concentration Enhance Adaptation in the Most Sensitive Glomeruli 85

Figure 3.7: Response Amplitudes are Diminished in Adapted Glomeruli 86

Figure 3.8: Sustained Adaptation is Enhanced by Relative Odour Concentration ...88

Figure 3.9: Adaptation Delays Recovery to Baseline Response Amplitudes.....90

Figure 4.1: Measuring Changes in Odour Perception as a Function of Concentration 92

Figure 4.2: Assessing Odour Detection Thresholds Independent of Motivation.....94

Figure 4.3: Neural Code Underlying Odour Percepts 97

Figure 4.4: Characteristics of the Primary Glomerulus 99

Figure 4.5: Rapid Adaptation Evolves through Distinct Phases.....100

Figure 4.6: Odour Percepts are Classifiable within Primacy Time Constraints.....102

Figure 4.7: Rapid Adaptation Originates at the First Synapse 103

Figure 4.8: Rapid Adaptation is not a Consequence of Feedback Inhibition.....104

Figure 4.9: A Model of Depolarising Block in Olfactory Receptor Neurons and Rapid Glomerular Adaptation 106

Figure 5.1: Olfactory Learning Protocols 109

Figure 5.2: Mice Learn to Associate an Odour with Food and Develop a Preference for it 110

Figure 5.3: Mice Connect a Wide Range of Odour Concentrations to the Same Object 112

Figure 5.4: Associative Learning Abolishes Rapid Adaptation in the Primary Glomerulus 113

Figure 5.5: Perceptual Constancy Arises from Dynamic Range Matching and Functional Changes in the Primary Glomerulus.....115

Figure 5.6: Associative Learning Shifts Sensitivity of Responsive Glomeruli 118

Figure 5.7: Associative Learning Reduces the Fraction of Dual-Responsive Glomeruli 119

Figure 5.8: Odour Learning Increases the Detection Threshold for Glomeruli Responsive to the Conditioned Odour.....121

Figure 5.9: Associative Learning reduces the Fraction of Dual-Responsive Glomeruli II 123

Figure 5.10: Odour Learning Increases the Detection Threshold for Glomeruli Responsive to the Conditioned Odour II.....125

Figure 6.1: A Model for Perceptual Constancy in Olfaction.....136

Chapter 1: Introduction

1.1 The Olfactory System

1.1.1 Overview

In order for any living organism to thrive in its habitat, it must gather data about its environment and respond to it appropriately. Airborne volatile molecules serve as carriers of information related to food, predators, and the reproductive cycles of conspecifics. It is the olfactory system that is responsible for analysing and making sense of this information.

In evolutionary terms, olfaction is among the most ancient sensory systems. From bacteria and protozoans, to funghi, plants, and animals, all forms of life have the capacity to perceive chemicals in their environment. Vertebrate olfactory systems likely began with simple sensory cells in the skin of our distant common ancestor (*3*). Over the course of evolution, distinct regions dedicated to odour-detection were formed, giving rise to a specialised system capable of more sophisticated odour analysis.

Unlike the domains of vision and audition, where the physical properties of light and sound waves can predictably influence perception, the olfactory system is faced with the challenge of distinguishing potentially more than a trillion structurally diverse odour molecules ((*4*), but see (*5*, *6*)). This immense variety allows for the identification of a virtually limitless array of distinct odours. For example, in coffee alone, > 800 different volatile components give rise to its unique aroma (*7*). In contrast, the recognisable aroma of banana contains ~24 active components (*8*), yet can be meaningfully recreated with just a single compound, isoamyl acetate.

The olfactory system interfaces with the external world and converts odourant information into electrochemical signals in the brain (Figure 1.1). This is achieved by multiple classes of receptor neurons, which collectively express a diverse range of chemosensitive receptors. Olfactory receptor neurons bind to odour molecules entering the nasal cavity and project to glomeruli, dense bundles of nerve fibres in the olfactory bulb. Within a glomerulus, sensory information is transmitted to a pool of output neurons, the mitral/tufted cells, where it is modulated through multiple layers of

inhibition before being relayed to the olfactory cortex. Chapter 1.1 describes each part of this process and the underlying structures involved.

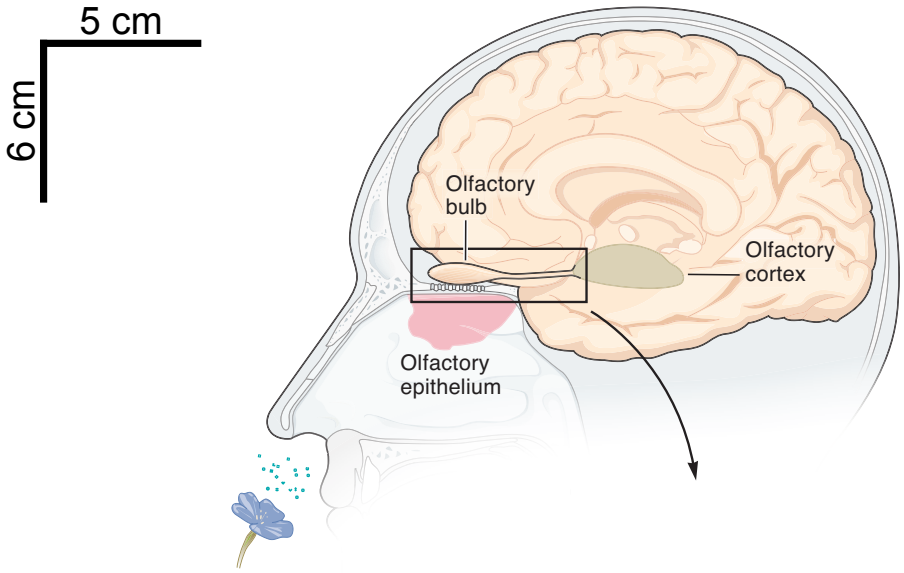

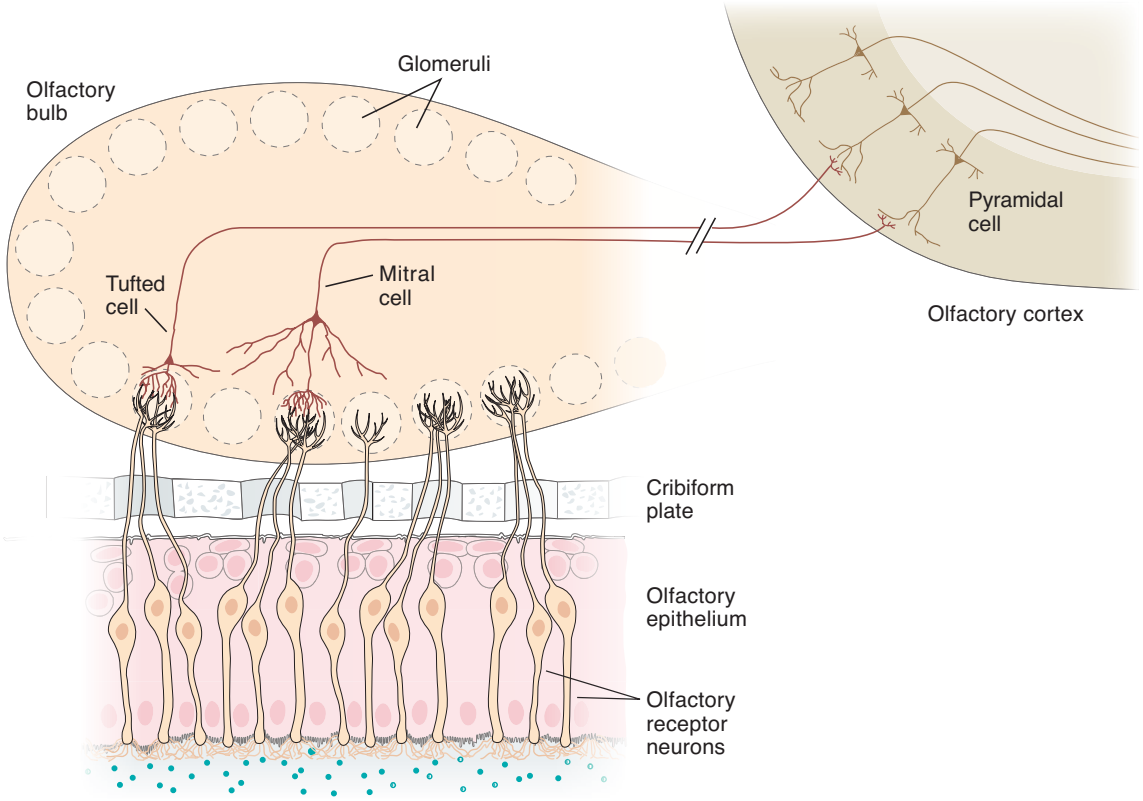

Figure 1.1: The Olfactory System

Odourants entering the nose are detected by olfactory receptor neurons embedded within the olfactory epithelium lining the nasal cavity. These neurons extend their axons to glomeruli, compact clusters of nerve fibres within the olfactory bulb. Here, odour information is transmitted to mitral/tufted cells, where it undergoes modulation before being relayed to the olfactory cortex. Figure adapted with permission from Kandel *et al.* (*9*).

1.1.2 The Nasal Cavity

Odour perception unfolds when odour molecules enter the nasal cavity directly through sniffing (orthonasal) or find their way indirectly via the oral cavity (retronasal). The nasal cavity houses several distinct subsystems which contribute to the sense of smell. Both orthonasal and retronasal routes of entry provide the required airflow to transport volatile compounds towards these specialised regions.

The main olfactory epithelium lines the dorsal portion of the nasal cavity, and its sensory neurons project to glomeruli in the main olfactory bulb (Figures 1.1-2). Volatile odours migrate from the air into the fluid that encapsulates the cilia of these neurons, where receptor-odourant binding takes place. Located beneath the ventral nasal cavity lies the vomeronasal organ, an area shown to participate in innate sexual and social behaviours between conspecifics. Sensory neurons within the vomeronasal organ express a variety of pheromone-sensitive receptors and establish connections with the accessory olfactory bulb. Despite this delineation, there is compelling evidence of significant overlap between the main olfactory epithelium and the vomeronasal organ. Neurons in the main olfactory system respond to certain pheromones, playing a crucial role in multiple sexual and social behaviours (*10-14*). Similarly, the accessory olfactory system is sensitive to certain odourants which can influence behaviour without recruiting the main olfactory system (*13*, *15*, *16*). In humans, the vomeronasal organ appears to be vestigial and non-functional.

A third mammalian structure, the septal organ (organ of Masera), is a small island of epithelium situated near the ventral base of the nasal septum (*17*, *18*). As with the main olfactory epithelium, olfactory sensory neurons reside in the septal organ, and

the majority extend their axons to ventromedial positioned glomeruli in the main olfactory bulb (*18*). Consequently, numerous volatile odourants cause overlapping activation in both regions (*19*, *20*). Moreover, certain neurons within both the septal organ and main olfactory epithelium function as dual sensors, capable of detecting odour molecules and shifts in air pressure brought about by sniffing (*20*).

In more recent years, another olfactory subsystem was discovered at the nasal vestibule, just at the entrance to the naris in mice: the Grueneberg ganglion (*21*, *22*). Olfactory receptor neurons from this zone participate in olfaction by responding to volatile alarm pheromones, inducing freezing behaviour in mice (*23*). Axons from Grueneberg ganglion neurons take a unique projection path, ramifying in a distinct class of glomeruli surrounding the caudal end of the main olfactory bulb, known as 'necklace glomeruli' (*24-29*).

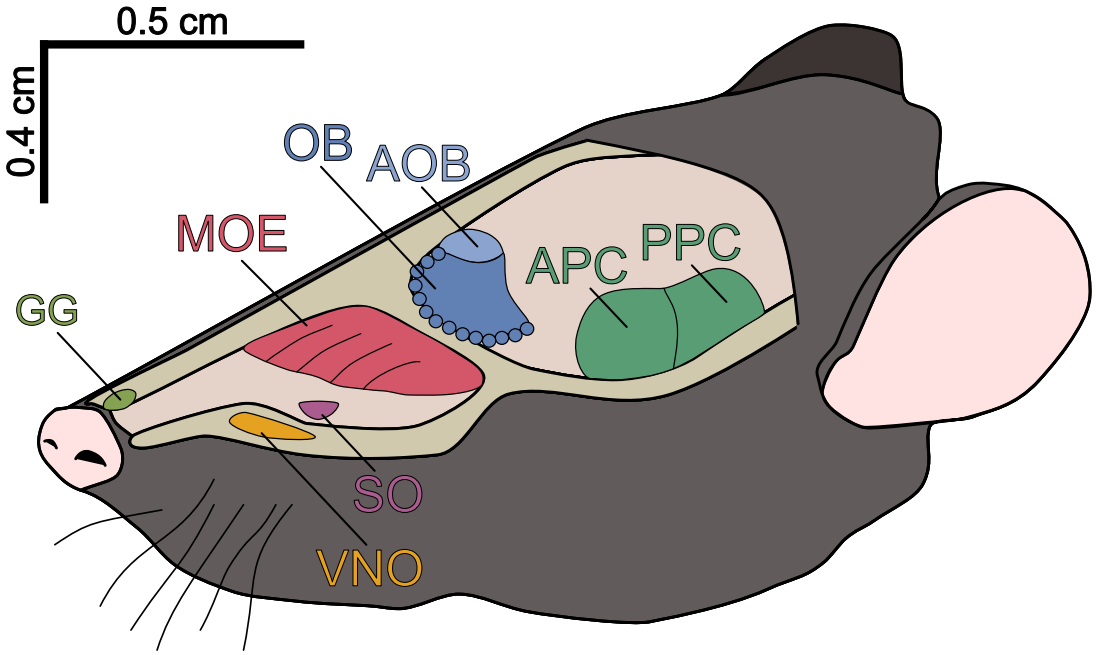

Figure 1.2: Olfactory System Anatomy

Sagittal view of mouse olfactory system anatomy. Olfactory receptor neurons located in the main olfactory epithelium (MOE), Grueneberg ganglion (GG), and the septal organ of Masera (SO) all extend their axons to the main olfactory bulb (OB), while those residing in the vomeronasal organ (VNO) project to the accessory olfactory bulb (AOB). Output neurons from the olfactory bulb—the mitral/tufted cells—transmit modulated olfactory information to distinct regions of the olfactory cortex, including the anterior

and posterior piriform cortex (APC and PPC, respectively), which collectively form the primary olfactory cortex. Figure adapted with permission from Su *et al.* (*30*).

1.1.3 Olfactory Receptors

Odourant receptors constitute the largest family of G-protein-coupled receptors (GPCRs) in the mammalian genome. The mouse genome contains 1,141 functional olfactory receptor genes, whereas 389 have been identified in humans (*31*). Among these, mature olfactory receptor neurons express only one receptor gene (*32*), and they express only one allele of that particular gene (*33*). The expressed olfactory receptor governs the odour-response profile of an olfactory receptor neuron (*34*) and the target glomerulus its axon innervates (*35*). Thus, this expression profile across neurons confers a high degree of dimensionality to odour representations, and enables olfactory receptor neurons to arrange themselves into functional units.

In mammals, olfactory receptors generally consist of seven-transmembrane domains (Figure 1.3) (*36*). Ligand binding occurs within the hydrophobic regions of the GPCR, which span the membrane. Unlike traditional GPCRs that interact with only a specific ligand, olfactory receptors bind to a range of both full and partial agonists with varying affinities (*32*, *34*, *37-41*). The amino acid sequences within the binding pocket, which constitute the most variable regions of the GPCR (*36*), are considered the foundation for the receptor repertoire's ability to recognise a vast array of odourous ligands. Given the broad receptive field of olfactory receptors, a single odourant molecule can induce different levels of activation in numerous receptor types, generating unique patterns of activity across the olfactory receptor neuron population (*42*). This phenomenon is referred to as combinatorial coding (*32*) and it allows for the discrimination of a seemingly limitless number of odours.

Olfactory receptor genes represent the most extensive gene family in the mammalian genome and are categorised into several distinct subfamilies. The vast majority of receptors in the main olfactory epithelium and septal organ are olfactory receptors. However, a subset of olfactory receptor neurons express trace amine-associated receptors (TAARs) that are sensitive to volatile amines. Amines, which are

abundant in animal bodily fluids such as urine and semen, are generated during protein degradation. As such, TAARs provide key social cues between conspecifics, facilitate sexual attraction, alert animals to predators, and serve as markers of spoiled food (reviewed in (*43*)). There are only 15 TAARs in the mouse genome (*44*), 14 of which are expressed in the main olfactory epithelium (*36*). As with canonical olfactory receptors, TAAR-expressing neurons converge at demarcated glomeruli in the olfactory bulb (*45*). A collection of TAARs however are expressed by neurons in the Grueneberg ganglion, and extend their axons to distinct glomeruli encircling the caudal region of the main olfactory bulb, referred to as the 'necklace glomeruli' (*22*).

In the vomeronasal organ, two distinct families of vomeronasal receptors are expressed: type-1 (V1R) and type-2 (V2R), with 187 (*46*) and 127 (*47*) functional genes present in the mouse genome, respectively. Neurons expressing type 1 vomeronasal receptors occupy the apical portion of the organ and target their axons to the anterior accessory olfactory bulb, whereas type 2 receptor neurons reside in the basal layer of the vomeronasal epithelium and project to the posterior accessory olfactory bulb (*48-50*). One particular vomeronasal receptor, V2r83, is expressed by Grueneberg ganglion neurons (*21*). Despite their different expression and projection patterns, both vomeronasal receptor types detect pheromones originating from urine and bodily secretions, together facilitating a range of innate sexual behaviours, maternal aggression, and the Bruce effect during pregnancy (reviewed in (*30*, *51*)). In more recent years, ~1% of vomeronasal receptor neurons have been found to express a novel family of formyl peptide receptors (*52*), which have an affinity for compounds released during disease and thus allow animals to detect illness in conspecifics.

Guanylyl cyclase D (GC-D) are another receptor type expressed in a subpopulation of sensory neurons residing in the main olfactory epithelium and septal organ. Unlike other receptors in the olfactory system, GC-D receptors consist of only a single transmembrane domain (Figure 1.3). Neurons expressing GC-D receptors have been shown to detect semiochemicals, a class of chemical substances which influence behaviour in conspecifics. It was first found that GC-D receptor neurons were responsive to the urinary peptides guanylin and uroguanylin (*28*), which have since

been shown to promote the acquisition of food preferences in mice (*53*). Carbon-disulfide (CS_2), a component of mouse breath, has also been shown to activate GC-D receptor neurons and transmit food preferences to conspecifics (*54*). Additionally, GC-D receptors are sensitive to carbon dioxide (*55*), an odour which (unlike humans) mice can perceive. The axons of neurons expressing GC-D receptors synapse onto ~15 aptly named 'necklace' glomeruli which encircle the dorsal and ventrolateral aspects of the main olfactory bulb (*25-27*).

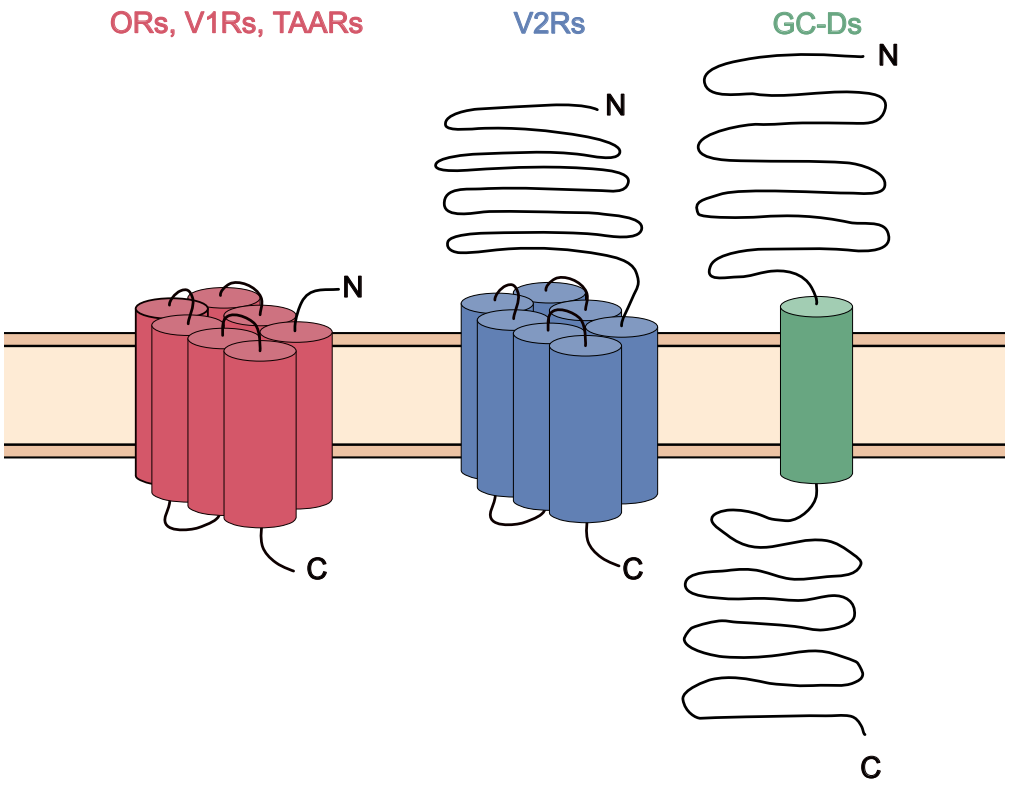

Figure 1.3: Olfactory Receptors

Olfactory receptors (ORs), vomeronasal type-1 receptors (V1Rs), trace amine-associated receptors (TAARs), and vomeronasal type-2 receptors (V2Rs) all consist of seven-transmembrane domains, whereas guanylyl cyclase receptors (GC-D) contain only one transmembrane domain. In all these receptor types, the N-terminus is positioned on the extracellular side of the cell membrane, while the C-terminus is located intracellularly. Like GC-D receptors, V2Rs possess a substantially large N-terminus. Additionally, the C-terminus of GC-D receptors is also notably prolonged, further distinguishing them from other olfactory receptors. Figure recreated and adapted with permission from Fleischer *et al.* (*56*) https://creativecommons.org/licenses/by/4.0/

1.1.4 The Main Olfactory Epithelium

1.1.4.1 Organisation

The main olfactory epithelium is the primary site of odour detection. It lines the roof of the nasal cavity and is situated ~7 cm posterosuperior to the nostrils (*57*). Around ~10 million bipolar olfactory receptor neurons are housed here in mice (*58*). Olfactory receptor neuron dendrites protrude into the epithelium, where hair-like cilia emanate from each knob into the surrounding mucus which coats the nasal cavity (Figure 1.4). The cilia are equipped with olfactory receptors and the requisite transduction machinery to transform odourant attributes into electrical signals. In mammals, olfactory receptor neurons positioned in the anterior regions of the epithelium have cilia which are up to five times as long and almost three times as numerous as those situated at the posterior, endowing greater sensitivity to odourants (*59*). The axons of olfactory receptor neurons project through the cribriform plate and terminate at their target glomeruli in the olfactory bulb.

Each olfactory receptor neuron expresses only one type of olfactory receptor (*32*), and all neurons expressing the same receptor converge at the same two glomeruli in the olfactory bulb (*35*). In the main olfactory epithelium, neurons expressing the same olfactory receptor are scattered in a mosaic fashion (*60-63*), and consequently there is evidence of spatial clustering between olfactory receptor neurons that respond to the same odour (*42*). Olfactory receptor neurons were classically thought to be spatially segregated into one of four non-overlapping zones in the main olfactory epithelium. However, in more recent years, 3D mapping of 68 (of the > 1,000) olfactory receptors revealed nine highly overlapping zones (*31*), suggesting there may well be more.

Interspersed with olfactory receptor neurons are several classes of supporting cells (Figure 1.4). Among these are basal stem cells, which serve to replace olfactory receptor neurons over the lifespan of the organism, and sustentacular cells, which function similarly to glial cells. Sustentacular cells provide structural support, engage in the metabolic processing of odourants, and maintain the ionic balance crucial for signal transduction by effectively isolating olfactory receptor neurons. In all terrestrial

mammals, including humans, olfactory receptor neurons are continuously generated throughout life from basal stem cells (*64-66*). These neurons have a relatively short lifespan, ranging from several weeks to a year, with survival and proliferation rates varying by location within the epithelium (*67-70*). The production of olfactory receptor neurons increases in response to chemical exposure, physical injury, or viral infections, enabling the olfactory epithelium to rapidly regenerate even after substantial neuronal loss (*71-73*). This continual regeneration enables the olfactory system to adapt to dynamic odour landscapes while safeguarding against environmental insults.

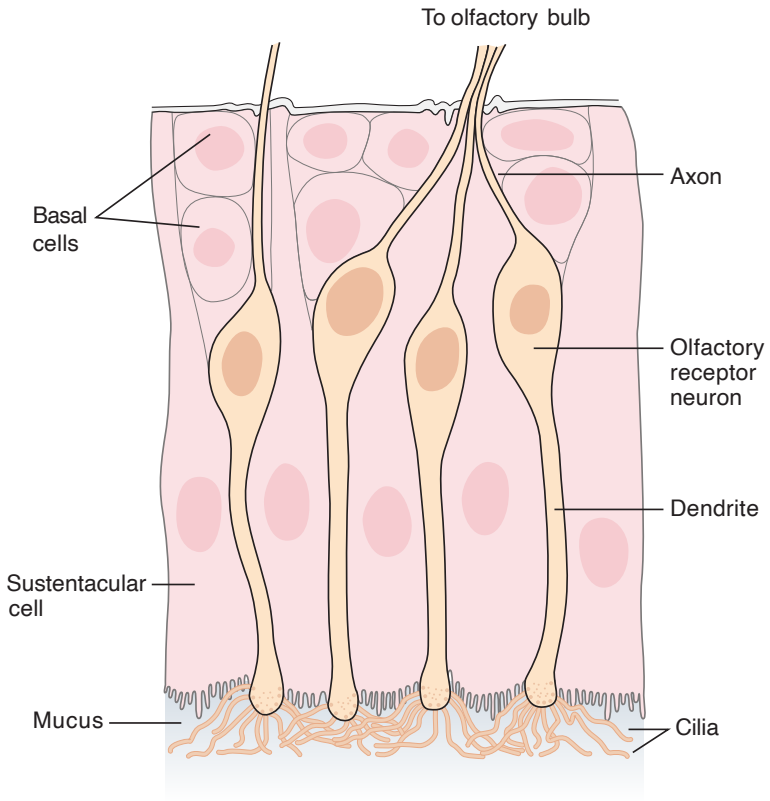

Figure 1.4: The Main Olfactory Epithelium

Olfactory receptor neurons are embedded within the olfactory epithelium, supported by sustentacular cells and basal stem cells. The dendritic knobs of these olfactory receptor neurons extend towards the epithelial surface, from which sensory cilia radiate into the surrounding mucus. The axons of olfactory receptor neurons project to the olfactory bulb. Figure adapted with permission from Kandel *et al.* (*9*).

1.1.4.2 Odour Transduction

For an odour to be perceived, its molecular attributes must first be converted into an electrical signal that the brain can interpret. Odourous ligands transported through the nasal cavity dissolve in the mucus layer, where they come into contact with the cilia which radiate from the dendritic knobs of olfactory receptor neurons (Figure 1.5). The binding of an odourant molecule to a receptor triggers an intracellular signalling pathway that depolarises the olfactory receptor neuron. In canonical olfactory receptors, the activated receptor first binds to the G protein $G\alpha_{olf}$, a guanosine triphosphate (GTP)-binding protein (*74*). $G\alpha_{olf}$ is the alpha component of a heterotrimeric complex, and in its resting state it is coupled with guanosine diphosphate (GDP). Once activate, $G\alpha_{olf}$ dissociates from the β- and γ-subunits ($G\beta\gamma_{olf}$), and exchanges GDP for guanosine triphosphate (GTP). GTP-bound $G\alpha_{olf}$ stimulates adenylyl cylclase III (*75*), which converts adenosine triphosphate into the secondary messenger cyclic adenosine monophosphate (cAMP). Sufficient elevation of cAMP inside the cilium prompts the opening of a cyclic nucleotide-gated (CNG) channel permeable to Na^+ and Ca^{2+} (*76*, *77*). Cation influx drives an inward depolarising current into the ciliary membrane, with the accumulation of intraciliary Ca^{2+} inducing activation of another transduction channel: the Ca^{2+}-gated Cl^- channel Anoctamin 2 (*78-82*). In resting conditions, high concentrations of Cl^- are maintained in the ciliary lumen by the Na^+-K^+-2Cl^- cotransporter NKCC1 (*83-85*). Thus, gating of Anoctamin 2 promotes the rapid efflux of Cl^-, further reinforcing depolarisation in the neuron. The Cl^- current markedly amplifies the signal of the initial response, accounting for up to 90% of the total receptor current in mice (*86*). As such, evidence suggests that Anoctamin 2 determines the number of action potentials generated (*87*) and contributes to odour learning (*87*, *88*). The overall magnitude of the receptor current and in turn the frequency of action potential firing is also graded with odourant concentration, until a saturation point is reached at concentrations which surpass a neurons dynamic range (*89*). The depolarising current travels along the dendrite towards the axon hillock, where action potentials are generated. Trains of action potentials propagate along the axon and stimulate glutamate release from olfactory receptor neuron terminals onto the

dendritic tufts of principal neurons in the olfactory bulb (*90*).

Whilst the majority of olfactory receptors rely on intraciliary cAMP to initiate odour transduction, there are known receptor types which instead utilise cyclic guanosine monophosphate (cGMP). Neurons expressing guanylyl cyclase D (GC-D) receptors were the first class of neurons shown to transduce odour information using a cGMP signalling cascade (*24*, *28*, *91*). Numerous neurons within the Grueneberg ganglion have also been found to express components of the cGMP transduction pathway (*92-95*). Interestingly, both of these neuronal subpopulations project to distinct regions of the atypical necklace glomeruli which encircle the most caudal region of the main olfactory bulb (reviewed in (*96*)).

Similar principles of signal amplification are observed in other sensory systems. For instance, transduction cascades within retinal rod photoreceptors are amplified to such an extent that these neurons are capable of detecting individual photons of light (*97*). Within the time it remains active, a single light-activated rhodopsin can trigger multiple G proteins (*98*, *99*). However, this is a stark contrast to the olfactory bulb, where interactions between odourant molecules and receptors tend to be so transient

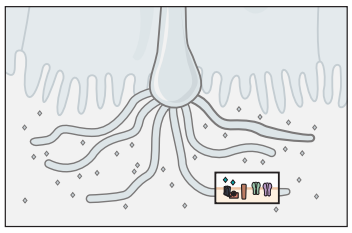

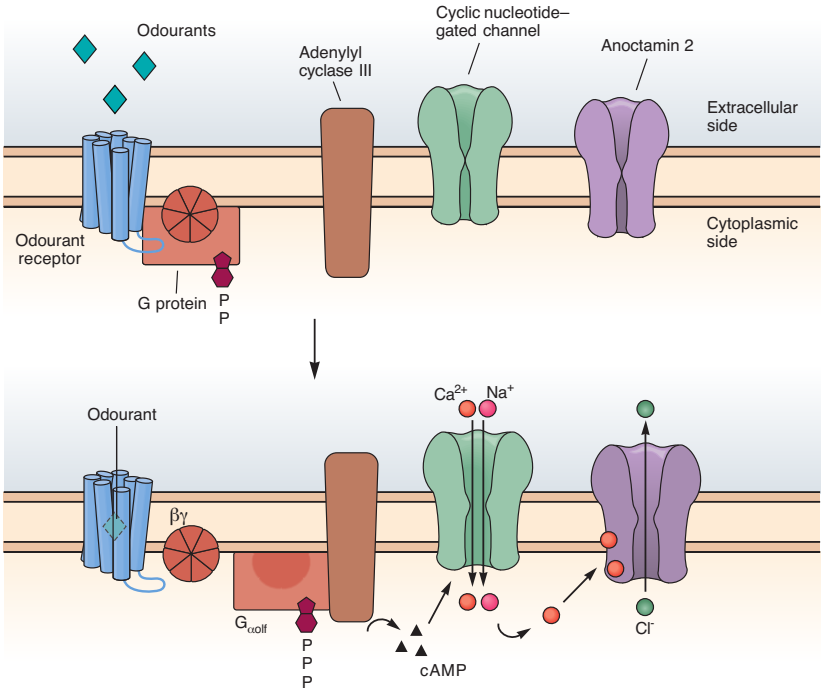

Figure 1.5: Odour Transduction

Odourants bind to olfactory receptors housed within the cilia, initiating an intracellular signalling cascade. Activated olfactory receptors interact with the α-subunit of the heterotrimeric G-protein ($G\alpha_{olf}$). This prompts $G\alpha_{olf}$ to dissociate from the β- and γ-subunits and exchange guanosine diphosphate (GDP) for guanosine triphosphate (GTP). Once bound with GTP, $G\alpha_{olf}$ stimulates adenylyl cyclase III, resulting in cyclic adenosine monophosphate (cAMP) generation. Rising levels of intracellular cAMP prompt the opening of the cyclic nucleotide-gated channel, promoting the influx of Ca^{2+} and Na^{+}. Ca^{2+} accumulation within the cilium triggers the opening of Antoctamin 2, dramatically amplifying the odour signal via the rapid efflux of Cl^{-}. Figure adapted with permission from Kandel *et al.* (*9*).

that they seldom lead to the activation of even a single G protein (*100*). As a result, a significant portion of these odourant-receptor binding events end up having little to no impact. Moreover, successful odourant-binding events yield small unitary currents (around only 0.15 pA in mouse olfactory receptor neurons), of which ~35 are estimated to be necessary to generate action potentials (*101*, *102*).

1.1.5 The Olfactory Bulb

1.1.5.1 Organisation

The olfactory bulb is the region of the brain where odour processing first takes place. Its defining characteristic is the vast array of glomeruli, ellipsoidal clusters of nerve endings which envelope the bulbs surface. Each one of the ~1,800 glomeruli (*103*) receive axon terminals from several thousand olfactory neurons expressing the same receptor gene (*35*, *104*, *105*). This extensive convergence serves to amplifiy odour sensitivity in the olfactory system. The two glomeruli which represent a given olfactory receptor are mirrored on the lateral and medial hemispheres of the olfactory bulb (*104*, *105*), and occupy stereotyped positions with minor variations (*106-108*). Thus, glomeruli are discrete modules whose activity is determined by the receptor type which innervates them. Within a glomerulus, the terminals of olfactory receptor neurons release glutamate as they make synaptic connections with a pool of output neurons, the mitral/tufted cells, and a diverse population of interneurons, including external tufted cells, periglomerular cells, and short axon cells (Figure 1.6).

Mitral/tufted cells are glutamatergic and the principal neurons of the olfactory bulb. They typically extend their apical dendrite into a single glomerulus, where the dendrite expands into an intricate tuft of branches that establish synapses with olfactory receptor neuron terminals and the lateral dendrites of periglomerular cells (*109*). Although generally referred to collectively, mitral and tufted cells represent distinct classes of principal neurons, identifiable by their arborisations and soma location (*109-111*). In mice, ~25 mitral cells and ~50 tufted cells share a glomerulus (*112*). Mitral cell somata are generally larger than tufted cells (*113*), and they typically possess far longer secondary dendrites (*109*, *114*). Current data suggests that the depth of soma location correlates with secondary dendrite length, with projection neurons located in deeper regions of the olfactory bulb generally having longer secondary dendrites (*115*). While the secondary dendrites of mitral cells are mostly confined to the deepest regions of the external plexiform layer, those of tufted cells extend throughout the superficial regions, proximal to the glomerular layer (*109*, *111*, *116*, *117*). Mitral/tufted cell axon collaterals project across both lateral sides of the olfactory bulb to form the lateral olfactory tract. Tufted cell axons target the anterior olfactory nucleus and olfactory tubercule, whereas those of mitral cells cover the olfactory cortex in its entirety (*110*, *114*, *118*). However, the axons of some projection neurons terminate within the olfactory bulb, synapsing onto the soma and dendrites of granule and deep short axon cells situated the granule cell layer (*119-121*).

Before being transmitted to the olfactory cortex, the olfactory signal is shaped by numerous classes of interneurons. Tufted cells situated in the external plexiform and glomerular layers are classified as external tufted cells. External tufted cells whose somata reside in the glomerular layer lack secondary dendrites (*116*, *122-126*). Like mitral and other tufted cells, external tufted cells are almost exclusively glutamatergic, providing excitatory drive onto periglomerular cells, superficial short axon cells, (*122*) and other mitral/tufted cells via dendrodendritic synapses (*127*). However, at least a subset of external tufted cells send axonal projections to the anterior olfactory nucleus and olfactory tubercule (*126*). Periglomerular cells represent the most abundant neuron type in the glomerular layer (*128*). Periglomerular cells are axonless, with their dendrites

predominantly ramifying within a single glomerulus (*129*, *130*). A population of periglomular cells receives input directly from the axon terminals of olfactory receptor neurons, while some are driven by feedforward excitation from external tufted cells (*131*). The vast majority of periglomerular cells are GABAergic, with a subset co-releasing both dopamine and GABA (*128*, *132*). The release of GABA from periglomerular cells inhibits neurotransmitter release from olfactory receptor neuron terminals by activating $GABA_B$ receptors (*133*, *134*), whereas activation of $GABA_A$ receptors inhibits mitral cells (*135*) and allows periglomerular cells to regulate their own excitability (*136*). Dopamine's role in the olfactory bulb is complex and not yet fully understood. Dopamine, through D2 receptors, inhibits glutamate release from olfactory receptor neuron terminals (*137*). In contrast, activation of D1 receptors enhances feedforward excitation from external tufted cells to mitral cells, while also modulating activity in periglomerular cells, superficial short axon cells, and granule cells, partly in coordination with GABA (*138*, *139*). Superficial short axons cells are housed in the interglomerular space and (despite their name) extend their axons across multiple glomeruli to facilitate interglomerular communication (*113*, *129*, *140-143*). Via the co-release of GABA and/or dopamine, superficial short axons cells concomitantly induce inhibition in mitral cells (*143*) and exert a biphasic inhibition-excitation response in external tufted cells (*142*) from neighbouring glomeruli. These neurons also presynaptically inhibit olfactory receptor neurons by modulating their release probabilty (*144*). The deep granule cell layer is occupied predominantly by granule cells, GABAergic, axonless neurons which establish reciprocal dendrodendritic connections with the lateral dendrites of mitral/tufted cells in the external plexiform layer (*109*, *119*). Deep short axon cells, another category of GABAergic interneurons, are also situated in the granule cell layer and have multiple axonal targets, including tufted cells and other interneurons (*121*, *145*).

The circuits of the olfactory bulb exhibit remarkable plasticity. The olfactory bulb is one of only two regions in the adult nervous system, alongside the dentate gyrus of the hippocampus, that continuously integrates newborn neurons across the lifespan (*146*). Neural progenitor cells migrate from the subventricular zone of the forebrain

through the rostral migratory stream to the olfactory bulb, where they reach their target layer and differentiate into at least one of three interneurons—granule cells, periglomerular cells, or short axon cells (*147-153*). Each day, over 30,000 neuroblasts leave the rodent subventricular zone and travel along the rostral migratory stream (*154*). Although neural progenitors reach their target layers within a few days, it typically takes 2-4 weeks for them to fully mature into their destined interneurons (*155*, *156*), the vast majority of which become granule cells (*109*, *157*). The ongoing turnover of bulbar neurons is highly regulated, enabling animals to adapt their behaviour to an ever-changing environment while affording protection against injury (see (*149*, *158*) for in-depth review).

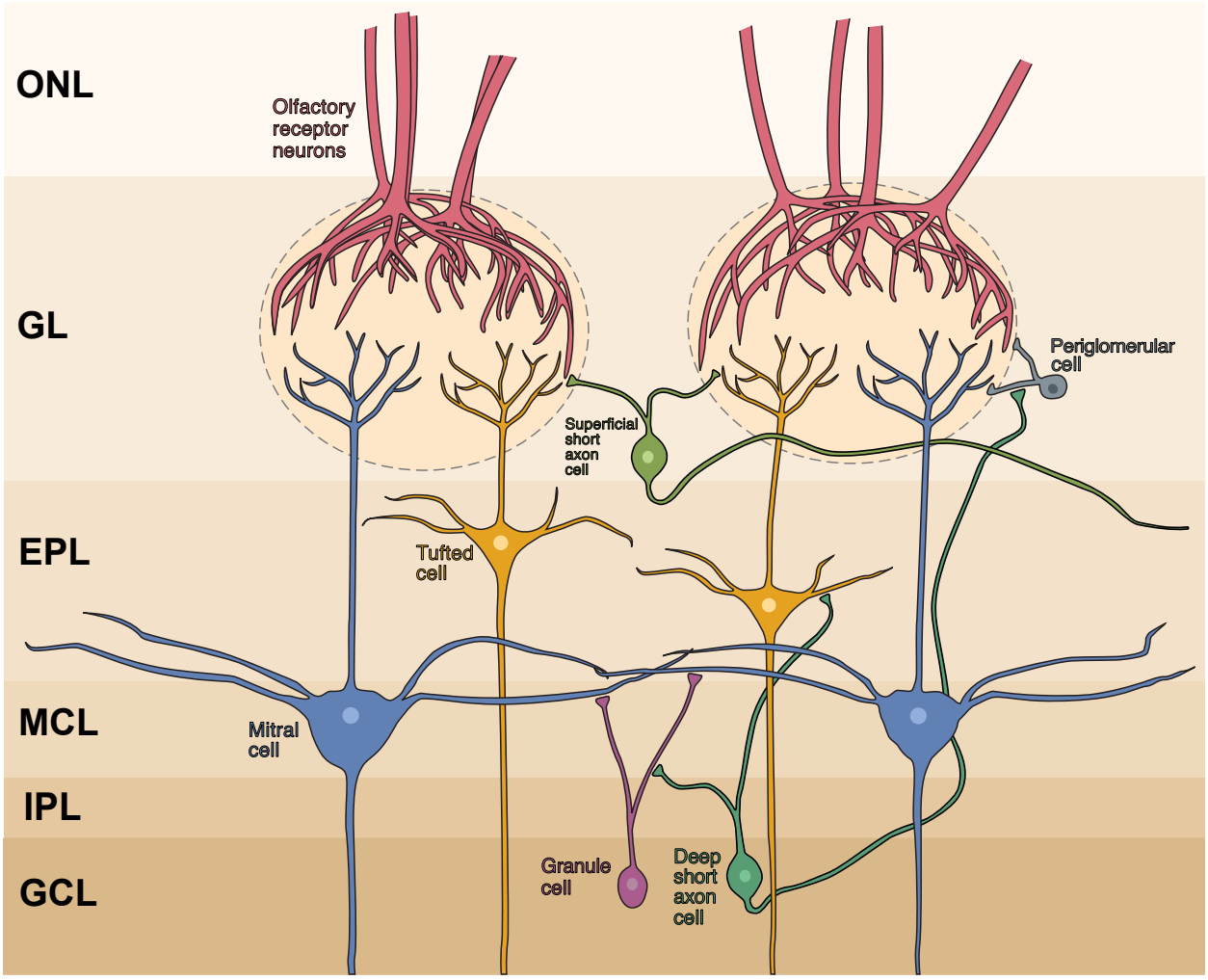

Figure 1.6: The Olfactory Bulb

The olfactory bulb is organised into multiple layers comprising morphologically distinct cell types. Axons from olfactory receptor neurons occupy the superficial olfactory nerve layer (ONL), with those expressing the same receptor terminating at the same glomerulus. The bodies of mitral and tufted cells are located in the mitral cell layer (MCL) and external plexiform layer (EPL), respectively, with both extending their primary dendrites to a single glomerulus. Within each glomerulus, the axon terminals of olfactory receptor neurons form synaptic connections with the primary dendrites of mitral/tufted cells, as well as with superficial short axon cells and periglomerular cells, both residing in the glomerular layer (GL). The primary dendrites of mitral/tufted cells ramify within the glomerulus, facilitating contact with olfactory receptor neurons, periglomerular cells, and superficial short axon cells. Superficial short axon cells facilitate interglomerular communication by projecting their axons to nearby glomeruli. Additionally, the lateral dendrites of mitral/tufted cells establish reciprocal dendrodendritic connections with granule cells and deep short axon cells, originating from the deep granule cell and internal plexiform layers (GCL and IPL, respectively). Figure created with permission using elements sourced from Imamura *et al.* (*115*), https://creativecommons.org/licenses/by/4.0/, and Kandel *et al.* (*9*).

1.1.5.2 Top-Down Feedback

In addition to complex intra-bulbar circuits, the olfactory bulb receives extensive top-down feedback from other regions of the brain, which serve to further modulate neuronal activity based upon behavioural state, attention, memory, motor output, and learning (Figure 1.7). Broadly, top-down feedback can be categorised into two groups: those which mostly originate from nuclei in the brain stem and basal forebrain and release neuromodulators such as noradrenaline, serotonin, and acetylcholine, and those which originate from regions of the olfactory cortex that olfactory bulb afferents project to.

Noradrenergic fibres extend from the locus coeruleus to all layers of the olfactory bulb and comprise ~40 % of all output fibres from this region in rat (*159*). The density of fibre innervation is correlated with layer depth, with the deepest layer—the granule cell layer—receiving the highest density, and progressively sparser innervation observed in more superficial layers. Granule cells are subjected to noradrenergic modulation via α2 and β receptors which consequently disinhibits mitral/tufted cells (*160*, *161*). Noradrenergic inputs have also been shown to enhance mitral cell

responses to weak olfactory nerve input (*162*, *163*) and to directly excite mitral cells via α1-receptors (*164*), implying they may facilitate the detection of low-concentration odours. Additionally, noradrenergic modulation seems to orchestrate mitral/tufted cell synchrony, where discrimination training alters their spike timing to encode odour value (i.e. whether an odour is associated with a reward), rather than odour identity (*165*). Moreover, glomerular input is subject to noradernergic modulation, with locus coeruleus stimulation shown to suppress odour-evoked responses in olfactory receptor neurons (*166*). In neonates, noradrenaline is crucial for forming odour associations (*167-169*) and preferences (*170-173*). In adults, it has been shown to enhance odour memory (*174-176*), improve discriminability of perceptually similar odourants (*177*), and facilitate learning in reward-based association tasks (*178*). Noradrenaline also influences behaviours like spontaneous investigation (*179*) and habituation (*180-182*), but see (*178*, *179*). Furthermore, both repeated exposure to novel odourants and associative conditioning have been linked to increased noradrenaline in the olfactory bulb (*174*, *176*).

The olfactory bulb receives a substantial amount of serotonergic fibres from the raphe nuclei (*183*), which project to all layers of the olfactory bulb but most notably to the glomerular layer (*184*). The glomerular layer predominantly contains fibres from the median raphe nucleus, whereas the granule cell layer is mainly innervated by the dorsal raphe nucelus (*185*). In the olfactory bulb, the primary two subtypes of serotonin receptors are 5-HT1A and 5-HT2A (*186*). The effects of serotonergic fibres in the olfactory bulb include: 1) excitation of external tufted cells via 5-HT2A receptors (*187*). 2) increased excitatory drive onto and consequent activation of GABAergic periglomerular cells, granule cells, and superficial short axon cells (*188-190*). 3) reduced glutamate release from olfactory receptor neuron terminals via $GABA_B$ receptors (*189*). 4) bimodal inhibition and excitation of mitral cells via $GABA_A$ receptors and 5HT2A receptors, respectively (*188*). The functional effects of serotonergic modulation are not well understood, though serotonergic input has been shown to play a key role in the acquisition of odour preference in neonates (*191*, *192*), potentially in coordination with noradrenaline (*193*). In adults, serotonin has been reported to support

discrimination between learned odourants (*194*), while modulation of 5-HT4 receptors specifically influences short-term memories involved in social recognition (*195*) and learning reward-based association tasks (*196*).

Cholinergic fibres extend primarily from the horizontal limb of the diagonal band of Broca in the basal forebrain (*197*, *198*) and innervate most layers of the olfactory bulb, chiefly the glomerular layer (*199*, *200*). Acetylcholine activates muscarinic and nicotinic receptors expressed throughout the olfactory bulb. Cholinergic fibres modulate inhibition by either exciting or inhibiting granule cells through M1 or M2 muscarinic receptors, respectively (*201*, *202*), and activating both periglomerular cells and superficial short axon cells via nicotinic receptors (*201*, *203*). Cholinergic-mediated increases in GABA suppress glutamate release from olfactory receptor terminals by way of $GABA_B$ receptors (*203*), and inhibit mitral/tufted cells via $GABA_A$ receptors (*203*, *204*). Additionally, acetylcholine directly exerts opposing effects on mitral cells, inducing excitation via nioctinic receptors (*201*, *203*) or inhibition by activating M2 muscarinic receptors (*205*). Taken together, these data suggest that acetylcholine serves dual functions: to enhance glomerular odour sensitivity by acting on M2 muscarinic receptors, or to decrease sensitivity utilising nicotinic receptors (*206*). Functionally, acetylcholine has been implicated in mediating habituation to novel odourants (*207-211*), but see (*212*), in forming short-term odour memories (*212-215*), and seems to play an important role in both learning odour associations (*216-220*) and discriminating between perceptually similar odourants (*221-223*).

Feedback projections emanating from the olfactory cortex establish reciprocal connections with the olfactory bulb. These fibres predominantly originate from the piriform cortex and anterior olfactory nucleus (collectively referred to as the anterior olfactory cortex), and the entorhinal cortex (*224-230*). Olfactory cortex-derived feedback densely innervates the olfactory bulb, outnumbering even olfactory receptor neuron inputs (*231*, *232*). Cortico-bulbar fibres are glutamatergic and primarily target granule cells, and to a smaller degree deep short axon cells, periglomerular cells, superficial short axon cells, and mitral cells. As a result, they can induce either feedforward inhibition onto or directly activate mitral cells (*233-238*). Top-down

feedback from the olfactory cortex offers an ideal substrate for transmitting the significance of stimuli, by either enhancing or suppressing odour-specific responses in mitral cells (but not in tufted cells, interestingly), or precisely altering spike timing in these neurons (*232*, *232*, *236*). Despite this, direct evidence of the functional significance of this type of feedback is limited. However, research has shown that a subdivision of the anterior olfactory nucleus, the pars medialis, plays a key role in modulating odour sensitivity and olfaction-dependent behaviours (*239*). Additionally, computational modelling suggests that feedback originating from the piriform cortex regulates the balance of excitation and inhibition in mitral cells, adjusting spike timing in piriform cortical cells and enhancing odour discriminability (*240*).

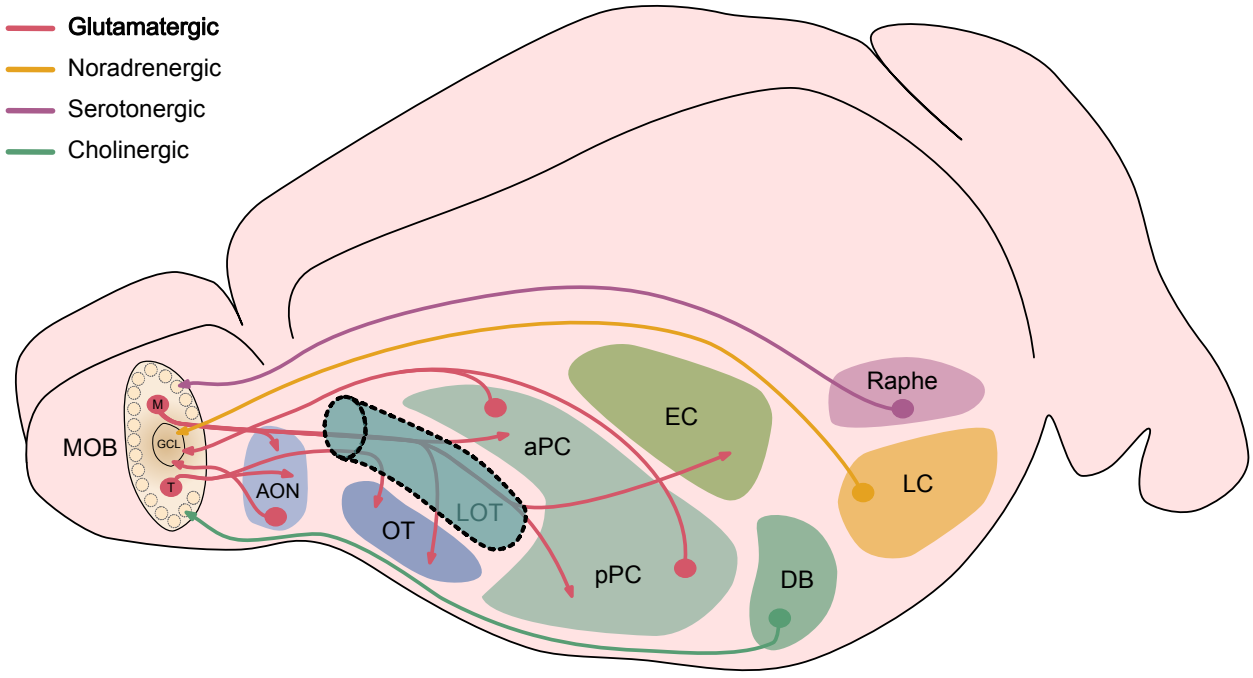

Figure 1.7: Olfactory Bulb Projection and Top-Down Feedback

Projection patterns of olfactory bulb neurons and top-down feedback in rodents. Mitral cells (M) send their axons to the anterior olfactory nucleus (AON), as well as the olfactory tubercle (OT), anterior and posterior piriform cortex (aPC and pPC, respectively), and entorhinal cortex (EC) via the lateral olfactory tract (LOT). In contrast, the axons of tufted cells (T) extend only to the AON and OT. Neuronal activity within the olfactory bulb is modulated by fibres originating from higher brain regions: Noradrenergic fibres from the locus coeruleus (LC) predominantly target the granule cell layer; serotonergic fibres and cholinergic fibres emanating from the raphe nuclei (Raphe) and the horizontal limb of the diagonal band

of Broca (DB), respectively, primarily innervate the glomerular layer; glutamatergic fibres from the aPC and pPC provide dense top-down feedback primarily to granule cells. Figure recreated and adapted with permission from Imamura *et al.* (*115*) https://creativecommons.org/licenses/by/4.0/.

1.2 Odour Encoding

1.2.1 Overview

To accurately represent the external odour landscape, the olfactory system must navigate significant challenges that alter perception, such as variations in odour concentration, air turbulence, and the rhythmic patterns introduced by natural breathing (*241-243*). Moreover, in natural settings, we predominantly encounter complex mixtures of odours at varying concentrations, rather than single, isolated molecules delivered at a constant flow, as in controlled laboratory conditions. Yet, the nose can discriminate an extraordinary array of volatile chemicals, a number far surpassing the available olfactory receptors in any given species (*244*). Consequently, the olfactory system must rely not only on its vast receptor repertoire but also on sophisticated encoding mechanisms to define odour identity.

Considerable advances have been made in understanding how odours are detected and processed at the periphery. Yet, how these olfactory signals are transformed into perceptual experiences remains elusive. A single odourant molecule can evoke intricate patterns of activity within the brain, but identifying which features of these patterns are essential to odour perception continues to be a major focus of research. The involved mechanisms likely encompass both the specific combination of activated receptors and the timing of neuronal responses relative to the sniff cycle. This section will explore the predominant models of odour identity encoding, reviewing how each contributes to our understanding of odour perception.

1.2.2 Combinatorial Coding

1.2.2.1 Combinatorial Receptor Codes

The foundational principles governing how olfactory receptors respond to

odourants were initially uncovered from recordings of individual olfactory receptor neurons in the olfactory epithelium. These early investigations revealed that each olfactory receptor neuron can detect more than one odourant, and that individual odourants activate distinct groups of olfactory receptor neurons (*245-247*). In 1999, groundbreaking research employing a combination of calcium imaging and single-cell reverse transcriptase unveiled for the first time the specific odourant receptors expressed in olfactory receptor neurons. This pioneering work by Malnic *et al.* (*32*) marked a significant milestone in understanding odour perception, demonstrating unequivocally that different odourants activate unique sets of olfactory receptor neurons. It provided the first indication that the olfactory system uses a 'combinatorial receptor code' to encode odour identities (Figure 1.8). Further, the research discovered that different concentrations of an odourant generate different codes, which are also sensitive to minor changes in chemical structure. Thus, each odourant, at any given concentration, is represented by a unique combinatorial receptor code.

Just over a decade later, the largest-scale analysis of olfactory receptor neuron response profiles to date was conducted by Nara *et al.* (*248*). Using calcium imaging, they examined responses from 3,000 mouse-derived olfactory receptor neurons to 125 chemically diverse odourants, resulting in a staggering 375,000 potential receptor/odourant pairings. Their study uncovered remarkable diversity of the olfactory receptor repertoire, which exhibited bias towards certain chemical classes. While most olfactory receptor neurons were specialised to detect only one or a few structurally similar odourants, there was also a subset of receptors with broader sensitivity, capable of recognising many. Notably, the vast majority of odourants evoked a unique combinatorial pattern of activity, involving the activation of at least two or more olfactory receptor neurons, encompassing both narrowly and broadly tuned receptors.

This body of research greatly expanded our understanding of how odours are detected and encoded in the olfactory epithelium. It elucidates why different odourants, especially those closely related in structure, can produce markedly different percepts. Crucially, the sophisticated combinatorial codes employed by the olfactory system, while initially identified and explored in earlier studies (*38*, *41*, *249-254*), have

been extensively corroborated and expanded upon by many subsequent studies across a variety of species (*255-260*). In the olfactory bulb, the unique combinatorial receptor code translates to unique patterns of activated glomeruli. These glomerular patterns are bilaterally symmetrical and stereotyped between animals, and as in the olfactory receptors they represent, are sensitive to variations in odourant structure and concentration (*261-265*).

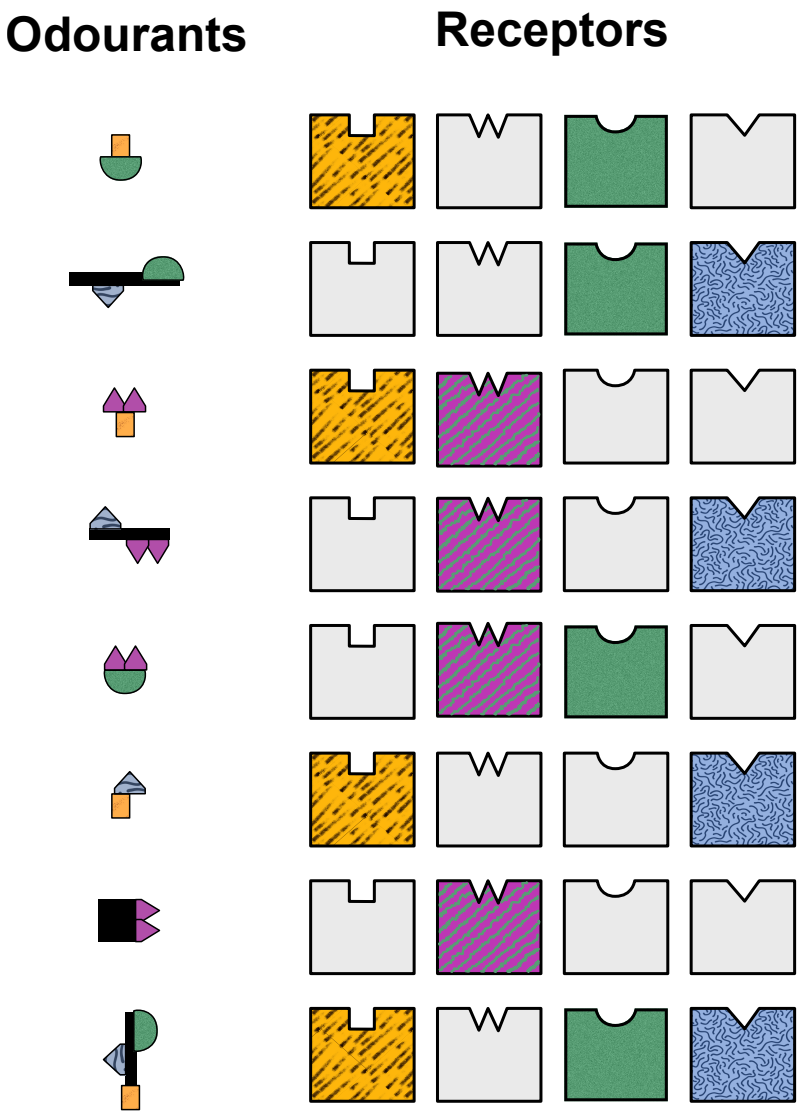

Figure 1.8: Combinatorial Receptor Code for Odourants

In this model, the receptors highlighted with coloured patterns recognise the odourants illustrated on the left. Odour identity is encoded by unique combinations of these receptors. Additionally, each odourant

receptor can contribute to the codes for multiple odourants. Given the vast array of possible receptor combinations, this coding strategy could potentially allow for the discrimination of an almost infinite number and variety of odourants. Figure recreated and adapted with permission from Malnic *et al.* (*32*).

1.2.2.2 Odourant-Receptor Interactions

The combinatorial receptor code model has been instrumental in elucidating how odourants interact with olfactory receptors. However, it falls short in fully capturing the complex interactions between various odourants and the receptor repertoire. In natural odour environments, the olfactory system is typically exposed to complex mixtures of odourants, as opposed to a single odourant in isolation. For example, coffee alone is a rich blend of > 800 volatile compounds. Consequently, recent research has shifted focus towards exploring how the olfactory system handles complex odour mixtures. In doing so, our understanding of how odours are coded at the periphery has been altered. Notably, these experiments revealed that an individual odourant can assume multiple roles - as an agonist, antagonist, inverse agonist, partial agonist, or even synergist. In 2020, a series of groundbreaking studies illuminated how the olfactory system normalises receptor inputs to prevent saturation and enhance signal transmission (*266-271*).

Technological advancements played a pivotal role in these discoveries, highlighted by the implementation of a novel light-sheet microscopy technique known as Swept Confocally Aligned Planar Excitation (SCAPE). SCAPE microscopy was used in a seminal experiment by Xu *et al.* (*270*) to image odour responses in mice that expressed the genetically encoded calcium indicator GCaMP6f in their olfactory receptor neurons. This technique allowed for simultaneous measurements from ~10,000 individual olfactory receptor neurons in intact mouse epithelia in response to various odour blends. Single-cell analysis revealed that the majority of neuronal responses were unaltered by other odours in the mixture, aligning with a simple additive model such as the combinatorial receptor code. However, in certain subgroups of cells, responses were liable to either enhancement, suppression, or complete inhibition. The prevalence of these interactions was shown to be odour specific and dose-dependent. In neurons that underwent suppression, this effect could

be reversed by increasing the concentration of the suppressed odour. Conversely, enhancement was evident in neurons that failed to respond to an odour in isolation, but did so robustly when the concentration of another odour in the blend was increased.

These phenomena have also been observed at the peripheral and glomerular level (*267*, *271*). Inagaki *et al.* (*267*) reported that enhancement was primarily observed in olfactory receptor neurons when an odour mixture was comprised of weaker concentrations, whereas stronger concentrations were more likely to induce antagonism. Furthermore, both enhancement and antagonism were observed at the glomerulus in double knockout mice lacking $GABA_B$ and D_2 receptors, effectively making them resistant to feedback inhibiton. This suggests that these effects are directly relayed to the olfactory bulb and arise independently of post-synaptic processing. These findings partially align with those from Zak *et al.* (*271*), who while also observing antagonism in both glomeruli and individual olfactory receptor neurons, reported that this effect was stable across concentrations spanning three orders of magnitude. Synergy, however, was a rare occurrence, observed in only ~12% of olfactory receptor neurons. Additionally, it was revealed that mixture-evoked suppression was more pronounced in complex blends composed of more odours.

Building on these insights using a combination of SCAPE microscopy and single-cell RNA sequencing, Pfister *et al.* (*269*) discovered that within a diverse collection of 800 odourants commonly used in perfumery, more than half exhibited antagonstic properties against the test odour. Notably, the vast majority were found to inhibit activity in more than one olfactory receptor. These findings suggest that odourant-induced antagonism is a common feature in odour encoding, functioning in a combinatorial fashion. Additionally, the dose-response curves from the *in vitro* data was shown to align with a mahematical model of competitive binding, as has been proposed previously (*272*). The observed synergy hints at allosteric modulation, a mechanism that, although elusive and seldom seen in class A GPCRs, could explain why certain olfactory receptors only respond to an odour when it is part of a mixture (*273-278*).

These studies collectively demonstrate that odourant-induced responses are

subject to various forms of modulation at the periphery. This modulation likely expands the dynamic range of the olfactory system, adjusting signal intensity to either enhance or suppress elements within an odour mixture. Figure 1.9 illustrates that a simple additive model, where each odourant molecule activates a specific set of receptors, could quickly saturate the receptor repertoire (Model 1), thus rendering distinct odour blends indistinguishable. However, subtle adjustments through suppression and enhancement endow each blend a unique signature (Model 2). Although this process might occasionally obscure the detection of individual blend components, it effectively imbues the mixture with a distinct identity. Accordingly, the psychological parallels of suppression and enhancement have been reported in odour mixture perception (*279-281*). Crucially, normalisation at the receptor level would allow for a sparser and more informative representation without imposing further demands on the neural circuits.

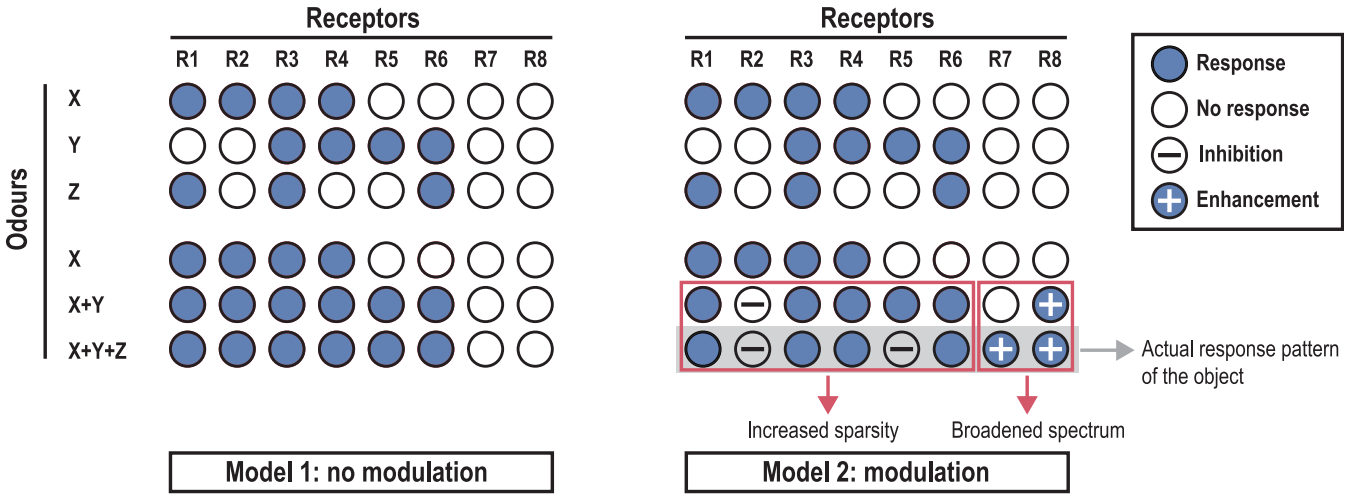

Figure 1.9: Odourant-Receptor Interactions in Odour Encoding

Two theoretical models for the encoding of odour mixtures. Monomolecular odourants X, Y, and Z each activate a unique set of receptors. (Model 1) No modulation: This assumes a linear summation of the activated receptors. Mixing odours X and Y would activate two additional receptors, however adding Z to the blend would not alter the percept. (Model 2) Modulation: In this scenario, receptors are modulated via odourant interactions. A blend of odours X and Y leads to the inhibition of receptor 2 and enhancement of receptor 8. Similarly, the inclusion of odour Z inhibits receptor 5 and enhances receptor 7. These adjustments are thought to allow for the separation of complex odour mixtures and thus

expand the coding capacity of the olfactory system. Figure adapted with permission from Xu *et al.* (*270*), https://creativecommons.org/licenses/by/4.0/

"*Perfumers have known for years that compounds with little or no odours—or even an unpleasant odour— are critical to the artistry of fragrance creation. In light of this new work, we may infer that these compounds likely have antagonistic effects that sharpen a perception or remove an unwanted note from the mixture*"

(*282*)

1.2.3 Phase Coding

In recent years, research increasingly indicates that encoding odour identity involves more than just variations in neuronal firing rates in response to an odour, commonly known as 'rate coding'; it also relies on changes in the timing of these neuronal spikes, or 'phase coding'. Phase code modulation can manifest as changes in spike latency, oscillation phase, and interspike intervals (*283-285*). However, for an odour to be perceived, it must first be sampled. Nasal airflow, driven by active sniffing, captures discrete snapshots of the odour landscape. The passage of air through the nostrils generates pressure that triggers mechanical responses, known as theta oscillations, in various cell types. Groundbreaking work by Iwata et al. (*286*) suggests that these theta oscillations are a crucial component of the odour identity code. Their research demonstrates that the mechanosensitivity of olfactory receptor neurons orchestrates spike timing in mitral/tufted cells, enabling concentration-invariant encoding of odour identity.

These experiments were performed on anaesthetised and tracheotomised animals using an artificial sniffing system that precisely controlled nasal airflow and simulated natural breathing rhythms. At the level of olfactory receptor neuron axon terminals within the olfactory bulb, calcium imaging revealed that brief pulses of air elicited widespread activity that was unique to each glomerulus, indicating receptor-specific mechanosensitivity—consistent with earlier research (*20*, *287*, *288*). Increasing

the airflow rate drove more activity in ~50% of glomeruli. In contrast, ~80% of mitral/tufted cells responded robustly at the onset of air pulse stimuli and activity declined thereafter. Furthermore, air-evoked theta oscillations within mitral/tufted cells were synchronised within each glomerulus, aligning with reports of synchrony among 'sister' mitral/tufted cells that share a common glomerulus (*289-291*). Remarkably, these glomeruli displayed distinct oscillatory activity, indicating that glomeruli are tuned to encode specific phases of the sniff cycle. Conversely, individual olfactory receptor neurons exhibited only binary high or low responses to periods of airflow-on and -off, respectively, suggesting that glomerulus-specific oscillations arise from olfactory bulb circuitry. These findings underscore the temporal complexity of odour encoding in the olfactory bulb, which is further exemplified by how different cell types function during the sniff cycle.

It is well-established that odourants activate different mitral/tufted cells at specific phases of the sniff cycle (*292-295*). For example, external tufted cells, which are among the initial transmitters of the odour signal, activate ~100 ms after inhalation and continue to fire throughout the inhalation phase (*114*, *296*). Similarly, middle/internal tufted cells initiate their high-frequency burst firings beginning at inhalation, but their activity extends to around the mid-point of the exhalation phase (*114*). In contrast, mitral cells exhibit a notably delayed response, beginning with low-frequency burst firing early in the exhalation phase and persisting throughout (*114*). A subset of mitral cells continue firing even after odour cessation (*297*, *298*). This temporal specialisation likely enhances rodents' ability to discriminate between optogenetic stimulations of a single glomerulus delivered at different phases of the sniff cycle (*299*). Although increases in airflow and the presentation of an odour both elicit activity in mitral/tufted cells (an increase in rate code), odour stimuli induce significantly larger changes in the timing of responses (shifts in phase code, measured by the time taken for a response to reach half its peak amplitude). These effects are both odour- and glomerulus-specific, and have been observed in both anaesthetised and awake states.

While it has been demonstrated that a single sniff provides enough information for trained mice to make odour discriminations (*295*, *300-302*), repetitive sniffing is

essential for other behaviours, including olfactory learning and scent tracking. When presented with a sustained odour stimulus, the rate-codes (response amplitudes) in mitral/tufted cells progressively declined across sniff cycles, with the last cycle looking markedly different from the first (*286*). In contrast, the phase code (timing of glomerular responses relative to the sniff cycle) was considerably more stable and conserved across multiple sniff cycles. Moreover, when animals were exposed to 14 different odours (comprised of both pure odourants and mixtures) across a concentration range spanning ~two orders of magnitude (1:8,100 - 1:100 dilutions), rate coding was altered dramatically, with the majority of glomeruli exhibiting a monotonic relationship with odour concentration. However, the phase code remained consistent and concentration-invariant, maintaining the same odour-induced phase advances or delays across the entire concentration range. Furthermore, in experiments where mice were exposed to either rhythmic odour pulses, designed to mimic mechanosensation, or a sustained odour pulse, the phase code was notably more precise and exhibited less variability across sniff cycles with the inclusion of the mechanistic component (Figure 1.10).

Phase coding appears to be a key mechanism used by the olfactory system to encode odour identity in a concentration-invariant manner, which is essential for

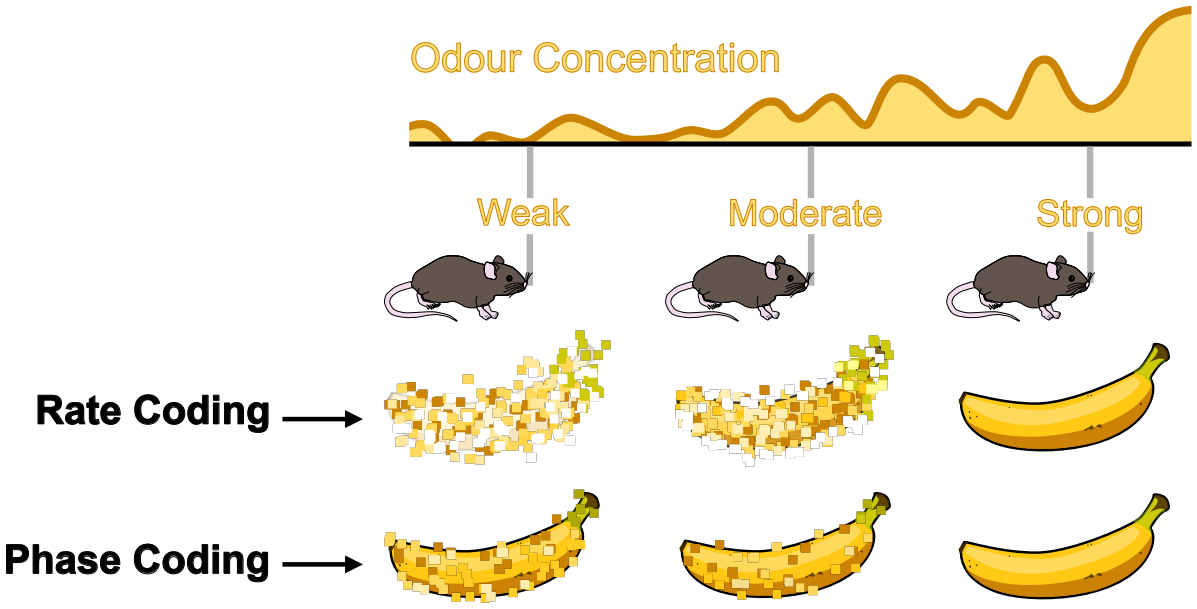

Figure 1.10: Phase Coding Model of Odour Identity

Proposed function of phase coding in olfaction. Rate coding, the odour-evoked change in neural spiking patterns, varies with concentration and across sniff cycles. In contrast, phase coding—the timing of these neuronal spikes—remains stable across various concentrations and sniff cycles. Consequently, phase coding is suggested to be a more reliable coding strategy for representing odour identity, especially in naturally turbulent environments. On the other hand, rate coding may be a more valuable indicator of odour intensity. Figure recreated and adapted with permission from Iwata *et al.* (*286*).

effective scent tracking. This constancy is proposed to be supported by intrinsic firing properties of mitral/tufted cells, subthreshold oscillations, and/or interglomerular inhibitory circuitry (*290*, *303-306*). Conversely, rate coding effectively represents odour intensity, evidenced by the markedly different firing patterns of mitral/tufted at different concentrations (*294*, *307*). Therefore, employing a dual-coding strategy that integrates both rate and phase coding could provide a more robust and stable representation of the odour environment.

1.2.4 Primacy Coding

It has been suggested that, for a given odour stimulus, only the first few activated glomeruli are necessary to encode odour identity. This model, referred to as 'primacy coding', purportedly explains the olfactory system's ability to identify the same odour over a wide range of concentrations (Figure 1.11) (*308*). An assumption of the model is that the first few responsive glomeruli during a sniff represent olfactory receptors that have the highest affinity for the odour. Although the primary set of glomeruli would change with each odour, this model posits that the sequence of activation—and thus odour identity—will be preserved across concentrations of the same odourant; less sensitive glomeruli are recruited at higher concentrations, but only after the primary set.

A fundamental premise of primacy coding is that the initial segments of neural activity elicited by an odour are crucial for its identification, rather than the entire pattern of activity. Indeed, rodents are capable of distinguishing between different

odours within a single sniff (< 200 ms) (*300-302*). However, these data suggest there is a trade-off between speed and accuracy: more challenging tasks, like distinguishing between very similar odour mixtures that evoke highly overlapping spatiotemporal patterns of glomerular activity, require longer sampling times. It is worth noting that these discrimination tasks did require extensive training periods, which may not wholly represent an animals's behaviour in natural settings and could potentially bias neural coding towards this task. Yet, when free to spontaneously discriminate odours, rats generally did so within 200 ms, and when discerning between a novel odour and a learned one, did so within a fraction of a sniff (as fast as 140 ms) (*309*). *In vivo* calcium imaging revealed that olfactory receptor neuron input arrives at the olfactory bulb 100-150 ms post-inhalation. Remarkably, animals often made discriminations as fast as 50 ms, even before the initial surge of receptor neuron firing had concluded and before the pattern of glomerular activity had fully developed. Building on this insight, Wilson *et al.* (*308*) demonstrated that optogenetically disrupting olfactory receptor neuron activity within the nose impaired odour discriminability in mice, but only when light was delivered within the 100 ms post-stimulus period. These findings were extended further by Chong *et al.* (*310*), who used optogenetics to activate a set of glomeruli on the dorsal olfactory bulb in a time-fixed sequence relative to inhalation. While mice could distinguish between this set sequence and random stimulations, substituting a glomerulus or delaying its activation within the set (by as little as 10 ms) impaired performance. Notably, there was a graded decline in performance based on timing, whereby altering the earliest activated glomeruli in the sequence had the most pronounced impact on discriminability. However, altering the specific activity pattern within a sniff produced relatively weak perceptual effects, suggesting that phase coding may have a minor contribution in comparison. Mice can also perceive light-driven activation of a single glomerulus, and are able to discern between different stimulation intensities and timing relative to the sniff cycle (*299*), implying that activity within a single glomerulus can inform behavioural decisions. Although optogenetic stimulation does not fully recapitulate the intricate patterns of activity driven by odour stimuli, these experiments suggest a key role for early activated neurons in encoding

odour identity. This phenomenon, where the earliest activating olfactory receptor neurons significantly shape behaviour, is similarly observed in flies (*311*).

Within multiple sensory systems, including olfaction, neurons are known to respond faster to stronger stimuli (*249*), leading to the idea that olfactory receptors of high affinity induce faster depolarisation in neurons than those of lower affinity (*293*, *303*, *312*). For air breathing animals, the act of sniffing controls the timing and concentration of odours entering the nose, thus generating a sequence of olfactory receptor neuron activation based on their affinity to the odour. This sequence changes with different odours but reportedly remains somewhat fixed across concentrations, albeit over a relatively narrow tenfold concentration range (*293*, *304*, *313*). Thus, primacy coding proposes that the timing of receptor activation encodes odour identity, with those possessing the highest affinity conveying the most information.

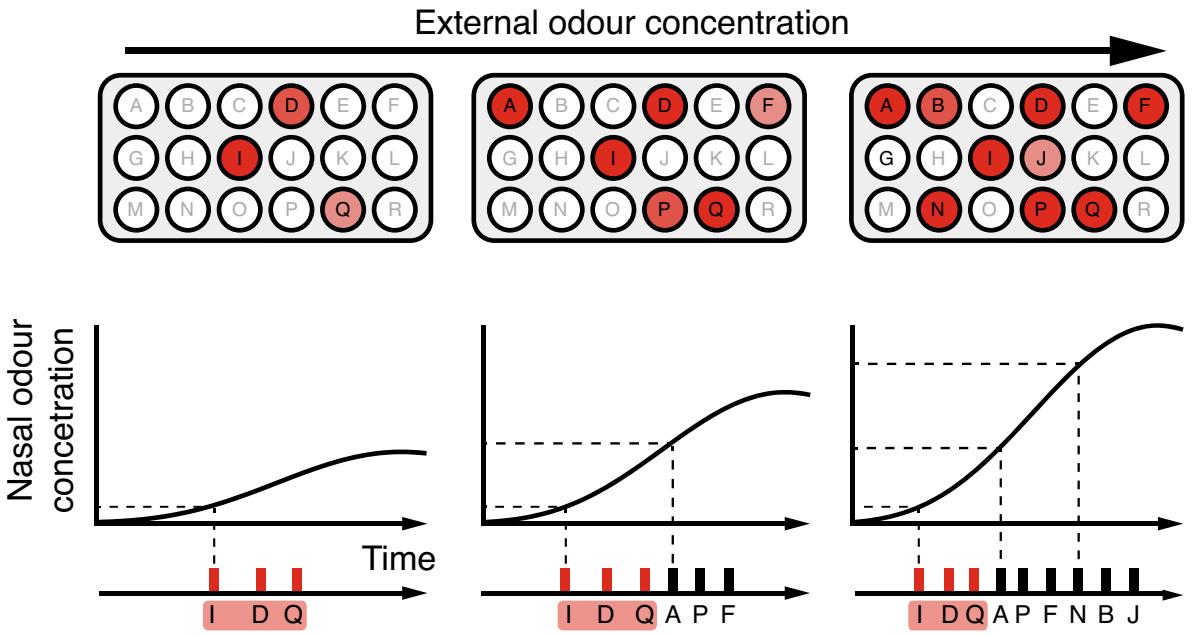

Figure 1.11: Primacy Model for Encoding Odour Identity

The primacy model proposes that only the initial few glomeruli activated by an odour are essential for encoding its identity. Glomeruli are denoted by letters, with those active marked in red. In this example, glomeruli I, D and Q exhibit the highest affinity for the odour, being the only ones to activate across three concentrations. Crucially, the sequence of activation—glomeruli I, D and Q, in that order—remains stable regardless of concentration, even when other less sensitive glomeruli are recruited at higher odour

concentrations. This model suggests that, for each given odour, a sparse, sequenced set of highly-sensitive glomeruli are sufficient to encode identity. Figure adapted with permission from Chong *et al.* (*310*), https://creativecommons.org/licenses/by/4.0/.

1.3 Odour Adaptation

1.3.1 Overview

In natural environments, animals are continually exposed to an extraordinarily vast array of odour stimuli across broad concentration spectra. Sensory adaptation ensures organisms remain attuned to their surroundings by filtering out redundant inputs, allowing animals to extract meaningful information from novel and salient stimuli (*314*). This process is crucial not only for preserving input sensitivity, but also for updating neural representations based on recent sensory experience. This section will discuss the various mechanisms by which the olfactory system optimally aligns with and interprets the surrounding odour environment.

1.3.2 Receptor Desensitisation

Repeated or prolonged exposure to an agonist leads to a marked decrease in responsiveness among the majority of G-protein coupled receptors (GPCRs), a phenomenon known as desensitisation. This process unfolds through various mechanisms, acting on different timescales. The earliest mechanism, receptor phosphorylation and consequent uncoupling of the receptor from the G-protein, occurs within seconds of ligand binding (*315-317*). Distinct classes of protein kinases target serine/threonine residues within the intracellular loops and C-terminal regions of GPCRs. This phosphorylation disrupts the linkage between the receptor and the heterotrimeric G-protein, effectively halting the signalling process (see (*318-320*) for more in depth discussion). GPCR kinases (GRKs), directly target receptors activated by an agonist, thereby triggering cytosolic proteins called arrestins that bind to and alter the conformation of the receptor, thus rendering it inactive (Figure 1.12) (*321*, *322*). Conversely, kinases that rely on secondary messengers such as cAMP-dependent protein kinase A (PKA) and calcium-dependent protein kinase C (PKC) can

phosphorylate both activated and inactive GPCRs (*323*).

While olfactory receptors constitute the largest subfamily of GPCRs, the specific manner in which GRKs and arrestins modulate these receptors is yet to be elucidated. GRK3 (originally referred to as β-adrenergic receptor kinase 2) and β-arrestin2 are highly enriched in olfactory receptor neurons, localised to the sites where odour transduction occurs in the dendritic knob and cilium. Incubating olfactory receptor neurons with antibodies that targeted GRK3 enhanced odour-induced increases of cAMP and mitigated desensitisation altogether (*324*). Upon odour stimulation, GRK3 has also been shown to translocate from the cytosol to the cell membrane, where it seemingly exerts its action (*325*). Moreover, olfactory cilia from mice lacking GRK3 do not desensitise following odour stimulation, and cAMP production is significantly reduced (*326*). These data collectively suggest that GRK3 and β-arrestin2 modulate the desensitisation of olfactory receptors. More recently however, the effects of GRK3 were assessed in human embryonic kidney (HEK293) cells and for the first time in intact olfactory receptor neurons using mOR-EG, a well characterised olfactory receptor sensitive to the odour eugenol (*327*). While over expression of GRK3 desensitised mOR-EG-expressing HEK293 cells, reducing both cAMP and in turn Ca^{2+} responses to eugenol, this did not alter adaptation kinetics. Additionally, when isolated olfactory receptor neurons derived from GRK3-deficient mice were presented with either an individual or double-pulse of eugenol, there were no differences when compared with wild type counterparts. This suggests that the impact of GRK3-mediated desensitisation of olfactory receptor neurons *in vivo* may be minimal, at least for shorter odour stimuli. However, inhibition of phosphatases, which counteract the action of protein kinases, was shown to enhance short-term adaptation in olfactory receptor neurons, evidenced by a more pronounced reduction in response amplitude to the second pulse in paired-pulse odour stimulation (*328*).

Besides detaching the G-protein from the olfactory receptor, the recruitment of arrestins, following agonist binding, initiates signalling pathways that direct olfactory receptors towards clathrin-coated pits for internalisation (Figure 1.12) (*319*). Clathrin is the major protein involved in vesicle formation for trafficking receptors from the

membrane to the endosome (for review, see (*329*, *330*)). This internalisation occurs over minutes and involves the temporary sequestration of receptors (*331*, *332*). Following odour stimulation, clathrin-mediated endocytosis of olfactory receptors has been demonstrated in olfactory receptor neurons from the channel catfish (*333*). Activated olfactory receptors can also interact with β-arrestin to undergo clathrin-dependent endocytosis, with inhibition of β-arrestin2 halting desensitisation and odour adaptation in olfactory receptor neurons (*334*).

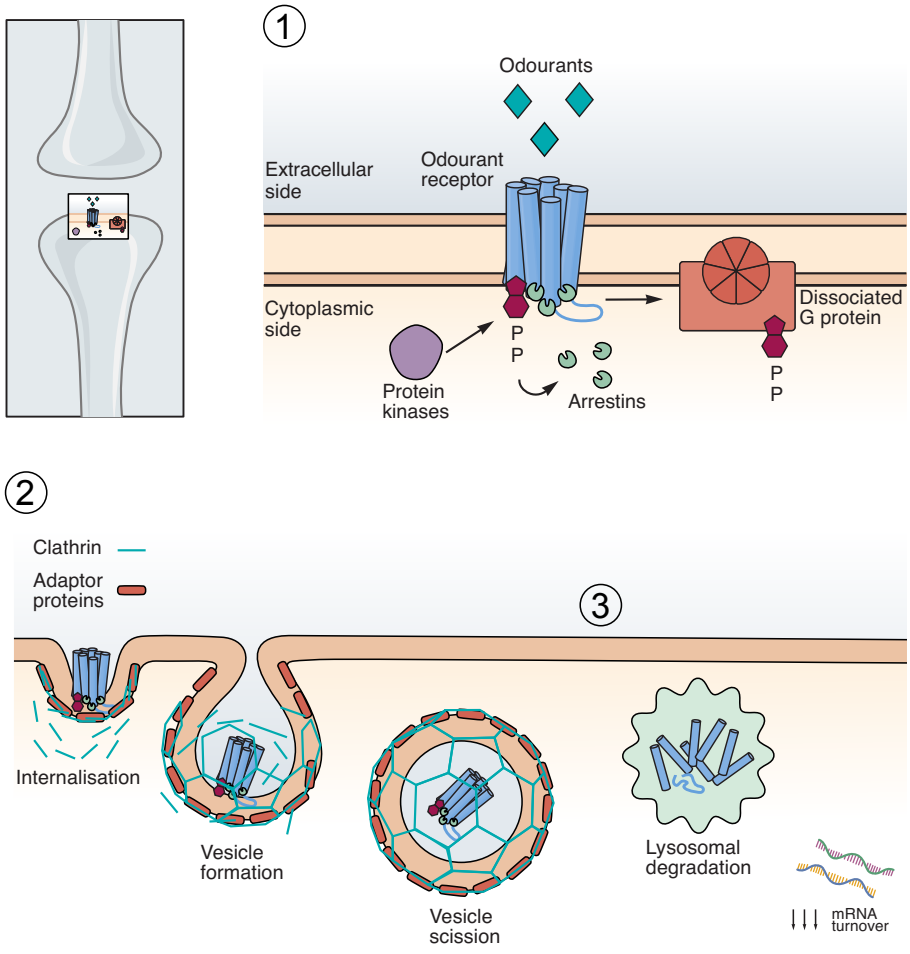

Figure 1.12: Olfactory Receptor Desensitisation

After prolonged odour exposure, olfactory receptors undergo three distinct stages of desensitisation: 1) Various classes of protein kinases either directly or indirectly phosphorylate the olfactory receptor, dissociating it from the G-protein and preventing odour transduction. This triggers the recruitment of arrestins, cytosolic proteins that bind to the receptor and change its conformation, rendering it

nonfunctional. 2) Clathrin, a protein essential for endocytosis, is recruited along with adaptor proteins to the receptor, forming clathrin-coated pits that induce membrane invagination. Clathrin proteins assemble into a lattice-like structure that surrounds the invaginated portion of the membrane, ultimately forming a vesicle that detaches from the membrane and temporarily sequesters the receptor. 3) Internalised receptors may be trafficked to lysosomes for degradation over longer timescales. Additionally, prolonged receptor activation can trigger signalling pathways that reduce receptor expression by downregulating the transcription of their mRNA, contributing to long-term receptor desentisation. Figure created with permission using elements sourced from Kandel *et al.* (*9*).

Receptor downregulation repesents the slowest form of GPCR desensitisation, occurring over several minutes to hours or even days. While internalisation transpires over shorter timescales, prolonged agonist exposure leads to the trafficking of receptors to lysozomes for degradation. This downregulation is also associated with reduced transcripts for receptor mRNA, which in turn decreases receptor expression at the plasma membrane (Figure 1.12) (*331*, *335*). In mice, it was found that 30 min odour exposure was sufficient to reduce mRNA transcript levels of responsive olfactory receptors *in vivo* (*258*). This receptor downregulation was enhanced by increasing odour concentration, with the most substantial decreases occurring after 2-24 hours of sustained stimulation. Remarkably, mRNA levels returned to normal after 12-48 hours once the stimulus was removed. These changes in mRNA levels have more recently been attributed to the downregulation of transcription, rather than degradation of existing mRNA molecules (*336*). This reflects a long-term regulatory mechanism, distinct from receptor internalisation, which impacts receptor availability at the cell surface. Together, these data indicate that the receptor abundance is highly dynamic, responding to the environment in a manner that adjusts receptor availability and sensitivity.

1.3.3 Adaptation of the Transduction Machinery

When exposed to an odour for a prolonged period, olfactory receptor neurons generate receptor currents that initially rise to a peak and thereafter decline, often falling to or near baseline levels even before odour cessation. Historically however,

olfactory adaptation has largely been studied using a paired-pulse approach, revealing that the amplitude of the second pulse is incrementally diminished as the time between pulses is reduced. What mechanisms could underlie such response adaptation?

A key determinant in olfactory receptor neuron adaptation is calcium (Ca^{2+}) influx via the cyclic nucleotide gated (CNG) channel. In the presence of calmodulin (CaM), an abundant ciliary protein that pre-associates with the CNG channel at rest (*337*), Ca^{2+} lowers the CNG channel's affinity for cyclic adenosine monophosphate (cAMP) up to 20-fold (Figure 1.13) (*337*, *338*).

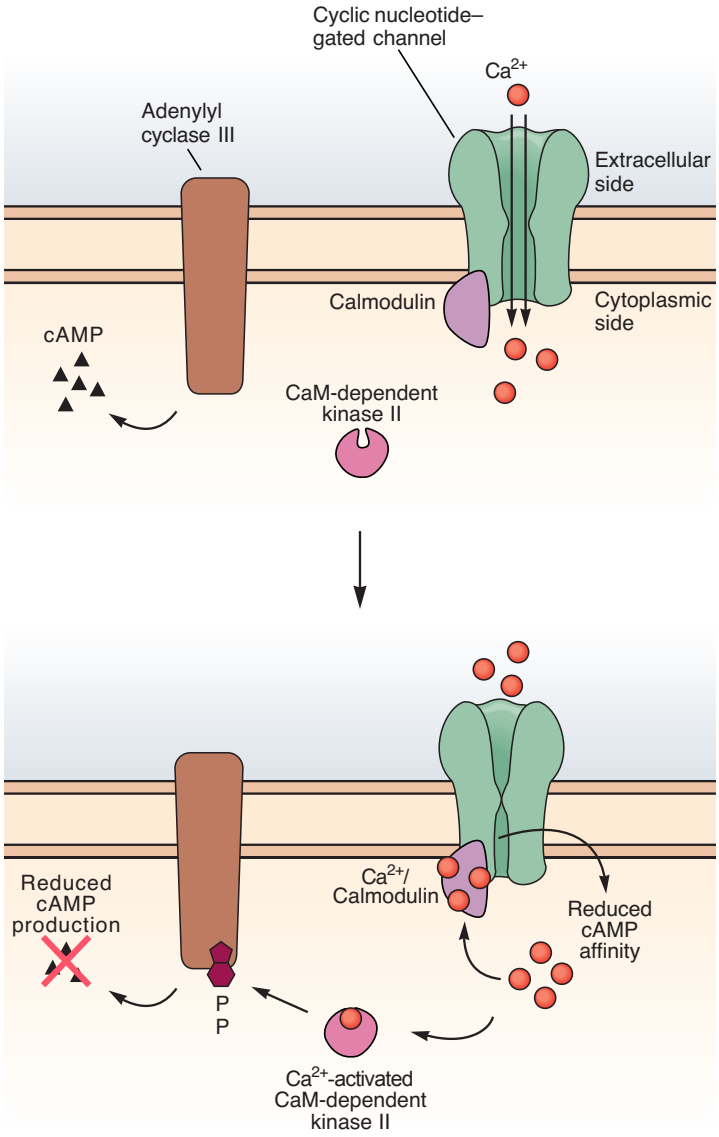

Figure 1.13: Mechanisms of Ca^{2+}-Mediated Adaptation in Olfactory Receptor Neurons

(Top) Upon binding of an odourant, stimulated adenylyl cyclase 3 (ACIII) generates cyclic adenosine monophosphate (cAMP). This triggers the opening of the cyclic nucleotide-gated (CNG) channel, allowing Ca^{2+} influx. (Bottom) The accumulation of intracellular Ca^{2+} contributes to adaptation through two primary mechanisms: 1) Forming a complex with calmodulin (CaM), which reduces the CNG channel's affinity for cAMP and ultimately leads to its closure. 2) Activating CaM-dependent kinase II (CaMKII), which phosphorylates ACIII and thereby down regulates cAMP production. Figure created with permission using elements sourced from Kandel *et al.* (*9*).

Moreover, paired-pulse experiments whereby extracellular Ca^{2+} was chelated or neurons were positively clamped during whole-cell recordings dramatically impeded the adaptive current decline (*339-341*). The CNG channel is a heterotetramer, composed of two CNGA2 subunits, and a single CNGA4 and CNGB1b subunit (*342-344*). Whilst CNGA2 (*345*), CNGA4 (*346*), and CNGB1b (*347-349*) subunits all house CaM-binding domains, deletion of the CaM-binding domain exclusively in either the A4 or B1b subunits was sufficient to eliminate Ca^{2+}/CaM sensitivity in heterologously expressed CNG channels altogether (*346*). Building on this, a mouse line was generated that lacked the CaM-binding domain of the B1b subunit, which interacts with CaM via an IQ-motif (*350*). Despite impeding CNG channel desensitisation ~100 fold, paired-pulse stimulation resulted in suppression of the second stimulus as seen in wild type mice, indicating that Ca^{2+}/CaM-mediated desensitisation of the CNG channel is not the sole adapting determinant. This approach did however slow the decline of the receptor current and prolonged responses by ~60 ms, most notably with longer stimuli, potentially arising from additional Ca^{2+} influx as a consequence of CNG channel desensitisation.

Another component of the olfactory transduction machinery seemingly subject to Ca^{2+}-mediated feedback and is thus implicated in adaptation is adenylyl cyclase 3 (ACIII). The influx of ciliary Ca^{2+} via CNG channels is thought to activate CaM-dependent kinase II (CaMKII), which indirectly down regulates cAMP production by phosphorylating ACIII (Figure 1.13). This theory largely stems from experiments where

CaMKII inhibitors were applied to human embryonic kidney 293 cells expressing ACIII (*351*, *352*), as well as to isolated olfactory cilia and olfactory receptor neurons (*353*, *354*). When exposed to a sustained odour stimulus, disrupting CaMKII dramatically delayed the onset of and recovery from adaptation in intact olfactory receptor neurons by three- and sixfold, respectively; however these effects did not extend to brief (100 ms) odour pulses (*354*). The inhibition mediated by Ca^{2+}/CAMKII has been attributed to the phosphorylation of ACIII at a single serine residue, serine^{1076} (*352*, *353*). Yet, in mice which were genetically engineered to harbour a mutation of serine^{1076} to alanine, olfactory receptor neuron response kinetics were not dissimilar to wild-type counterparts (*355*). Thus, despite being positioned as prime candidates, neither the phosphorylation of ACIII at serine^{1076} nor Ca^{2+}/CaM-mediated desensitisation of the CNG channel via the IQ-binding site fully accounts for odour adaptation, at least when investigated in isolation.

1.3.4 Response Termination

To preserve olfactory receptor neuron sensitivity, odour responses must be efficiently terminated prior to the subsequent stimulus. Termination of the odour response relies on intraciliary cAMP and Ca^{2+} returning to baseline levels, enabling the closure of CNG channels (directly opened by cAMP) and Ca^{2+}-activated Cl^- channels. Theoretically, the kinetics of response termination should thus be dictated by whichever occurs last: either the removal of cAMP or the removal of Ca^{2+} from the cilium.

In olfactory receptor neurons, cAMP is hydrolysed by phosphodiesterases (PDEs), of which two are currently known: PDE1C, which is localised to the cilium, and PDE4A, which is found throughout the olfactory receptor neuron excluding the cilia (*356-358*). Following odour stimulation, the ciliary cAMP produced by adenlyl cyclase 3 (ACIII) could be degraded on-site by PDE1C or by PDE4A after diffusing into the dendrite (Figure 1.14). While the specifics of cAMP dynamics within the cilia remain unclear, independently knocking out PDE1C or PDE4A does not delay response termination in olfactory receptor neurons (*359*), implying that either PDE1C or PDE4A

alone are sufficient to rapidly clear cAMP. Interestingly however, disrupting the *Pde1c* gene, but not the *Pde4A* gene, resulted in reduced response amplitudes and slower response decays when compared with wild type olfactory receptor neruons, most likely due to PDE1C's proximity to cAMP production within the cilium (*359*). Furthermore, short-term adaptation, which refers to a neurons ability to rapidly recover its sensitivity after being exposed to repetitive stimuli, was unaffected by application of the broad-spectrum PDE inhibitor IBMX, as well as by the direct stimulation of the transduction cascade using caged-cAMP (*341*). In contrast, IBMX application was shown to prolong response decays and significantly reduce the response amplitude to the second pulse in paired-pulse odour stimulation (*328*). The simple diffusion of cAMP from the cilia to the cell body (where PDE4A exerts its action) is thought to partially account for intraciliary cAMP reduction (*341*, *360*, *361*), further supported by the finding that the concomitant disruption of both PDE1C and PDE4A do indeed impede response termination (*359*). Nevertheless, these data together suggest that cAMP degradation within cilia is not a rate-limiting factor for response termination.

A growing body of literature indicates that it is in fact the rate of Ca^{2+} removal from the cilium which largely determines the rate of response termination. Since olfactory cilia do not house vesicular organelles (*362*), Ca^{2+} expulsion has long been thought to occur through the action of Ca^{2+} transporters within the membrane, such as Na^{+}/Ca^{2+} exchangers and adenosine triphosphate-fuelled Ca^{2+} pumps (*363*, *364*). Indeed, preventing intraciliary Ca^{2+} clearance by reducing extracellular Na^{+} (thereby eliminating the gradient necessary for Na^{+}/Ca^{2+} exchange) extends odour-induced receptor currents and reduces the amplitude of the second pulse in double-stimulation paradigms to a greater extent than in wild-type olfactory receptor neurons, due to a sustained Ca^{2+}-activated chloride (Cl^{-}) current (*365*, *366*). Numerous Na^{+}/Ca^{2+} exchangers have been identified in olfactory receptor neurons (*363*, *367*), however one such potassium-dependent Na^{+}/Ca^{2+} exchanger, NCKX4, has been identified as critical for response termination and adaptation kinetics (*368*). Mouse olfactory receptor neurons lacking NCKX4 exhibit dramatically prolonged odour responses, and in double-stimulation protocols, the amplitude of the second pulse is severely diminished.

These findings are akin to what is observed in wild-type olfactory receptor neurons bathed in low extracellular Na^+ solutions (*365*, *366*), further presenting Ca^{2+} extrusion as the rate-limiting factor for response termination. Moreover, when NCKX4-deficient olfactory receptor neurons were bathed in a Na^+-free solution, odour responses were only marginally extended further (*368*), reinforcing the idea that NCKX4 is the dominant Na^+/Ca^{2+} exchanger in olfactory receptor neurons (Figure 1.14). Interestingly, response amplitudes following a single odour pulse are not affected in NCKX4-knockout olfactory receptor neurons, suggesting that the simple diffusion of Ca^{2+} from the cilium to the dendrite adequately maintains low intraciliary Ca^{2+} at rest. Response amplitudes following successive odour pulses (and the consequent inability to generate action potentials) were more severe in olfactory receptor neurons lacking NCKX4 than in those harbouring CNG channels which cannot bind CaM (*350*), highlighting the significance of NCKX4 in Ca^{2+} clearance.

Disentangling the mechanisms that facilitate response termination from those that underlie adaptation is complicated by the fact that both phenomena appear to be inseparable. For example, in paired-pulse experiments, the attenuation observed to the second pulse could stem from either delayed termination or altered sensitivity. The olfactory system's ability to rapidly initiate and terminate neuronal responses is critical for perceiving odours that arrive within bursts of inhalation. However, it has yet to be determined whether these mechanisms adapt to the respiration cycle or are simply constrained by it (see (*369*) for a more in depth review).

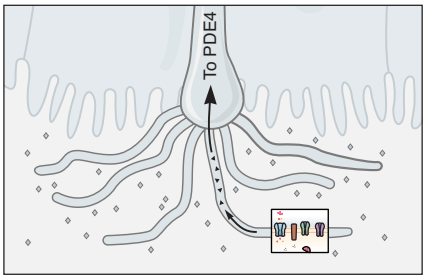

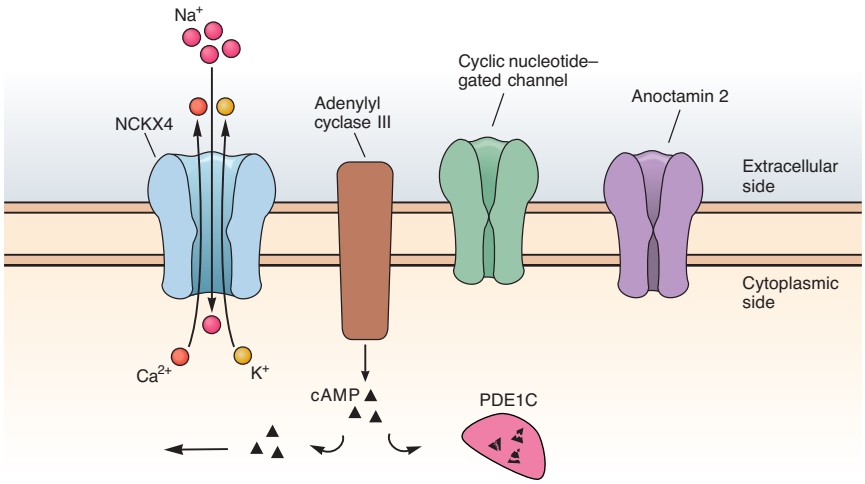

Figure 1.14: Proposed Mechanisms of Response Termination in Olfactory Receptor Neurons

Termination of the odour-evoked response is believed to depend on cAMP breakdown and Ca^{2+} extrusion. Phosphodiesterases PDE1C and PDE4A are thought to hydrolyse cAMP within the cilium and in the dendrite, respectively. The potassium-dependent Na^{+}/Ca^{2+} exchanger NCKX4 is speculated to play a key role in removing Ca^{2+} from the cell. Combined, these mechanisms promote the closure of the cyclic nucleotide gated channel and the Ca^{2+}-gated Cl^{-} channel, Anoctamin 2, thus terminating the transduction current. Figure created with permission using elements sourced from Kandel *et al.* (*9*).

1.3.5 Stimulus-Induced Depression

The concentration and frequency at which a given odourant is presented crucially dictates the speed and rate of action potential generation in olfactory receptor neurons. Depression, characterised by a decrease in the efficacy of neuron-to-neuron communication, represents a distinct form of adaptation. This phenomenon is often triggered by either strong or sustained stimulation and culminates in diminished responsiveness to subsequent stimuli.

As odour concentration rises, response latencies are shortened and firing rates increase. Responses can be initiated as rapid as ~30 ms and isolated olfactory receptor neurons can reach firing rates as high as 200 Hz when saturated**.** Generally, olfactory receptor neurons have a narrow dynamic range, often saturating within 2 log units of odourant concentration above threshold (*365*, *370*). The relationship between odour concentration and action potential firing is not monotonic, with spiking rates increasing up to intermediate concentrations and declining at higher concentrations often to only a few action potentials or failing to respond altogether. In such instances, action potentials are restricted to the stimulus onset during the rising phase of the receptor current (*89*, *365*, *370-373*). Despite often persisting substantially longer, receptor currents induced by higher odour concentrations fail to generate any further action potentials while the current is still active (Figure 1.15) (*374*). Thus, whilst an odour could still be present in an animals environment, neurons which experience such high receptor currents would not transmit odour signals to the brain. Compression of

the spike train is a consequence of progressively diminished action potential amplitudes, likely stemming from the inactivation of voltage-gated Na^+ channels following sustained depolarisation (*355*, *375*, *376*).

The ability of an olfactory receptor neuron to fire action potentials to repeated stimuli is contingent upon termination of the receptor current and sufficient membrane hyperpolarisation. Traditionally, varying the time between presentations of odour stimuli has been used to simulate the turbulent nature of plumes in natural environments and/or the periodicity introduced by breathing. Such experiments have revealed that olfactory receptor neuron response amplitudes are attenuated at inter-stimulus intervals ranging between 6-10 s (*377-379*). At lower stimulation frequencies which resemble normal breathing (2 Hz, with 400 ms between pulses), olfactory receptor neurons reliably fire action potentials when odour stimuli are presented at moderate concentrations. However, at higher stimulation frequencies more analogous to active sniffing (5Hz, with 100 ms between pulses), action potentials are sporadic (*380*), owing to the receptor current's inability to fall to baseline levels prior to the subsequent stimulus. Furthermore, when stimulated repeatedly with high odourant concentrations, olfactory receptor neurons fail to respond altogether. Accordingly, olfactory receptor neuron activity was reportedly attenuated *in vivo* when either awake animals exhibited high sniffing rates (*287*, *381*) or anaesthetised animals were presented with high frequency odour stimuli that mimicked sniffing behaviour (*382*). However, depression measured at the glomerulus *in vivo* (*381*, *382*) are less pronounced than those reported *in vitro* (*378*, *383-385*). Together, these observations indicate that for fixed stimulation frequencies, it is primarily the olfactory receptor neurons that are only moderately activated by an odour that encode the entire stimulus, whereas the most sensitive neurons seemingly transmit only the onset of the odour signal. This implies that olfactory receptors themselves are a significant determinant in response kinetics. Yet, this area remains to be explored, as the majority of studies to date have been performed with randomly selected olfactory receptor neurons.

Depression in olfactory receptor neurons does not only arise from odourant binding at the periphery. Bypassing peripheral-mediated adaptation by directly

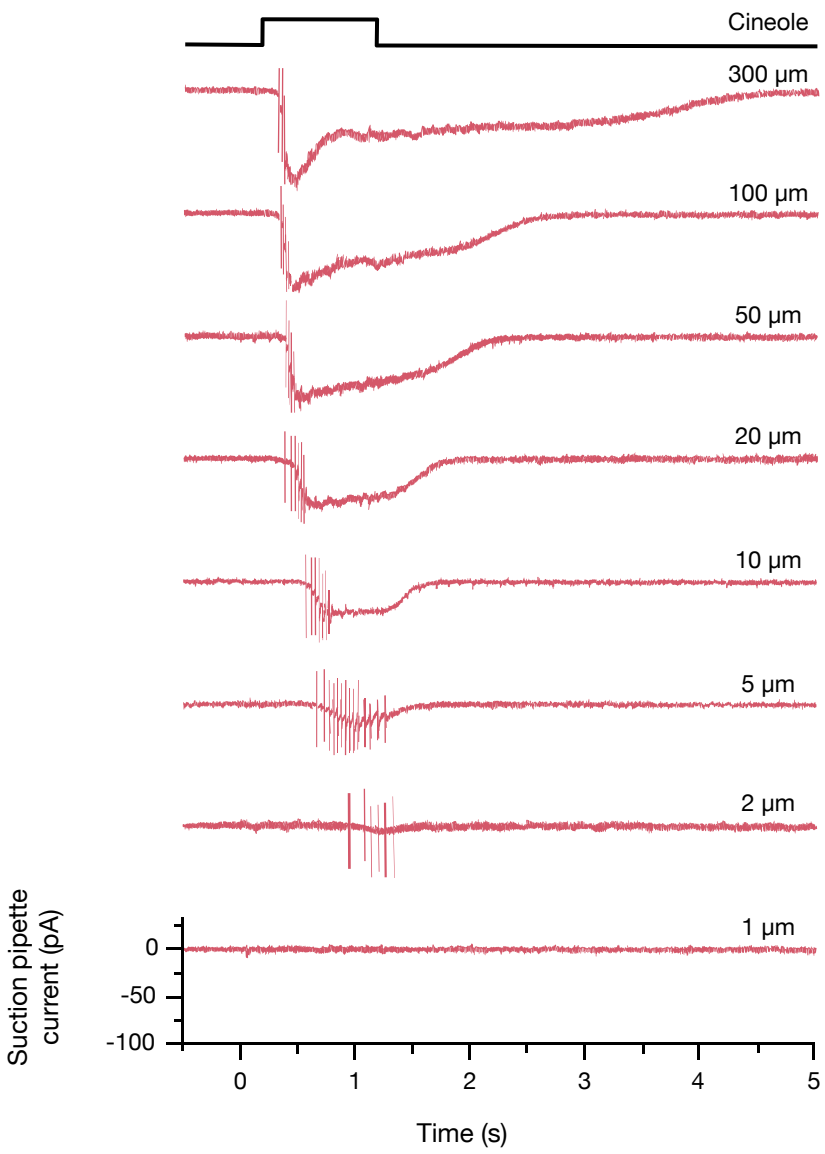

Figure 1.15: Stimulus-Induced Depression in an Olfactory Receptor Neuron

Based on suction pipette recordings from an isolated olfactory receptor neuron, stimulated by a 1 s pulse of cineole at various concentrations. Response latency in olfactory receptor neurons decreases as odour concentration increases. However, firing rates increase only up until moderate concentrations and decline at higher concentrations, despite larger receptor currents being generated. Figure recreated from real data with permission from Reisert and Matthews (*374*).

stimulating the olfactory nerve has also been shown to modulate glutamate release onto mitral/tufed cells both *in vitro* (*133*, *137*) and *in vivo* (*386*). In line with this, paired-pulse electrical stimulation was shown to reduce Ca^{2+} influx *in vitro* and consequent

gluatamate release *in vivo*, the effects of which were recovered when inter-stimulus intervals were extended to longer than 1 s (*134*, *385*, *387*). Simultaneous recordings from both olfactory receptor neurons and mitral/tufted cells revealed that this adaptation originates from olfactory receptor neuron terminals, as the effects of paired-pulse depression are fed-forward to mitral/tufted cells (*90*). Comparably, in *Drosophilia*, strong electrical stimulation of olfactory receptor neurons induced depression and consequently reduced excitation of projection neurons, the invertebrate homolog of mitral/tufted cells (*388*). These adaptive mechanisms, functioning at both the central and peripheral levels, introduce an additional layer of sophistication, enhancing the olfactory system's ability to modulate odour perception in an ever-changing environment.

1.4 Olfactory Learning

1.4.1 Overview

Successfully navigating complex olfactory environments is essential for survival-based behaviours such as foraging and predator evasion, and relies heavily on the olfactory system's remarkable capacity to adapt and learn. Animals assign value to behaviourally-relevant odours through experience by forming associations with seemingly disparate stimuli, thus shaping their physiological responses and perception. In response to these odours, olfactory receptor neurons dynamically adjust their transcriptomes and gene expression, undergo rapid synaptic turnover, and alter their survival rates to effectively capture prominent features of the odour landscape. The underlying mechanisms of these adaptive processes are multifaceted, and additional modifications—such as changes at pre- and post-synaptic sites and alterations in neuronal excitability—are observed under conditions of sensory deprivation. Additionally, the olfactory bulb is remarkably plastic and, along with the dentate gyrus of the hippocampus, is one of only two regions in the adult nervous system that continuously integrate newly generated neurons (*146*). These newborn neurons mature into granule cells or periglomerular cells, and learning enhances their incorporation into

the bulbar circuitry. This section explores the behavioural outcomes and underlying mechanisms that facilitate various forms of olfactory learning.

1.4.2 Passive Experience

Passive experience encompasses forms of odour exposure that do not involve reinforcement or consequences that could influence learning outcomes, such as enrichment by altering the odour environment, or perceptual learning through discriminating between perceptually similar odours. A common method of odour enrichinment involves placing tea balls filled with either odourised cotton swabs or filter paper in the animal's home cage. Research shows that exposing animals to two perceptually similar monomolecular odourants for 1-2 hrs daily over a period of 10-20 days enhances their ability to differentiate these odourants, both individually and when combined (*389-392*). Notably, this enhanced discriminability applied only to odourants that evoked at least partially overlapping patterns of glomerular activity in the olfactory bulb. Furthermore, inducing widespread activity throughout the olfactory bulb with local injections of NMDA replicated these performance gains. Conversely, blocking NMDA receptors prevents odour exposure from exerting the same effect (*390*). Thus, increased sensory input enhances the olfactory systems ability to distinguish between experienced odours, in both animals and humans alike (*393*, *394*). This raises the question: What structural and functional changes underpin these improvements?

Olfactory Learning Glossary

Passive Experience: Exposure to sensory stimuli without any associated reinforcement or consequences that could affect learning outcomes.

Odour enrichment: A form of passive experience, involving the enhancement of an environment (typically the home environment) with one or multiple odours.

Perceptual Learning: The process by which sensory perception is refined and improved through passive experience, enhancing the ability to distinguish between perceptually similar stimuli.

Associative Learning: A form of conditioning in which an animal learns to connect a previously neutral stimulus with a significant stimulus/ event, resulting in changes in behaviour.

Classical Conditioning: A learning process that occurs when two stimuli are repeatedly paired; a response that is at first elicited by the second stimulus (e.g. reward or punishment) is eventually elicited by the first stimulus alone.

Operant Conditioning: A method of associative learning that employs rewards and punishments for behaviour, encouraging the animal to associate certain behaviours with consequences.

1.4.2.1 Changes at the Periphery

Olfactory receptor neurons are highly dynamic, with more than 20 % of the population undergoing activity-dependent synaptic turnover within 3 hours (Figure 1.16) (*395*). Single-cell RNA sequencing has revealed that each of the ~1,000 olfactory receptor neurons possess a unique transcriptome that dynamically responds to the sensory environment within hours of odour exposure (*336*, *396*). Groundbreaking research by Tsukahara *et al.* (*396*) has shown that expression levels of more than 70 genes—including those coding for voltage-gated ion channels, calcium-binding proteins, and secondary-messenger molecules—dynamically adjust within hours of exposure to new odour environments. These bidirectional changes, which either amplify or attenuate odour responses, correlate with the degree of transcriptional change, thereby predicting the extent to which olfactory receptor neuron responses will be modulated (*396*). Additionally, receptor mRNA levels are also modulated in an activity-dependent manner (*336*). Thus, odour perception is constrained by previous experience. Additionally, prolonged odour enrichment resulted in larger responses amplitudes in the olfactory epithelium for the exposed odour in mice (*397*, *398*). Conversely, brief odour exposures over several days did not alter olfactory receptor neuron responses, indicating stability under short-term exposure conditions (*399*). While odour perception is influenced by previous experiences at the level of olfactory receptor neurons, it is further refined in the olfactory bulb before being relayed to higher brain regions.

1.4.2.2 Modulation of Olfactory Bulb Output

Unlike olfactory receptor neurons, brief daily exposure to odours—as little as 20 min—over several days has been shown to result in more sparse and diminished responses from mitral/tufted cells in rodents (*399-403*). These effects were specific to the odours used and gradually reversed over months once exposure ceased (*399*). Strikingly, when mice were passively exposed to perceptually similar odours, the responses from mitral/tufted cell ensembles diverged. In contrast, exposure to perceptually distinct odours caused these cells' response patterns to become more

similar (*402*). Rather than a reduction in the responsive fraction, it was found that affected neurons switched from excitatory to inhibitory response profiles, or vice versa (*403*). This suggests that experience shapes olfactory representations, optimising reliability and reducing redundancy based on the similarity of ambient odours. Additionally, in flies, chronic odour exposure enhanced the sensitivity of projection neurons, though this effect occurred only when the odour was presented at low concentrations, indicating that the direction of change may be influenced by odour concentration (*404*).

1.4.2.3 A Role for Inhibition

Mounting evidence suggests that the activity of mitral/tufted cells is shaped by inhibition, which reorganises their output patterns. Optogenetic stimulation of GABAergic granule cells enhances the distinctiveness of mitral/tufted cell activity patterns elicited by similar odours. Crucially, this enhanced pattern separation improved animals' ability to discriminate between these odours. On the other hand, suppressing granule cell activity has been found to reduce pattern separation and impair performance in odour discrimination tasks (*405*). These findings align with earlier reports that genetic modification to increase or decrease granule cell activity can either improve or impair odour discriminability in mice, respectively (*406*). Additionally, pharmacological blockade of the adrenergic system, which densely innervates the granule cell layer, not only reduced the number of newborn granule cells but also hindered discriminability (*407*).

Dendritic spines on granule cells, crucial sites for synaptic signalling, are highly dynamic and exhibit significant plasticity. This constant remodelling and turnover reflect their integral role in learning and memory processes (*408*). Exposure to odours over 10 days stabilises synaptic turnover in granule cells, increases spine density, cell survival, and granule cell responsiveness to the learned odours (*392*, *409-411*). Functional changes in granule cells correlate with improved discriminability, with more difficult discrimination tasks having a more pronounced effect on increasing spine density (*392*, *411*).

Evidence also indicates that perglomerular cells—the other major type of inhibitory neuron in the olfactory bulb—play a role in remodelling the olfactory bulb following odour exposure. Constant exposure to odours during early development enhances the selectively of adult-born periglomerular cells for these specific odours. Whereas established periglomerular cells exhibited a mix of excitatory and inhibitory responses, adult-born periglomerular cells exhibited only excitatory responses to the experienced odours (*412*). Synaptic turnover was also reportedly stabilised in mature adult-born neurons (which could constitute both granule and periglomerular cells) following 10 days of odour exposure (*409*). Thus, the inhibitory network of neurons is highly dynamic and seemingly shapes olfactory bulb output following odour exposure, thereby supporting future perception (Figure 1.16).

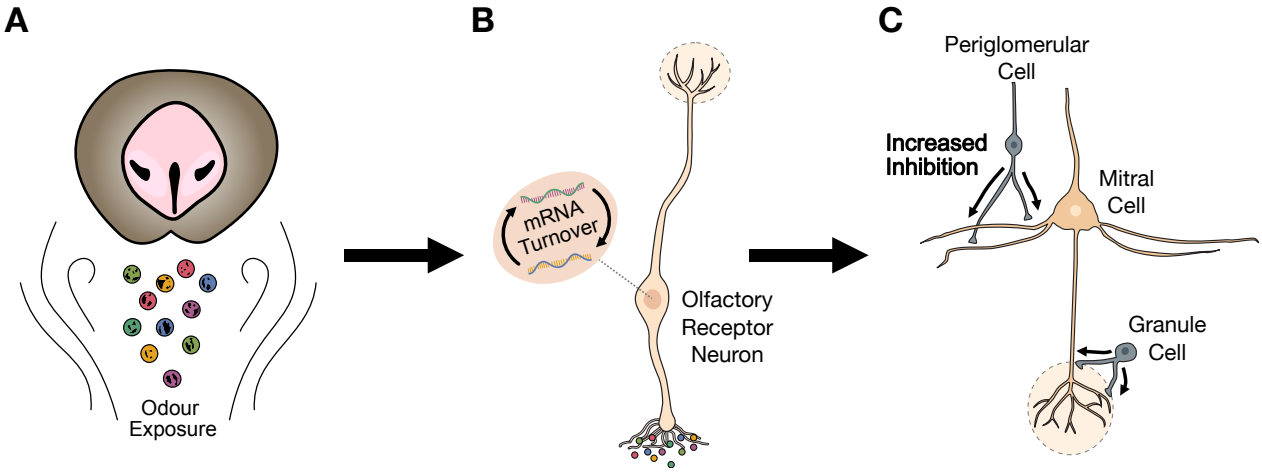

Figure 1.16: Odour Exposure-Induced Plasticity

(A) Prolonged odour exposure triggers multiple forms of plasticity in the early olfactory system. B) At the periphery, olfactory receptor neurons can rapidly remodel their synapses, modulate receptor mRNA levels and alter the expression of numerous genes directly involved in odour transduction. C) Cell survival is increased and synaptic turnover is stabilised in inhibitory granule cells and periglomerular cells, which enhances learning by shaping output from mitral/tufted cells. Figure created using elements sourced from Kandel *et al.* (*9*).

1.4.2.4 Bulbar Dynamics During Sensory Deprivation

Experiments involving sensory deprivation, such as naris occlusion (typically achieved by inserting a small plug into the nostril), have provided valuable insights into olfactory bulb dynamics. Occluding the nostril for a few weeks was found to increase the probability of glutamate release from olfactory receptor neurons onto external tufted and periglomerular cells (*413*). This also increased the amplitude of AMPA- and NMDA-type miniature excitatory postynaptic currents (mEPSCs), likely due to the upregulation of these receptors in the glomerular layer. Consistent with these findings, a longer period of nostril occlusion (3 weeks) has been shown to reduce the activity-dependent turnover of olfactory receptor neurons by 3.5 fold (*395*). This reduced turnover may contribute to the sustained increase in glutamatergic signalling by maintaining and potentially strengthening existing synaptic connections. Additionally, naris occlusion lasting between 20 days to 2 months increases the number of odour-responsive mitral/tufted cells (*414*, *415*), the effects of which were mimicked by blocking dopamine D2 receptors (*415*).

These changes in excitatory neurons are mirrored by alterations in inhibitory circuits. Sensory deprivation via olfactory receptor neuron ablation was shown to decrease the amplitude of spontaneous inhibitory postsynaptic currents (IPSCs) in external tufted cells (*416*). This reduction was accompanied by fewer GAD67-positive synapses surrounding these cells; GAD67 is a critical enzyme involved in GABA synthesis, and its reduction suggests diminished GABA production at inhibitory synapses. Naris occlusion has also been shown to reduce the number of dopaminergic neurons neurons, with a 22 % decrease observed within 7 days (*417*), increasing to ~40 % by 4 weeks (*417*, *418*). Furthermore, the density of presynaptic terminals formed by these neurons declines, suggesting that synaptogenesis in the remaining dopaminergic neurons is not upregulated to compensate for this loss (*417*). Even briefly plugging a nostril for a day can structurally alter the axon initial segment in dopaminergic short axon cells in the glomerular layer (*419*). Since the axon initial segment is crucial for action potential generation (*420*, *421*), this shortening reduces

the intrinsic excitability of these neurons (*419*), likely diminishing both neurotransmitter release from olfactory receptor neurons and inhibitory drive onto mitral/tufted cells (*142-144*). After 3 weeks of naris occlusion, the density of granule cell synapses decreases in the internal plexiform layer but remains unaffected in the external plexiform layer. However, synapse density returns to control levels following 6 weeks of plug removal (*422*). Prolonged naris occlusion also affects newborn neurons, preventing the expansion of inhibitory sensory maps, which normally occurs via the integration of these granule cells (*423*). Additionally, it remodels both the input and output synapses on these newborn neurons (*424*). Together, these findings underscore the influence of sensory input on regulating olfactory system plasticity and functional architecture, emphasising the dynamic regulation of both excitatory and inhibitory synapses in response to sensory deprivation.

1.4.3 Associative Learning

Associative learning allows the brain to assign predictive value to sensory inputs and modify behaviour accordingly—a crucial process for survival. This process falls under two main categories: classical (Pavlovian) conditioning and operant conditioning (Figure 1.17). In classical conditioning, an animal learns to connect two seemingly disparate stimuli, such as pairing an odour with either a positive stimulus like a food reward or a negative stimulus like a mild electric shock. On the other hand, operant conditioning involves forming an association between a stimulus and the animal's own behaviour. This method typically requires extensive training, where animals learn to discriminate between odours and receive rewards for correct choices. While all associative in nature, research indicates that the specific way in which associations are formed leads to distinct changes within the early olfactory system.

1.4.3.1 Reward-Based Classical Conditioning

Some of the earliest research into the effects of associative learning on the olfactory system was conducted with neonatal rat pups, involving the pairing of an odour stimulus with tactile stimulation (stroking). These studies exposed rat pups to an

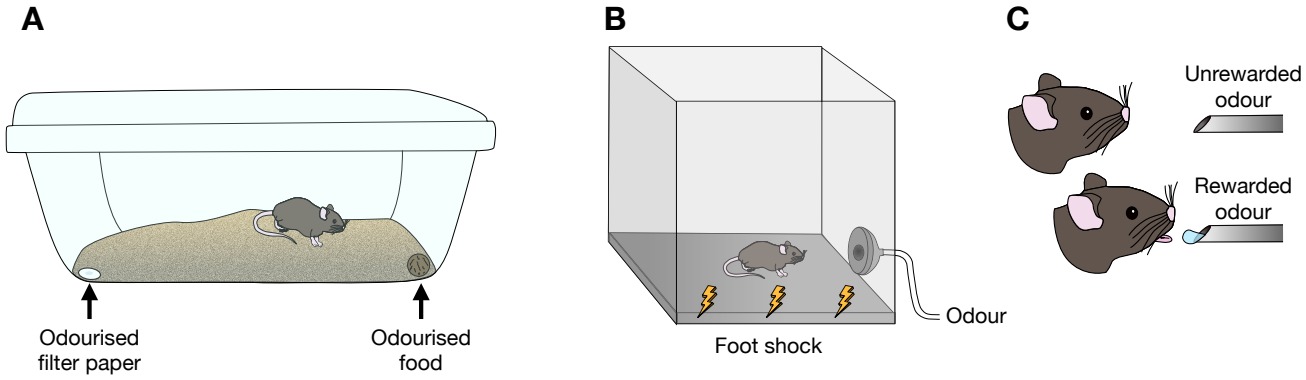

Figure 1.17: Olfactory Associative Learning Paradigms

A) Reward-based classical conditioning. Food-deprived animals are placed in a cage with two buried odours. Each odour is typically introduced in separate sessions, one of which is consistently paired with a food reward. Through repeated trials, animals are trained to identify and dig at the location of the rewarded odour. B) Fear-based classical conditioning. Animals are placed in an enclosure with an electrified metal plate and exposed to specific odours that are simultaneously paired with a foot shock. In this setup, animals learn to associate the odours with an aversive experience. C) Operant conditioning. Water-deprived animals are trained to distinguish between odours where only one is associated with a reward. Animals learn to perform a specific action (such as licking a sensor) in response to the rewarded odour to receive water.

odour while concurrently being stroked daily during the postnatal period. This pairing led the animals to develop a preference for the conditioned odour, as evidenced by their increased time spent associating with it compared to a non-conditioned alternative. Notably, this behavioural outcome was only observed when the odour was simultaneously presented with stroking; presenting the odour after the tactile stimulation had no effect (*425-427*).

In vivo single-unit recordings revealed that mitral/tufted cells exhibited more inhibitory and less excitatory responses specifically to the conditioned odour (*425*, *426*). Further studies demonstrated that blocking adrenergic receptors or creating bilateral lesions in the locus coeruleus—the primary source of noradrenergic innervation to the olfactory bulb—prevented the acquisition of this learning (*428*, *429*). Additionally, presenting an odour while either activating noradrenergic receptors locally

within the olfactory bulb or pharmacologically stimulating the locus coeruleus elicited conditioned behaviour (*430*). Similarly, octopamine—the insect homologue of noradrenaline—is reportedly essential for reward-based learning in flies (*431*). These findings suggest that noradrenergic signalling is a critical component of associative learning when an odour is paired with a positive stimulus.

Another approach in associative learning paradigms involves burying an odour and measuring an animal's digging time. Typically, odours are hidden beneath bedding material, and food-restricted rodents undergo multiple training sessions in which they are exposed to either a rewarded and or non-rewarded odour separately. Ultimately, animals are simultaneously exposed to both odours without any rewards, and learning is inferred if they dig significantly more at the site of the conditioned odour. Initially developed by Shellinck *et al.* (*432*), this method has been foundational in numerous subsequent studies (*433-436*). Pairing a reward with an odour has been shown to enhance discriminability between perceptually similar odours. For instance, naïve rats initially unable to distinguish between enantiomers of limonene and terpinen-4-ol can do so effectively when one is paired with a reward (*433*, *437*).

A notable variable in this method is how animals are trained to dig, with some researchers progressively burying the sugar reward deeper to encourage more vigorous digging behaviour in successive trials. This raises a question: does this method of reinforcement qualify as learned behaviour? If so, could this task then be considered operant in nature? While the underlying mechanisms supporting non-operant forms of associative learning remain less understood, it has been demonstrated that, unlike operant conditioning, it occurs independently of neurogenesis (*436*).

1.4.3.2 Fear-Based Classical Conditioning

Pairing an odour with an aversive stimulus like an electric shock typically triggers a conditioned fear response in animals, often manifesting as behaviours such as freezing or an increased startle response upon subsequent encounters with the odour. Alongside these behavioural changes, neuroanatomical changes also occur. For

example, when the odour acetophenone—known to activate the M71 odourant receptor (*34*)—is used in fear conditioning, it not only intensifies the startle response but also leads to the enlargement of the M71 glomerulus (*438*). Accordingly, conditioned freezing behaviour is accompanied by enhanced olfactory receptor neuron input solely for the conditioned odour, resulting in greater separation of glomerular activity patterns between the conditioned and unconditioned odour. This enhancement is not concentration-dependent, and the increase in amplitude from the fear response is comparable to that caused by a fourfold increase in odour concentration (*439*). Additionally, when a single glomerulus is stimulated optogenetically in conjunction with a foot shock, mice exhibit freezing behaviour in response to subsequent light stimulation. This behavioural response correlates with an increase in neurotransmitter release from olfactory receptor neurons and a decrease in $GABA_B$ receptor expression in the stimulated glomerulus (*440*).

Remarkably, the odour-fear association can be inherited. Mice whose parents were conditioned to fear an odour exhibited an increased startle response to the conditioned odour, despite having never encountered it. This heightened behavioural sensitivity, along with an increase in glomerulus size, was passed down two generations, likely through epigenetic mechanisms (*441*). Strikingly, the formation of an odour-evoked fear response and its associated structural changes can also be reversed through a process known as 'fear extinction'. Repeated exposure of fear-conditioned mice to the conditioned odour without the aversive stimulus not only abolishes the odour-elicited fear response but also reverses the increase in the number of olfactory receptor neurons that resulted from the initial fear conditioning (*442*).

1.4.3.3 Operant Conditioning

In typical operant conditioning paradigms, water-deprived mice are trained to identify a conditioned odour and receive a water reward for correct decisions (signalled by licking) during its presentation (Figure 1.17). Animals must make a decision within a short time window, which promotes rapid decision-making. This learning process requires extensive training, often involving hundreds of trials each day over several

days to effectively discriminate between odours. Given the demanding nature of this training, the brain adapts specifically to optimise task performance.

Mice trained with this method can distinguish between perceptually dissimilar odours in < 200 ms (*300-302*). However, distinguishing between more complex odour mixtures, which generate highly overlapping spatiotemporal patterns of glomerular activity, requires longer for effective discrimination. This type of learning has also been shown to improve odour detection thresholds, enabling mice to detect and discriminate between some odours as dilute as $1x10^{-5}$ % SV (*443*).

Associated with this improvement is a threefold increase in the number of responsive glomeruli on the dorsal surface of the olfactory bulb and enhanced response amplitudes. These changes were measured using intrinsic signal imaging, which indirectly represents the activity of olfactory receptor neurons (*443*). However, when Ca^{2+} activity in olfactory receptor neuron axon terminals was measured at the glomerulus, no changes were detected following an operant learning protocol. While this discrepancy could stem from differences in the task or imaging technique, it suggests that the improvements in discriminability originate downstream in the olfactory bulb network (*444*).

Indeed, using the same operant learning protocol, it was revealed that odour encoding efficiency in mitral/tufted cell ensembles is enhanced. When mice were tasked with discriminating between perceptually similar odours, mitral/tufted cell ensembles' representations were decorrelated. Conversely, the representations of perceptually distinct odours converged, becoming more alike. Although the same patterns of neural rearrangement were observed with simple odour exposure, operant learning notably accelerated these effects (*402*).

Data suggest that inhibition modulates olfactory bulb output to facilitate operant-based learning. Optogenetic stimulation or pharmacological silencing of GABAergic granule cells has been shown to enhance or decrease pattern separation in mitral/tufted cell ensembles, respectively; consequently, these interventions accelerate or impede an animal's ability to effectively distinguish odours (*405*). Additionally, this form of associative conditioning expands inhibitory sensory maps on the dorsal surface

of the olfactory bulb. Formed by newborn granule cells, these maps respond more robustly to both rewarded and unrewarded odours after learning (*423*). Accordingly, in mice trained to associate an odour with a reward through a behavioural task, there is an increased survival of newborn neurons in regions of the granule cell layer activated by the conditioned odour (*212*, *436*, *445-447*).

1.5 Aims

This research aims to investigate how animals reliably identify the same odour object despite variations in sensory input—a phenomenon known as perceptual constancy. Using mice as a model organism, we probed perception across a wide range of odour concentrations, combining behavioural testing, *in vivo* imaging, and learning paradigms to uncover the neural mechanisms supporting perceptual constancy.

Chapter 2: Methods

2.1 Animals

Animal handling and experimentation was carried out according to UK Home Office guidelines and the requirements of the United Kingdom (Scientific Procedures) Act 1986 and the University of Leeds animal welfare ethical review board. Mice were housed under a 12:12 hr light/dark cycle with free access to food and water. All efforts were made to minimise animal suffering and the number of animals used. OMP-Cre mice (B6;129P2(Cg)-Omp<tm4(cre)Mom>/MomTyagRbrc (RBRC02138)) and Pcdh21-nCre mice (C57BL/6Cr-Tg(Pcdh21-cre)BYoko (RBRC02189)) were crossed with floxed GCaMP6f mice (GCaMP6f.flox, stock 028,865, B6J.CgGt(ROSA)26Sor < tm95.1 (CAGGaMP6f)) to generate OMPxGCaMP6f mice and Pcdh21xGCaMP6f mice, respectively (Figure 2.1). The OMP promoter drives targeted expression of the genetically encoded Ca^{2+} indicator GCaMP6f (*448*) specifically in mature olfactory receptor neurons (*449*, *450*), while the Pcdh21 promoter restricts GCaMP6f expression to mitral and tufted cells (*451*). Both OMP-Cre and Pcdh21-nCre mouse lines were originally obtained from RIKEN BioResource Research Center (Ibaraki, Japan).

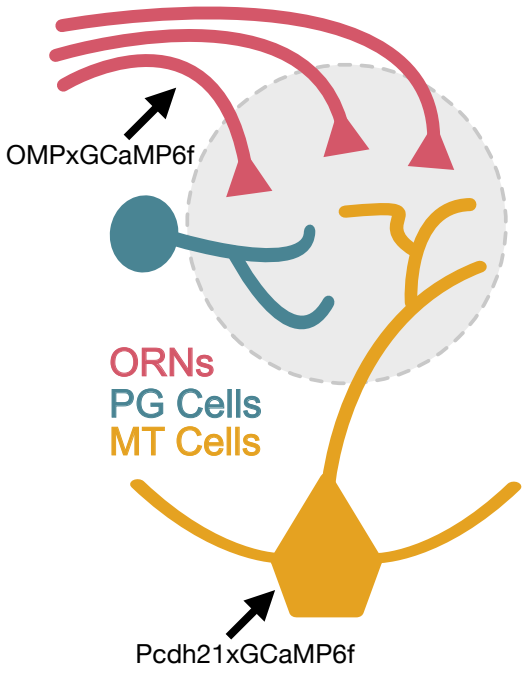

Figure 2.1: Genetically Engineered Mouse Lines

Simplified olfactory bulb circuit. Olfactory bulb input and output neuron activity is measured by driving expression of GCaMP6f under OMP-Cre and Pcdh21-nCre promoters, respectively. ORN = olfactory receptor neuron, PG = periglomerular cell, MT = mitral/tufted cell.

The GCaMP6f mouse line was originally obtained from Jackson Laboratory (Maine, USA). All mouse lines were maintained in house. Consistent with the NC3Rs guidelines (https://www.nc3rs.org.uk/who-we-are/3rs), both males and females aged

2-4 months old were used in this study. Throughout results Chapters 3-5, N refers to the number of animals, whereas n denotes the number of glomeruli.

2.2 Olfactometry

Odourants were obtained from Sigma-Aldrich, or Alfa Aesar. Liquid dilutions of odourants were prepared to achieve desired concentrations of approximately $3x10^{-5}$ %, $1x10^{-4}$ %, $3x10^{-3}$ %, $1x10^{-2}$ %, 0.1 %, 1 %, 3 % and 100 % using 1:100 and 1:1000 serial dilutions. Odourants were diluted in either mineral oil (Sigma-Aldrich, 69794) or caprylic/capric triglyceride oil (Spectrum Chemical, C3465) within ~one week of experiments. Diluted odorants were delivered in vapour phase using either an 8 or 16 channel olfactometer (Aurora Scientific, 206A or 220A, respectively). Total flow rates were kept constant at 1000 sccm. In imaging experiments, the output tubing of the olfactometer was positioned 1-2 cm in front of the mouses nose, while the exhaust valve was connected to charcoal. Odourants were delivered independent of inhalation timing, in protocols typically consisting of 14 presentations per odour (Figure 2.2). Prior to odour stimuli, three presentations of solvent oil were given. Odourant presentations followed an order of increasing concentration. Each odour stimulus was presented up to three times within a given field of view for each animal. The duration of odourant stimuli was either 3 s, 60 s, or 80 s. Inter-stimulus intervals were extended as odour concentration increased, varying between 20 - 120 s to minimise neural adaptation. All odour concentrations are reported as % saturated vapour. The odour flow stabilisation delay (the time it takes an odour to flow from the vial to the final valve) was set to either 10 s or 20 s. Synthetic medical air was continually delivered to the mouse between odour trials to eliminate odour residues. Olfactometer tubing was purged with synthetic medical air for 20 min after every animal and periodically cleaned with 70 % isopronanol to prevent contamination. Odour concentrations delivered to the behaviour boxes were measured with a miniPID (Aurora Scientific, 200B) placed at the nose port and are reported relative to the % saturated vapour used for imaging experiments.

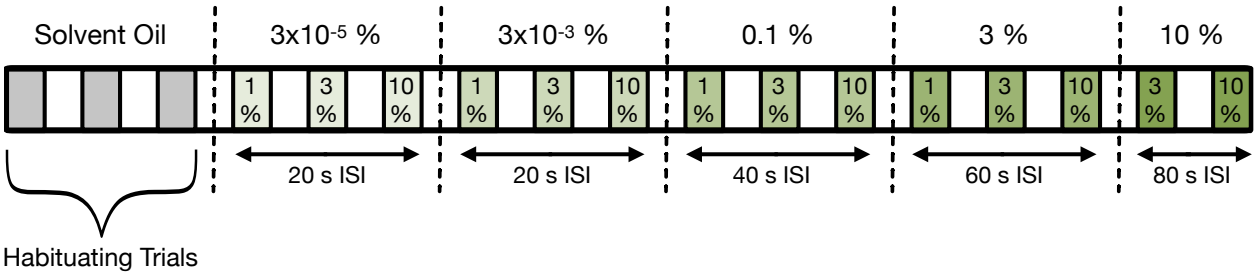

Figure 2.2: Odour Delivery Protocol

Standard odour delivery protocol used to measure dynamic range of individual glomeruli. Following three consecutive presentations of solvent oil, odourants (green) were delivered in increasing concentrations, with the time between stimuli increasing as odour concentration increased.

2.3 Behaviour

2.3.1 Cross-Habituation Test

Cross-habituation experiments were set up similarly to the method described by Qiu *et al.* (*452*). 2–3-months old mice were placed in a 25 x 25 cm perspex chamber with all sides opaque. Each chamber was fitted with an odour port and exhaust tube positioned 1 cm above the base at opposing sides (Figure 2.3A). The output of the olfactometer was connected to the odour ports of all boxes via tubing and used to deliver odours to the mice at a rate of 100 sccm. There was no difference in the concentration of odour delivered to each box as measured with a miniPID. Each odour port housed an IR beam brake sensor (The Pi hut, Figure 2.3B). This allowed us to measure investigation time by recording beam break events and vale openings in binary using a MicroPython pyboard lite (v1.0) and pyControl GUI (v1.6). A mini vacuum pump (SLS2602) was attached to the exhaust tubes of all four chambers via tubing with n identical path length and air was extracted at a rate of 5.5 l/min. In each trial, mice were presented with either a solvent oil or a test odour for 60 s, followed by 60 s of synthetic medical air (21 % oxygen V/V medicinal gas, compressed). Wild type C57bl6 mice were first habituated to the test environment for 10 min before starting the stimulus protocol (Figure 2.3C). Each presentation lasted 60 s with 60 s of medical air

between presentations. In all instances, animals were naïve to the testing odour. Initially, each animal was tested with mineral oil as a familiarisation stage. Each animal was tested with 2-heptanone and ethyl tiglate with 1 day between experiments, with half the cohort tested with ethyl tiglate first and the other half with 2-heptanone.

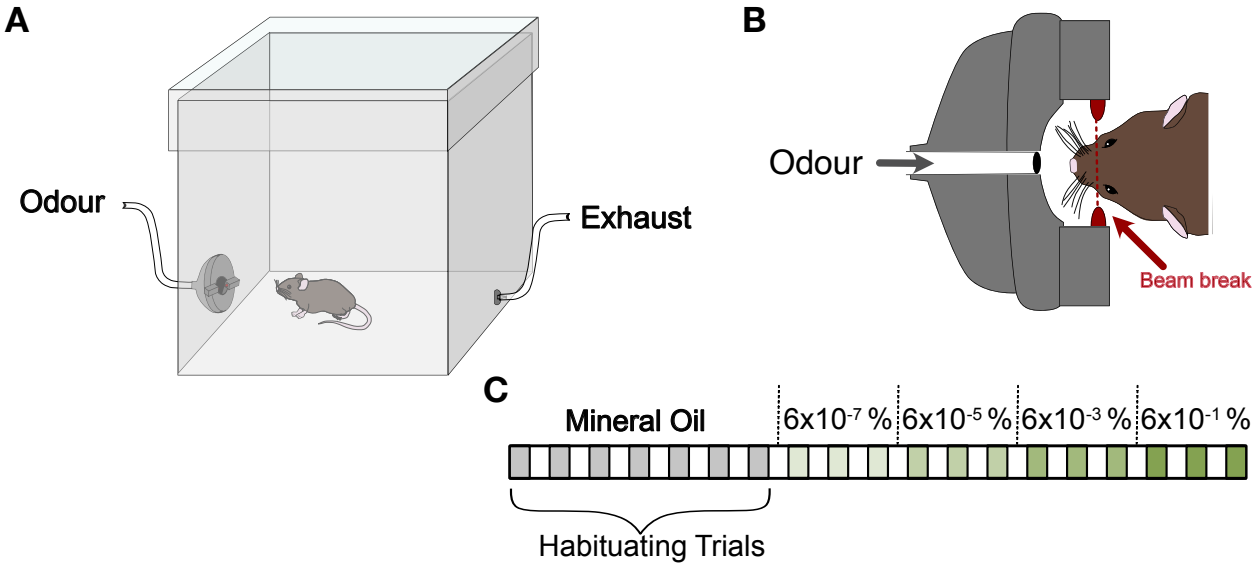

Figure 2.3: Cross-Habituation Test

A) Experimental paradigm, mice were placed in a test chamber equipped with an odour delivery port and exhaust. B) Contained within the odour delivery port was a nose poke and beam break sensor to record investigation time. C) Odour delivery protocol, each block represents 60 s (60 s stimulus, 60 s inter-stimulus interval).

2.3.2 Odour Learning Protocols

2.3.2.1 Odour Exposure

The environments of either wild type C57bl6 or Pcdh21xGCaMP6f mice were enriched with an odour for 7 or 10 days. Odours were diluted in mineral oil (1:40) and 1 ml was applied to Whatman qualitative filter paper No.1, before being folded inside a metal teaball and placed inside the animals home cage (Figure 2.4), replenished daily at ~17:30.

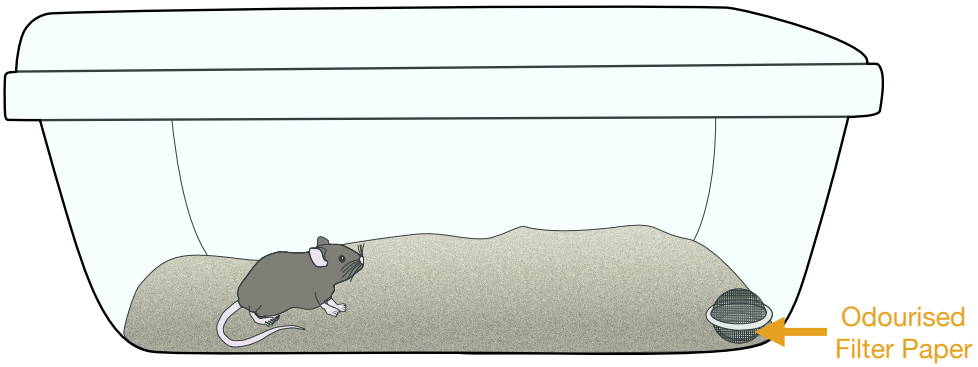

Figure 2.4: Odour Exposure Setup

For 1 week, mice were exposed to odourised filter paper contained within a tea ball, referred to herein as the ‘exposed’ cohort. The odour used was ethyl tiglate at a concentration of 2.5 % SV. Odourised filter paper were replenished daily.

2.3.2.2 Food-Odour Association

The diets of either wild type C57bl6 or Pcdh21xGCaMP6f mice were supplemented with an odour for either 7 or 10 days. Odours were first diluted in distilled water (1:40), before being combined with their regular diet in powdered form (equal W/V) and shaped into a single ball (~5 g per ball). Each mouse received a fresh food ball daily at ~17:30 in a glass Gü dessert dish (7.5 cm W, 4.25 cm) (Figure 2.5).

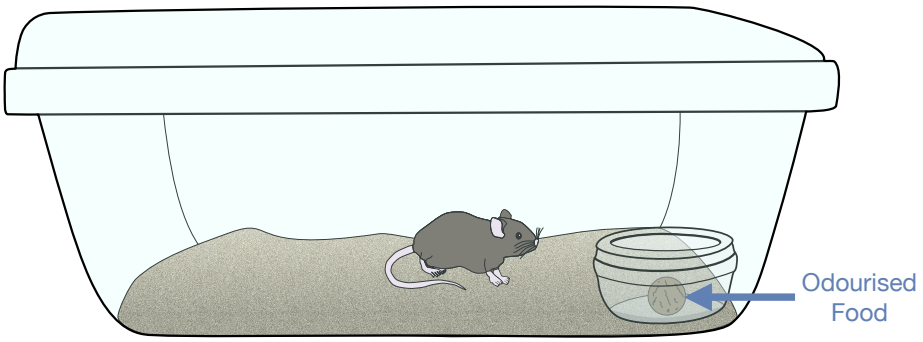

Figure 2.5: Food-Odour Association Setup

For 1 week, mice were exclusively fed standard chow supplemented with an odour, herein referred to as the ‘associated’ cohort. The odour used was ethyl tiglate at a concentration of 2.5 % SV. Odourised food was replenished daily.

2.3.2.3 Food Preference Test

Wild type C57bl6 mice were fasted for ~16 hr prior to testing commenced to ensure they were motivated to eat. Two glass Gü dessert dishes (7.5 cm W, 4.25 cm) containing 5 g of food odourised with either ethyl tiglate or isoamyl acetate (1:40) were placed at opposite corners of the animals home cage (Figure 2.6). Preference was determined by measuring the amount of food eaten over the course of 1 hr.

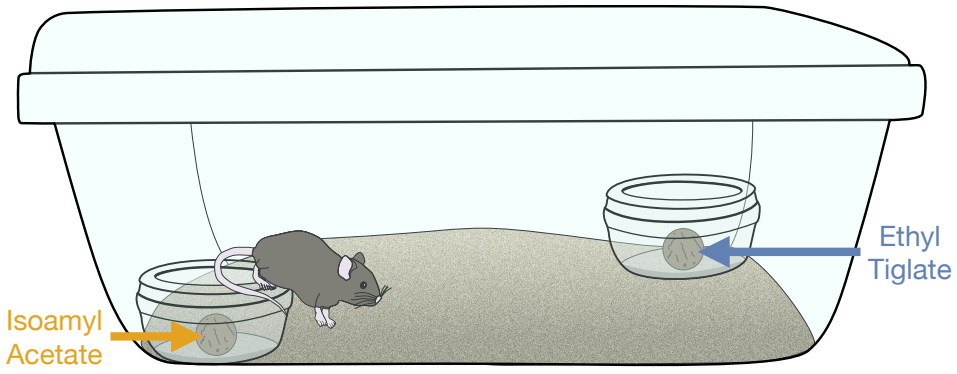

Figure 2.6: Food Preference Test

Fasted mice were presented with two food pellets, each odourised with either 2.5 % SV ethyl tiglate, or 2.5 % SV isoamyl acetate. Mice were left to feed for 1 hour, and the amount eaten from each food pellet was measured.

2.3.2.4 Food- and Odour-Finding Tests

Wild type C57bl6 mice were fasted for ~16 hr before testing commenced to ensure they were motivated to eat. A clean housing cage was filled with ~4 cm of fresh bedding and an odourised food or cotton ball (~1.5 cm^3) was hidden beneath the bedding in a single corner (Figure 2.7). Care was taken not to leave odour trails during food/cotton ball placement. Mice were individually placed in a cage and a timer was set once a clear perspex lid had been attached. The time taken for mice to locate (defined as when the majority of the food/cotton ball became visible) and start eating the food/cotton ball was manually recorded.

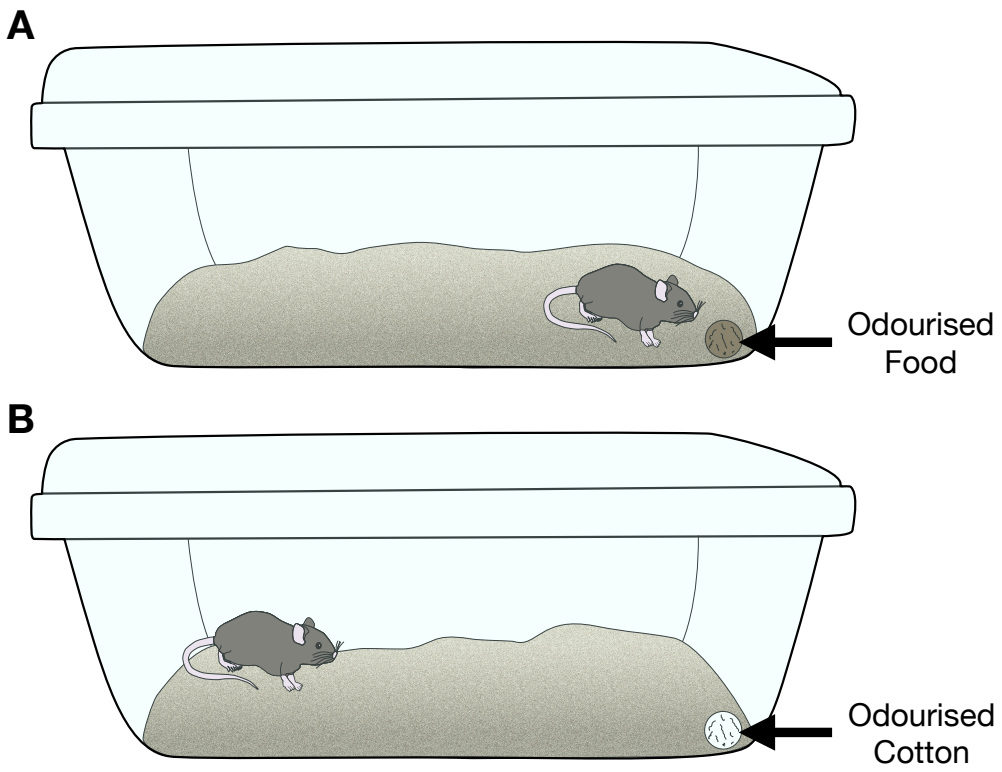

Figure 2.7: Food- and Odour-Finding Test Setup

Either a A) food pellet or B) cotton ball odourised with ethyl tiglate was buried in one corner of the test cage. Fasted mice were individually placed in the test cage, and time taken to locate and begin eating the odourised pellet/cotton was recorded. If mice did not locate and/or attempt to eat the pellet/cotton within 10 min, the test was abandoned.

2.4 *In Vivo* Imaging

2.4.1 Surgery

Mice were anaesthetised with an intraperitoneal injection of Urethane (1.5 g/kg). Body temperature was maintained at 37°C using a custom-made thermostatic heat pad and monitored with an anal temperature probe. A protective eye ointment (HYLO Night) was applied to prevent the animals eyes from drying. Mice received an intramuscular injection of Dexamethasone (2 mg/kg) to minimise inflammation. Analgesia was induced by subcutaneously injecting Meloxicam (5 mg/kg). To prevent severe cardiorespiratory depression and limit mucus accumulation in airways, Atropine (0.02 mg/kg) was subcutaneously injected prior to surgery; with additional top-ups (0.01 mg/

kg) administered if necessary. Surgery commenced once the animals pedal withdrawal reflex was completely absent. A scalpel (Swann-Morton, non-sterile blade No.10) was used to make a midline incision from the anterior edge of the nasal bone to the intraparietal bone. Skin covering this region was removed using surgical scissors and the underlying skull was cleared from hair and periosteum using cotton bud tips. The parietal bone was scored using a scalpel (Swann-Morton, non-sterile blade No.11) to facilitate adhesion of dental cement (UNIFAST Trad). A stainless steel head bar (4.5 x 66 mm) was fixed with dental cement caudal to the inferior cerebral vein. Dental cement was applied using the tip of a halved wooden cotton bud. The animals head was secured for the remaining procedures and imaging session using a stereotaxic frame (Thor labs). A micro-motor dental drill (Strong 90) was used to perform a craniotomy covering roughly half of the dorsal surface of the olfactory bulb (Figure 2.8). Surgical sponge soaked in artificial cerebrospinal fluid (7.4 pH, 135 mM NaCl, 5.4 mM KCl, 5 mM HEPES, 1.8 mM CaCl2 2H2O) was used to periodically cool the skull during bouts of drilling and to address any bleeding. The exposed bulb was covered with 2 % low-melting point agarose in artificial cerebrospinal fluid and a 3 mm glass coverslip (Biochrom, Harvard Bioscience) was fixed with dental cement. Silicone rubber (Body Double™ Fast Set) was applied to the skull surrounding the cranial window to create a well for the water dipping objective of the microscope. For experiments where drugs were topically applied, segments of the dura were removed using fine forceps (Fine Science Tools, Dumont #5SF) and the animal was imaged without a coverslip.

2.4.2 2-Photon Ca^{2+} Imaging

Mice fitted with a cranial window over one hemisphere of the olfactory bulb were positioned under a custom built 2-photon laser scanning microscope (Figure 2.8). GCaMP6f fluorescence was excited at 940 nm using a pulsed Mai Tai eHP DeepSee TI:sapphire laser system (SpectraPhysics). A resonant-galvo mirror assembly (Sutter instruments) scanned the beam through a 16 x water-dipping objective (N16XLWD-PF, NA 0.8, Nikon). Fluorescence was detected using GAasP photo-multiplier tubes and appropriate filters and dichroic mirrors. Images were acquired at 30-120Hz, using

ScanImage software (*453*).

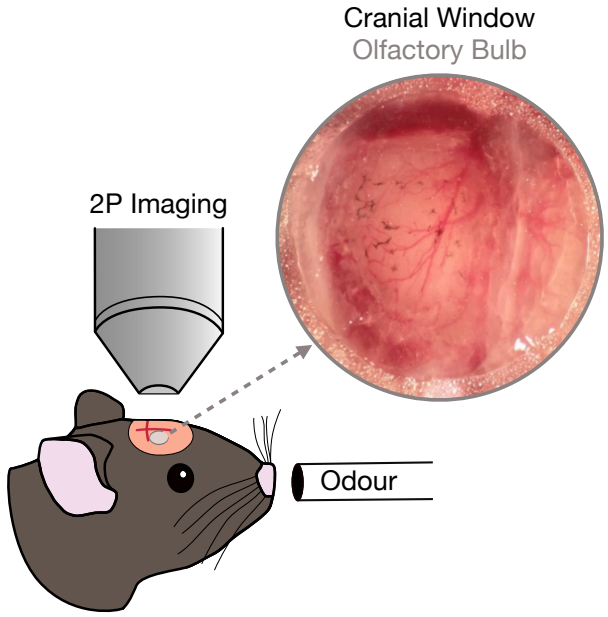

Figure 2.8: Surgery and 2-Photon Ca^{2+} Imaging

Anaesthetised mice were fitted with a cranial window on the dorsal surface of the olfactory bulb. Neural activity was measured using 2-photon microscopy while mice were presented with odours. Inset shows example surgery.

2.4.3 Head-Fixed Perception Tests

Wild type C57bl6 mice were anaesthetised with isoflurane on a custom stereotaxic frame (Thor Labs) for head-bar attachment. Anaesthesia was maintained at a level of ~1.5-2 % isoflurane, 1 l/min O2 during surgery. Metacam (5mg / kg S.C.) and buprenorphine (0.1 mg / kg I.P.) were administered as analgesics. A small piece of skin above the skull, big enough for placing the head bar was carefully removed and cleaned with sterile saline solution. Superglue was initially applied over the exposed skull followed by dental cement to affix a custom 3D printed head bar. Dental cement was applied using the tip of a halved wooden cotton bud. Additional dental cement (UNIFAST Trad) was applied to cover the head bar and the exposed skull. Post surgery mice were given soaked diet and buprenorphine (0.1 mg / kg I.P.) for the following two days, all mice were allowed 1 week for recovery before habituation to head-fixation began. Mice were handled 5 min each day for 2 days prior to behavioural tests, aiming to acclimate them to the experimenter. Mice were head-fixed upon on a treadmill, described in (*454*), and habituated for 10 to 20 min per day for 2-3 days before recordings. The mouse face was imaged with a Basler camera (Cat. No: 107652) with

12 mm Edmund Optics lens (Cat. No: 33-303) and videos were captured at 120 Hz with 750 nm illumination (outside the visual range of mice). Odours were delivered using an olfactometer (220A, Aurora Scientific) and custom written code. The recording and synchronisation of data was performed with Bonsai-Rx (*455*) and a Teensy 4.2 microcontroller (PJRC). Each video acquisition was 35 s, composed of 10 s of baseline, 10 s stimulus and 15 s post stimulus. Each mouse was first presented with 5-7 oil trials before the the odour and all trials were spaced ≥ 60 s apart. A deeplabcut (*456*) neural net was trained on 15 frames from each mouse and used to extract the xy coordinates of the key points from every frame (Figure 2.9).

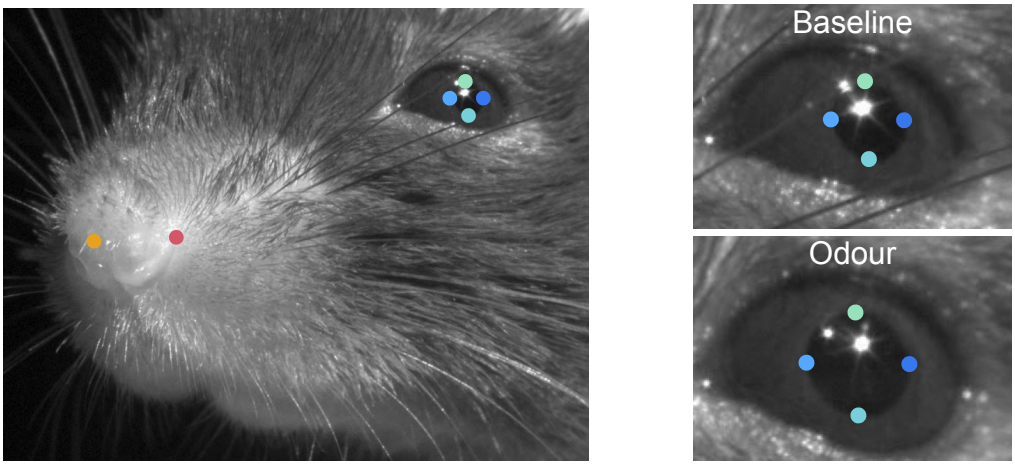

Figure 2.9: Head-Fixed Perception Tests

Mice were head-fixed and presented with odours while awake and freely moving on a treadmill. Key facial features (indicated by coloured dots) were tracked using deeplab cut to measure odour-evoked changes in pupil diameter and sniff rate.

2.4.4 Pharmacology

The $GABA_B$-receptor antagonist CGP 54626 hydrochloride (Tocris Bioscience) was used at a concentration of 5 μM. The dopamine D_2-receptor antagonist Raclopride (Tocris Bioscience) was used at a concentration of 100 μM. Both drugs were dissolved in artificial cerebrospinal fluid (7.4 pH, 135 mM NaCl, 5.4 mM KCl, 5 mM HEPES, 1.8 mM CaCl2 2H2O) and topically applied to the olfactory bulb ~20 minutes before

imaging recommenced (Figure 2.10).

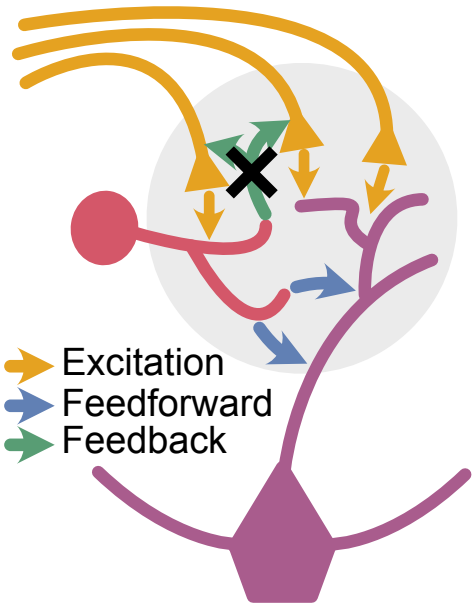

Figure 2.10: Pharmacology

Pharmacological blockade of $GABA_B$ and dopamine D_2 receptors using CGP 54626 and Raclopride, respectively, inhibits feedback inhibition onto olfactory receptor neuron terminals.

2.5 Data Analysis

2.5.1 Image Segmentation of Glomeruli

We used the Suite2p pipeline (v0.10.1) to register imaging data, applying the default settings ('nimg_init': 300, 'batch_size': 500, 'maxregshift': 0.1, 'smooth_sigma': 1.15). Suite2p is an open-source pipeline designed for processing calcium imaging data, including motion correction, region of interest extraction, and signal analysis (*457*). Regions of interest corresponding to glomeruli were manually drawn using Suite2p-registered data in FIJI (Fiji Is Just ImageJ), an open-source image processing software specialised for biological research (*458*). Glomeruli were manually drawn using the mean projection of the time series and were validated against the corresponding time series data. Each glomerulus exhibited a discrete fluorescent signal (Figure 2.11). Raw fluorescence was extracted from manually drawn glomeruli using the extraction.create_masks_and_extract function in Suite2p. Extracted fluorescent traces were normalised as ΔF/F using the following equation: $F\text{-}F^0/F^0$, where F is the raw fluorescent trace and F^0 is the baseline fluorescence recorded 5 s prior to the odour

stimulus. Background subtraction was performed by setting the darkest region of the recorded image to zero and subtracting the offset.

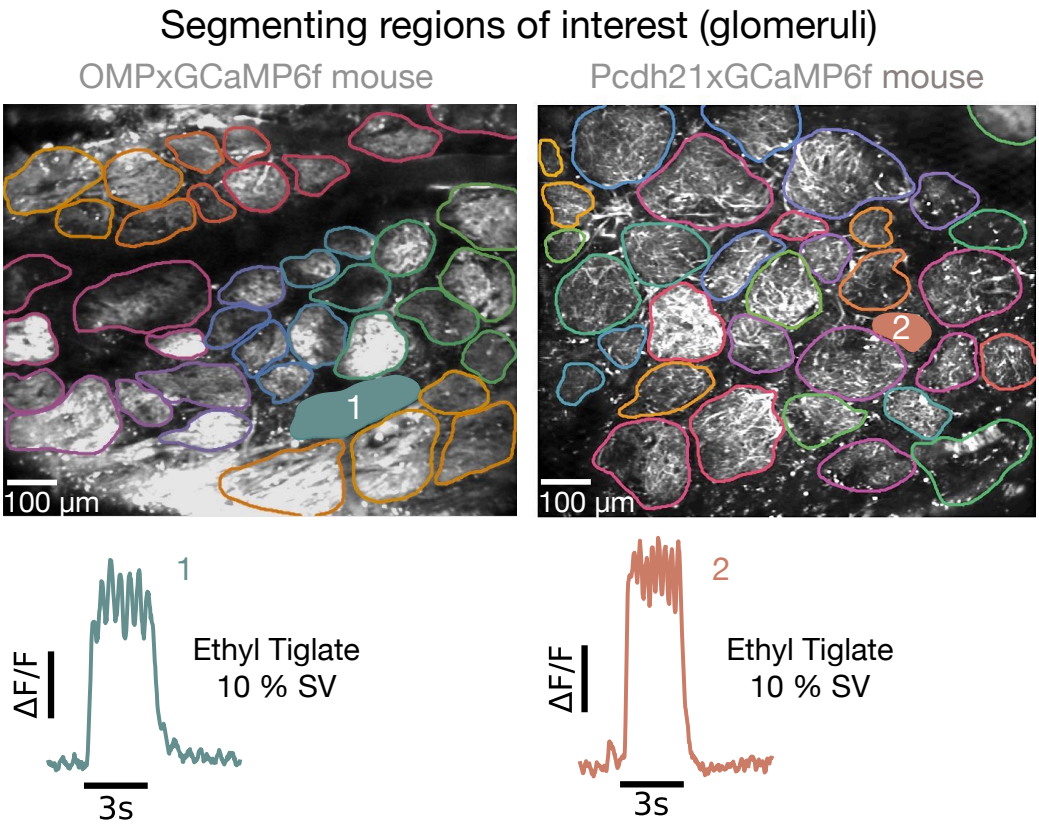

Figure 2.11: Image Segmentation of Glomeruli

Top: Fields of view in both genetically engineered mouse lines. Regions of interest (glomeruli) are manually drawn in FIJI and the fluorescent signal is segmented. Bottom: Responses from example glomeruli in both mouse lines to a 3 s presentation of ethyl tiglate at 10 % SV.

2.5.2 Defining Glomerular Responses

To consistently identify responsive glomeruli, we first applied a signal-to-noise ratio (SNR). We define the SNR for stimuli as: (mean amplitude over stimulus window - mean amplitude over 3 s preceding the stimulus) / standard deviation over 3 s preceding the stimulus. A glomerulus was classified as responsive if it met the following two criteria: 1) the SNR for a given stimulus must be ≥ 5, and 2) all subsequent odour presentations higher in concentration must also generate a response with an SNR ≥ 5. If the highest concentration tested was the stimulus being evaluated, the glomerulus was classified

as responsive if it met the SNR criterion. Trials where irregular breathing was apparent (i.e. a drop in activity across all glomeruli) were excluded.

2.5.3 Response Integral

The response integral (∫) was calculated over the stimulus period. For trials with multiple repeats, the average response integral was calculated for each stimulus across all trials. Trials where irregular breathing was apparent (i.e. a drop in activity across all glomeruli) were excluded from the computation of the mean.

2.5.4 Jaccard Index

We used a Jaccard index to quantify the overlap between responsive glomeruli for two distinct odours. We defined the Jaccard index as the intersection (the number of glomeruli responsive to both odours) divided by the union (the total number of glomeruli responsive to either odour, excluding those responsive to both). For trials with multiple repeats, the average number of responsive glomeruli across all trials was used to calculate the Jaccard index at each concentration.

2.5.5 Adaptation Index

We used an adaptation index (AI) to quantify the amount of adaptation exhibited by glomeruli. For 3 s odour stimuli, we defined the adaptation index (AI) as the mean of the last 100 ms of the stimulus period (B in Figure 2.12) divided by the peak response (A in Figure 2.12). For 60 s odour stimuli, B in Figure 2.12 corresponded to the mean of the last 1 s of the stimulus period. To minimise point-to-point fluctuations, a convolution filter of 5 was applied using the ‘np.convolve’ function from NumPy, a core library for numerical computing in Python, prior to calculating the adaptation index. For trials with multiple repeats, the average adaptation index was calculated for each stimulus across all trials. Instances where a glomerulus was inactive during an odour presentation were omitted from the computation of the mean.

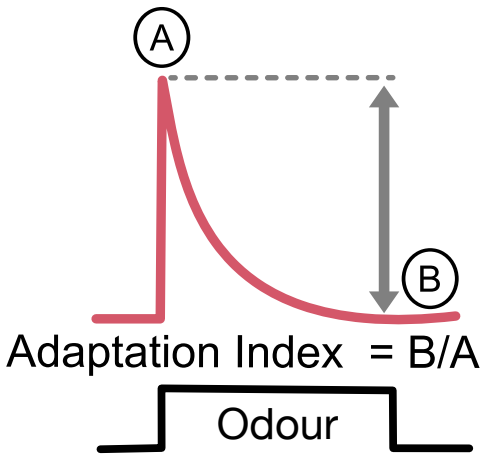

Figure 2.12: Adaptation Index

Adaptation index calculation, where A represents the peak response amplitude and B represents the mean response amplitude over the last 100 ms / 1 s of the stimulus period.

2.5.6 Response Maps

For each stimulus, response maps (Figures 4.3A, 4.7C, 5.4A & C) were generated using the following equation: $F\text{-}F^0/F^0$, where F is the raw fluorescent trace and F^0 is the baseline fluorescence recorded 3 s preceding the odour stimulus. Maps are displayed after 2D gaussian filtering with a sigma of 2 and areas outside the segmented glomeruli were set to zero.

2.5.7 Support Vector Machine (SVM) Classification

For each glomerulus, we calculated the mean amplitude of the Ca^{2+} signal over the odour delivery period (3 s stimulus) and 1 s second after odour cessation (4 s window in total, accounting for delayed activation observed in a subset of glomeruli). To minimise point-to-point fluctuations, a convolution filter of 5 was applied using the 'np.convolve' function from NumPy, a core library for numerical computing in Python. In a single odour delivery protocol (Figure 2.2), the mean response amplitudes to various concentrations were normalized relative to the maximum response for each glomerulus. We included only glomeruli that were classified as responsive in our analyses (see '2.5.2. Defining Glomerular Responses'). To determine which features of our dataset were most important for classifying odour percepts, we used a linear support vector machine (class weight = balanced) from scikit-learn, a widely-used

machine learning library in Python. Odour responses were assigned a percept label ('weak' or 'strong') if they were within 50 % of the boundary concentration shown in Figures 4.3A, 4.4A, and 4.8A. We evaluated the classifiers accuracy using the Leave-One-Out cross-validator from the sci-kit learn library to calculate weighted average F1 scores, as reported in Figures 4.3B & D, and 4.6A & C. The Leave-One-Out cross-validator is a cross-validation technique particularly suited for small datasets, where each data point is used once as a test sample while the model is trained on all remaining points. Relative glomerular weighting (Figures 4.3C and 4.6B) was obtained by calculating the absolute values of the coefficients for each glomerulus and normalising each value to the largest assigned weight.

2.5.8 Ranking Glomerular Activation Times

To determine the first active glomerulus for a given stimulus, we identified the first frame during the 4 s stimulus window (3 s stimulus period + 1s post-stimulus, see above) with a signal-to-noise ratio ≥ 5. The timestamp of this initial frame from was taken as the activation time for the glomerulus. For each stimulus, all responsive glomeruli were assigned a rank, with the first active glomerulus assigned a rank of 1 (Figures 4.4B and 5.5C). Trials where irregular breathing was apparent (i.e. a drop in activity across all glomeruli) were excluded. For trials with multiple repeats, the primary glomerulus was assigned the mean rank it received across all trials of the same concentration.

2.5.9 Glomerular Size Measurements

To measure the maximal cross-sectional area of primary glomeruli, we obtained a z-stack at 2-4 μm increments of the olfactory bulb in each mouse. Glomerular outlines were manually drawn in Fiji (Fiji Is Just ImageJ), an open-source image processing software specialised for biological research (*458*). The largest outline from all planes was used to determine the maximal cross-sectional area for Figure 5.5D. These results were confirmed by a labeller blind to the groups. Where glomerulus structure was

difficult to determine in stacked images alone, outlines were drawn using time series data from odour-evoked recordings.

2.5.10 Statistical Analysis

For all statistical parameters data were first tested for normality with Shapiro Wilk and are reported as mean ± standard error of the mean if normal or median ± median absolute deviation if not. Paired comparisons were made using either a paired t-test or Wilcoxon signed-rank test, and unpaired comparisons were assessed using either an unpaired t-test or a Mann-Whitney U test, as appropriate. Comparisons across multiple groups were made using either a one-way ANOVA or a Kruskal-Wallis H-test. Linear correlations between datasets were assessed using the Pearson correlation test. Figure 3.8D data was analysed using repeated measures ANOVA with post-hoc paired t-tests comparing initial response amplitudes to the mean of all subsequent odour responses. For Figures 4.1D, E, & 5.3D, Friedman's test was used to compare the median of the last 5 oil presentations with each odour delivery, followed by post-hoc Wilcoxon signed-rank tests with Bonferonni correction. Figures 5.6, 5.7 & 5.9 were analysed using two-way ANOVA, with post-hoc Tukey's HSD test for cohort comparisons. In Figures 5.8 & 5.10, spatial pattern analyses were conducted with PERMANOVA on Euclidean distances, comparing detection thresholds between dual-responsive glomeruli across cohorts, followed by post-hoc PERMANOVA pairwise comparisons between individual cohorts. All p values were adjusted for multiple comparisons with Bonferroni correction, except for Figures 5.8 & 5.10, which were corrected using the Benjamini-Hochberg method due to the high-dimensionality of the dataset. When asterisks are used to indicate significance, * = $p<0.05$, ** = $p<0.01$ and *** = $p<0.001$.

2.6 Depolarising Block Model

Morphologically realistic models of olfactory receptor neurons and their receptor input were simulated in NEURON 8.2 by Jamie Johnston (*459*, *460*). Each olfactory receptor neuron consisted of 4 compartments: an axon of length 1.6 mm and diameter of 0.6 µm, a soma with diameter of 5 µm, a dendrite with a length of 12 µm and 0.8 µm

diameter and an endbulb of 2 μm diameter. Axial resistance was 180 Ω * cm and membrane capacitance was 1 μF cm^{-2}. Standard Hodgkin-Huxley channels were used at a uniform density throughout the cell with the following conductance densities: Na = 32 mS cm^{-2}, K = 8 mS cm^{-2}, passive = 0.02 mS cm^{-2}, passive reversal -50 mV. This gave an input resistance of 4.6 G Ω similar to the reported membrane resistance of olfactory receptor neurons (*379*). To mimic the basal firing activity of olfactory receptor neurons evoked by spontaneous Nav channel openings in the cell body (*461*), gaussian noise with a mean of 1 pA and SD of 0.021 was injected into the somatic compartment which generated spontaneous firing at ~4 Hz, similar to the reported spontaneous rates (*379*). The receptor currents were modelled as a point process placed on the tip of the endbulb, with a time course described by 3 piecewise functions obtained from fits to the synaptic currents reported in (*374*). The 3 piecewise functions correspond to the onset and duration of the odour stimulus (a), the decay after the stimulus (b), and the adaptation during the steady-state phase of the stimulus (c). The synaptic conductance (g) was therefore g = m(a+b-c), where m is a scaling factor. For the weak odour concentration:

$$a(t) = \begin{cases} \frac{0.0415}{1+e(\frac{190+t_0\ -t}{40})} & if\ t_0 < t < t_0\ + t_d \times t_x \\ 0 & otherwise \end{cases}$$

$$b(t) = \begin{cases} \frac{0.017}{1+e(\frac{-200.55+t_0+t-t_d \times t_x}{100.14})} & if\ \ t_0 + t_d \times t_x < t < t_0 + t_d \times t_x + 1500 \\ 0 & otherwise \end{cases}$$

$$c(t) = \begin{cases} 0.041 - (0.010774 + 0.03674e(\frac{-t + t_d + 190}{1232.7} & if\ \ t_0 + 190 < t < t_0 + t_d \times t_x \\ 0 & otherwise \end{cases}$$

And for the strong odour concentration:

$$a(t) = \begin{cases} \frac{0.08}{1+e(\frac{90+t_0\ -t}{20})} & if\ \ t_0 < t < t_0 + t_d \times t_x \\ 0 & otherwise \end{cases}$$

$$b(t) = \begin{cases} \dfrac{0.0482}{1 + e(\frac{-606.55 + t_0 + t - t_d \times t_x}{240.14})} & if \;\; t_0 + t_d \times t_x < t < t_0 + t_d \times t_x + 2500 \\ 0 & otherwise \end{cases}$$

$$c(t) = \begin{cases} 0.08 - (0.04474 + 0.03674e(\dfrac{-t + t_d + 190}{454.54} & if \;\; t_0 + 190 < t < t_0 + t_d \times t_x \\ 0 & otherwise \end{cases}$$

Where t_0 is the odour stimulus onset in ms, t_d is the stimulus duration in ms, and t_x is a duration multiplier to reflect that receptor current outlasts the stimulus with this duration, increasing with both the intensity and duration of the stimulus (*365*, *374*, *383*, *462*). For the weak stimulus t_x was set at 1 and for the strong stimulus t_x was 1.65 + a value drawn at random from a gaussian distribution, with a mean of 0.2 and SD of 0.25 to reflect heterogeneity in the response decay across neurons carrying the same receptor (*40*). Peri-stimulus time histograms were computed for 500 olfactory receptor neurons at each concentration with bin widths of 50 ms. To estimate the Ca^{2+} signal that GCaMP6f would report for each odour concentration the mean spike rate was convolved with a kernel representing the kinetics of GCaMP6f (*448*).

Chapter 3: Odour Adaptation in the Olfactory Bulb

3.1 Odour Sensitivity Varies Widely Across Glomeruli

To understand how odour identity is encoded, we studied the region of the brain where odours are first processed, the olfactory bulb. We used two genetically modified mouse lines: Those which had the genetically encoded Ca^{2+} indicator GCaMP6f (*448*) expressed in mature olfactory receptor neurons (OMPxGCaMP6f mice (*449*, *450*)), and those which had GCaMP6f targeted to mitral and tufted cells (Pcdh21xGCaMP6f (*451*)) (Figure 3.1A, see methods). We next fitted anaesthetised mice with a cranial window that covered roughly half of the dorsal surface of the olfactory bulb and imaged this region using two-photon microscopy, positioning the output of an olfactometer directly in front of the mouse's nose (Figure 3.1B). We imaged at the glomerular layer, allowing us to visualise the spatiotemporal patterns of odour-evoked activity (Figure 3.1C) (*463*). Glomeruli are discrete functional modules whose activity corresponds to input from a single olfactory receptor (*35*). Thus, by segmenting the fluorescent signals of each glomerulus within a field of view, we were able to infer how a given odour activates an assortment of receptors. Each of the ~1000 olfactory receptors (*31*) possess a unique affinity for every single odourant molecule (*32*, *34*, *37-41*), defining the dynamic range

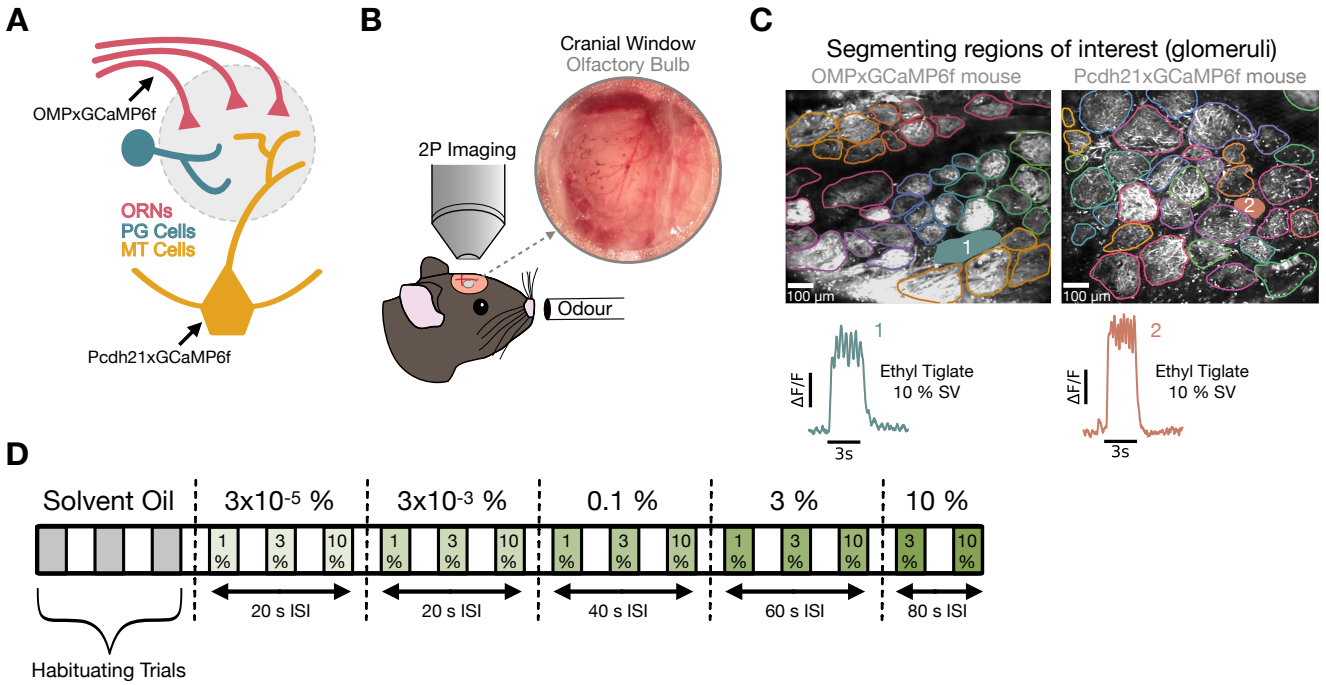

Figure 3.1: Visualising Neural Activity in the Olfactory Bulb

A) Simplified olfactory bulb circuit. Olfactory bulb input and output neuron activity is measured by driving expression of GCaMP6f under OMP-Cre and Pcdh21-nCre promoters, respectively. ORN = olfactory receptor neuron, PG = periglomerular cell, MT = mitral/tufted cell. B) Anaesthetised mice are fitted with a cranial window on the dorsal surface of the olfactory bulb, neural activity is measured using 2-photon microscopy, inset shows example surgery. C) Top: Fields of view in both mouse lines. Regions of interest (glomeruli) are manually drawn in FIJI and the fluorescent signal is segmented. Bottom: Responses from example glomeruli in both mouse lines to a 3 s presentation of ethyl tiglate at 10 % SV. D) Odour delivery protocol used to measure dynamic range of individual glomeruli. See methods for more detailed information.

of the glomerulus (*35*). However, odour-evoked patterns of activity also change drastically with concentration (*261*, *262*). To assess the influence of odour concentration on identity coding, we presented mice with 3 s presentations of multiple monomolecular odours across a wide range of concentrations (Figure 3.1D). We increased the duration of the inter-stimulus interval in line with odour concentration to minimise adaptation between stimuli (Figure 3.1D). This approach enabled us to visualise the dynamic ranges of responsive glomeruli within a field of view, which we refer to herein as input-output curves.

We first focused on olfactory receptor neurons, which together form the olfactory nerve and provide the input to the olfactory bulb (Figure 3.2A). The fluorescent signal measured at the glomerulus in OMPxGCaMP6f mice is the signal that drives glutamate release from olfactory receptor neuron terminals (Figure 3.2B). Diversity in receptor affinity is reflected in response time courses from individual glomeruli (Figure 3.2C). Glomeruli were generally more responsive to either ethyl tiglate or isoamyl acetate (Figure 3.2C, top and bottom, respectively), responding to a broader range of concentrations and displaying larger response amplitudes for the preferred odour. Less common were glomeruli which exhibited similar responsiveness to both test odours (Figure 3.2C, middle). We calculated the response integral for the example glomeruli shown in Figure 3.2B & C, which serves as a measure of calcium accumulation and thus more closely reflects the total number of action potentials

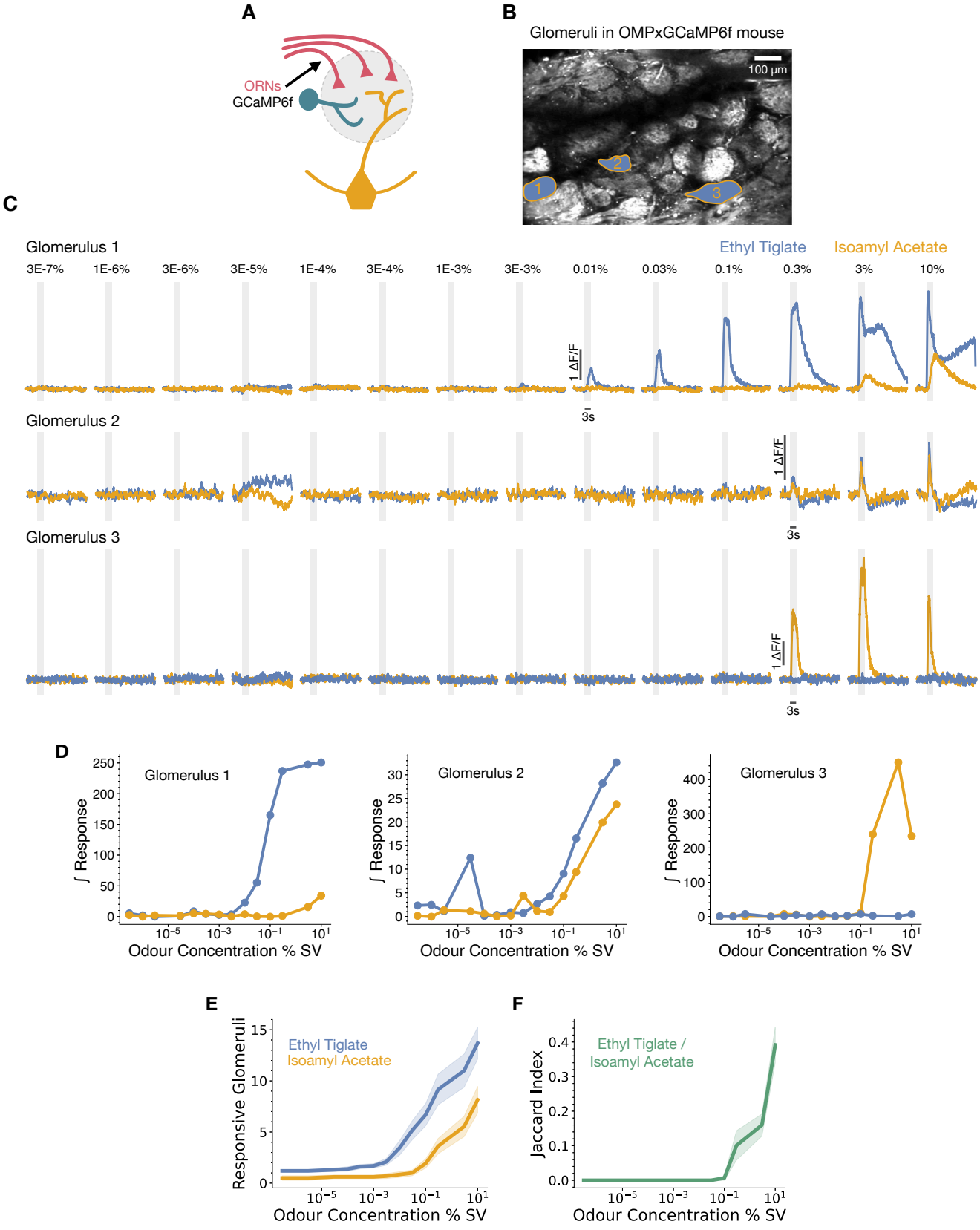
A
ORNs
GCaMP6f
B
Glomeruli in OMPxGCaMP6f mouse
100 µm
1
2
3
C
Glomerulus 1
Ethyl Tiglate
Isoamyl Acetate
3E-7%
1E-6%
3E-6%
3E-5%
1E-4%
3E-4%
1E-3%
3E-3%
0.01%
0.03%
0.1%
0.3%
3%
10%
1 ΔF/F
3s
Glomerulus 2
Glomerulus 3
D
Glomerulus 1
Glomerulus 2
Glomerulus 3
∫ Response
Odour Concentration % SV
E
Responsive Glomeruli
Ethyl Tiglate
Isoamyl Acetate
Odour Concentration % SV
F
Jaccard Index
Ethyl Tiglate /
Isoamyl Acetate
Odour Concentration % SV

Figure 3.2: Odour Sensitivity Varies Widely Across Olfactory Receptor Neurons

A) Imaging was conducted at the glomerular layer to detect GCaM6f-mediated fluorescence in olfactory receptor neurons. B) Field of view in an OMPxGCaMP6f mouse, with example glomeruli highlighted. C) Time course and D) integral response curves for 3 s presentations of ethyl tiglate and isoamyl acetate for glomeruli highlighted in B. E) Number of responsive glomeruli as a function of odour concentration for 3 s presentations of ethyl tiglate and isoamyl acetate (N = 13). F) Extent of glomerular overlap between ethyl tiglate and isoamyl acetate for data shown in E, expressed as a Jaccard index. See methods for more detailed information.

generated by a given odour stimulus (Figure 3.2D). As expected and as has been reported previously (*261-265*), we found that the number of responsive glomeruli increased linearly with odour concentration for both test odours ethyl tiglate and isoamyl acetate (Figure 3.2E). We quantified the degree of glomerular overlap between these two odours at each concentration using a Jaccard index (Figure 3.2F). A Jaccard index of 0 indicates that no glomeruli were dual-responsive to both odours at the concentration in question, whereas an index of 1 signifies that all responsive glomeruli were activated by both odours. Accordingly, we found that the degree of overlap in glomeruli responding to these odours was highest at the strongest concentrations (Figure 3.2F). These results can simply be attributed to differences in receptor affinities, whereby glomeruli that represent receptors with lower affinities for an odour molecule are recruited at higher concentrations, increasing the total number of active glomeruli (Figure 3.2E) and in turn the likelihood of glomerular overlap between both odours (Figure 3.2F) (*32*).

Next, we shifted our focus to the output neurons of the olfactory bulb by imaging PCDH21xGCaMP6f mice. We measured calcium signals at the glomerulus, which indicates the glutamatergic input from olfactory receptor neurons (Figure 3.3A & B). While we continued to use ethyl tiglate as a test odour, we replaced isoamyl acetate with 2-heptanone in these experiments. As a component of mouse urine (*464*), 2-heptanone activates not only the main olfactory bulb but also neurons in the vomeronasal organ (*465*) and accessory olfactory bulb (*13*). As expected, we observed similar response characteristics as those observed in OMPxGCaMP6f mice (Figure

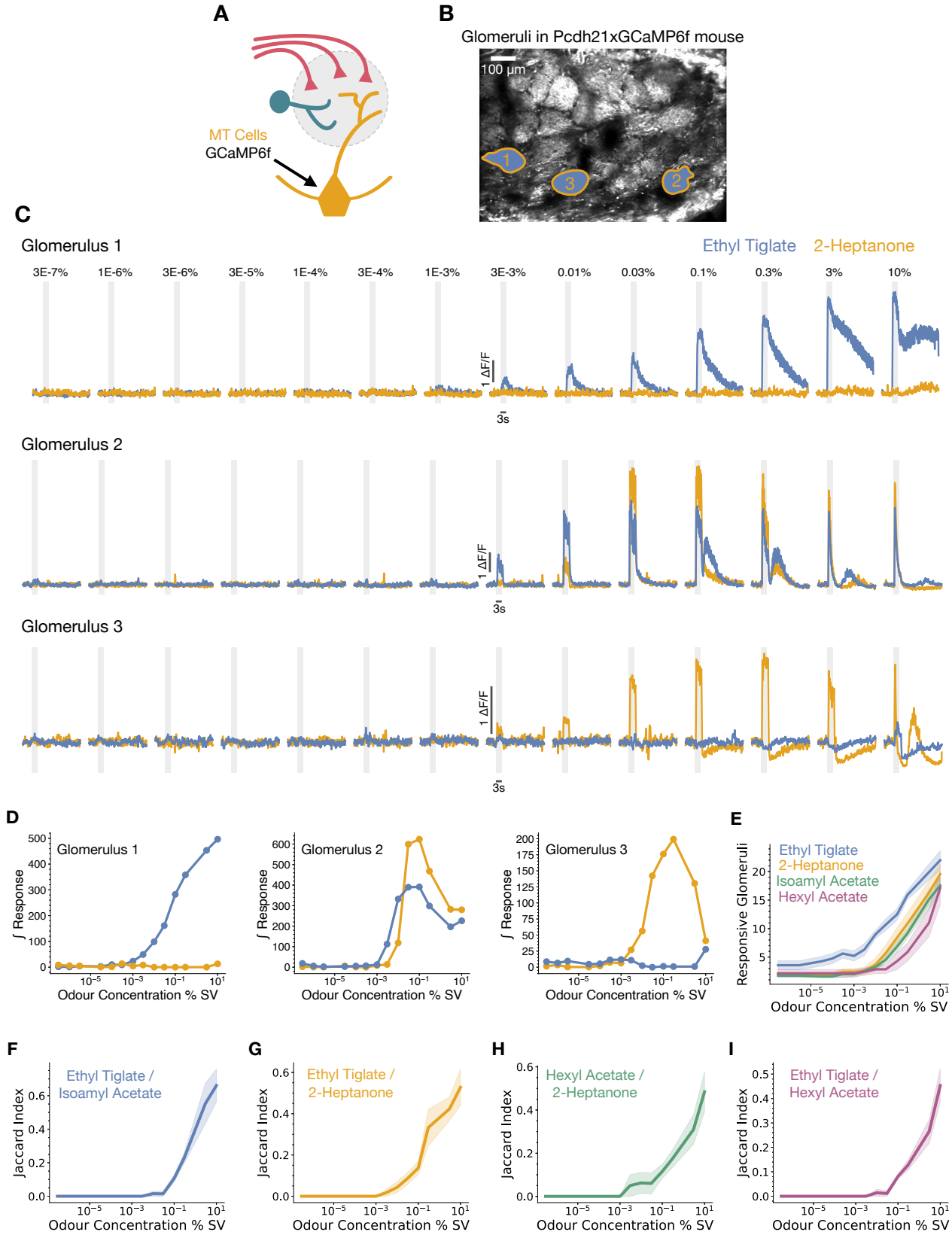
A
MT Cells
GCaMP6f
B
Glomeruli in Pcdh21xGCaMP6f mouse
100 µm
1
3
2
C
Glomerulus 1
Ethyl Tiglate
2-Heptanone
3E-7%
1E-6%
3E-6%
3E-5%
1E-4%
3E-4%
1E-3%
3E-3%
0.01%
0.03%
0.1%
0.3%
3%
10%
1 ΔF/F
3s
Glomerulus 2
Glomerulus 3
D
Glomerulus 1
Glomerulus 2
Glomerulus 3
∫ Response
Odour Concentration % SV
E
Ethyl Tiglate
2-Heptanone
Isoamyl Acetate
Hexyl Acetate
Responsive Glomeruli
Odour Concentration % SV
F
Ethyl Tiglate / Isoamyl Acetate
G
Ethyl Tiglate / 2-Heptanone
H
Hexyl Acetate / 2-Heptanone
I
Ethyl Tiglate / Hexyl Acetate
Jaccard Index
Odour Concentration % SV

Figure 3.3: Odour Sensitivity Varies Widely Across Mitral and Tufted Cells

A) Imaging was conducted at the glomerular layer to detect GCaM6f-mediated fluorescence in mitral/tufted cells. B) Field of view in a Pcdh21xGCaMP6f mouse, with example glomeruli highlighted. C) Time course and D) integral response curves for 3 s presentations of ethyl tiglate and 2-heptanone for glomeruli highlighted in C. E) Number of responsive glomeruli as a function of concentration for 3 s presentations of ethyl tiglate (N = 10), 2-heptanone (N = 7), isoamyl acetate (N = 7) and hexyl acetate (N = 7). F-I) Extent of glomerular overlap odour pairs for data shown in A, expressed as a Jaccard index.

3.3C & D, note that numbered glomeruli are not the same as those shown in Figure 3.2B-D for OMPxGCaMP6f mice). Glomeruli again displayed varying levels of sensitivities to the test odours, with some more selective to either ethyl tiglate or 2-heptanone, while a fraction exhibited comparable responsiveness to both (Figure 3.3C, top, bottom, or middle, respectively). The similarities observed between PCDH21xGCaMP6f and OMPxGCaMP6f mice (Figure 3.2) are not surprising, since output neuron response kinetics reflect contributions from several thousand olfactory receptor neurons converging at the same glomerulus (*35*, *104*, *105*). For all four of the odours tested, we again found that the number of responsive glomeruli increased with odour concentration (Figure 3.3E). Furthermore, the degree of overlap between responsive glomeruli also increased with odour concentration for all odour pairs (Figure 3.3E-I). Together, these data highlight that neurons which input to and output from the olfactory bulb exhibit a broad range of odour sensitivities, with patterns of glomerular activity becoming more similar across odours at higher concentrations.

3.2 Relative Odour Strength and Stimulus Duration Influence Adaptation

How do neurons of the olfactory bulb adapt their responses to sustained stimuli? Do the features of adaptation differ based on the strength of the stimulus and the sensitivity of the olfactory receptor? To address these questions, we presented mice with 60 s odour stimuli to more closely mimic the conditions encountered when an animal enters a new odour environment. We implemented a simple metric to quantify the degree of neuronal adaptation evoked by an odour stimulus, which we

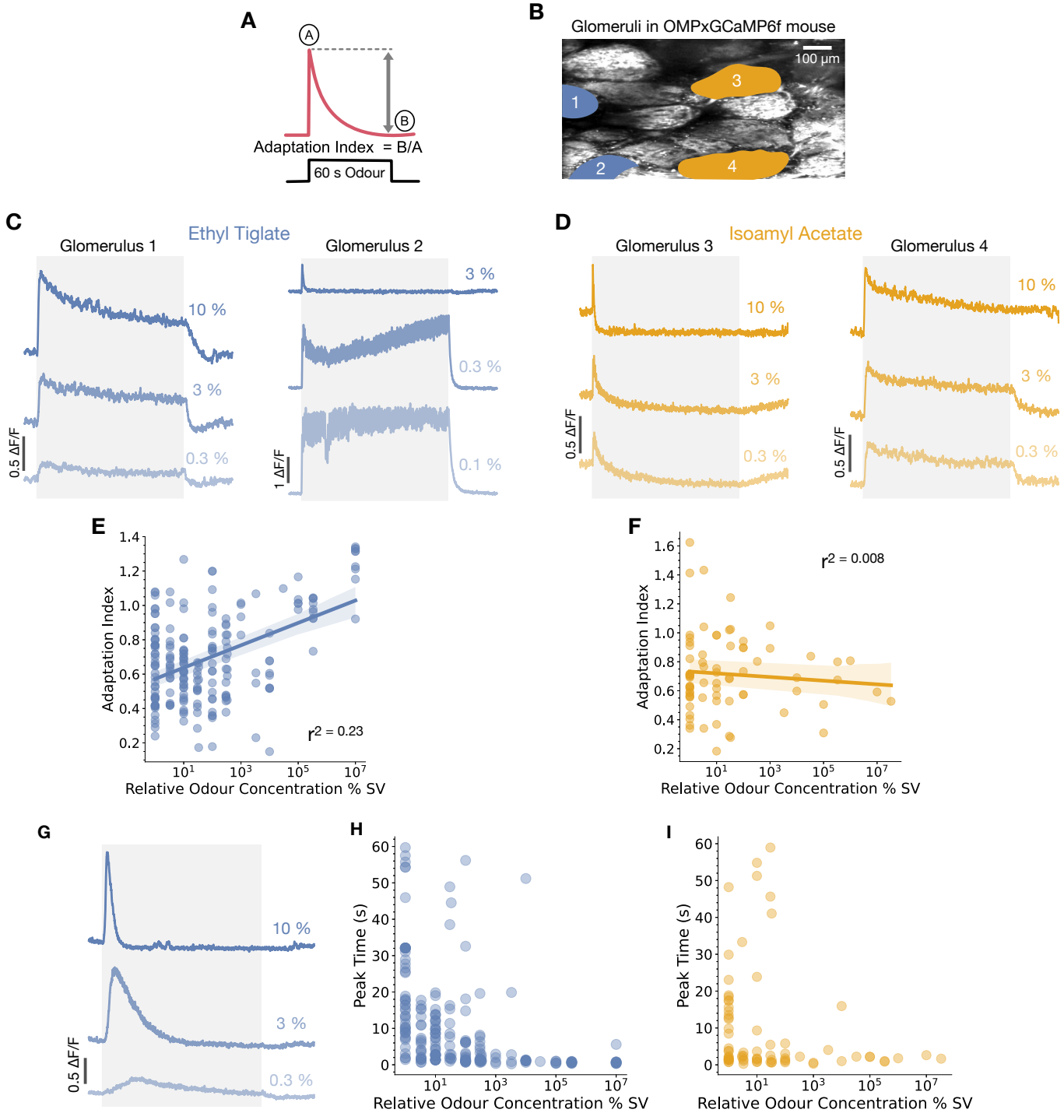

Figure 3.4: The Extent and Rate of Adaptation Vary with Relative Odour Strength

A) Adaptation index calculation, where A represents the peak response amplitude and B represents the mean response amplitude over the last second of the stimulus period. B) Field of view in an OMPxGCaMP6f mouse. C) Responses from example glomeruli for 60 s presentations (grey) of ethyl

tiglate and D) isoamyl acetate, highlighting the influence of odour concentration on adaptation. E) Adaptation indices for glomeruli as a function of relative odour concentration for ethyl tiglate (N = 13, p = < 0.001, Pearson correlation test) and F) isoamyl acetate (N = 7, p = 0.46, Pearson correlation test). Relative odour concentration was calculated by dividing the presented concentration by the lowest concentration of a given odour that a glomerulus first responded to. G) Responses from example glomerulus highlighting the acceleration of response peaks with increasing concentrations of ethyl tiglate. H) Peak response times as a function of relative odour concentration for ethyl tiglate (N = 13) and I) isoamyl acetate (N = 7).

refer to as an 'adaptation index' (AI) (Figure 3.4A). The AI is calculated by dividing the mean response amplitude over the final 1 s of the odour stimulus (B) by the peak response amplitude across the entire stimulus period. An AI of 1 reflects complete adaptation during the stimulus period, whereas an AI >1 indicates that the ΔF/F signal has dropped below the pre-stimulus baseline, which could arise from a decline in the basal firing rates of the several thousand olfactory receptor neurons that converge at the glomerulus. We first measured odour adaptation in olfactory receptor neurons by imaging glomeruli in OMPxGCaMP6f
mice (Figure 3.4B). Within a field of view, the extent of odour adaptation differed markedly based on both the odour and the concentration at which it was presented (Figure 3.4C & D). For the odour ethyl tiglate, the amount of adaptation exhibited by glomeruli generally increased with odour concentration (Figure 3.4C). In contrast, concentration seemed to have little effect on adaptation to isoamyl acetate (Figure 3.4D). Could these differences be explained by receptor affinities? If a receptor has a greater affinity for a particular odour molecule, the strength of the response—and consequently, the degree of adaptation, assuming these two variables are related—would be greater compared to others when presented at the same concentration. Using data obtained from our input-output curves (Figures 3.1-3), we plotted adaptation indices for all glomeruli as a function of what we term 'relative odour concentration'. This metric was calculated by dividing the presented concentration by the lowest concentration of the odour that elicited a response. Across all mice, the amount of glomerular adaptation increased with the relative concentration of ethyl

tiglate (Figure 3.4E). Although the strength of this linear relationship was weak, this association was statistically significant ($r^2 = 0.23$, $p = < 0.001$, Pearson correlation test, N = 13), whereas for isoamyl acetate these paramters werent related (Figure 3.4F, N = 7, $r^2 = 0.008$, $p = 0.46$, Pearson correlation test). We also noted a relationship between relative odour strength and the time taken for odour-evoked amplitudes to reach their peak (Figure 3.4G-I). Across all glomeruli, the latency to peak response amplitude reduced with increasing concentrations of both ethyl tiglate (Figure 3.4H, N = 13) and isoamyl acetate (Figure 3.4I, N = 7). This is consistent with reports that stronger stimulation accelerates the onset of action potentials in olfactory receptor neurons (*89*, *365*, *370-373*). These data indicate that relative odour strength influence the extent and rate of glomerular adaptation, at least for ethyl tiglate.

In a small subset of glomeruli, we observed a distinct transition from a sustained odour response at lower concentrations, to rapid adaptation at higher concentrations (Figures 3.4C, glomerulus 2, Figure 3.4D, glomerulus 3, and Figure 3.5B-D). Within a given mouse, only a few of these glomeruli were detected for each of the test odours (ethyl tiglate = 1.7 ± 0.2 glomeruli, 2-heptanone = 2.4 ± 0.7 glomeruli, hexyl acetate = 1.2 ± 0.2 glomeruli, isoamyl acetate = 1.2 ± 0.2 glomeruli, mean ± SEM); however, it is worth noting that our ability to detect these adaptive glomeruli was biased by both the size of the cranial window and the imaging location on the dorsal surface of the olfactory bulb. Nevertheless, we observed that ethyl tiglate-adaptive glomeruli were consistently situated within the medial region of the dorsal surface, whereas hexyl acetate and 2-heptanone-adaptive glomeruli were almost invariably positioned more caudally (Figure 3.5A, two separate medial and lateral field of views merged). A common trait among these adaptive glomeruli is that they are generally the most sensitive to the odour to which they rapidly adapt, being the first and often only to respond to relatively dilute concentrations (Figure 3.5B-D). Furthermore, the dynamic ranges of these glomeruli were similar for their preferred odour across animals, as illustrated in Figure 3.5E-H, for the ~2 glomeruli detected for each odour in each mouse. Aside from a couple of glomeruli (2 out of 15), ethyl tiglate-sensitive glomeruli responded robustly to the full suite of odour concentrations presented ($3x10^{-7}$ ± 0 %

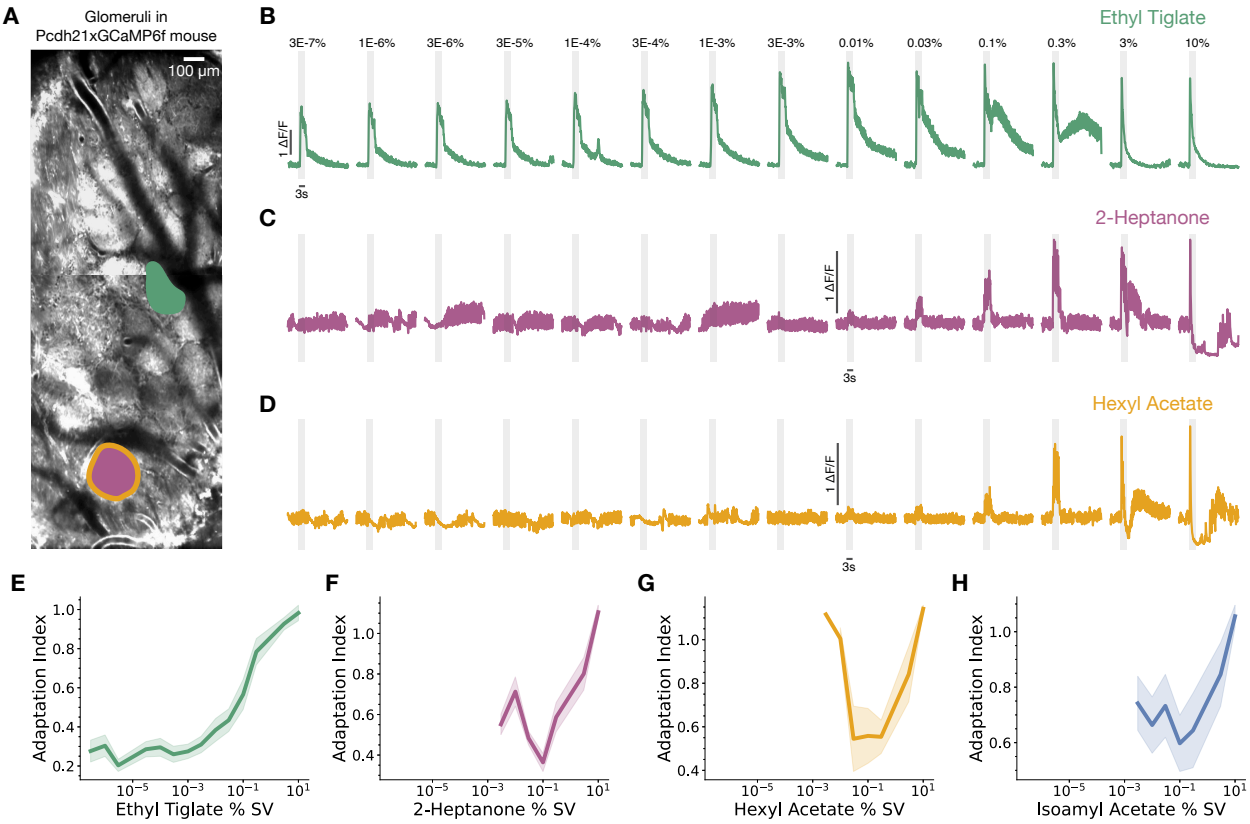

Figure 3.5: Glomeruli Most Sensitive for an Odour Rapidly Adapt at High Concentrations

A) Two fields of view merged in an Pcdh21xGCaMP6f mouse, with responses from example glomeruli across a wide range of concentrations for B) ethyl tiglate, C) 2-heptanone and D) hexyl acetate. E-H) Adaptation indices for glomeruli which transition from a sustained odour response to rapid adaptation at higher concentrations for E) ethyl tiglate (N = 9), F) 2-heptanone (N = 7), G) hexyl acetate (N = 5) and H) isoamyl acetate (N = 5).

SV response threshold), rapidly adapting to concentrations in the range of 0.1 - 10 % SV (3 ± 2.6 % SV, median ± MAD, N = 9). In contrast, responses from glomeruli sensitive to 2-heptanone, hexyl acetate, and isoamyl acetate were restricted to 0.01 - 10 % SV, with thresholds of 0.01 ± 0 % SV (N = 7), 0.02 ± 0.01 % SV (N = 5), and 0.02 ± 0.1 % SV (median ± MAD, N = 5), respectively, rapidly adapting at 3 - 10 % SV (10 ± 0 % SV, median ± MAD for all three odours). Interestingly, we found that glomeruli which rapidly adapt to higher concentrations of hexyl acetate always did so for higher concentrations of 2-heptanone (6 out of 6 glomeruli detected, N = 5), most likely due to

their structural similarity.

The transition from a mostly sustained odour response to a rapid adaptive one was even more apparent with 60 s odour presentations (Figure 3.6A & B). Within a single field of view, glomeruli which switched response profiles were detected for multiple odours (Figure 3.6A), and when compared with 3 s odour pulses of the same strength, the extent of adaptation was greater for 60 s stimuli (Figure 3.6B, $p = 0.048$ for $1x10^{-3}$ % SV, $p = 0.0048$ for $3x10^{-3}$ % SV, $p = 0.001$ for 0.1 % SV, $p = 0.005$ for 3 % SV, $p = 0.003$ for 1E-3 %, N = 11, paired t-tests, two-tailed with Bonferroni correction, odours included were ethyl tiglate, 2-heptanone, isoamyl acetate and hexyl acetate). The impact of odour concentration on adaptation was also more notable in this subset of adaptive glomeruli than in the glomerular fraction combined (compare Figure 3.6C with 3.4C, $r^2 = 0.41$, $p = < 0.001$, Pearson correlation test, N = 11, odours included were ethyl tiglate, 2-heptanone, isoamyl acetate, hexyl acetate and methyl valerate). These data show that a small number of glomeruli on the dorsal surface of the olfactory

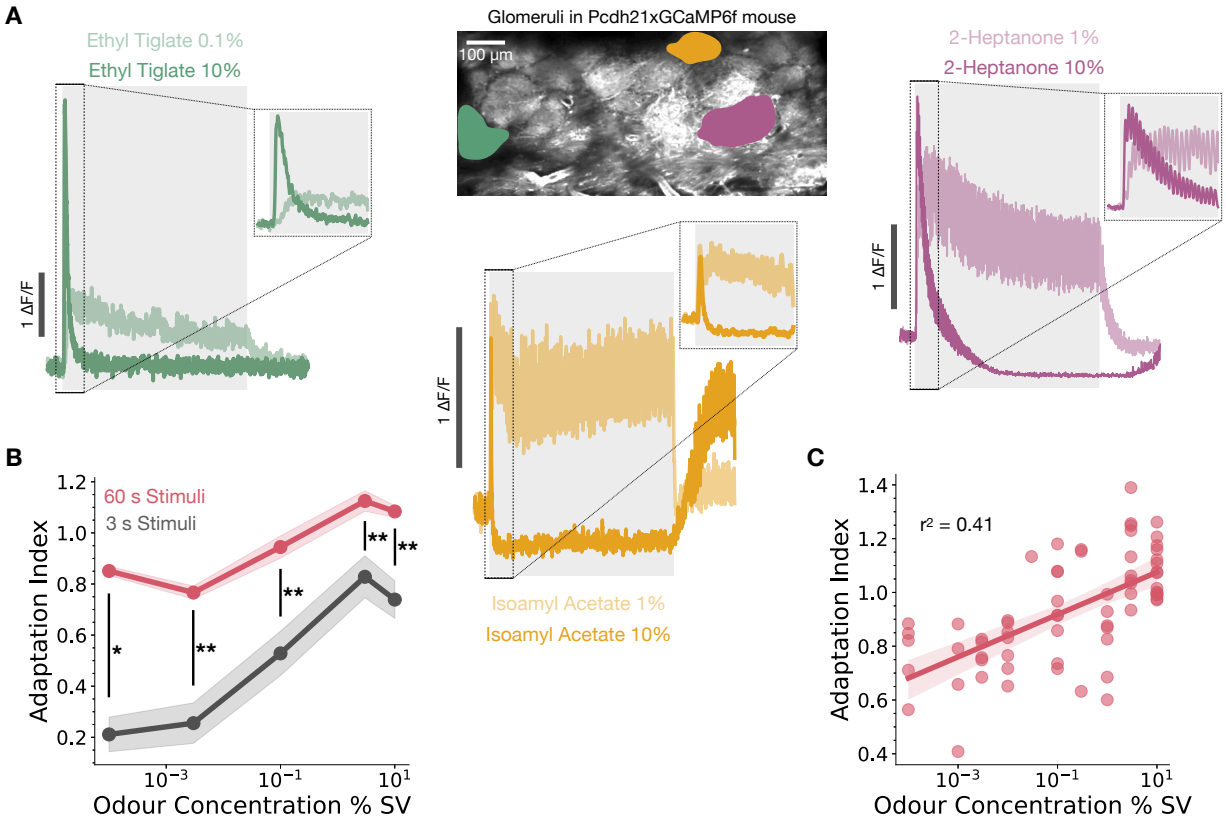

Figure 3.6: Stimulus Duration and Odour Concentration Enhance Adaptation in the Most Sensitive Glomeruli

A) Field of view in a Pcdh21xGCaMP6f mouse and responses from example glomeruli for 60 s presentations of ethyl tiglate, isoamyl acetate and 2-heptanone. Note the transition from a sustained odour response at low concentrations to rapid adaptation at high concentrations. B) Adaptation indices for glomeruli in response to 3 s and 60 s presentations of ethyl tiglate, isoamyl acetate, 2-heptanone, and hexyl acetate (N = 11). Two-tailed paired t-tests with Bonferroni corrections were carried out at $1x10^{-4}$% SV (p = 0.0096, N = 2), $3x10^{-3}$ % SV (p = < 0.001, N = 3), 0.1 % SV (p = < 0.001, N = 6), 3 % SV (p = 0.001, N = 6) and 10 % SV (p = 0.0029, N = 5). C) Adaptation indices as a function of absolute odour concentration for the subset of glomeruli that exhibited an adaptive phenotype for ethyl tiglate, isoamyl acetate, 2-heptanone, hexyl acetate and methyl valerate (p = < 0.001, Pearson correlation test, N = 11).

bulb have a broader dynamic range for each monomolecular odour, rapidly switching from sustained to adapted response profiles at higher concentrations.

How do adapted neurons of the olfactory bulb recalibrate to changes in odour intensity? We sought to answer this question by exposing OMPxGCaMP6f mice to a sustained odour stimulus before giving a test step that was either up or down in concentration relative to the adapting concentration. Mice were presented with ethyl tiglate at either 1 % or 10 % SV for 60 s, after which the concentration was either reduced to 1 % or increased to 10 % SV for 20 s, respectively (Figure 3.7A). In line with Figures 3.1-6, there were an assortment of odour responses profiles and adaptation rates detected among glomeruli in a field of view, owing to varying receptor affinities for ethyl tiglate. To assess how glomerular responses are altered in adapted olfactory receptor neurons, we plotted the % change in amplitude of the test pulse due to the 'pre-adapting' step as a function of the AI during the pre-adapting phase. Given that diminished response amplitudes are a hallmark of odour adaptation (*339-341*, *384*), we anticipated that odour-evoked responses would be smaller in adapted neurons than in unadapted ones. Indeed, the amount of adaptation exhibited during the 60 s stimulus predicted the magnitude of amplitude decrement, irrespective of whether the succeeding stimulus was stronger (Figure 3.7B, $r^2 = 0.77$, p = <0.001, N = 7, Pearsons correlation test) or weaker (Figure 3.7C, $r^2 = 0.79$, p = < 0.001, N = 7, Pearson

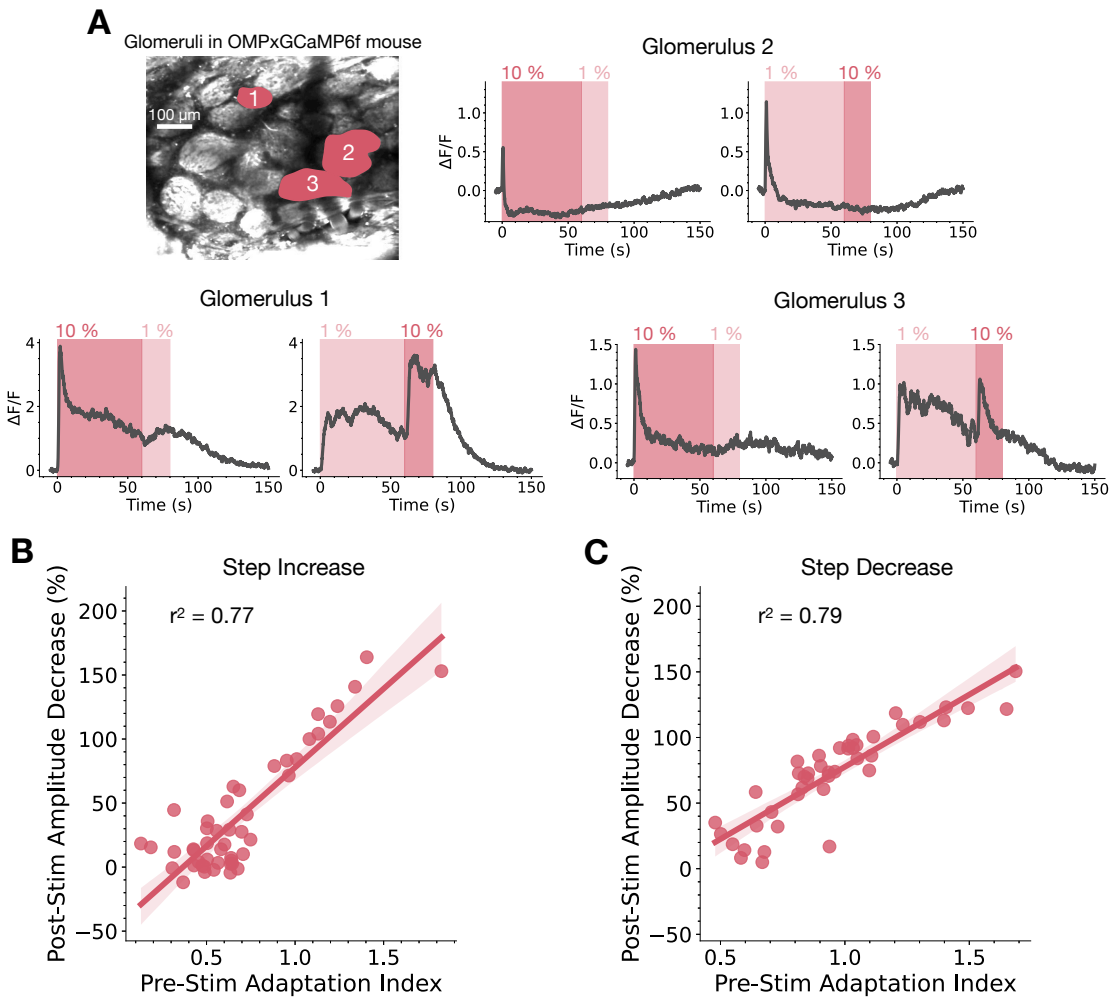

Figure 3.7: Response Amplitudes are Diminished in Adapted Glomeruli

A) Field of view in an OMPxGCaMP6f mouse and responses from example glomeruli to 80 s presentations of ethyl tiglate. Stimulus presentations consisted of a 60 s stimulus at either 10 % or 1 % SV which either decreased to 1 % SV ('step decrease') or increased to 10 % SV ('step increase') for the remaining 20 s, respectively. B & C) Percent amplitude decrease of 20 s odour responses relative to those which were not preceded by a 60 s stimulus, plotted as a function of adaptation indices during the 60 s adapting stimulus for B) step increases and C) step decreases in odour concentration ($p = < 0.001$ for both B and C, Pearson correlation test, N = 7).

correlation test) than the initial adapting stimulus. When mice were presented with a step increase in odour concentration, reductions in response amplitude were most notable in glomeruli that adapted to or beyond baseline during the 60 s adapting stimulus (Figure 3.7A, glomerulus 2). Amplitude shifts were less variable when mice

were presented with a step decrease in odour concentration (Figure 3.7C). This largely stemmed from the fact that responses to 1 % SV were consistently smaller in the adapted state, and glomeruli often even failed to respond at all when the test stimulus was weaker than the initial adapting one (Figure 3.7A, all glomeruli). Interestingly, glomeruli which were particularly sensitive to ethyl tiglate across a wide range of concentrations (shown in Figure 3.5A,B & E) responded to neither a step increase or step decrease in odour concentration, rapidly entering into an adapted state that persisted throughout the entire stimulus periods (Figure 3.7A, glomerulus 2). These data demonstrate that the amount of adaptation a glomerulus undergoes during a given odour stimulus largely determines the strength at which it responds to subsequent stimuli.

3.3 Recovery is Delayed in Adapted Neurons

It has been widely reported that neurons adapt to stimuli delivered in rapid succession (*339-341*). We quantified this adaptation in mitral/tufted cells by presenting mice with a sequence of odour pulses identical in identity and concentration (Figure 3.8A). There was a significant difference detected between glomerular response amplitudes across consecutive odour presentations (Figure 3.8B, $p = < 0.001$, repeated measures ANOVA, $N = 5$). We found that, on average, the initial odour pulse was 58 % larger in amplitude than the subsequent 7 pulses, with response amplitude stabilising from the second pulse onward (Figure 3.8B, 1st pulse = 2.81 ± 0.35 ΔF/F, 2nd-8th pulse = 1.77 ± 0.16 ΔF/F, mean ± SEM, $p = 0.03$, paired t-test, two-tailed, $N = 5$). Based on our finding that relative odour strength influences the amount of adaptation (Figures 3.4C-F and 3.6C), we probed whether relative odour concentration also influenced this fast and seemingly stable level of adaptation, by presenting mice with odour pulse sequences at different concentrations (Figure 3.8C). In line with our previous data, the pulse-evoked amplitude decrease that a given glomerulus exhibited increased linearly with relative odour concentration (Figure 3.8D, $r^2 = 0.42$, $p = < 0.001$, Pearson correlation coefficient, $n = 4$). This effect would have likely been more

pronounced if all mice had been presented with the full suite of odour concentrations used in our earlier experiments (Figure 3.1), as a portion of animals were exposed to only part of it. For these glomeruli the lowest concentration delivered was set to 1, which is likely to give larger % decreases at lower relative concentrations. Nevertheless, these data demonstrate that the relative strength of the odour pulse predicts the amplitude decrement exhibited to subsequent stimuli. This short-term adaptation likely originates in olfactory receptor neurons (*339-341*), and recent data indicate that full recovery in mitral/tufted glomeruli takes only a few minutes (*466*). Aside from minor pulse-to-pulse variability, the response amplitude was largely stable after the first pulse; therefore, we did not focus on this phenomenon.

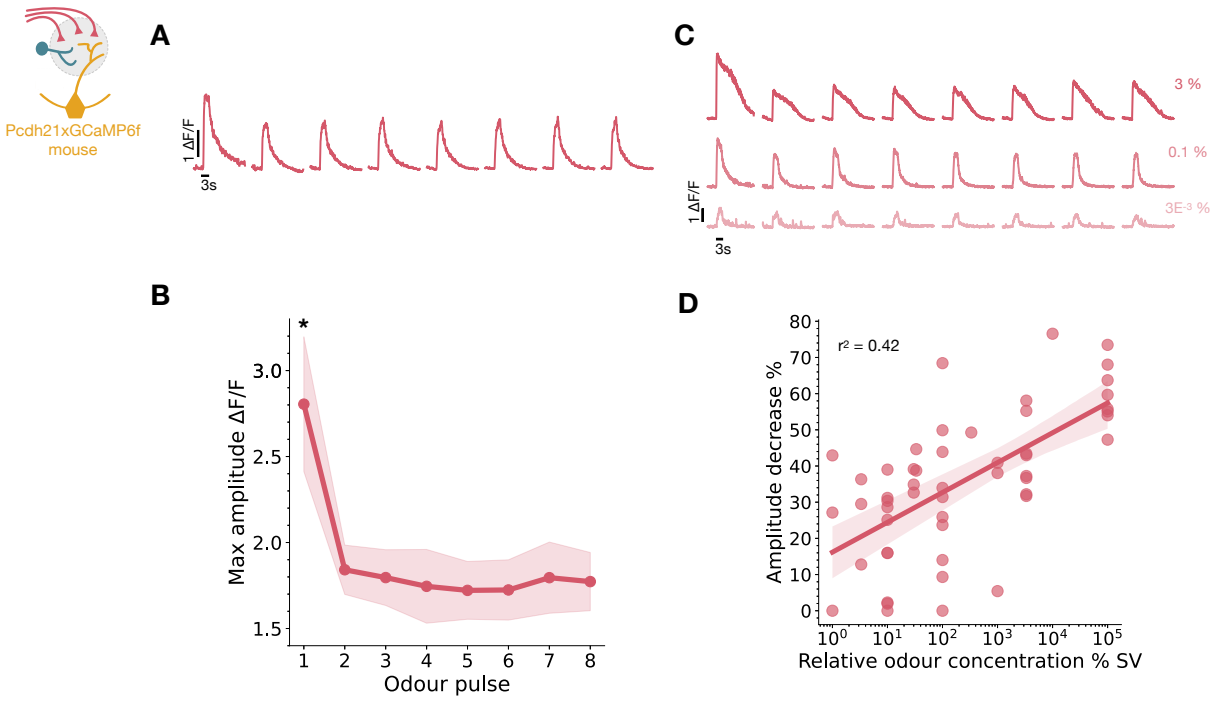

Figure 3.8: Sustained Adaptation is Enhanced by Relative Odour Concentration

A) Glomerular response time course, representative example of 'sustained adaptation' following 3 s presentations of equal concentration odour pulses, 20 s inter-stimulus interval, 0.1 % SV ethyl tiglate. B) There was a significant difference detected in glomerular response amplitudes across consecutive odour pulses ($1x10^{-4}$ - 3 % SV ethyl tiglate testing stimulus, data is presented as mean ± SEM, p = < 0.001, repeated measures ANOVA, N = 5). Asterisk indicates significance of 1st pulse compared to the mean of the remaining pulses (p = 0.03, paired t-test, two-tailed, N = 5). C) Glomerular response time course for three concentrations of ethyl tiglate pulse trials, representative example of the impact relative odour

concentration has on sustained adaptation. D) The extent of amplitude decrease during fast adaptation increases with relative concentration of ethyl tiglate, n = 4, p = < 0.001, r2 = 0.33, Pearson correlation test. Relative odour concentration was calculated by dividing the test concentration by the lowest concentration a glomerulus responded to.

Once neurons enter into an adapted state, how long does it take for them to recover? We defined recovery rate as the time constant taken for response amplitudes to return to their pre-adapted levels. We again presented mice with a series of same-strength odour pulses with 20s inter-stimulus-intervals, this time followed by a 60 s stimulus which was either weaker, equal to, or stronger than the pulse stimuli, before resuming pulse delivery (Figure 3.9A). Recovery was evaluated by comparing the post-60 s peak response amplitudes to the average peak amplitude of 3-5 pulses immediately preceding the 60-s stimulus. An exponential function was fit to determine the recovery time course, as demonstrated in Figure 3.9B for the example glomerulus responding to a stronger stimulus, shown in Figure 3.9A. The majority of glomeruli in both OMPxGCaMP6f and Pcdh21xGCaMP6f mice (1 in 10 and 2 in 8, respectively) did not exhibit a decrement in response amplitude following 60 s presentations of any strength. However, as illustrated in Figure 3.9B, a sustained stimulus stronger than the initial pulses delayed recovery in some glomeruli, characterised in this instance by a time constant (τ) of 26.7 s. After observing that the amount of adaptation induced by stronger stimuli was often larger in these affected glomeruli (FIgure 3.9A), we plotted the adaptation indices from stronger 60 s stimuli against the time constants for these affected glomeruli. We found that, although not significant, the amount of adaptation a glomerulus underwent was predictive of the time it took to recover (Figure 3.9C, r^2 = 0.31, p = 0.095, Pearson correlation test, N = 3 Pcdh21xGCamp6f, N = 2 OMPxGCaMP6f). This effect would likely have been more pronounced given a larger n number, as there were only ever one to a few of these glomeruli detected in each mouse. Together, these data indicate that neurons of the olfactory bulb enter an adapted state after first experiencing an odour, and those that undergo the most adaptation take longer to recover.

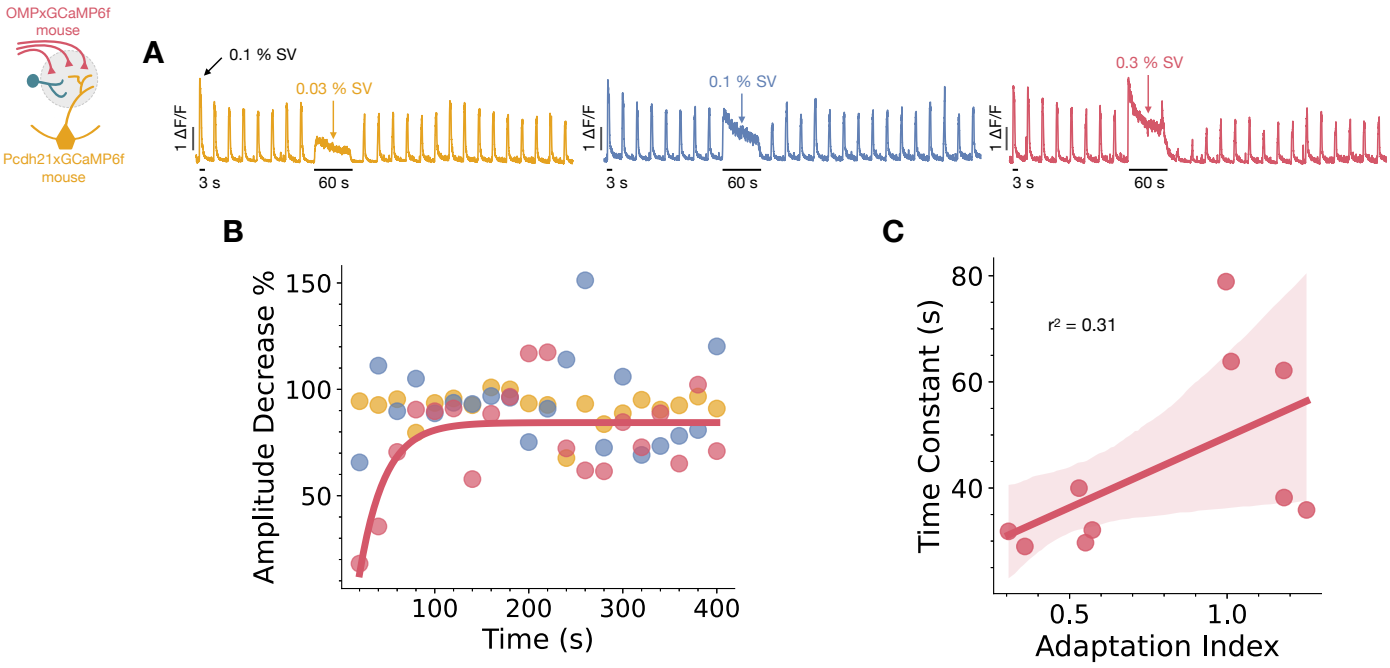

Figure 3.9: Adaptation Delays Recovery to Baseline Response Amplitudes

A) Response time courses for example glomerulus in a Pcdh21xGCaMP6f mouse. Odour delivery protocols consisted of 3 s odour pulses at a fixed concentration (in this case, 0.1 % SV ethyl tiglate) followed by a 60 s presentation of the same odour at a concentration that was either weaker (yellow, 0.03 % SV), equal (blue), or stronger (red, 3 % SV) in concentration, after which pulse presentations were resumed. B) Percent peak amplitude decrease (points) of post-60 s odour pulses relative to the average peak amplitude of the 3-5 odour pulses preceding the 60 s stimulus, plotted as a function of time, for example glomerulus and concentrations shown in A. Red line represents recovery time constant (τ = 26.7 s) following the 60 s stimulus presented at a stronger concentration. C) Time constants as a function of adaptation indices for glomeruli which exhibited delayed recovery to their pre-60 s peak response amplitudes, each point represents a glomerulus ($p = 0.095$, Pearson correlation test, N = 3 Pcdh21xGCamp6f, N = 2 OMPxGCaMP6f).

Chapter 4: Transmission Failure to a Single Glomerulus Culminates in Odour Constancy Break Down

4.1 Odour Concentration Generates Perceptual Shifts

To evaluate whether varying concentrations of an odourant are perceptually distinct to mice, we utilised a cross-habituation assay, a commonly used method for assessing a rodent's ability to distinguish between different odours (*467-471*). We employed an automated approach based on Qiu *et al.* (*452*), where mice were placed in a test chamber equipped with a nose-poke odour port featuring a beam-break that logged investigation time (Figure 4.1A & B, see methods). In a traditional cross-habituation assay, mice habituate to a given odour when repeatedly presented with it, evidenced by a gradual reduction in investigation time. When exposed to a novel odour, mice typically begin to re-investigate the odour source, indicating they perceive the new odour as distinct from the initial odour. We adapted this protocol by habituating mice to varying concentrations of the same odourant (Figure 4.1C). Mice were first habituated to the solvent mineral oil before being exposed to ascending concentrations of the test odourant, with each concentration presented in triplicate (60 s stimulus, 60 s inter-stimulus interval).

Interestingly, the initial presentation of mineral oil always evoked more interest than subsequent presentations (Figure 4.1D, N = 32), corroborating an earlier report that mice are able to detect mineral oil (*472*) despite it generally being considered an odourless solvent. The cross-habituation assay relies on mice being able to detect an odour and choosing to investigate it. To this end, we first used 2-heptanone, a component of mouse urine (*464*), anticipating that mice would be inherently interested in this odourant, providing they could detect it. Indeed, when presented with the most dilute concentration tested ($6x10^{-7}$ %), mice investigated the odour source significantly more than the solvent ($p = < 0.001$, post-hoc Wilcoxon signed-rank test, Bonferroni corrected, N = 32) and quickly habituated to subsequent exposures (Figure 4.1D). This habituated state persisted even when mice were exposed to a 100-fold stronger

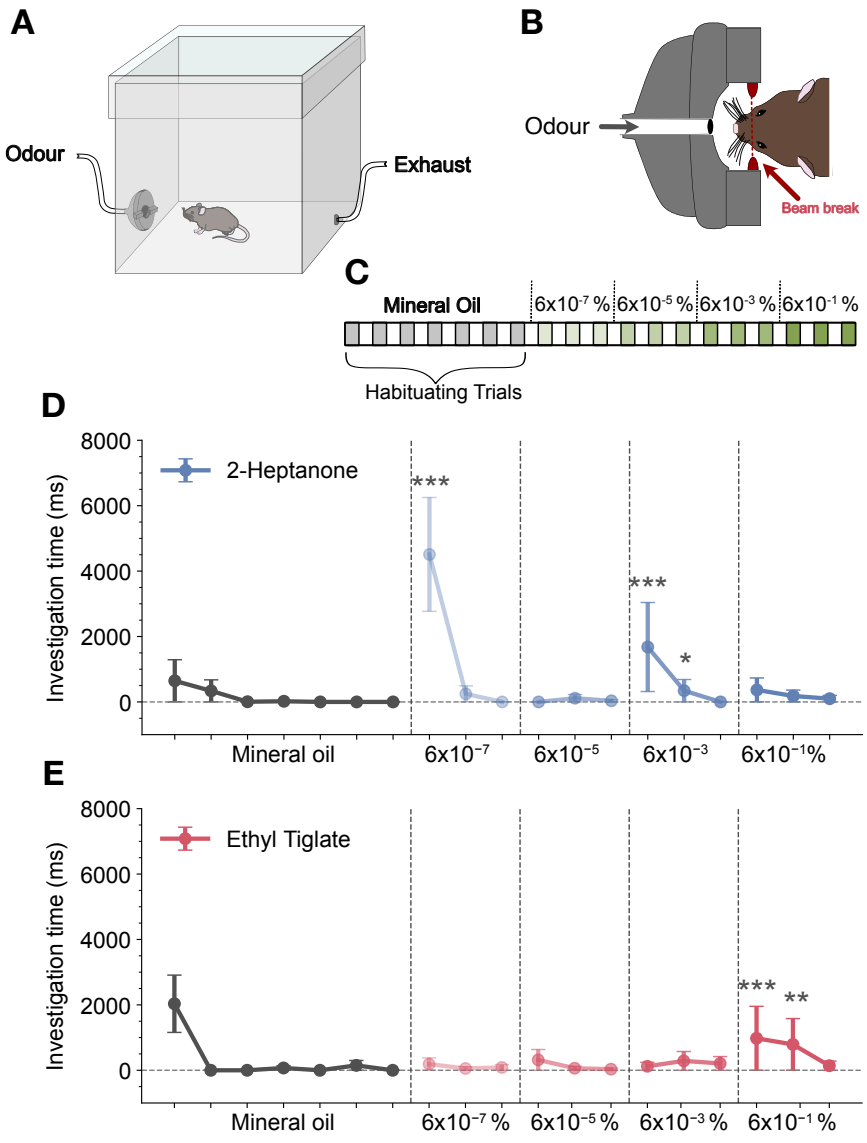

Figure 4.1: Measuring Changes in Odour Perception as a Function of Concentration

A) Experimental paradigm, mice were placed in a test chamber equipped with an odour delivery port and exhaust. B) Contained within the odour delivery port was a nose poke and beam break sensor to record investigation time. C) Odour delivery protocol, each block represents 60 s (60 s stimulus, 60 s inter-stimulus interval). D) Odour investigation times during the stimulus period for 2-heptanone and E) ethyl tiglate, data are displayed as median ± the median absolute deviation, N = 32. Horizontal dashed lines indicate baseline levels of investigation, calculated from the average across the final 5 solvent presentations. There were significant differences detected between the last 5 oil presentations and presentations of ethyl tiglate ($p = < 0.001$, Friedman test). Asterisks indicate post-hoc significance tests above baseline investigation (Wilcoxon signed-rank test with Bonferroni correction, see methods for

asterisks significance). Odour concentrations are presented as the final concentration measured at the nose poke using a photo-ionization detector. See methods for more detailed information.

concentration at $6x10^{-5}$ % (Figure 4.1D). It was only upon increasing the concentration to 10,000 times that of the original that mice began to investigate significantly more than mineral oil again (Figure 4.1D, $p = < 0.001$, post-hoc Wilcoxon signed-rank test, Bonferroni corrected), displaying a similar habituation pattern to repeated stimuli (Figure 4.1D). This indicates mice perceived a qualitative shift in the odourant between concentrations of $6x10^{-5}$ % and $6x10^{-3}$ %, but not between the lowest and highest pairs of concentrations. We next used ethyl tiglate (Figure 4.1E), an ester family odourant which the mice were naive to. In these instances, mice did not exhibit any interest above that of the solvent until the strongest concentration of $6x10^{-1}$ % was presented (Figure 4.1E, $p = < 0.001$, post-hoc Wilcoxon signed-rank test, Bonferroni corrected). These data suggest mice perceive a qualitative change between concentrations of $6x10^{-3}$ % and $6x10^{-1}$ % for ethyl tiglate (Figure 4.1E).

Esters are reported to have a neutral valence (*473*), and the absence of innate attraction could explain why mice failed to investigate concentrations spanning 6x10-7 - 6x10-3 %. However, to rule out the possibility that this lack of investigation was due to an inability to detect lower concentrations, we developed a method to measure odour sensitivity in mice that is independent of their internal motivation. We surgically fitted mice with a head bar and fixed them in a stereotaxic frame above a treadmill (*474*). The olfactometer output was positioned directly in front of the mouse's nose, enabling us to present odours to the mouse irrespective of the animals interest. With video recording, we tracked key facial features using deeplapcut (*475*) (Figure 4.2A). Pupil dilation is known to occur in both humans and rodents after detection of a novel stimulus (*476-480*), and we find that the lowest concentration of ethyl tiglate (1x10-7 %) induces a notably greater increase in pupil size than solvent presentations which precede them (Figure 4.2B & C, N = 6). Additionally, tracking key points surrounding the snout revealed that nose tip movement relative to the cheek is seemingly in sync with breathing. Moreover, plotting the distance between these keypoints confirmed that

oscillations are in line with typical resting respiration frequencies of ~2-5 Hz (*467*). Strikingly, exposure to ethyl tiglate at 1x10-7 % prompted a significant elevation in frequency content, indicative of sniffing/active exploration (Figure 4.2D-F, N = 6). These data demonstrate that mice can perceive the lowest concentration of ethyl tiglate (6x10-7 %), with detection evoking an increase in pupil size and sniffing behaviour. Collectively, these findings indicate that mice can detect both test odourants at the most dilute concentrations tested, and that increasing concentration generates a perceptual shift, between 6x10-5 - 6x10-3 % for 2-heptanone, and between 6x10-3 - 6x10-1 % for ethyl tiglate. We next sought to uncover the neural basis underlying these seemingly distinct odour percepts which are formed at different concentrations.

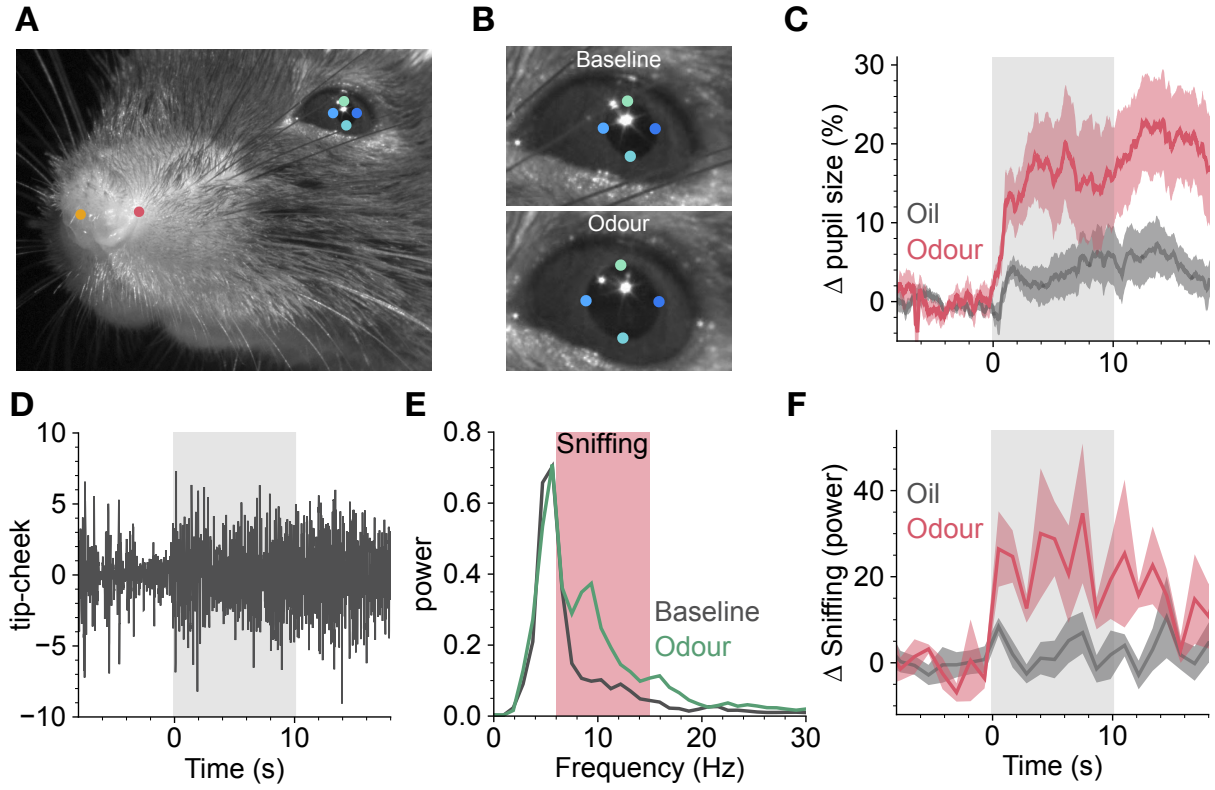

Figure 4.2: Assessing Odour Detection Thresholds Independent of Motivation

A) Mice were head-fixed and key facial features (indicated by coloured dots) were tracked using deeplab cut (see methods for more detailed information). B) Pupil diameter before and after odour exposure, calculated as the mean from the cardinal points. C) Relative change in pupil diameter (mean ± SEM) in response to 1x10^{-7} % ethyl tiglate (red) and three preceding solvent blanks (grey), N = 6, shaded grey area indicates stimulus period. D) Oscillations in the distance between key points for the note tip and

cheek. E) Fourier transforms of data shown in D, for 10 s preceding the stimulus (grey) and during odour exposure (green), shaded red box indicates sniffing band. F) Change in sniffing band power (mean ± SEM) during presentation of $1x^{10}$-7 % ethyl tiglate (red) and three preceding solvent blanks (grey), N = 6, shaded grey area indicates stimulus period. Head-fixed perception tests were conducted by Merve Oncul, and this figure was made by Jamie Johnston.

4.2 A Sparse Code Underlies Odour Percepts

To explore how the brain represents the concentration spectrum presented in Figure 4.1C, we examined our neural recordings captured using *in vivo* 2-photon imaging discussed in Chapter 3. We began by analysing data gathered in mice which had the genetically encoded Ca^{2+} indicator GCaMP6f (*448*) expressed in mitral and tufted cells of the olfactory bulb, driven by the Pcdh21 promoter (*451*) (Pcdh21xGCaMP6f mice, see methods). Mitral and tufted cells constitute the output of the olfactory bulb, receiving direct input from the olfactory nerve on their dendritic tufts situated within a single glomerulus (*109*, *481*, *482*). This single-glomerulus input organisation, combined with active voltage-dependent conductances in the primary dendrite that promote firing (*483-485*), suggests that cell body responses closely mirror those observed in the apical tuft, as shown in previous studies that demonstrated similar response dynamics between glomerular tufts and mitral cell somas (*486-488*). Both mitral and tufted cells are also subject to feedback and feedforward inhibition, which they receive via the dendrodendritic connections they form with periglomerular cells (*109*). The rationale behind first examining activity in the output neurons stemmed from their exposure to this diverse array of circuit mechanisms, increasing the likelihood of detecting key phenomena. We focused our efforts on odour-evoked responses obtained in the glomerular layer, the origin of where these output neurons receive excitation. This approach enabled us to broadly visualise the spatiotemporal pattern of activity that reaches the olfactory bulb (*463*), with each glomerulus corresponding to input from a single olfactory receptor (*35*).

We examined response maps for ethyl tiglate, after observing its wide-ranging effects on the dorsal surface of the olfactory bulb, as previously documented (*487*).

Additionally, we were unable to identify glomerular responses for 2-heptanone at the low end of the concentration range (Figure 3.5C & F), despite evidence that mice can perceive this in our cross-habituation experiments (Figure 4.1D). This implies that the glomeruli detecting 2-heptanone at the lower concentration ranges are not on the dorsal surface of the olfactory bulb. Response maps for ethyl tiglate were generated by averaging glomerular activity over the 3 s stimulus period (Figure 4.3A). As in the cross-habituation experiments, mice were first exposed to the most dilute concentration, with each successive stimulus 3-10 fold stronger. Glomerular responses were detected across the entire concentration spectrum (Figure 4.3A), corroborating our finding that mice can perceive ethyl tiglate over 6 orders of magnitude (Figure 4.1E). Consistent with recent findings (*489*), glomerular responses at the weak end of the concentration spectrum were sparse, with activation generally only evident in a single glomerulus (Figure 4.3A). Each olfactory receptor type is represented by two glomeruli (*104*, *105*); therefore, at least one additional glomerulus—and potentially more—would have been co-active within this range, located either outside our recorded fields of view or beyond the dorsal surface. As expected, the total number of active glomeruli increased dramatically with odourant concentration (Figure 4.3A), as shown in Figures 3.2E & 3.3E, and in accordance with previous reports (*263-265*). Based on our cross-habituation experiments, we assigned labels to the responses to represent each seemingly distinct percept, with concentrations ranging between the weakest stimulus and ~$6x10^{-3}$ % labelled as the 'weak percept', and those above ~$6x10^{-1}$ % labelled as the 'strong percept' (Figure 4.3A). We were unable to effectively identify the precise concentration at which the perceptual shift occurs, a measure likely to vary with nasal patency (*490*); however, it lies between $6x10^{-3}$ and $6x10^{-1}$ %, which we have termed the 'transition range' (Figure 4.3A).

To identify key features of our dataset that may underlie odour percepts, we used a support vector machine (see methods), which attempted to predict the odour percept based on glomerular response amplitudes. Strikingly, this linear classifier was able to categorise neural activity with a 99.8 % success rate (Figure 4.3B, N = 9). Given that the performance was not dependent on the number of glomeruli within a field of

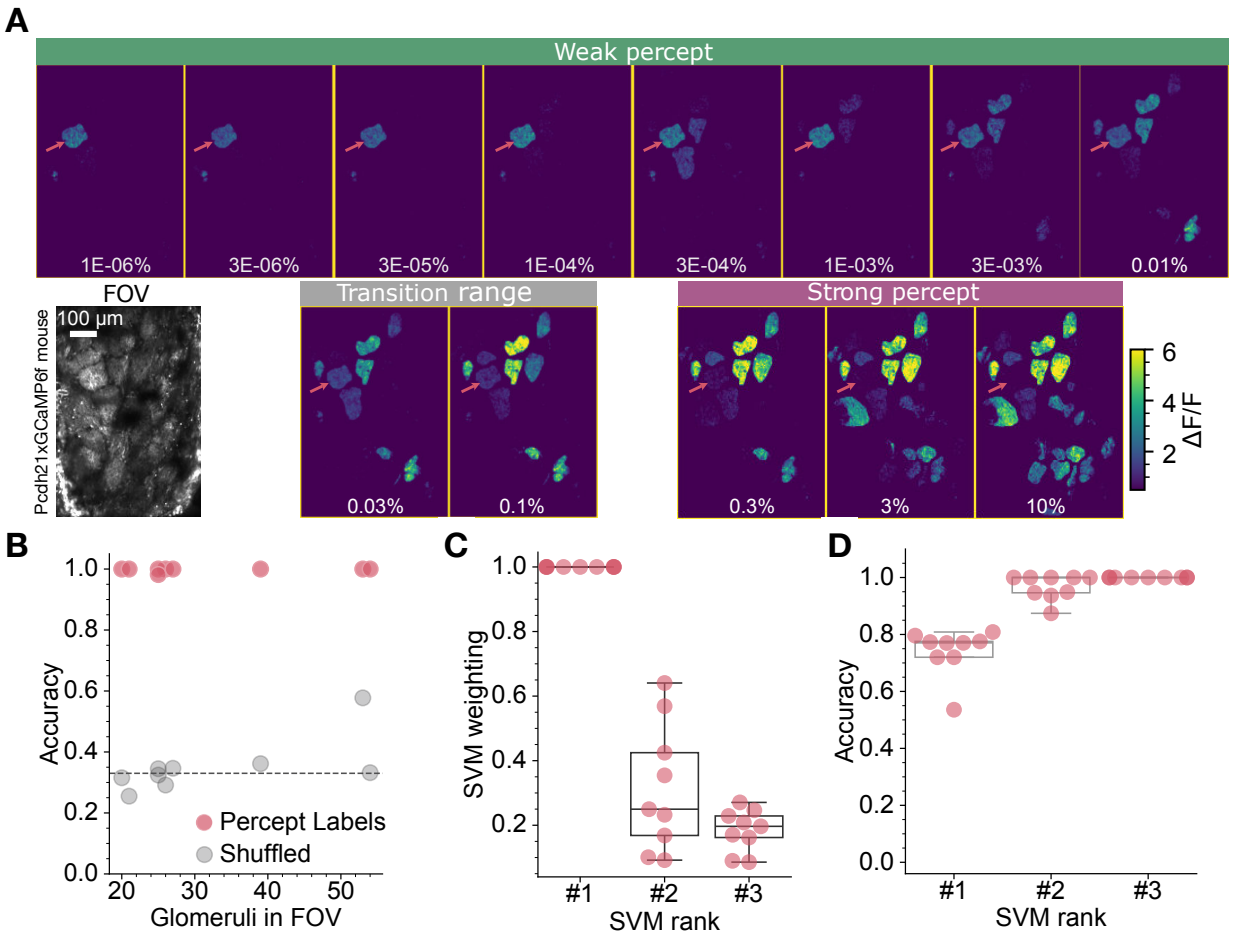

Figure 4.3: Neural Code Underlying Odour Percepts

A) Response maps and corresponding field of view in a Pcdh21xGCaMP6f mouse, displaying mean activity during 3 s presentations of ethyl tiglate at varying concentrations (shown in white). Responses are labelled as weak (green) or strong (purple) percepts (see text). Red arrows highlight the primary glomerulus. B) Performance of a linear SVM classifier using labelled glomerular response amplitudes (red dots, N = 9, see methods), compared with results when labels were shuffled (grey dots). C) Relative weights assigned to the three most important glomeruli for classification, N = 9, the primary glomerulus has a weight of 1. D) Classifier performance using only the top three most important glomeruli identified in B, N = 9. See methods for more detailed information.

view, we next analysed the weights assigned to each glomerulus used in classification, which directly signify the level of contribution a glomerulus makes towards the decision boundary. We find that for each mouse, a single glomerulus is the predominant contributor, with the 2nd and 3rd most important glomeruli weighted as 25 ± 15 % and

19 ± 3 % that of the foremost (Figure 4.3C, mean ± SEM). Remarkably, using responses from only the most important glomerulus, the classifier achieved a mean accuracy of 74 %, which increased to 96.7 % with the inclusion of just the top two glomeruli (Figure 4.3D). This performance is almost equivalent to that obtained using all glomeruli (Figure 4.3B), suggesting that only a few key glomeruli—at least on the dorsal olfactory bulb—are required to encode odour percepts, rather than a widespread pattern of activity.

Earlier work has proposed that odour identity is encoded through a sparse 'primacy' code (*308*, *310*), with the fastest activating glomeruli holding the most importance. Our findings support such a primacy code; for each odour stimulus, we measured the activation time of all responsive glomeruli and ranked each glomerulus in order of activation (Figure 4.4A & B), revealing that glomeruli with the highest predictive value for percept classification were almost invariably the first to activate (Figure 4.4B**,** N = 9). However, this trend held true only for the weak percept; in the strong percept, these glomeruli trailed behind others that became active at higher concentrations (Figure 4.4A & B, N = 9). Notwithstanding, given that these glomeruli made the largest contribution to classifying odour percepts, we refer to them henceforth as 'primary' glomeruli. The most striking characteristic of primary glomeruli is that their response dynamics are distinct for each odour percept, transitioning from a sustained response in the case of the weak percept to rapid adaptation in the strong percept. We employed our adaptation index (AI) metric introduced in Figure 3.4A to quantify the extent of adaptation exhibited by primary glomeruli as a function of concentration. An AI of 1 reflects complete adaptation, whereas an AI > 1 indicates that the ΔF/F signal has fallen below the pre-stimulus baseline, possibly due to a decline in the basal firing rates of the several thousand olfactory receptor neurons that input to a glomerulus. Figure 4.4C illustrates that the amount of adaptation indeed covaries with odour concentration, increasing from 0.34 ± 0.03 at the highest concentration of the weak percept to complete adaptation at the highest concentration of the strong percept with an AI of 1 ± 0.05 (mean ± SEM, p = < 0.001, paired t-test, two-tailed, N = 9). Notably, this shift to near-complete adaptation occurs within the transition range. Together,

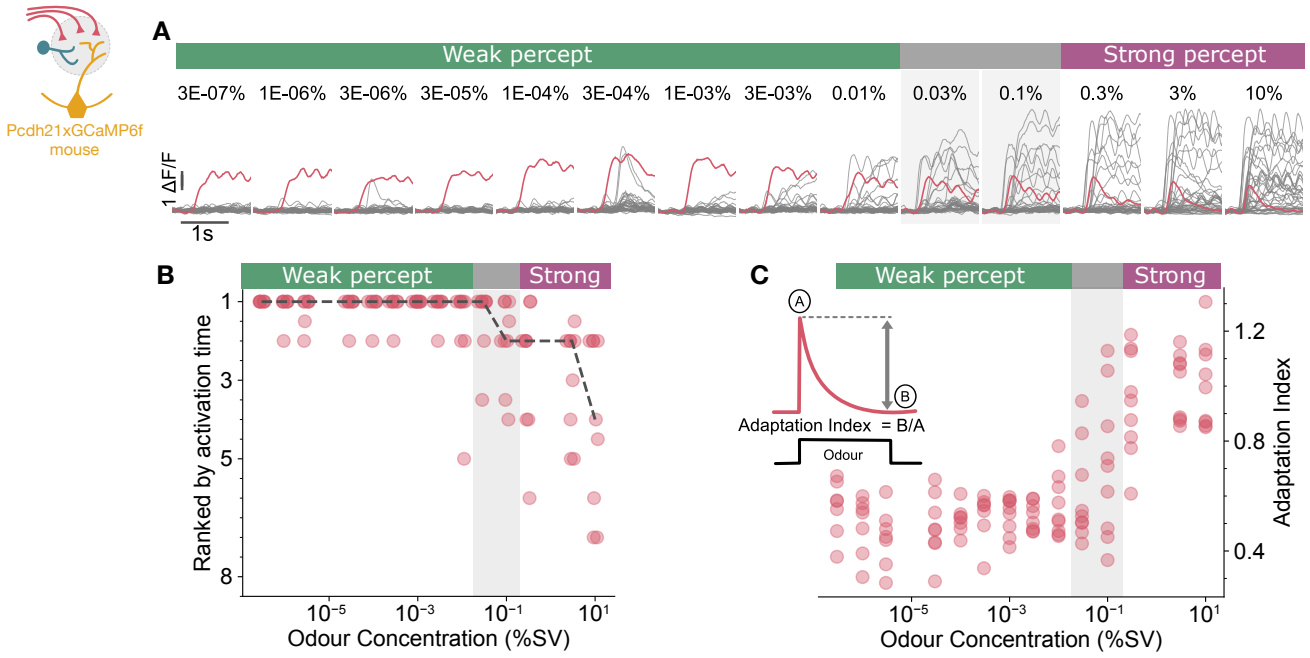

Figure 4.4: Characteristics of the Primary Glomerulus

A) Activity time courses for all glomeruli within a field of view (shown in Figure 4.3A response maps), with the primary glomerulus highlighted in red, sampled at 42 Hz. Coloured bars (top) indicate odour percepts. B) Glomeruli ranked by activation time for all concentrations presented, each dot represents a mouse, with jitter added for clarity. Dashed black line represents the median N = 9. C) Adaptation indices for primary glomeruli as a function of odour concentration, inset shows adaptation index calculation N = 9. See methods for more detailed information.

these data imply that a sparse code comprising only a few glomeruli underlie odour percepts, with rapid adaptation in the primary glomerulus corresponding to a perceptual change.

The dichotomy in primary glomeruli response dynamics to weak and strong percepts is particularly pronounced when a 60-second stimulus is presented to mice (Figure 4.5A), as was used in our cross-habituation experiments (Figure 4.1C). Responses to the weak percept exhibit slow and partial adaptation (AI = 0.75 ± 0.05 N = 5), whereas strong percept concentrations elicit rapid and complete adaptation (Figure 4.5B). Remarkably, responses to these higher concentrations dropped below baseline, with an AI of 1.15 ± 0.04 (Figure 4.5B, mean ± SEM, p = 0.0008, t-test, two-

tailed, for the 5 animals where a 60 s stimulus from both percepts were delivered). Two other notable differences were observed between weak and strong percept responses from primary glomeruli; firstly, peak amplitudes were larger for the weak percept than those for the strong (Figure 4.5C, 2.03 ± 0.54 vs 3.26 ± 1.19 ΔF/F, respectively, p = 0.004, Wilcoxon matched-pairs signed rank test, N = 9), and secondly, strong percept stimuli induced post-stimulus rebound activity, the delay to which extended with stimulus intensity (Figure 4.5D, 1.35 ± 0.28 ΔF/F, N = 8).

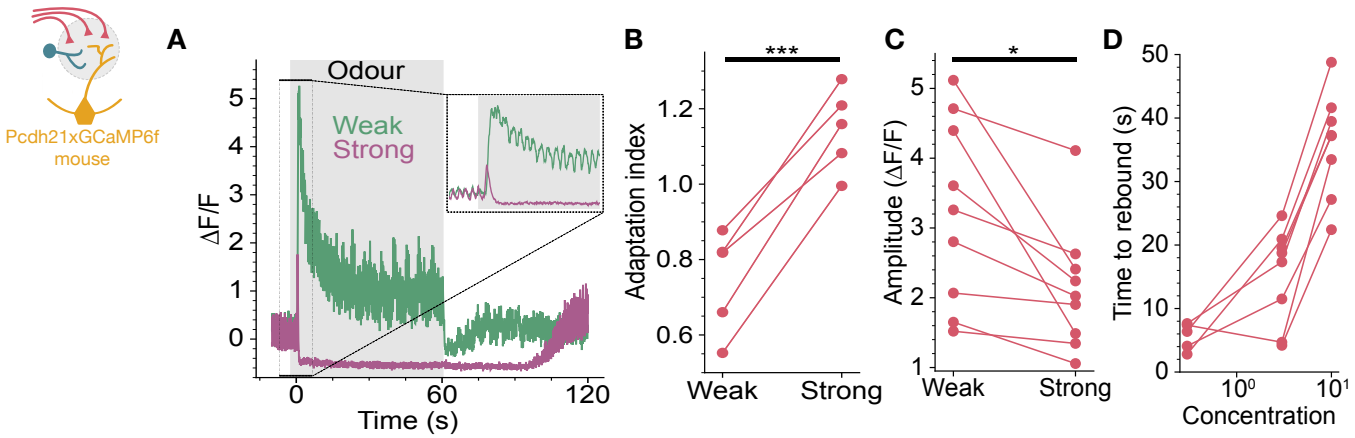

Figure 4.5: Rapid Adaptation Evolves through Distinct Phases

A) Response from a primary glomerulus to a 60 s presentation of ethyl tiglate from the weak ($1x10^{-6}$ %) and strong (3 %) percept. Inset provides an expanded view of the brief peak and sharp drop below baseline. Note the rebound in activity which arises long after the stimulus period. B) Adaptation indices exhibited by primary glomeruli in response to 60 s presentations of ethyl tiglate from the weak and strong percept, p = 0.0008, t-test, two-tailed, N = 5. C) Response amplitudes from primary glomeruli were larger for a 3 s stimulus from the weak percept ($3x10^{-3}$ %) than those from the strong (10 %), p = 0.004, Wilcoxon matched-pairs signed rank test, N = 9. D) Delay of the rebound activity extends as stimulus strength increases, obtained from 3 s stimuli N = 8.

A key premise of the aforementioned primacy code rests on the ability of mice to innately identify odours within < 200 ms and < 100 ms with training (*308*, *310*). To explore the neural mechanisms underlying this, we trained a linear classifier on mean glomerular response amplitudes across the initial 200 and 100 ms post-stimulus. Remarkebly, it was able to label 200 ms responses under the correct odour percept

with a 91.9 % success rate (Figure 4.6A, N = 9) and 100 ms responses with a 87.9 % success rate (Figure 4.6A, N = 9). As found using response amplitudes over the entire stimulus period, contribution from a single glomerulus predominated (Figure 4.6B), albeit with the 2nd and 3rd most important glomeruli carrying greater weighting than what was assigned across the entire stimulus period (200 ms = 38 ± 5 % and 27 ± 4 %, 100 ms = 53 ± 7 % and 39 ± 6 %, full stimulus = 25 ± 15 % and 19 ± 3 %, mean ± SEM). Moreover, the glomeruli which were assigned the highest weighting were the same primary glomeruli identified in Figure 4.3C & D. The mean performance of the classifier using only primary glomeruli was 68 % for 200 ms responses and 69.1 % for 100 ms responses (Figure 4.6C). When the 2nd most important glomerulus was included, mean accuracy increased to 90.5 % for 200 ms responses and 84.2 % for 100 ms responses (Figure 4.6C), both of which are again comparable to results obtained using all glomeruli (Figure 4.3D). These data are consistent with the primacy code. Perception remains stable as long as the activation rank is maintained, but then changes in concert with the activation rank.

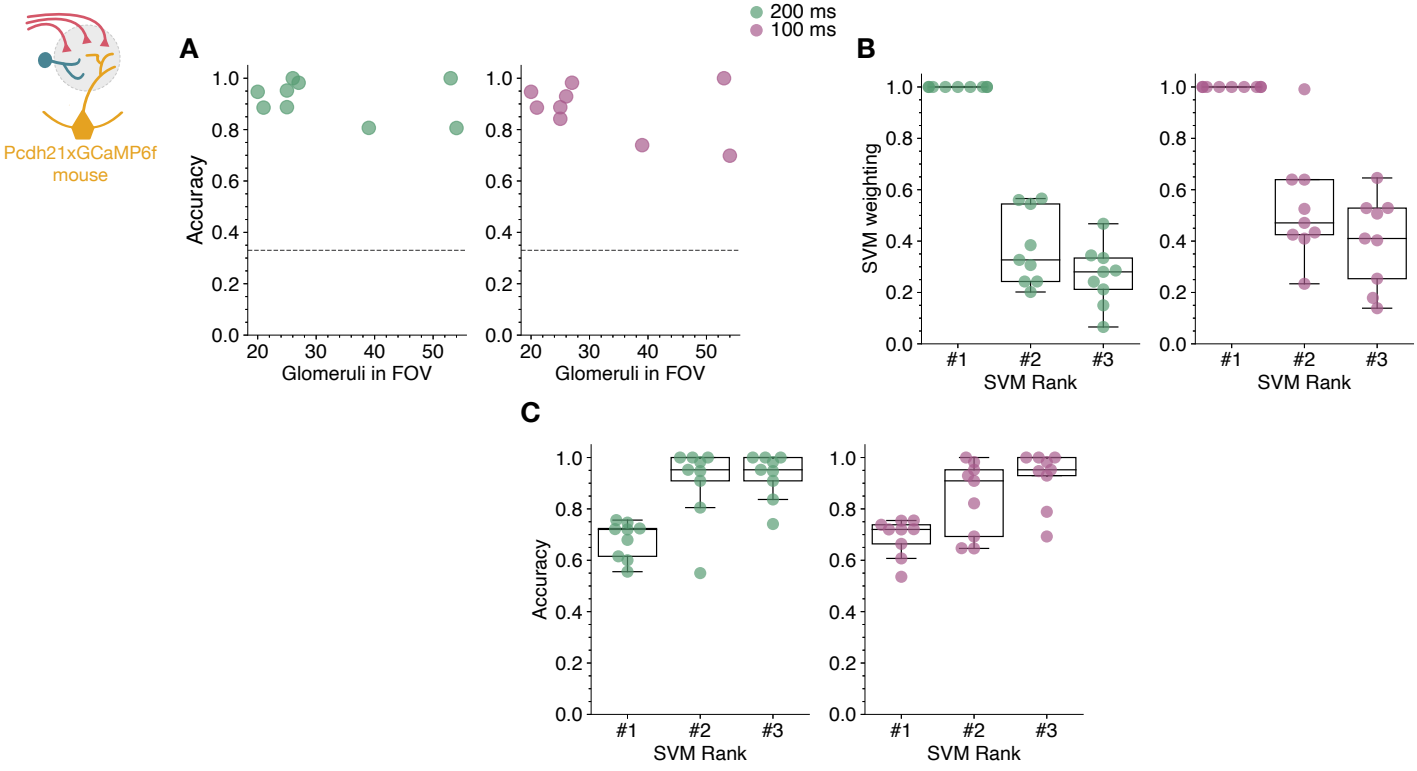

Figure 4.6: Odour Percepts are Classifiable within Primacy Time Constraints

A) Left: Performance of a linear SVM classifier using labelled glomerular response amplitudes spanning the initial 200 ms (green dots) and Right: 150 ms (purple dots) post-stimulus period (N = 9, see methods). B) Relative weights assigned to the three most important glomeruli for classification of A, N = 9, the primary glomerulus has a weight of 1. C) Classifier performance using only the top three most important glomeruli identified in B, N = 9.

4.3 Rapid Adaptation is Consistent with Depolarising Block in Olfactory Receptor Neurons

What mechanism could give rise to a diminished peak response that rapidly adapts below baseline, followed by rebound activity which is delayed by stimulus intensity? Such response characteristics exemplify feed-forward inhibition (*491*, *492*), a circuit pattern found in the glomerular layer (Figure 4.7A). At the glomerulus, where our measurements in Figures 4.3-6 were made, olfactory nerve terminals excite both mitral/tufted cells and inhibitory periglomerular neurons. Consequently, activated periglomerular neurons supply a delayed inhibitory drive onto mitral/tufted dendrites (*127*). To test whether we could attribute this mechanism to the rapid adaptation we see, we recorded from mice which had GCaMP6f expression restricted to mature olfactory receptor neurons (OMPxGCaMP6f, Figure 4.7B) (*449*, *450*). Should feedforward inhibition be the basis for the observed fast adaptation, this phenomenon would be confined to the mitral/tufted cells and not present in the olfactory nerve input. Identifying the same primary glomerulus in OMPxGCaMP6f mice was straightforward due to their near-identical positioning across animals (*108*), coupled with the observation that, in the weak percept, the primary glomerulus is often the only to activate (Figures 4.3A & 4.7C). To our surprise, we observed the same phenomenon in olfactory nerve terminals converging at primary glomeruli; an analogous shift to rapid adaptation became apparent when comparing responses to 60 s presentations of weak and strong percept stimuli (Figure 4.7D). The transition from sustained to adapting responses (Figure 4.7E) aligns with both the transition we observe in mitral/tufted cells (Figure 4.4C) and the perceptual shift that occurred in the cross-habituation

experiments (Figure 4.1E). Based on these findings, we can infer that this phenomenon originates at the first synapse, and is not the consequence of feedforward inhibition.

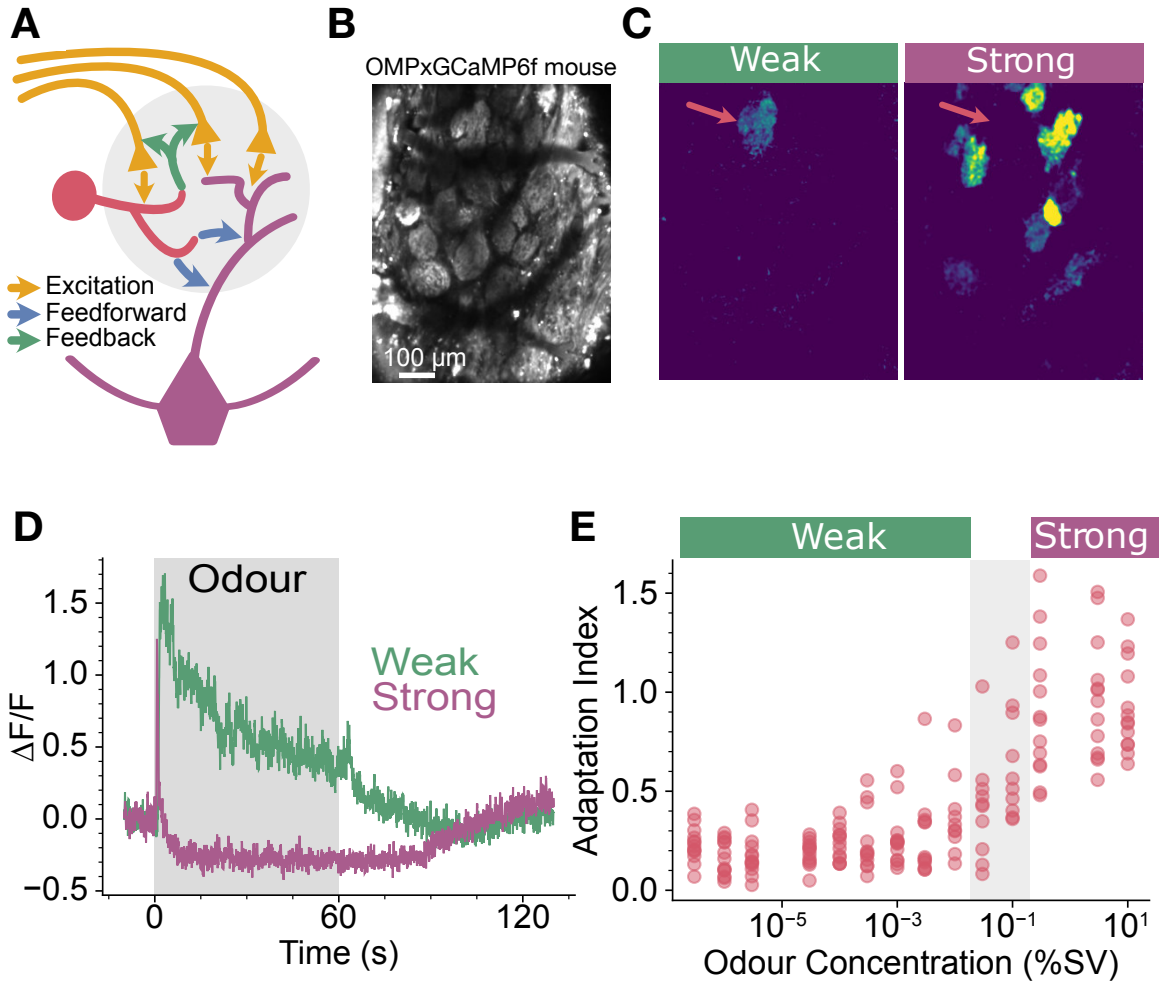

Figure 4.7: Rapid Adaptation Originates at the First Synapse

A) Intraglomerular inhibitory circuits within the olfactory bulb. Olfactory receptor neurons (yellow) excite periglomerular cells (red), prompting feedback and feedforward inhibition onto olfactory nerve terminals and mitral/tufted cells (purple), respectively. B) Field of view in an OMPxGCaMP6f mouse. C) Response maps for B, displaying mean activity in response to 60 s presentations of ethyl tiglate at weak ($1x10^{-4}$ %) and strong (3 %) percept concentrations. Red arrows indicate the primary glomerulus. D) Time course of responses from the primary glomerulus highlighted in C. E) Adaptation indices exhibited by primary glomeruli as a function of concentration, for 3 s presentations of ethyl tiglate N = 13.

However, olfactory receptor neurons are also subject to inhibitory modulation, which they receive from the peiglomerular neurons they synapse onto (Figure 4.7A)

(*387*) and from top-down feedback (*164*, *189*, *203*). This feedback inhibition functions to limit presynaptic calcium influx (*137*, *385*) and is mediated via $GABA_B$ and dopamine D_2 receptors expressed on olfactory nerve terminals (*164*, *189*, *203*). To ascertain whether the observed response dynamics were the result of feedback inhibition, we topically applied drugs known to block $GABA_B$ and D_2 receptors, CGP 54626 and raclopride, respectively (*493*, *494*). Disrupting feedback inhibition led to increased pre-synaptic Ca^{2+} influx for both weak and strong percepts (Figure 4.8A-C, p = 0.0018 weak control vs drug, p = 0.0058 strong control vs drug, paired t-tests, two-tailed, N = 9), indicating that the drugs were exerting their expected action. Despite this, rapid adaptation was still evident in olfactory nerve terminals when mice were presented with strong percept stimuli (Figure 4.8A & D, p = 0.33, paired t-test, two-tailed, N = 9). These data demonstrate that rapid adaptation in primary glomeruli, which coincides with a shift in odour perception, does not arise from neural circuit processing in the brain. Instead, this signal is a feature of olfactory receptor neurons residing in the nasal epithelium.

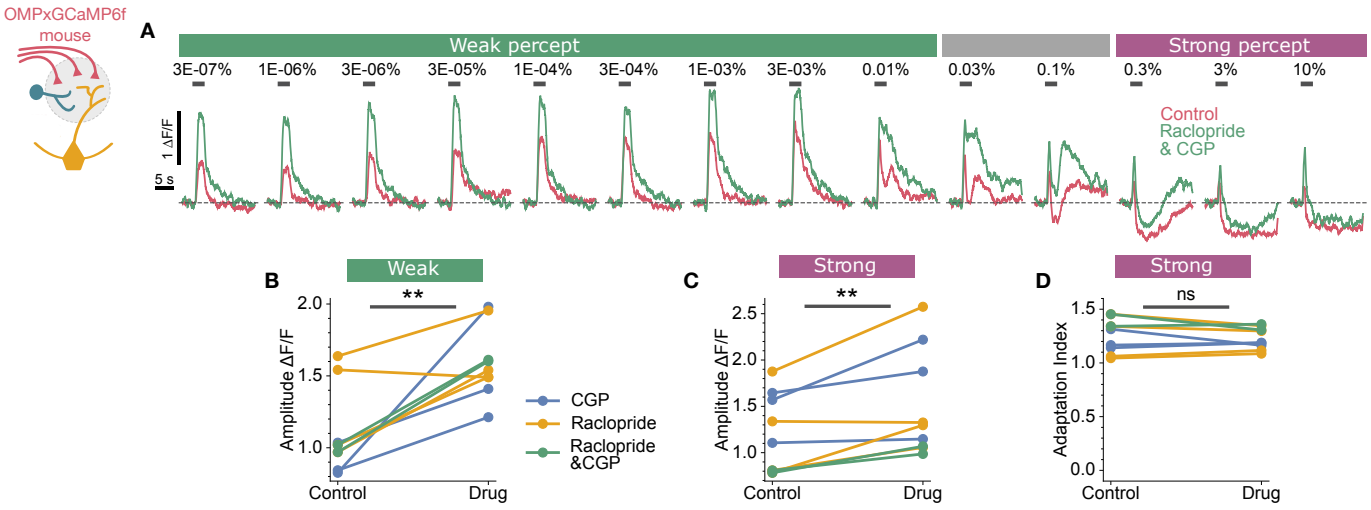

Figure 4.8: Rapid Adaptation is not a Consequence of Feedback Inhibition

A) Responses from a primary glomerulus to 3 s presentations of ethyl tiglate, before and after application of $GABA_B$ and D_2 antagonists CGP 54626 and raclopride, respectively. B) Peak response amplitudes of primary glomeruli to weak C) and strong percept concentrations of ethyl tiglate (3 s stimuli), before and after application of CGP 54626 and raclopride, p = 0.0018 weak control vs drug, p = 0.0058 strong control vs drug, paired t-tests, two-tailed, N = 9. D) Adaptation indices for primary glomeruli in response

to 60 s presentations of ethyl tiglate from the strong percept, pre and post drug application, p = 0.33, paired t-test, two-tailed, N = 9.

It is well-established that adaptation occurs in the olfactory transduction cascade (*374*, *383*, *462*). This process, characterised by a reduction in cyclic nucleotide-gated current sensitivity, stems from Ca^{2+}-dependant feedback (*383*). Nevertheless, this mechanism by itself does not go far enough to explain the rapid adaptation below baseline that we observe in olfactory nerve terminals (Figures 4.7D & 4.8D). To uncover the origin of this phenomenon, we constructed a morphologically and biophysically realistic model of olfactory receptor neurons (Figure 4.9A). Using membrane resistances and spontaneous spike rates similar to those obtained from *in vitro* recordings (*374*, *379*), we developed piecewise functions that closely match reported receptor currents, enabling us to replicate the receptor currents we measured *in vivo* (Figure 4.9A-F, see methods). With our model, we are able to simulate realistic receptor currents and measure the membrane potential in individual olfactory receptor neurons at both the soma and axon terminal (Figure 4.9C & D). However, in our imaging experiments (Figures 4.3-8), we utilised a calcium indicator to measure average activity across a glomerulus, which comprises input from several thousand olfactory receptor neurons (*495*). To produce analogous recordings in our model, we simulated transduction currents in 500 olfactory receptor neurons (Figure 4.9E), calculated their average spike rate, and convolved the result with the kinetics of the GCaMP6f reporter (Figure 4.9F). This model provides key insights into the mechanism that may underly rapid adaptation. We applied a weak stimulus that generated a peak receptor current of 13 pA and led to a sustained increase in the firing rate of individual olfactory receptor neurons. At the population level, this translated into a slow rate of adaptation across the stimulus period (compare Figure 4.9F with Figures 4.5A & 4.7D). In stark contrast, the application of a strong stimulus induced a prolonged depolarisation at the olfactory receptor neurons' soma, generating a brief series of action potentials only at the onset of the stimulus. This small train of action potentials rapidly decreased in amplitude, due to the accruing inactivation of voltage-gated Na^{+} channels. The somatic membrane

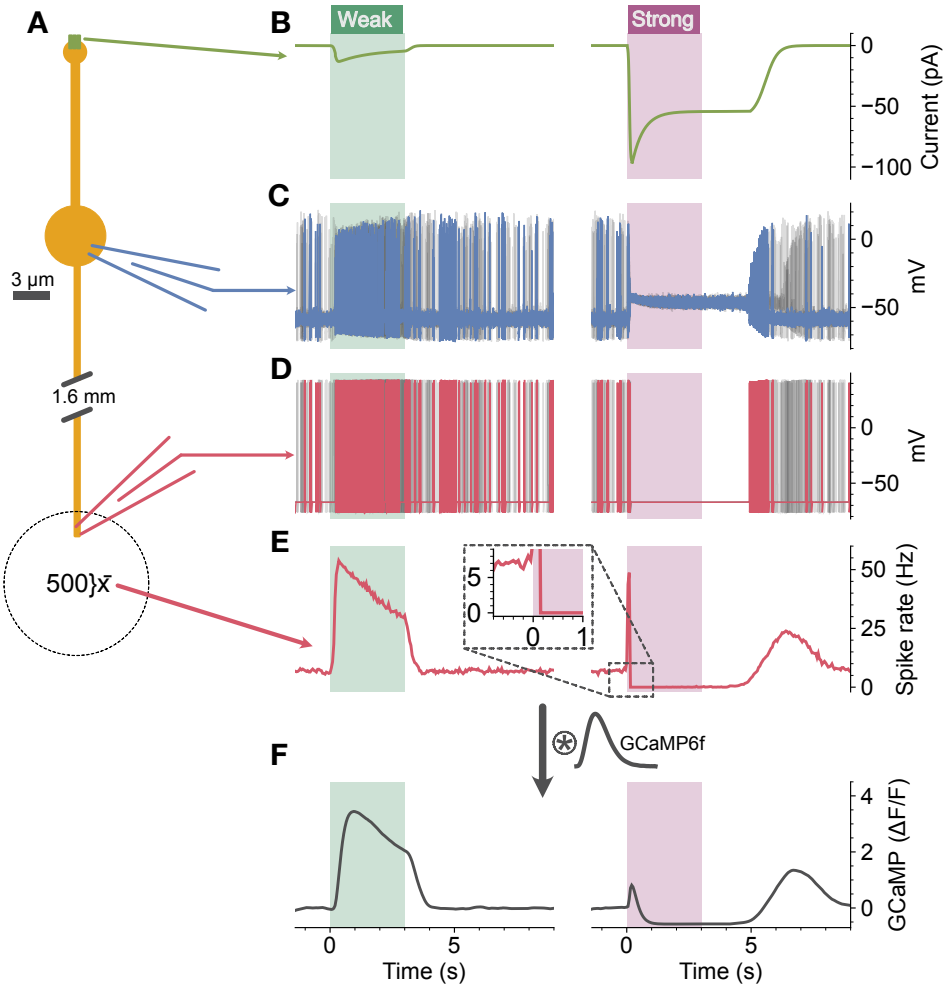

Figure 4.9: A Model of Depolarising Block in Olfactory Receptor Neurons and Rapid Glomerular Adaptation

A) Morphology of model olfactory receptor neuron. B) Receptor currents generated from weak and strong percept stimuli. C) Recording from the somatic membrane of an individual neuron in response to weak and strong percept stimuli (blue), four additional cells are shown in grey. D) Recording from the axonal membrane of an individual neuron in response to weak and strong percept stimuli (red), four additional cells are shown in grey. E) Peri-stimulus time histograms displaying the mean spike rate across 500 simulated neurons. Inset shows expanded view of the response onset for the strong stimulus, highlighting the rapid drop below baseline. F) Spike rates from E convolved with the kinetics of the GCaMP6f reporter (see methods for model details). This model and figure was created by Jamie Johnston.

remained locked in a depolarised state, impeding recovery from voltage-gated Na^+

channel inactivation and thus blocking action potential propagation along the axon. When convolved with the kinetics of the GCaMP6f reporter (Figure 4.9F), the aggregate spike rate from the population of olfactory receptor neurons exhibits all the traits reported in Figures 4.3A, 4.4C, 4.5, 4.7C-E & 4.8: 1) An initial, short-lived burst of action potentials which yields a smaller Ca^{2+} signal than that from the weaker stimulus; an effect of the GCaMP6f reporter's low pass filtering (Figure 4.9F vs Figures 4.5A & C). 2) A rapid decline in the response below pre-stimulus baseline, due to depolarising block halting spontaneous action potential generation, and thus preventing Ca^{2+} detection at the glomerulus (Figures 4.5A, 4.7D, 4.9E & F). 3) A resurgence of action potentials after stimulus cessation, which occurs once the somatic membrane potential is sufficiently hyperpolarised to recover from voltage-gated Na^{+} channel inactivation (Figure 4.9C). The strong stimulus we applied equated to a peak current of 96 pA, which is relatively modest given that odour-evoked receptor currents in rodents have been reported to exceed 200 pA (*365*, *379*, *462*, *496*). Collectively, these data suggest that the perceptual shift which occurs at higher concentrations (Figure 4.1E) may arise from action potential failure in primary sensory neurons residing in the nasal epithelium. These neurons possess and transmit signals from the olfactory receptor that has the greatest affinity for a given odourant.

Chapter 5: Adaptations in Primary Sensory Neurons Facilitate Perceptual Constancy for an Odour

5.1 Associative Learning Establishes Perceptual Constancy

Chapter 4 described the breakdown in perceptual constancy experienced when encountering a novel odour, and presented a mechanistic model that may drive this phenomenon. An inability to identify the same odour across varying intensities would undoubtedly be disadvantageous, especially for salient stimuli such as food. Engaging naturally with food items allows an animal to link a spectrum of concentrations to the same object. Notably, the act of food consumption itself induces a relatively weak activation of the olfactory epithelium via the retronasal route (*497*). We therefore explored whether a natural, 'passive' association of the odour with food could confer perceptual constancy for ethyl tiglate across the entire range of concentrations used in our experiments. We supplemented the animals standard chow with ethyl tiglate at a concentration that corresponded to the strong percept (2.5 %) (Figure 5.1A). To discern

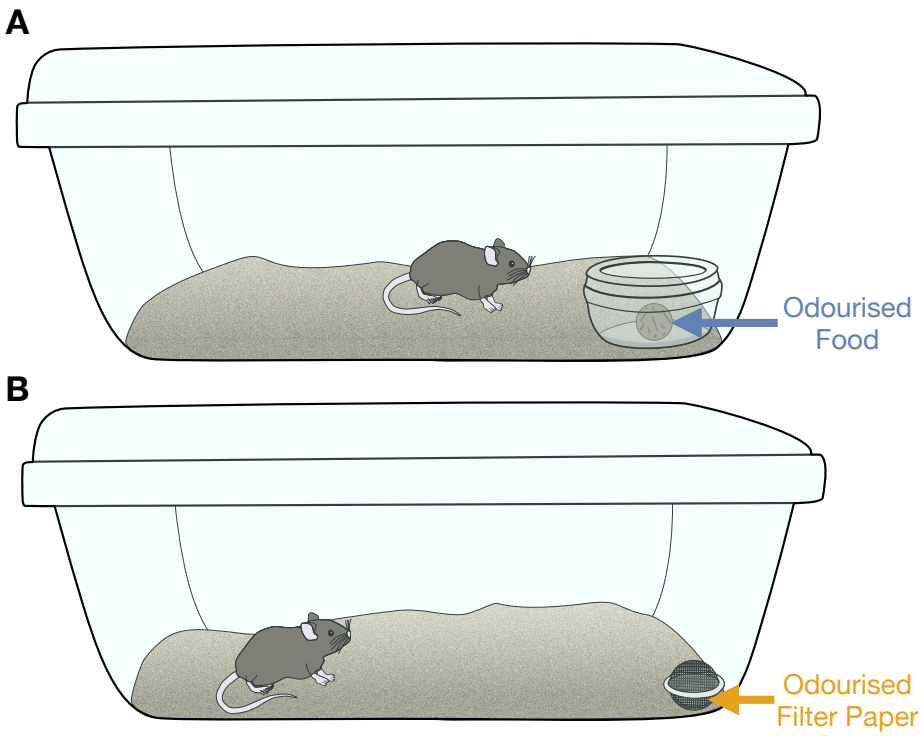

Figure 5.1: Olfactory Learning Protocols

For 1 week, mice were assigned to one of two protocols: A) exclusively fed standard chow supplemented with an odour ('associated' cohort), or B) exposed to odourised filter paper contained within a tea ball, with no dietary changes ('exposed' cohort). In both instances, the odour used was ethyl tiglate, at a concentration of 2.5 %. Both odourised food and filter paper were replenished daily.

whether any observed changes stemmed from food-odour association rather than mere odour exposure, we exposed a separate cohort of mice to the same concentration of ethyl tiglate on filter paper without altering their diet (Figure 5.1B).

After 1 week, we performed food-finding tests with mice that had either exclusively consumed ethyl tiglate-scented food or had simply been exposed to ethyl tiglate. Following an overnight fast, mice were placed in a cage with a buried food pellet, odourised with 2.5 % ethyl tiglate (Figure 5.2A & B). Mice that learned to associate ethyl tiglate with food located the pellet faster than those exposed to the

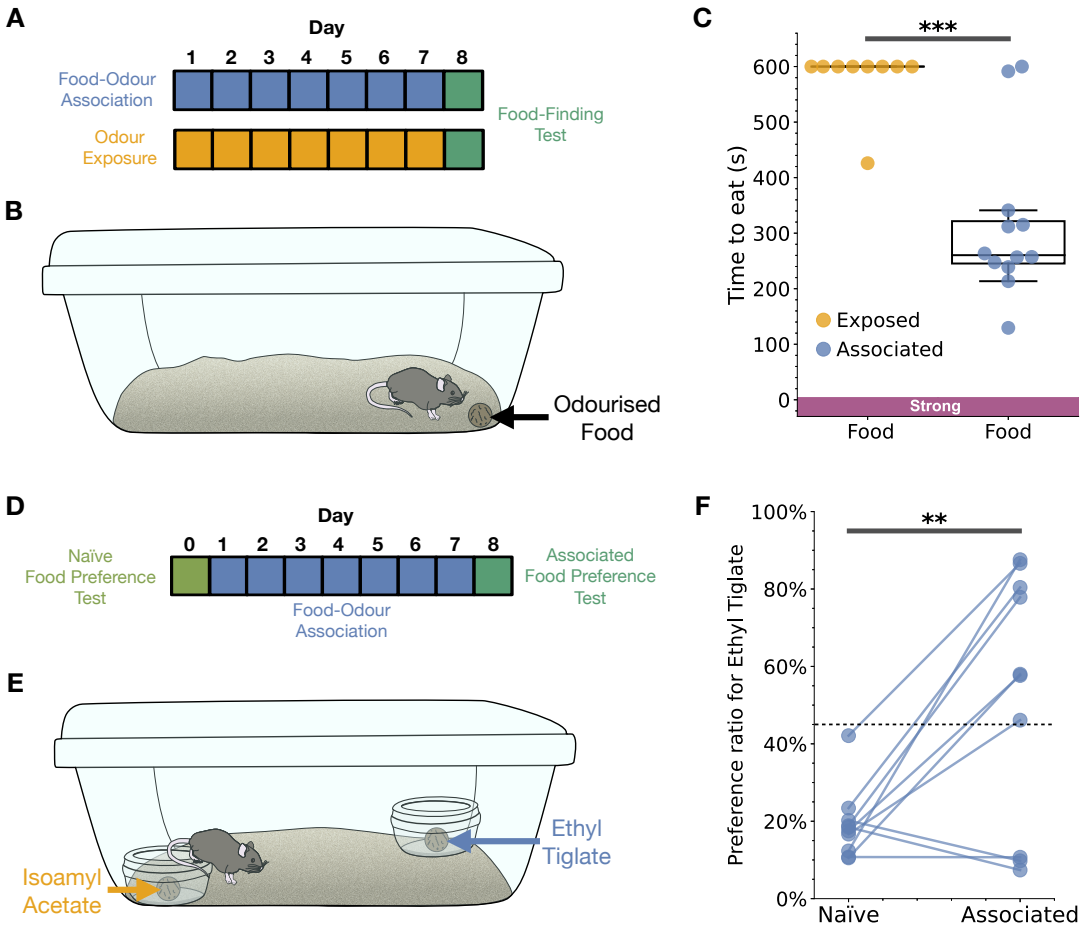

Figure 5.2: Mice Learn to Associate an Odour with Food and Develop a Preference for it

A) Food-finding test timeline. B) Food-finding test. A food pellet odourised with ethyl tiglate (2.5 %) was buried in one corner of the test cage. Fasted mice were individually placed in the test cage, and time taken to locate and begin eating the odourised pellet was recorded. If mice did not locate and/or attempt to eat the pellet within 10 min, the test was abandoned. C) Latency for both 'exposed' (N = 9) and 'associated' (N = 12) cohorts of mice to begin eating a buried food pellet odourised with 2.5 % ethyl tiglate. Note that only 1 of the 9 mice from the exposed cohort attempted to eat the food pellet, whereas 11 of the 12 mice from the associated cohort did (p = 0.0013, Mann-Whitney U test). D) Food preference test timeline. E) Food preference test, fasted mice were presented with two food pellets, odourised with either 2.5 % ethyl tiglate, or 2.5 % isoamyl acetate. Mice were left to feed for 1 hour, and the amount eaten from each food pellet was measured. F) Preference ratio for ethyl tiglate in naïve mice and those which associated the odour with food, calculated by dividing the amount of ethyl tiglate food pellet eaten by the total amount eaten from both food pellets, N = 10 (p = 0.0074, paired t-test, two-tailed). Note that all but 2 mice developed a preference for ethyl tiglate-scented food. The majority of food-finding tests in panel C were executed by Kate Allen.

odour for the same duration without any food link (Figure 5.2C, 154 ±96 vs 332 ±122 s, mean ± SEM, p = 0.0013, Mann-Whitney U, N = 21). Mice subjected to supplemented diets evidently formed a food-odour association with ethyl tiglate, as 11 of the 12 mice tested also began eating the pellet within the 10 min test period, as opposed to only 1 of the 9 'exposed' mice which did so (Figure 5.2C). Indeed, when given a choice between a food pellet scented with 2.5 % ethyl tiglate and one scented with 2.5 % isoamyl acetate, naïve mice prefer Isoamyl acetate, but mice that underwent associative learning developed a preference for ethyl tiglate (Figure 5.2D-F, 19.08 ± 2.88 vs 52.21 ± 10.29 %, mean ± SEM, p = 0.0074, paired t-test, two-tailed, N = 12). These findings suggest that mice established a connection between a strong percept concentration of ethyl tiglate and food.

We next assessed whether this association extended to weaker concentrations of ethyl tiglate, which naïve mice perceive as a distinct 'weak percept'. A separate cohort of mice fed 2.5 % ethyl tiglate for 1 week were again tested with a buried food pellet as in figure 5.3A & B, this time odourised with $1x10^{-3}$ % ethyl tiglate. Strikingly, all

mice rapidly located the pellet and began eating (Figure 5.3C). We were concerned that the scent of the standard chow may have aided their localisation of the food, given how dilute the odour was at this concentration. To address this, we conducted the test with a different group of mice using a cotton ball soaked in the same weak concentration of ethyl tiglate (Figure 5.3A & B), where remarkably, all mice quickly found and started nibbling on the cotton ball just as they did with the odourised food pellet (Figure 5.3C, 97.2 ± 23.9 s vs 145 ± 31.28 s, mean ± SEM, p = 0.24, independent t-test, two-tailed, N = 16). Moreover, mice that had formed this association investigated the odour at every concentration in the cross-habituation experiment (Figure 5.3D, N = 16). This, along with our data from head-fixed perception tests (Figure 4.2), indicates that animals were indeed capable of detecting the odour in the naïve state (Figure 5.3D inset & Figure 4.1E). It also suggests that, unlike naïve animals, those that learned the association perceive the entire spectrum of odour concentrations as a single odour object. These data demonstrate that mice, after consuming a strong concentration of

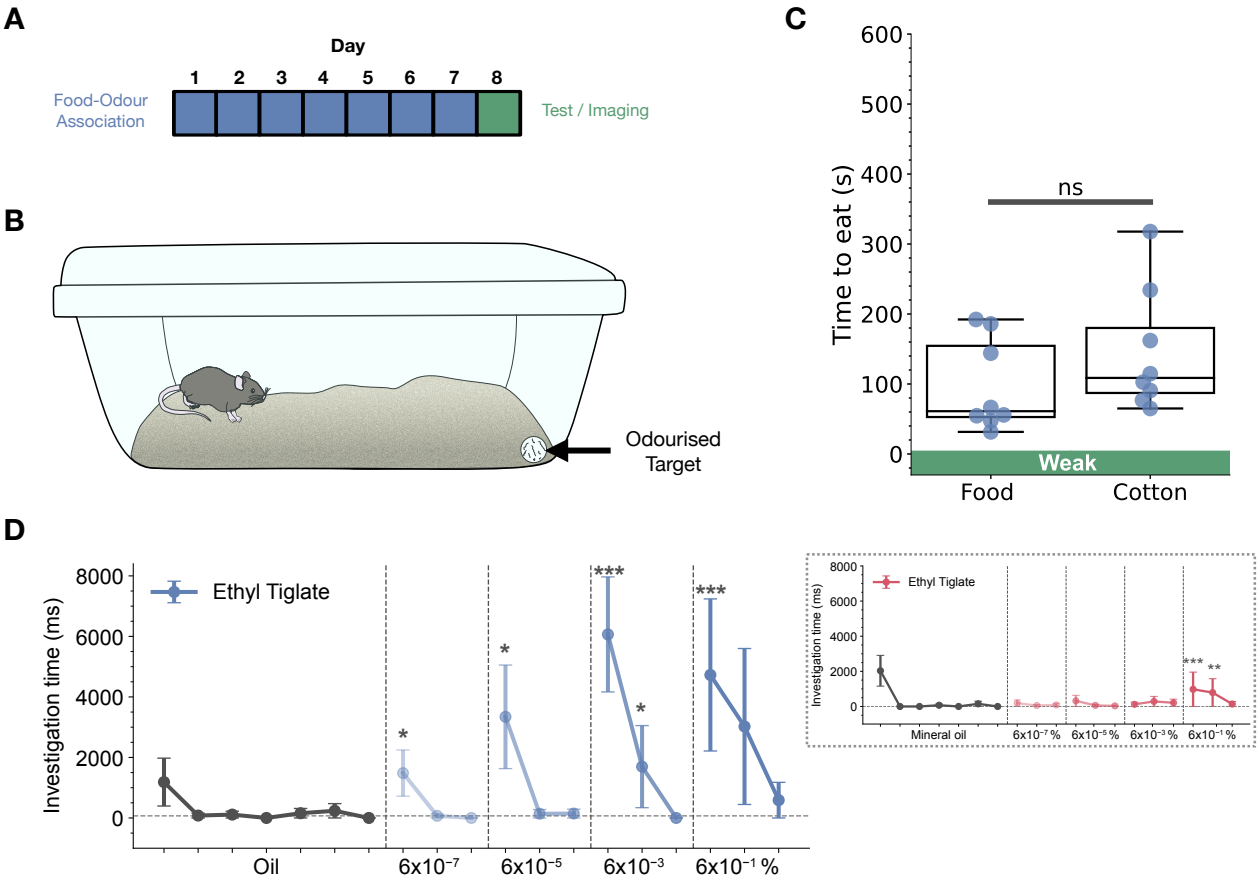

Figure 5.3: Mice Connect a Wide Range of Odour Concentrations to the Same Object

A) Food/odour-finding test timeline. B) Odour-finding test. A food or cotton ball odourised with ethyl tiglate ($1x10^{-3}$ %) was buried in one corner of the test cage. Fasted mice were individually placed in the test cage, and time taken to locate and begin eating the cotton ball was recorded. If mice did not locate and/or attempt to eat the cotton ball within 10 min, the test was abandoned. C) Latency for mice to begin eating either a buried food pellet (N = 8) or cotton ball (N = 8) odourised with $1x10^{-3}$ % ethyl tiglate ($p = 0.24$, independent t-test, two-tailed, N = 16). D) Cross-habituation test (see methods and Figure 4.1 for more info) in mice that had been fed 2.5 % ethyl tiglate-scented food for 7 days (blue). Odour investigation times during the stimulus period, data are displayed as median ± the median absolute deviation, N = 16. Horizontal dashed lines indicate baseline levels of investigation, calculated from the average across the final 5 solvent presentations. There were significant differences detected between the last 5 oil presentations and presentations of ethyl tiglate ($p = < 0.001$, Friedman test). Asterisks indicate post-hoc significance tests above baseline investigation (Wilcoxon signed-rank test with Bonferroni correction, see methods for asterisks significance). Odour concentrations are presented as the final concentration measured at the nose poke using a photo-ionization detector. Inset shows data from the same cross-habituation test conducted with naïve mice (red), as shown in Figure 4.1D.

an odour paired with food, retain this food-odour association across a wide range of concentrations, including those which previously elicited a different perceptual response.

5.2 Perceptual Constancy Emerges from Dynamic Range Matching in the Primary Glomerulus

What neural changes could underpin the learning-induced shift in perception? Could the 'primary' glomerulus functionally adjust its sensitivity to preserve responsiveness across the entire concentration range? If such a sensitivity shift occurred, would it consistently be the first glomerulus to activate at every concentration? To address these questions, we again employed *in vivo* 2-photon Ca^{2+} imaging to measure activity in mitral/tufted cell primary dendrites, using Pcdh21xGCaMP6f mice that had undergone 1 week of either exposure to, or diet supplementation with, 2.5 % ethyl tiglate (Figure 5.1). As detailed in Chapter 4 and

figures 4.3A & 4.7C, the primary glomerulus for ethyl tiglate was readily identifiable, as it was generally the only glomerulus to respond to every concentration presented and due to its predictable location on the dorsal surface of the olfactory bulb (Figure 5.4A). Strikingly, when we generated response maps as in Figures 4.3A & 4.7C, the primary glomerulus was clearly visible at both weak and strong concentrations of ethyl tiglate (Figure 5.4A). This was the result of sustained activity in the primary glomerulus throughout the entire stimulus period (Figure 5.4B), markedly different from responses observed in naïve mice (Figure 5 inset & Figure 4.5A). This difference is highlighted in Figure 5.4E, illustrating that adaptation indices (AIs) exhibited by primary glomeruli were significantly different from one another across naïve, exposed, and associated cohorts (p = < 0.001, one-way ANOVA, N = 23). AIs were substantially lower in mice

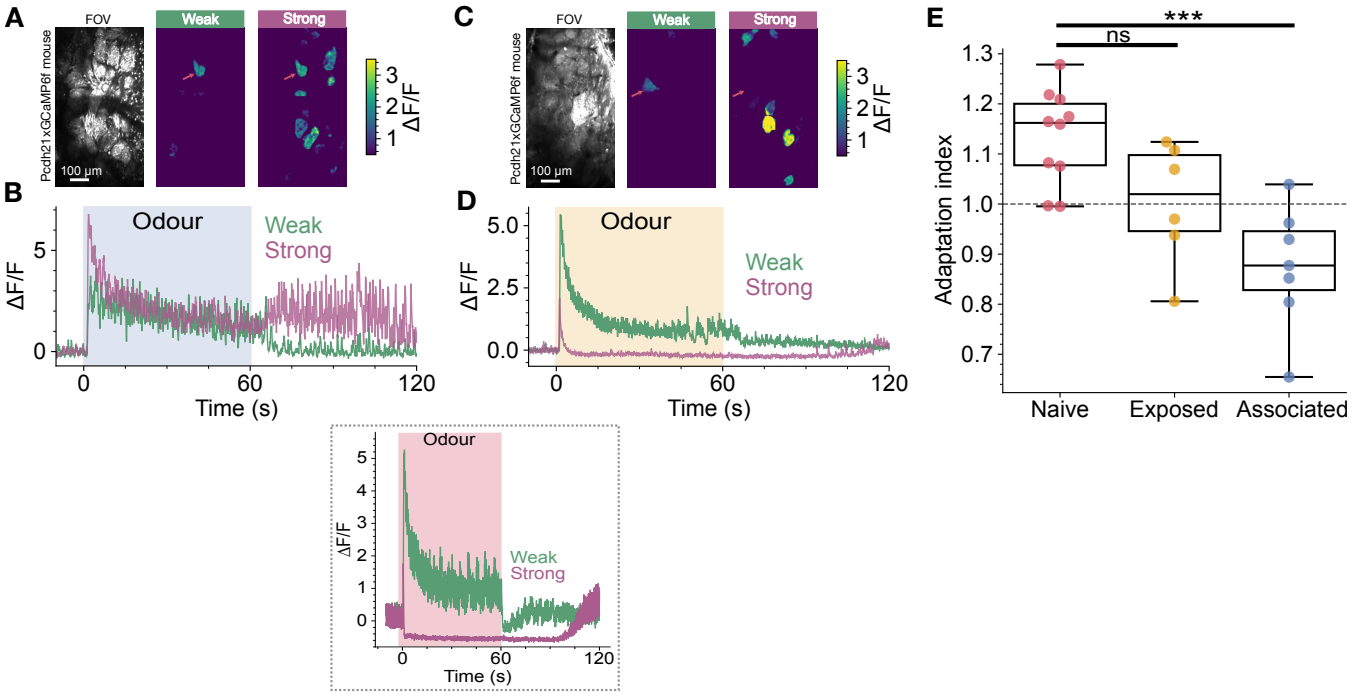

Figure 5.4: Associative Learning Abolishes Rapid Adaptation in the Primary Glomerulus

A) Field of view and response maps for weak ($1x10^{-3}$ %) and strong (3 %) percept concentrations of ethyl tiglate in mice that associated this odour with food. Note that the primary glomerulus is still visible in the strong percept. B) Time course of primary glomerulus response highlighted in A. C) & D) Same as A & B, for mice that were exposed to ethyl tiglate without any food association. E) A significant difference in the adaptation indices was detected across all cohorts (p = < 0.001, one-way ANOVA, N = 23). Adaptation

indices for primary glomeruli were lower for mice that formed food-odour associations with ethyl tiglate than those of naïve mice (p = 0.0003, post-hoc Tukey's HSD test, N = 17), whereas mice simply exposed to the odour were not significantly different to either the naïve cohort (p = 0.076, post-hoc Tukey's HSD test, N = 16) or the associated cohort (p = 0.12, post-hoc Tukey's HSD test, N = 13). Data from 3 mice in the associated cohort are attributed to work conducted by Kate Allen.

that had learned to associate ethyl tiglate with food than those in naïve mice (0.87 ± 0.047 vs 1.14 ± 0.03 AI, mean ± SEM, p = 0.0003, post-hoc Tukey's HSD test, N = 17). In contrast, mice simply exposed to ethyl tiglate in lieu of any food connection displayed almost complete adaptation in primary glomeruli (Figure 5.4C & D, 1.002 ± 0.05 AI, mean ± SEM, N = 6). Notably, the extent of primary glomerulus adaptation in exposed animals was intermediate among groups, yet this did not differ significantly to either the naïve cohort (Figure 5.4E, p = 0.076, post-hoc Tukey's HSD test, N = 16) or the associated cohort (p = 0.12, post-hoc Tukey's HSD test, N = 13).

The abolishment of rapid adaptation—which is consistent with our model of depolarising block in olfactory receptor neurons—coupled with sustained activity at stronger concentrations, hints at a sensitivity shift in the primary glomerulus. We confirmed this by plotting response time courses (Figure 5.5A) and response magnitude as a function of concentration (Figure 5.5B), revealing a marked shift in odour sensitivity. This shift was most pronounced when comparing naïve animals to those that associated ethyl tiglate with food, with mice merely exposed to ethyl tiglate falling somewhere in between the two groups (Figure 5.5B). Notably, the concentration of ethyl tiglate which elicited the maximal response shifted by approximately two orders of magnitude (Figure 5.5B), closely aligning with the concentration used to supplement the food (Figure 5.1A). Such an adjustment would enable the primary glomerulus to detect and respond to the entire spectrum of concentrations encountered when interacting with this specific food item. This is corroborated by our finding that mice which formed a food-odour association with ethyl tiglate investigated every concentration presented in the cross-habituation experiments (Figure 5.3D). We also observed a similar sensitivity shift in primary glomeruli from animals exposed to ethyl tiglate, though a sharp decline in response magnitude was still apparent at higher

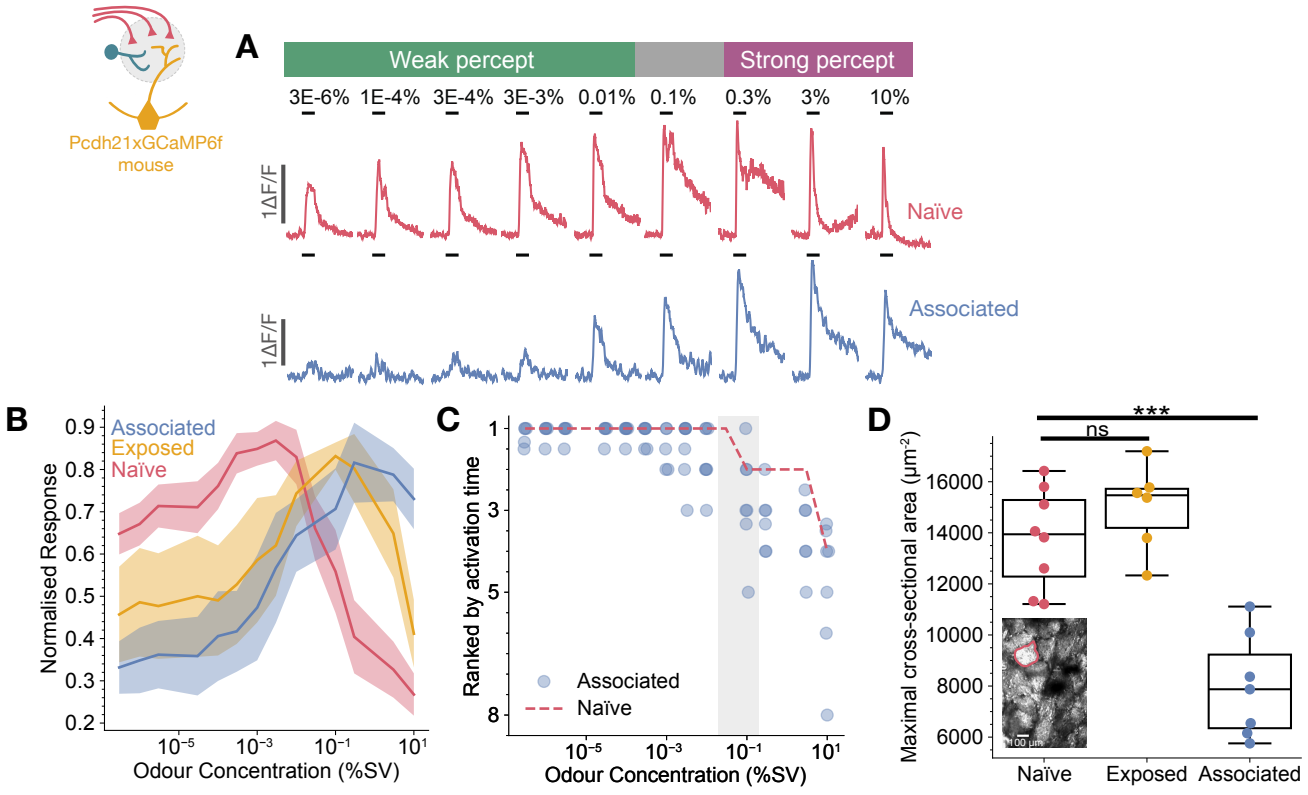

Figure 5.5: Perceptual Constancy Arises from Dynamic Range Matching and Functional Changes in the Primary Glomerulus

A) Representative response time courses for primary glomeruli as a function of concentration, for naïve and associated cohorts of mice (3 s presentations of ethyl tiglate). B) Normalised concentration-response curves for primary glomeruli across naïve (N = 9), exposed (N = 6), and associated (N = 7) cohorts of mice, displayed as mean ± SEM (3 s presentations of ethyl tiglate). C) Relative activation ranks for primary glomeruli as a function of concentration, with each mouse from the associated cohort represented by a dot (N = 7), dashed red line indicates the median for naïve mice (N = 9). D) There was a significant difference in the size of the primary glomerulus across cohorts (p = < 0.001, one-way ANOVA, N = 21). Primary glomerulus size was significantly smaller in mice that formed a food-odour association with ethyl tiglate compared to naïve mice (p = < 0.001, post-hoc Tukey's HSD test, N = 15) and exposed mice (p = < 0.001, post-hoc Tukey's HSD test, N = 13), whereas those from the exposed cohort did not differ from the naïve (p = 0.49, post-hoc Tukey's HSD test, N = 14). Data from 3 mice in the associated cohort are attributed to work conducted by Kate Allen.

concentrations, as in naïve animals (Figure 5.5B). Based on these data, we surmised that primary glomeruli in mice from the associated cohort may retain their activation

primacy across the entire concentration range. However, they again began to trail behind other glomeruli at concentrations which corresponded to the strong percept in naïve mice (Figure 5.5C). It is important to note that animals' regular food chow is not odourless and stimulates glomerular activity in the olfactory bulb. Thus, an odour mixture of both chow and ethyl tiglate could potentially alter the glomerular representation, either enhancing, suppressing, or altogether inhibiting ethyl tiglate responses in a glomerulus-specific manner (*266-271*). Examining whether this effect differs between naïve, exposed, and associated cohorts of mice in the primary glomerulus would be of particular interest. However, previous work in the lab has shown that only very high chow concentrations activate a few dorsal glomeruli, likely due to its low volatility. Nonetheless, as shown in Figure 5.3B-C, our data demonstrate that mice associate ethyl tiglate alone with food. Interestingly, we also found a significant difference in the size of the primary glomerulus across naïve, exposed, and associated cohorts ($p = < 0.001$, one-way ANOVA, $N = 21$). Primary glomeruli in the associated group of mice were significantly smaller than both those in the naïve group (Figure 5.5D, 7986 ± 768 vs 13,794 ± 693 μm^2, mean ± SEM, $p = < 0.001$, post-hoc Tukey's HSD test, $N = 15$) and exposed group (15007 ± 694 μm^2, mean ± SEM, $p = < 0.001$, post-hoc Tukey's HSD test, $N = 13$). In contrast, primary glomerulus size in mice merely exposed to ethyl tiglate was not significantly different from the naïve cohort ($p = 0.49$, post-hoc Tukey's HSD test, $N = 14$). This phenomenon is reminiscent of, yet distinctly opposite to, the structural changes that occur in olfactory receptor neurons with fear conditioning (*438*). Collectively, these data indicate that associating an odour with food leads to changes in the dendrites of mitral/tufted cells projecting to the primary glomerulus, modifying its size and sensitivity. However, simple odour exposure only partially alters odour sensitivity in primary glomeruli. These changes may originate from olfactory receptor neurons, potentially due to shifts in the receptor complement (*498*), intrinsic membrane properties (*396*), or indirect modulation from top-down feedback (*166-169*, *174*, *176*, *189*, *203*, *216-220*). Yet, the sequence of glomerular activation (primacy) remained fixed, and is seemingly unaltered by natural interaction with an odour object.

5.3 Odour Learning Shifts Sensitivity in Dual-Responsive Glomeruli for Unconditioned Odours

After finding that food-odour association shifts the sensitivity of the primary glomerulus for the conditioned odour, we next questioned whether other glomeruli are similarly affected. However, as our imaging of naïve and learned mice was carried out in different cohorts, we were unable to reliably identify specific non-primary glomeruli across different animals in our *in vivo* 2-photon Ca^{2+} imaging experiments (Figures 5.4 & 5.5). To circumvent this limitation, we quantified the overall fraction of glomeruli responsive to the conditioned odour within a field of view, excluding primary glomeruli (Figure 5.6A). Compared with naïve animals, there were significantly fewer glomeruli responsive to ethyl tiglate in mice that were either exposed to or had eaten food supplemented with 2.5 % SV ethyl tiglate for 7 days (Figure 5.6A, p = < 0.001 for both two-way ANOVAs and post-hoc Tukey's HSD tests, N = 21). This implies that both odour exposure and its association with food reduce the sensitivity of all glomeruli that respond to the conditioned odour. Among responsive glomeruli, we next examined odour-evoked response amplitudes across the range of odour concentrations presented (Figure 5.6B). In naïve animals, response amplitudes were significantly larger than those from both cohorts of learned animals (p = < 0.001 for both two-way ANOVA and post-hoc Tukey's HSD test, N = 21). These data indicate that, as with the primary glomerulus, both odour exposure and associative learning shift glomerular sensitivity and reduce the strength of responses to the conditioned odour.

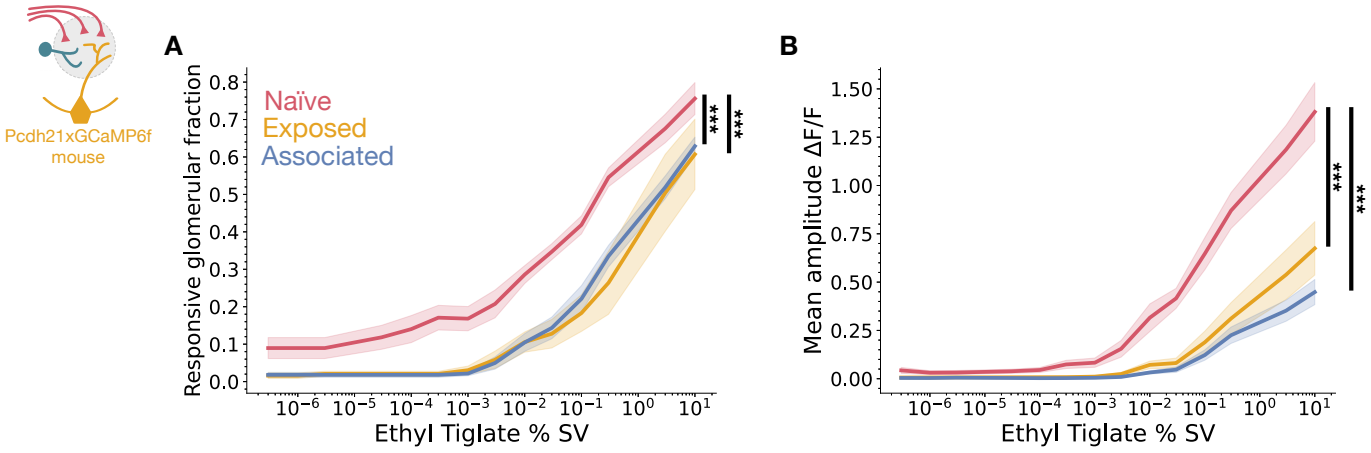

Figure 5.6: Associative Learning Shifts Sensitivity of Responsive Glomeruli

A) Fraction of responsive glomeruli and B) mean amplitude of all responsive glomeruli in a field of view, as a function of ethyl tiglate concentration, displayed as mean ± SEM for mice naïve to ethyl tiglate (N = 9), those exposed to the odour at 2.5 % SV for 7 days (N = 6), and those which learnt to associate the odour at 2.5 % with food for 7 days (N = 6, p = < 0.001 for two-way ANOVA and post-hoc Tukey's HSD tests done for both A and B).

Are the sensitivity shifts induced by learning odour specific? If the observed effects arise from changes in the receptor complement (*395*, *499*), one might expect to detect similar sensitivity changes in all odours that activate the same glomeruli as the conditioned odour. To analyse this, we quantified the fraction of glomeruli responsive to an unconditioned odour, 2-heptanone. Additionally, we segregated the glomeruli based on whether they responded to both the conditioned odour and 2-heptanone (termed 'dual-responsive'), or to 2-heptanone only (referred to as 'selective' glomeruli). As in Figure 5.6, we excluded primary glomeruli for ethyl tiglate from our analyses. Furthermore, we excluded glomeruli that only responded to ethyl tiglate at ≥ 3 % SV, as these would not have been active in naïve animals. Among the dual-responsive glomeruli, a significantly smaller fraction responded to 2-heptanone in the associated cohort of mice compared to naïve animals (Figure 5.7A left, p = 0.008, post-hoc Tukey's HSD test, N = 11), while the responsive fraction in exposed animals fell somewhere between the two groups but was not significantly different from the naïve cohort (p = 0.13, post-hoc Tukey's HSD test, N = 11). In contrast, the number of selective glomeruli that responded to 2-heptanone was stable across all groups (Figure 5.7A right, p = 0.063, two-way ANOVA, N = 16). These data imply that the learning-induced changes in sensitivity also affect novel odours, but only in glomeruli that are responsive to the conditioned odour. However, unlike with the conditioned odour (Figure 5.6B), the amplitude of 2-heptanone responses in dual-responsive glomeruli did not differ across cohorts (Figure 5.7B left, p = 0.31, two-way ANOVA, N = 16). Interestingly, we observed a significant difference in response amplitudes from 2-heptanone-selective glomeruli when comparing all groups (Figure 5.7B right, p = 0.0019, two-way ANOVA, N = 16), with the associated cohort exhibiting amplitudes

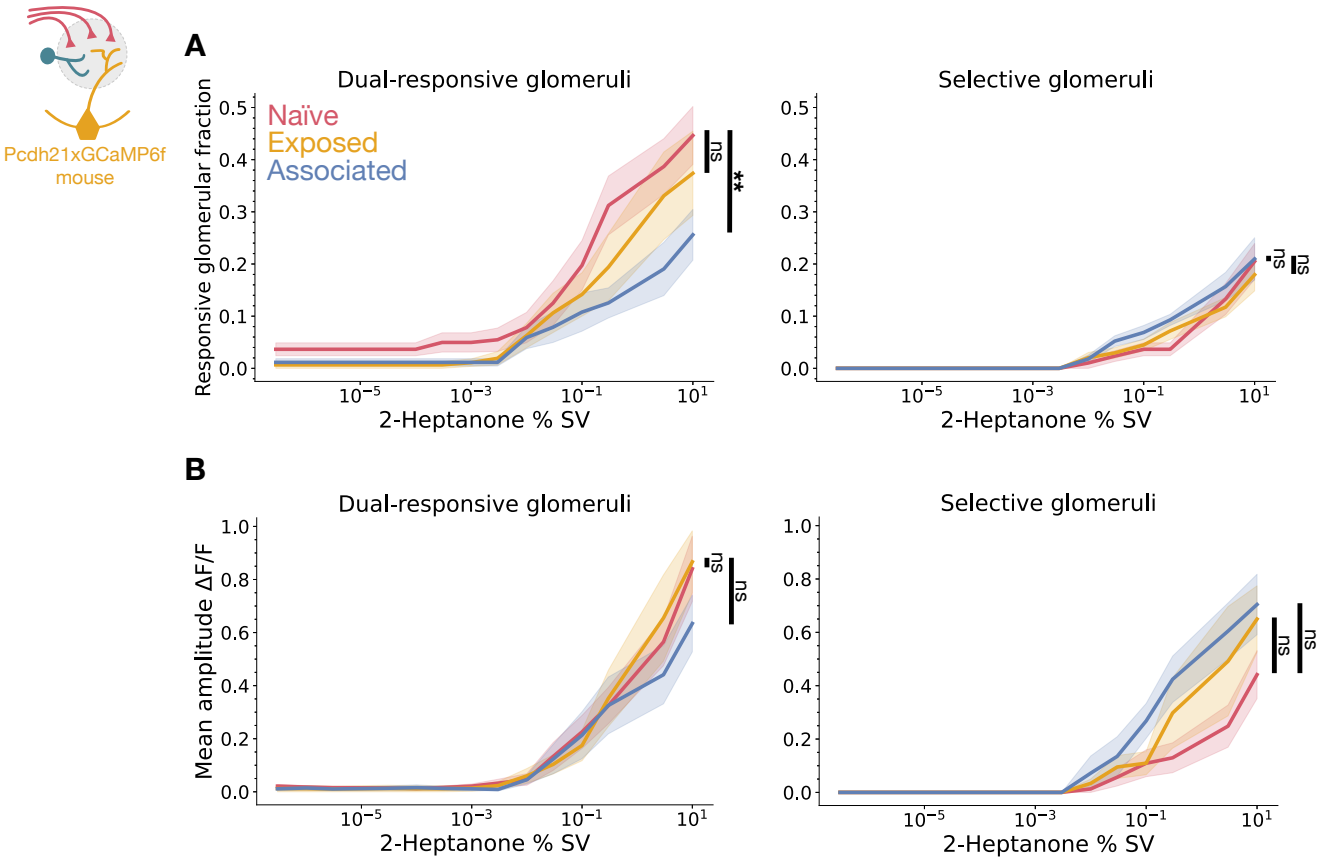

Figure 5.7: Associative Learning Reduces the Fraction of Dual-Responsive Glomeruli

A) Left: Fraction of glomeruli responsive to both ethyl tiglate and 2-heptanone in a field of view (naïve vs exposed: p = 0.13, naïve vs associated: p = 0.008, post-hoc Tukey's HSD test) and Right: glomeruli responsive to 2-heptanone only (p = 0.063, two-way ANOVA), as a function of 2-heptanone concentration. Data are displayed as mean ± SEM for mice naïve to ethyl tiglate (N = 5), those exposed to the odour for 7 days (N = 6), and those which learnt to associate the odour with food for 7 days (N = 5). B) Left: Mean response amplitude for dual-responsive glomeruli (p = 0.31, two-way ANOVA) and Right: selective glomeruli (naïve vs exposed: p = 0.41, naïve vs associated: p = 0.078, post-hoc Tukey's HSD test) shown in A.

marginally larger, yet not significantly so, than those from the naïve cohort (p = 0.078, post-hoc Tukey's HSD test, N = 11); amplitudes in exposed animals were again intermediate between the two (p = 0.41 compared to naïve, post-hoc Tukey's HSD test, N = 11). These findings suggest that responses to unconditioned odours are modestly

enhanced with associative learning. However, since 2-heptanone-selective glomeruli constitute only a small fraction of the total (just a few in number), we cannot confidently lend much credence to these results.

We next sought to further characterise the change in sensitivity observed with the unconditioned odour, 2-heptanone (Figure 5.7). In primary glomeruli for ethyl tiglate, we found that associating the odour with food shifts the concentration that elicits the maximal response by around two orders of magnitude (Figure 5.5B). This shift, accompanied by reduced response amplitudes at lower concentrations (Figure 5.5B), suggests that the threshold concentration required to activate these glomeruli increases with learning. However, we were unable to measure this parameter in primary glomeruli as they responded to the entire range of concentrations presented (Figures 4.3A, 4.4A, 4.8A & 5.5A). Does this change in threshold sensitivity also occur in non-primary glomeruli? If so, do these effects extend to unconditioned odours? We addressed these questions by identifying the lowest concentrations of both ethyl tiglate (the conditioned odour) and 2-heptanone (the unconditioned odour) to elicit robust responses (see 'defining glomerular responses' in methods), which we refer to as the 'detection thresholds' (Figure 5.8). In dual-responsive glomeruli, there was a significant difference in the detection threshold between the groups of mice (Figure 5.8, p = 0.001, PERMANOVA, N = 16). In the naïve cohort, the detection threshold was 0.1 ± 0.1 % (median ± MAD), which increased to 1.65 ± 1.35 % in the exposed cohort (p = 0.003, post-hoc PERMANOVA pair-wise comparisons, Benjamini-Hochberg corrected, N = 11).

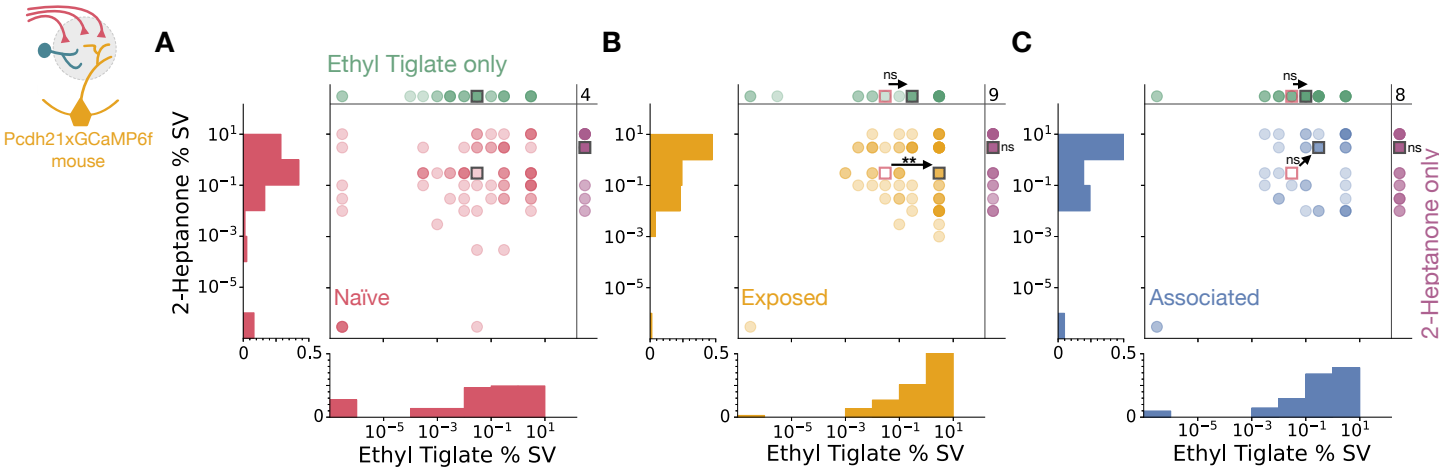

Figure 5.8: Odour Learning Increases the Detection Threshold for Glomeruli Responsive to the Conditioned Odour

Lowest concentration at which glomeruli responded to ethyl tiglate and 2-heptanone for Left panel: mice naïve to ethyl tiglate (red dots, N = 5), Middle panel: mice exposed to ethyl tiglate for 7 days (yellow dots, N = 6, p = 0.003 compared with naïve, PERMANOVA pair-wise comparisons, Benjamini-Hochberg corrected), and Right panel: mice that consumed food supplemented with ethyl tiglate for 7 days (blue dots, N = 5, p = 0.056, PERMANOVA pair-wise comparisons, Benjamini-Hochberg corrected). Green and purple dots represent glomeruli that were only responsive to ethyl tiglate (p = 0.066) or 2-heptanone (p = 0.33, Kruskal-Wallis H-test), respectively. Numbers in top right quadrants of each panel denote the mean number of glomeruli that were non-responsive to both odours, rounded to the nearest whole number. Black square boxes indicate the median for each cohort, arrows in the middle and right panels highlight the degree of change from naïve animals (represented by red boxes in middle and right panels). Histograms depict the distribution of dual-responsive glomeruli for both odours, categorised by the log-transformed lowest concentration of ethyl tiglate or 2-heptanone that elicited a response. Each bin represents a tenfold increase in concentration.

However, while a trend was apparent, the detection threshold for the associated cohort was not significantly different to that of naïve animals (0.3 ± 0.3 %, p = 0.056, post-hoc PERMANOVA pair-wise comparisons, Benjamini-Hochberg corrected, N = 11). These data suggest that after prolonged exposure to an odour, stronger concentrations of both conditioned and unconditioned odours are required to activate dual-responsive glomeruli, a phenomenon that may also extend to associative learning with a larger sample size. This is further exemplified by the detection thresholds for the specific odours (Figure 5.8). Here, the probability distributions indicate that the likelihood of ethyl tiglate eliciting a response at concentrations between 1-10 % SV increased from 24.7 % in the naïve cohort to 52.7 % in the exposed cohort and 39 % in the associated cohort (Figure 5.8). Similarly, for 2-heptanone, the detection threshold increased from 28.8 % in naïve animals to 47.3 % in exposed animals and 51.2 % in those that formed food-odour associations. Additionally, there were more than twice as many non-responsive glomeruli in learned mice than in naïve ones (Figure 5.8, naïve = 4, exposed = 9, associated = 8). Although the number of glomeruli can vary within a field of view, similar numbers of glomeruli were detected across all cohorts (p = 0.99, One-way

ANOVA, N = 16). It is therefore possible that the reduced number of responsive glomeruli in learned animals is due to a change in sensitivity, where less sensitive glomeruli cease to respond after learning. In contrast, detection thresholds for glomeruli that were selectively responsive to either 2-heptanone or ethyl tiglate were not significantly different across naïve and learned animals (Figure 5.8, $p = 0.33$ and $p = 0.066$, respectively, Kruskal-Wallis H-test, N = 16). The discrepancy observed for ethyl tiglate is surprising; nevertheless, the limited number of selective glomeruli may not provide enough power to detect a significant difference, although a trend was apparent. Together, these findings suggest that odour learning reduces glomerular sensitivity to all odours that activate the same receptor as the conditioned odour. Consequently, glomeruli with high detection thresholds in the naïve state may cease responding entirely after learning. However, as our comparisons between the naïve and learned state were not conducted on the same animals, we cannot definitively attribute the observed differences in sensitivity among non-primary glomeruli to learning.

Building on these findings, we conducted the same set of analyses with a second novel odour, isoamyl acetate (Figure 5.9). Segregating glomeruli based on odour selectively, we again found a significant difference in those that were dual-responsive to the conditioned and unconditioned odour (Figure 5.9A left, $p = < 0.001$, two-way ANOVA, N = 17). Compared with naïve animals, significantly fewer glomeruli were responsive in the exposed cohort ($p = 0.025$, post-hoc Tukey's HSD test, N = 10) with even more pronounced differences observed in the associated cohort ($p = 0.0007$, post-hoc Tukey's HSD test, N = 11). These results corroborate our earlier findings from Figure 5.7, indicating that learning-induced sensitivity changes affect responses to novel odours. Additionally, we detected a significant overall difference in the fraction of glomeruli selective to isoamyl acetate (Figure 5.9A right, $p = 0.001$, two-way ANOVA, N = 17). However, these differences were not significant in specific cohort comparisons (naïve vs exposed: $p = 0.63$, N = 10, naïve vs associated: $p = 0.26$, N = 11, post-hoc Tukey's HSD test). Given the particularly small number of isoamyl acetate-selective glomeruli, this could simply be an artifact of the limited sample size. The amplitude of isoamyl acetate-evoked responses in dual-responsive glomeruli were comparable

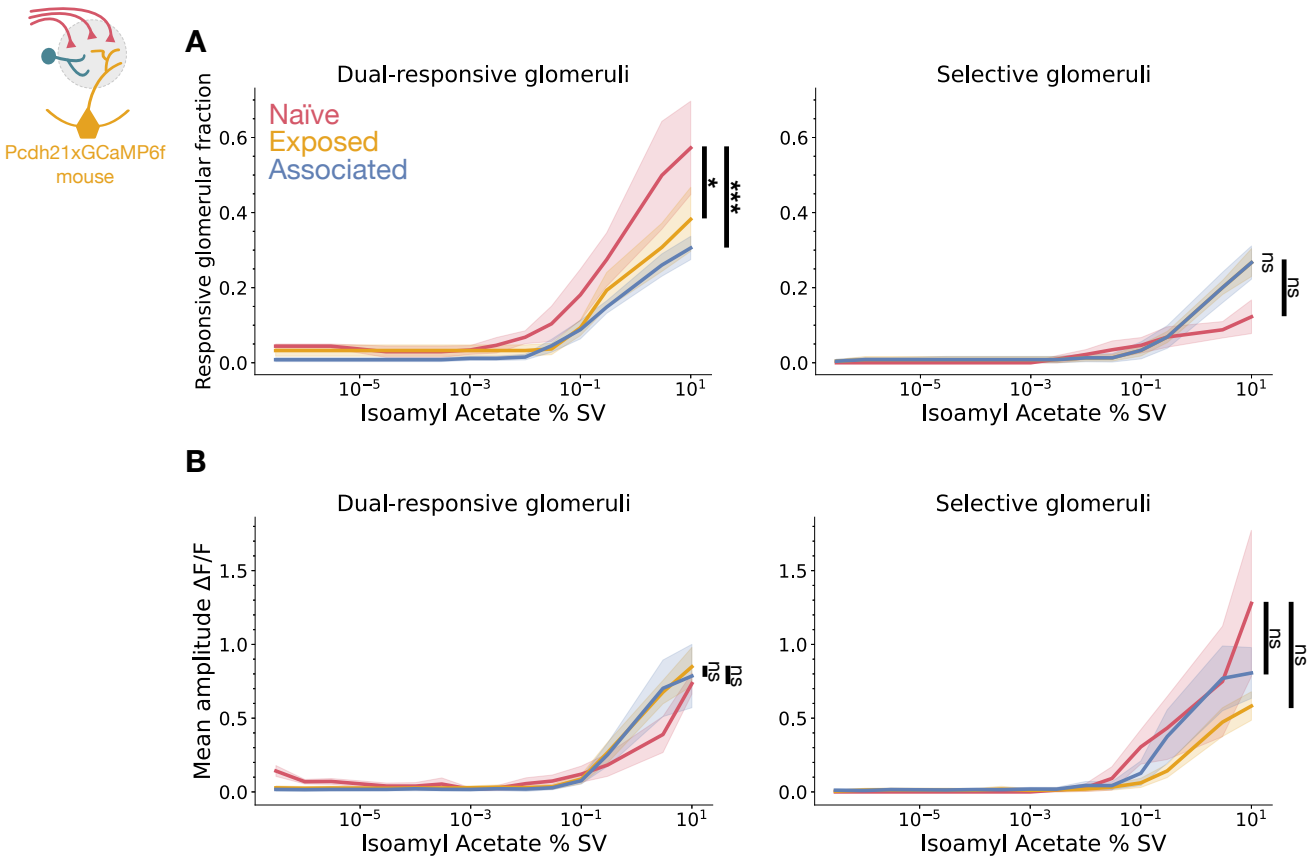

Figure 5.9: Associative Learning reduces the Fraction of Dual-Responsive Glomeruli II

A) Left: Fraction of glomeruli responsive to both ethyl tiglate and isoamyl acetate in a field of view (naïve vs exposed: p = 0.025, naïve vs associated: p = 0.0007, post-hoc Tukey's HSD test) and Right: glomeruli responsive to isoamyl acetate only (naïve vs exposed: p = 0.63, naïve vs associated: p = 0.26, post-hoc Tukey's HSD test), as a function of isoamyl acetate concentration. Data are displayed as mean ± SEM for mice naïve to ethyl tiglate (N = 4), those exposed to the odour for 7 days (N = 6), and those that learnt to associate the odour with food over 7 days (N = 7). B) Left: Mean response amplitude for dual-responsive glomeruli (p = 0.74, two-way ANOVA) and Right: selective glomeruli (naïve vs exposed: p = 0.55, naïve vs associated: p = 0.4, post-hoc Tukey's HSD test) shown in A.

across all cohorts (Figure 5.9B left, p = 0.74, respectively, two-way ANOVA, N = 17), with no significant differences detected between groups in glomeruli selective to isoamyl acetate either (naïve vs exposed: p = 0.55, N = 10, naïve vs associated: p = 0.4, post-hoc Tukey's HSD tests, N = 11). These data suggest that although learning alters sensitivity to novel odours that activate the same glomeruli, the strength of the

responses remains unchanged.

In glomeruli dual-responsive to isoamyl acetate and ethyl tiglate, the detection thresholds varied significantly across cohorts (Figure 5.10, p = 0.002, PERMANOVA, N = 17). Although all cohorts displayed a median concentration of 0.3 ± 0.3 % (median ± MAD), post-hoc analysis showed significant differences between the exposed (p = 0.001, N = 10) and associated (p = 0.0019, N = 11) cohorts compared to naïve (post-hoc PERMANOVA pair-wise comparisons, Benjamini-Hochberg corrected). Together with our findings from Figure 5.8, these data indicate that both forms of learning reduce the sensitivity of dual-responsive glomeruli, necessitating stronger input for activation. This is reflected in the probability distributions for both odours (Figure 5.10), where the likelihood of detecting ethyl tiglate at stronger concentrations (between 1-10 % SV) increased from 13.5 % in naïve animals to 49.3 % in exposed animals and 31.1 % in those that formed food-odour associations. For isoamyl acetate, detection thresholds were almost exclusively within the range of 0.1-10 % SV in dual-responsive glomeruli, increasing from 82.7 % in the naïve cohort to 90.7 % in the exposed cohort and 88.9 % in the associated cohort. Additionally, similar to observations with 2-heptanone (Figure 5.8), the number of non-responsive glomeruli in learned animals was notably larger, almost three times that of naïve animals (Figure 5.10, naïve = 2, exposed = 6, associated = 5). This supports the idea that the sensitivity changes induced by learning lead less sensitive glomeruli to stop responding altogether. In glomeruli selective for ethyl tiglate, there was a significant difference between detection thresholds across cohorts (Figure 5.10, p = 0.02, Kruskal-Wallis H-test, N = 15). Compared to naïve animals (Figure 5.10, 0.1 ± 0.1 %, median ± MAD), a significantly higher concentration of ethyl tiglate was required to activate selective glomeruli in those that were exposed to the odour for a week (3 ± 0 %, median ± MAD, p = 0.046, Mann-Whitney U pairwise comparisons, Bonferroni corrected, N = 10). However, in animals that associated the odour with food, the increase was not significant (0.3 ± 0.2 %, median ± MAD, naïve vs associated: p = > 1.0, N = 9, exposed vs associated: p = 0.08, N = 11, Mann-Whitney U pairwise comparisons, Bonferroni corrected, N = 9). These results were expected in animals from the exposed cohort and likely would have manifested in the associated

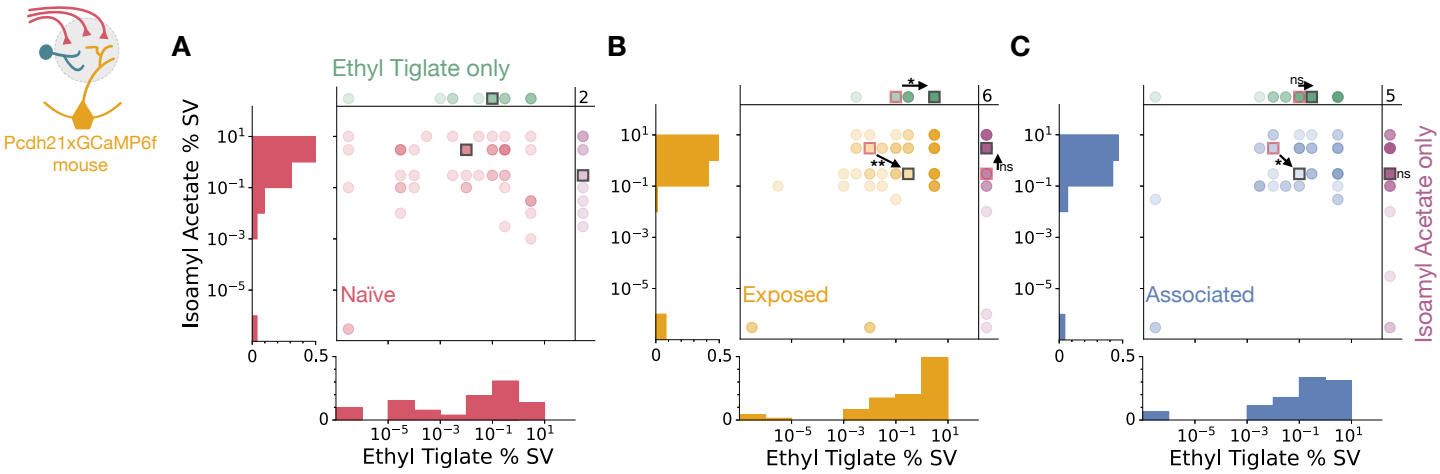

Figure 5.10: Odour Learning Increases the Detection Threshold for Glomeruli Responsive to the Conditioned Odour II

Lowest concentration at which glomeruli responded to ethyl tiglate and isoamyl acetate for Left panel: mice naïve to ethyl tiglate (red dots, N = 9), Middle panel: mice exposed to ethyl tiglate for 7 days (yellow dots, N = 6, p = 0.001 compared with naïve, PERMANOVA pair-wise comparisons, Benjamini-Hochberg corrected), and Right panel: mice that consumed food supplemented with ethyl tiglate for 7 days (blue dots, N = 6, p = 0.019 compared with naïve, PERMANOVA pair-wise comparisons, Benjamini-Hochberg corrected). Across cohorts, detection thresholds were significantly different in both glomeruli selectively responsive to ethyl tiglate (green dots, p = 0.02, Kruskal-Wallis H-test, N = 15, naïve vs exposed: p = 0.046, N = 10, naïve vs associated: p = 1.08, N = 9, exposed vs associated: p = 0.08, N = 11, Mann-Whitey U pairwise comparisons, Bonferroni corrected) or isoamyl acetate (yellow dots, p = 0.03, Kruskal-Wallis H-test, N = 15, exposed vs associated: p = 0.03, N = 11, naïve vs exposed: p = 0.64, N = 10, naïve vs associated: p = > 1, N = 9, Mann-Whitey U pairwise comparisons, Bonferroni corrected). Numbers in top right quadrants of each panel denote the mean number of glomeruli that were non-responsive to both odours, rounded to the nearest whole number. Black square boxes indicate the median for each cohort, arrows in the middle and right panels highlight the degree of change from naïve animals (represented by red boxes in middle and right panels). Histograms depict the distribution of dual-responsive glomeruli for both odours, categorised by the log-transformed lowest concentration of ethyl tiglate or isoamyl acetate that elicited a response. Each bin represents a tenfold increase in concentration.

cohort given a larger sample size. While detection thresholds for isoamyl acetate-selective glomeruli were also significantly different across cohorts (Figure 5.10, p = 0.03, Kruskal-Wallis H-test, N = 15), post-hoc comparisons showed that these

differences were only significant between animals exposed to ethyl tiglate and those that formed food associations with it (exposed vs associated: 3 ± 2.97 % vs 0.3 ± 0.3 %, median ± MAD, p = 0.03, N = 11, naïve vs exposed: 0.3 ± 0.3 % vs 3 ± 2.97 %, median ± MAD, p = 0.64, N = 10, naïve vs associated: 0.3 ± 0.3 % vs 0.3 ± 0.3 %, median ± MAD, p = > 1, N = 9, Mann-Whitney U pairwise compairsons, Bonferroni corrected). These results suggest that the observed effects are specific to glomeruli responsive to the conditioned odour.

These data collectively indicate that exposing animals to or supplementing their food with an odour reduces the sensitivity of all responsive glomeruli. This shift in sensitivity increases the activation threshold and also affects novel odours that engage the same receptor as the conditioned odour. Interestingly, a reduction in response strength was specific to the conditioned odour. A possible explanation is that the mean amplitudes for ethyl tiglate are notably larger than those generated by either 2-heptanone or isoamyl acetate (compare Figure 5.6B with Figures 5.7B left and 5.9B left), thus rendering them less susceptible to noise variations and more likely to exhibit a greater effect size. Nevertheless, it is important to note that these analyses were conducted using separate cohorts of naïve and learned animals, which prevents us from conclusively attributing the observed differences solely to the effects of learning.

Chapter 6: Discussion

In Chapter 3, we identified a small subset of glomeruli that were notably more sensitive to each given odour, rapidly adapting at high concentrations (Figures 3.5 & 3.6). In the case of ethyl tiglate, these glomeruli are exquisitely sensitive, responding to concentrations as low as $3x10^{-7}$ % SV. Our findings from Chapter 4 reveal that mice experience a concentration-induced shift in odour perception (Figures 4.1-2), paralleling reports in humans (*500*, *501*). This perceptual shift coincides with transmission failure from receptor neurons projecting to a single 'primary' glomerulus within the olfactory bulb (Figures 4.3-9). However, upon associating the odour with food, transmission failure is prevented, unifying the odour percept across a broad concentration spectrum (Chapter 5, Figure 5.1-5.5). These data lend credence to the theory that odour identity relies on a sparse code.

6.1 Temporal Dynamics in Odour Encoding

It has been suggested that the relative activation times of glomeruli are the determinant feature of such a sparse code, with the central tenet being those that activate earliest convey the most information (*308*, *310*). Our data align with this model at weaker concentrations and for naïve odours only. In these scenarios, the primary glomerulus is almost invariably the first to activate. However, at odour intensities that generate a distinct percept, this temporal sequence shifts (Figures 4.1E & 4.4B). Yet, after learning, when a broad spectrum of concentrations elicit the same 'food' percept, the primary glomerulus still lags behind others at higher concentrations (Figure 5.5C) despite notable shifts in odour sensitivity (Figures 5.4, 5.5A & B), suggesting that this occurs independent of depolarising block.

It is possible that the coding strategy utilised may be contingent upon the nature of the task. For instance, in operant discrimination tasks, mice are rewarded for making rapid behavioural responses (*300-302*, *308*, *310*), though it requires considerable training. This is in stark contrast to how animals interact with odour objects in natural environments. In our experiments, mice were free to interact with odourised food,

thereby experiencing a range of concentrations that they learn to associate with their proximity to the object (*502*). Under these conditions, the activity of the most sensitive glomerulus will exhibit the highest level of covariance with the odour stimuli; for example, at farther distances from the object, it will be the only glomerulus to activate. With repeated exposures, the primary glomerulus would become the most reliable indicator of the object's presence.

This can be understood within the framework of coherent covariation, a concept which helps explain how we learn the meanings of words (*503*). Just as our brains deduce word meanings by analysing usage patterns across different contexts, an odour stimulus can be discerned by recognising distinct glomerular activity patterns across different object distances. This is in accordance with recent reports that chemical space is represented by sparse and structured glomerular activity at low concentrations (*489*), further reinforcing the idea that coherent covariation is likely to give rise to a sparse odour identity code. Given that natural odours are comprised of complex mixtures, sparse coding for monomolecular odours is likely driven by efficiency, enabling the linear combination of sparse representations elicited by an odour's individual constituents (*504*).

Monomolecular odourants, especially at the high concentrations used in our experiments, are seldom, if ever, encountered in natural settings. Nonetheless, our data show that these odourants can generate a perceptual change (Figure 4.1D-E) that aligns with rapid adaptation in exquisitely sensitive neurons (Figures 4.5A & 4.7D) and is consistent with depolarising block (Figure 4.9). This suggests that individual components of natural odourants may alter the perceived quality of an overall mixture by inducing action potential failure in a subset of neurons encoding that blend. Notably, odour mixtures are known to produce distinct percepts, often perceived at intensities different from the sum of their individual components (*279-281*)—a phenomenon thought to be exploited by perfumers when crafting fragrances (*282*). Animals are also well-documented to discriminate odours within a single sniff and as quickly as 100 ms with training (*300-302*, *308-310*). Our data support these findings (Figure 4.6), indicating that rapid adaptation in the primary glomerulus occurs fast enough to meaningfully

alter the odour code and shape perception.

6.2 Signal Failure and Sensory Adjustment

Our data indicate that the rapid adaptation underlying a perceptual shift for a novel odour is consistent with action potential failure within the olfactory receptor neuron (Figure 4.9). There have been many reports of olfactory receptor neuron recordings where action potential failure has been observed at higher odour concentrations (*59*, *365*, *374*). This arises from an imbalance between the membrane resistance and the odour-evoked receptor currents. Olfactory receptor neurons have exceptionally high input resistances of ~4-5 GΩ (*379*), while the currents induced by odours can be as large as 200 pA (*365*, *379*, *462*, *496*). A basic 'ohmic' calculation would predict that these large receptor currents would result in a dramatic electrical shift within the neuron in the range of 800-1000 mV. However, the reality is more complex due to the reversal potential, which is largely governed by the Ca^{2+}-activated Cl^- current ANO2 (*462*, *505*). Before such a shift can occur, the membrane potential is clamped at a depolarised potential and voltage-gated Na^+ channels remain locked in their inactivate state, preventing action potential transmission along the axon.

On the surface, one might consider this a flaw in the olfactory system. However, the foremost aim of the olfactory system is to detect odours and then to classify them. After prolonged exposure to an odour, olfactory receptor neurons recalibrate their sensitivity, aligning their peak response with the maximum concentration of the odour in their environment. This adjustment averts transmission failure that would otherwise occur at high intensities, thereby maintaining perceptual constancy (Figures 5.3-5.5). It is possible that the changes we observed are in fact due to mere odour exposure, rather than an association between odour and food. Indeed, adaptation indices from primary glomeruli of mice exposed to the odour were lower than those of naïve animals (Figure 5.4E), and although this did not reach a level of statistical significance, this would likely be the case with a larger sample size. The greater effects observed in the associated cohort (Figure 5.4E) may simply be due to the longer durations that mice inevitably spent in close proximity to the odour during feeding times. However,

changes in glomerular size—likely unrelated to depolarising block—were only observed in the associated cohort (Figure 5.5D), indicating that association-dependent modifications are occurring at the level of the glomerulus.

Such plasticity within the nose is akin to that observed with aversive conditioning, where pairing an odour with a foot shock enhances glomerular input for that odour by increasing the population of olfactory receptor neurons which possess the corresponding receptor (*438*, *439*). In contrast, we observed reduced sensitivity in mitral/tufted cell dendrites projecting to primary glomeruli for the conditioned odour (Figures 5.4A, B, E, 5.5A & B), alongside a decrease in glomerular size within the associated cohort (Figure 5.5D). Both observations may reflect a reduction in active olfactory receptor neuron numbers, leading to remodelling of mitral/tufted cell dendrites. Additionally, top-down feedback from noradrenergic (*166*), serotonergic (*189*), and cholinergic (*203*) fibres indirectly modulates olfactory nerve input. Noradrenaline (*167-169*) and acetylcholine (*216-220*) each play important roles in forming odour associations, while increased bulbar noradrenaline has been linked to repeated odour exposure and associative learning (*174*, *176*). Moreover, in developing animals, both noadrenergic (*170-173*) and serotonergic (*191*, *192*) input is reported to be crucial for acquiring odour preferences, potentially working in coordination with one another (*193*). It therefore seems that both the olfactory bulb network and nasal epithelium (*336*, *395*, *396*) have a remarkable capacity to dynamically adjust dendritic architecture, cell generation, receptor densities, and even modulate input through top-down feedback to best capture salient features of the odour environment. Consistent with earlier reports on fear conditioning, simple exposure to the odour does not alter glomerular size (Figure 5.5D); instead, alterations in mitral/tufted cell dendrites and possibly olfactory receptor neuron numbers appear to occur only in response to meaningful stimuli. It remains a puzzling and open question as to how the nasal epithelium is able to discern the salience of an odour.

6.3 Input Strength and Adaptation

Our data demonstrates that higher concentrations of ethyl tiglate, relative to the

response threshold of a given glomerulus, increases the extent of adaptation in olfactory receptor neurons (Figure 3.4C & E). This implies that olfactory receptor neurons adapt more as they approach their responsive capacity. The observed adaptation likely stems primarily from Ca^{2+}-mediated feedback within the odour transduction cascade. Intracellular Ca^{2+}, once bound with calmodulin (CaM), lowers the cyclic nucleotide gated (CNG) channel's affinity for cAMP (*337*, *338*), prompting CNG channel closure and thereby diminishing the odour-evoked current.

Interestingly, we did not observe the same enhancement of adaptation with increasing relative concentrations of isoamyl acetate (Figure 3.4D & F). This discrepancy may be attributable to the dynamic range profiles of glomeruli on the dorsal surface of the olfactory bulb. Compared to isoamyl acetate, ethyl tiglate activated a greater proportion of glomeruli on the dorsal surface and did so at lower concentrations (Figures 3.2E and 3.3E). Consequently, ethyl tiglate likely stimulated a larger fraction of olfactory receptors closer to their maximal range—where this phenomenon is most evident, particularly in cases of suspected depolarising block—compared to isoamyl acetate (Figure 3.4E & F). This is consistent with the finding that, although olfactory receptor neurons exhibit robust receptor currents when subjected to high concentrations of an odour to which they are exquisitely sensitive, this does not lead to further generation of action potentials, despite prolonging the receptor current (*374*). Additionally, at lower concentrations, our adaption index metric is unable to differentiate between weak glomerular activation (which results in a brief peak followed by response termination) and glomerular adaptation. Increasing relative concentrations of both ethyl tiglate and isoamyl acetate reduced the latency for glomeruli to reach their peak response (Figure 3.4G-I). It is well documented that the onset of action potentials are accelerated as olfactory receptor neurons are more strongly stimulated (*89*, *365*, *370-373*), thus higher odour concentrations would enable faster Ca^{2+} detection at the glomerulus.

When presented with a series of identical odour stimuli, we found that glomerular responses were invariably larger for the initial presentation than for all subsequent ones (Figure 3.8). In our setup, clean air was continually delivered to the

mouse, creating an atypical condition. In natural environments a background odour is always present, which likely leads to an overestimation of this adaptation. Nevertheless, a decline in response amplitude to successive stimuli has been extensively reported and is partially mitigated by preventing the inward flux of Ca^{2+} (*339-341*). This pattern of short-term adaptation remained stable after the first pulse (Figure 3.8A & B). We did not explore the time course to complete recovery beyond this adapted state, although recent reports suggest that this occurs within 3 minutes in mitral/tufted glomeruli (*466*). However, we found that neurons which undergo more adaptation take longer to recover their pre-adaptation response amplitudes (Figure 3.9). This was expected, as higher relative concentrations, induced more significant adaptation (Figure 3.4B & C) and thus generate larger receptor currents (*374*). These currents take longer to dissipate, thereby prolonging the inactivation of Na^{+} channels (*355*, *375*, *376*). Consequently, we adjusted inter-stimulus intervals based on odour concentration in an attempt to minimise the impact of adaptation induced by preceding stimuli (Figure 3.1D).

6.4 High-Affinity Glomeruli

For each of the monomolecular odours used, we identified a small number of glomeruli that underwent rapid adaptation at higher concentrations. Among all glomeruli detected in a given mouse, these adaptive glomeruli almost invariably possessed the broadest dynamic range for the odour to which they rapidly adapted (Figure 3.5). Excluding those sensitive to ethyl tiglate, rapid-adapting glomeruli typically responded to their preferred odour across 2-3 log units, the upper limit reported in the literature (*365*, *370*). Additionally, both the dynamic range and concentrations at which these glomeruli rapidly adapt is very similar across mice, although this is likely influenced by nasal patency (*490*). This suggests that rapid adaptation—which our model attributes to depolarising block—is not a feature exclusive to the primary glomerulus; rather, it likely occurs in neurons that have surpassed the limits of their dynamic range. Glomeruli that exhibited this pattern of activity failed to respond even to higher concentrations when presented (Figure 3.7). This is consistent with reports

that high odourant concentrations attenuate and ultimately abolish action potential generation in olfactory receptor neurons (*89*, *365*, *370-373*), which would translate to a reduced input at the glomerulus as spontaneous action potentials will no longer reach the terminals. Since our imaging was confined to the dorsal surface, it is possible that higher-affinity glomeruli might be present elsewhere in the olfactory bulb, potentially limiting our ability to detect an odours 'primary' glomerulus. Indeed, our data from Figure 4.1D suggests that such a glomerulus may exist for 2-heptanone, as animals can detect the odour at concentrations much lower than those at which we observed glomerular responses on the dorsal olfactory bulb.

6.5 Olfactory Learning as a Modifier of Odour Sensitivity

We find that odour exposure and associative learning lead to a reduced proportion of responsive glomeruli (Figure 5.6A). As expected, the observed effects were confined to glomeruli that responded to the conditioned odour, but did extend to novel odours that activated the same glomeruli as the conditioned odour (Figures 5.7A left & 5.9A left). This reduction in the responsive fraction stems from a shift in glomerular sensitivity, whereby the concentration threshold for activation increases for glomeruli that respond to the conditioned odour (Figures 5.8 & 5.10). The amplitudes of glomerular responses were also significantly smaller in learned cohorts of mice compared to those in naïve cohorts, but this was observed only for the conditioned odour (Figures 5.6B). In line with these data, odour exposure has been shown to shift odour tuning and consequently decrease the number of responsive mitral/tuted cells (*399-403*). Contrastingly, it has been reported that operant learning, but not odour exposure, enhances input strength from olfactory receptor neurons, improving discriminability between odours at lower concentrations (*443*). However, this study differed from ours in a few important ways: 1) Our recordings were made in the output neurons of the olfactory bulb, the mitral/tufted cells. It has been proposed that post-synaptic inhibition could explain this discrepancy between enhanced input and diminished output in the olfactory bulb (*399*, *402*, *405*, *443*). Whilst we can not definitively rule this out, we have demonstrated that inhibition does not account for the

rapid adaptation we observe in olfactory receptor neurons (Figure 4.8), which we attribute to depolarising block (Figure 4.9). Moreover, the transition from a sustained odour response at lower concentrations to rapid adaptation at higher concentrations is also observed in mitral/tufted cells (compare Figure 4.5A with 4.7D), and this adaptation is abolished with associative learning (Figure 5.4A, B & E). 2) The associative learning protocol incorporated a go/no-go learning paradigm, whereby mice were trained to discriminate between rewarded and unrewarded odours, as opposed to naturally interacting with the odour. Input strength has been shown to increase preferentially for rewarded odours (*506*) and for odours paired with an aversive stimulus (*439*), indicating that the nature of the task itself can be the sole determinant of plasticity and is thus not directly comparable to passive interaction. 3) The total duration of odour exposure equated to less than one hour, whereas in our setup animals were exposed to the odour continuously over a week. Nevertheless, long-term chronic odour exposure has also been shown to enhance sensitivity of olfactory receptor neurons in mice (*397*) and projection neurons in flies (*404*). Interestingly, in both cases, the animals were exposed to weak concentrations of the conditioned odour, supporting the idea that olfactory receptor neurons adjust their dynamic range to optimally represent the odour environment. It is possible that the direction of sensitivity changes in olfactory receptors may depend on their initial sensitivity. These adjustments in sensitivity could be achieved via synaptic and/or receptor turnover (*395*, *499*) and/or processes driven by transcriptional adaptations in response to environmental stimuli (*336*, *396*). Such changes occur rapidly in both immature and mature olfactory receptor neurons (*507-509*), and can even be inherited across generations (*441*).

6.6 A Model for Odour Identity

To accurately identify odours, the olfactory system must overcome two primary challenges: 1) Constancy, the system's capacity to recognise an odour regardless of variations in concentration, which results in different patterns of neural activity. 2) Discrimination, the ability to distinguish between neural activity patterns elicited by

different odourant molecules. Building on our collective findings, we propose a model of how perceptual constancy and identity coding develops in the olfactory system with associative learning (Figure 6.1).

In the naïve animal, the primary glomerulus is sensitive to a broad spectrum of food-odour concentrations. However, at very high concentrations that surpass the dynamic range of the olfactory receptor neurons projecting to these primary glomeruli, action potentials fail to generate, resulting in a loss of signal. In contrast, the number of responsive non-primary glomeruli increases linearly with the concentration of both food and unconditioned odours.

If we apply the combinatorial model, where odour identity is presumed to be encoded by the specific pattern of active glomeruli, this increase in activity would simply add extraneous 'noise' to the neural signal, thereby reducing the robustness of the food-odour percept (compare F1 with F4) and, consequently, the animal's ability to distinguish between food and unconditioned odours (compare F4 with U4, respectively). Contrastingly, in a model where a singular primary glomerulus serves as the sole carrier for odour identity, the food-odour percept would remain stable across a range of concentrations, up until the point of depolarising block. This configuration implies that discriminability between food and unconditioned odours would also be improved for all but the highest concentration (Figure 6.1).

After associative learning, where the animal has been conditioned to a specific odour, there is a marked shift in the glomerular response to that odour - a sensitivity decrease by orders of magnitude (Figure 6.1). Within the combinatorial framework, the animal would now retain a consistent and food-odour perception over a larger portion of the concentration range. However, at the strongest concentrations, the food-odour percept is altered (compare F1 with F4) and still shares pattern similarities with the unconditioned odour (compare U4 with F4). In the primary model which we propose, a sensitivity adjustment in the primary glomerulus alone would preserve the food-odour identity across all encountered concentrations, completely dissociating the salient stimulus from unconditioned odours, thereby optimising the olfactory system's representation of the odour environment.

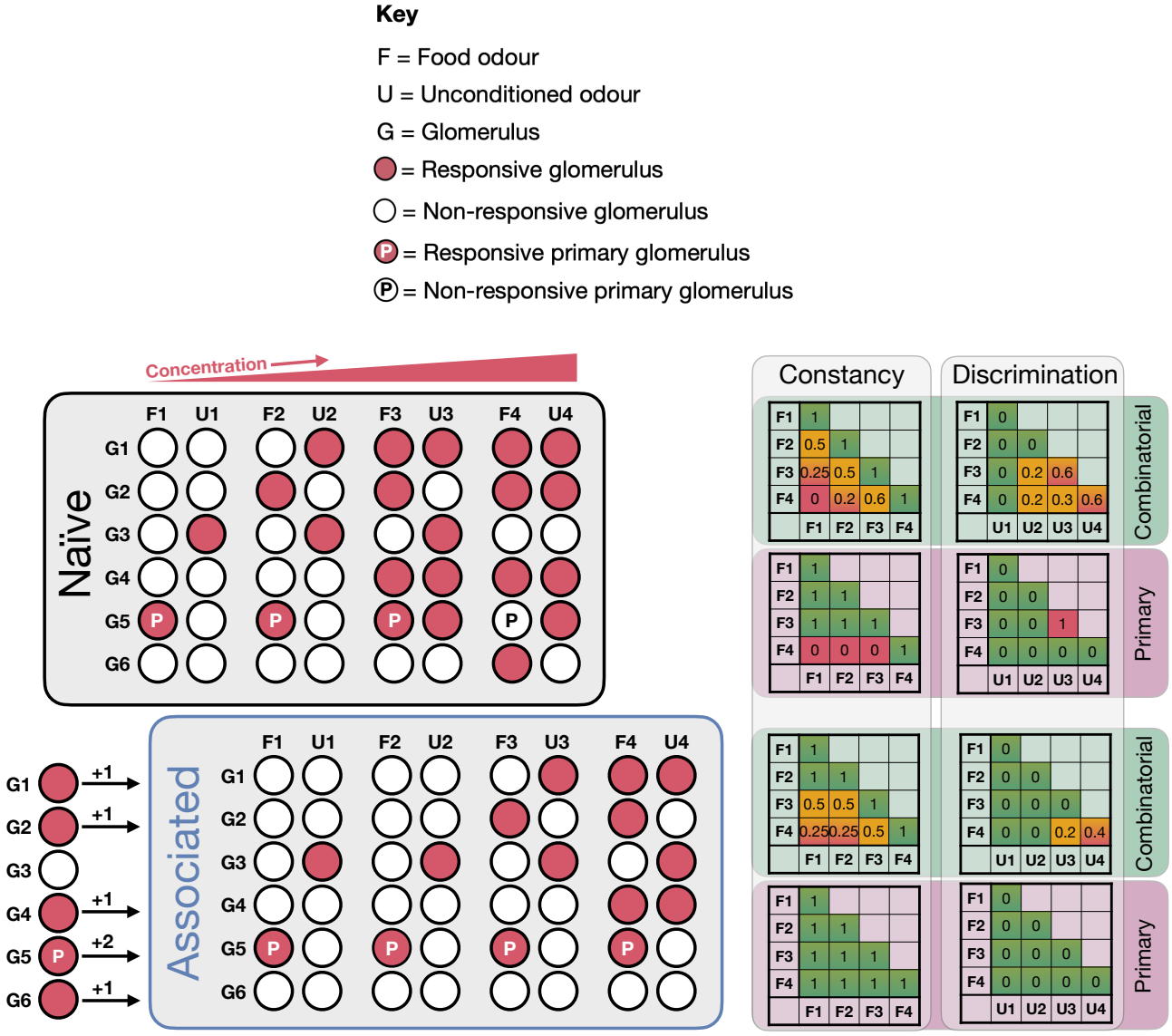

Figure 6.1: A Model for Perceptual Constancy in Olfaction

Top Left: In the naïve state, the food odour percept breaks down at higher concentrations when the primary glomerulus stops responding. Bottom Left: After associative learning, glomerular sensitivity shifts by orders of magnitude (denoted by numbers and arrows), preserving the food odour percept across the entire range of concentrations. Right: Matrices quantifying constancy (where 1 represents a wholly preserved odour percept) and discrimination (0 indicates no similarity between odour percepts) for naïve and associated cohorts of mice, within the framework of both combinatorial and primary models of odour coding. F1-4 = food-odour at four different concentrations, U1-4 = unconditioned odour at four different concentrations, G1-6 = six different glomeruli, P = primary glomerulus for the food-odour.

6.7 Conclusion & Future Directions

The mechanisms by which animals consistently recognise the same object, despite variations in sensory input within a dynamic odour landscape, are not well understood. To our knowledge, we provide the first evidence suggesting that rapid adaptation in a single glomerulus can lead to a perceptual change in mammals. We further propose a model in which this rapid adaptation may result from depolarising block in primary sensory neurons that project to this glomerulus. Depolarising block has been reported to induce a perceptual switch from attraction to aversion in flies expressing only a single high-affinity receptor (*510*). However, it is possible that what the authors interpret as aversion may actually be the flies' inability to detect the odour, given the absence of other glomeruli capable of sensing it. Additionally, our findings indicate that perceptual constancy arises through dynamic range matching in a single glomerulus. We propose a model that explains how sensory experiences enable animals to maintain a stable neural representation of an odour's identity.

In our recordings from learned mice, we measured Ca^{2+} activity in mitral/tufted cell glomeruli. While we observed a concentration-induced rapid decline in olfactory receptor neuron activity below baseline and confirmed that this occurs independently of feedback inhibition, we cannot conclusively state that postsynaptic processing does not play a role in mitigating this phenomenon. We reported a sensitivity shift among glomeruli responsive to the conditioned odour following learning. However, as our imaging of naïve and learned mice was performed in separate cohorts, we could not determine how learning specifically alters the sensitivity of individual glomeruli. Moreover, despite the primary glomerulus for ethyl tiglate being readily identifiable due its stereotyped position and unparalleled sensitivity, we were unable to demonstrate that learning abolishes rapid adaptation in the same animal. Additionally, although we observed a concentration-dependent perceptual shift with 2-heptanone, we did not identify any glomeruli that responded to this odour across the entire concentration range on the dorsal surface. Therefore, we cannot definitively extend our model to all odours.

Measuring the input to the olfactory bulb in learned mice could clarify whether

the elimination of rapid adaptation is solely due to peripheral changes or also influenced by postsynaptic mechanisms, particularly through the pharmacological blockade of feedback inhibition. Additionally, monitoring neural activity in the same animals before and after learning would offer clearer insights into how odour sensitivity changes in specific glomeruli. Are sensitivity shifts most pronounced in high-affinity glomeruli? Our findings indicate that the primary glomerulus adjusts its dynamic range to effectively respond to strong concentrations of ethyl tiglate. How would the primary glomerulus respond if animals' diets were supplemented with a 'weak percept' concentration? Would rapid adaptation still ensue at high concentrations? Furthermore, imaging at regular intervals throughout the learning process could map the progression of dynamic range matching. Tagging the primary glomerulus with a fluorescent marker would enhance this analysis by enabling the monitoring of changes in its size over time. Optogenetics could be utilised to conclusively demonstrate that the primary glomerulus is the sole carrier of odour identity; presumably, stimulating this glomerulus in freely-behaving learned mice would elicit food-seeking behaviour. Our model of perceptual constancy could be further supported by identifying primary glomeruli for other odours that induce perceptual shifts. This could be achieved by focusing on the medial, lateral, caudal and rostral edges of the olfactory bulb—areas that were not thoroughly explored in our imaging sessions. Finally, it remains unclear whether the diverse range of response dynamics we observed are primarily dictated by the olfactory receptors themselves. Employing genetic labelling of specific olfactory receptors combined with measurements from neurons that input to, modulate, and output from the olfactory bulb, could elucidate whether these dynamics are shaped via network processes or are directly inherited from the receptor currents of input neurons.

Ultimately, our data indicate that odour identity relies on a sparse code. Through experience, the olfactory system adjusts its sensitivity to maintain the integrity of this code, thus ensuring perception remains constant in a turbulent environment. These findings underscore the remarkable plasticity of the primary sensory organ and move us closer to understanding how animals navigate and perceive their sensory environments.

Bibliography

1. Y. Sugita, Experience in early infancy is indispensable for color perception. *Curr Biol* **14**, 1267–1271 (2004).
2. J. Yang, S. Kanazawa, M. K. Yamaguchi, I. Motoyoshi, Pre-constancy Vision in Infants. *Curr Biol* **25**, 3209–3212 (2015).
3. G. Poncelet, S. M. Shimeld, The evolutionary origins of the vertebrate olfactory system. *Open Biol* **10**, 200330 (2020).
4. C. Bushdid, M. O. Magnasco, L. B. Vosshall, A. Keller, Humans can discriminate more than 1 trillion olfactory stimuli *Science* (2014).
5. R. C. Gerkin, J. B. Castro, The number of olfactory stimuli that humans can discriminate is still unknown *Elife* (2015).
6. M. Meister, On the dimensionality of odor space *Elife* (2015).
7. W. B. Sunarharum, D. J. Williams, H. E. Smyth, Complexity of coffee flavor: A compositional and sensory perspective *Food Research International* **62**, 315–325 (2014).
8. M. Schubert, B. S. Hansson, S. Sachse, The banana code-natural blend processing in the olfactory circuitry of Drosophila melanogaster. *Front Physiol* **5**, 59 (2014).
9. E. R. Kandel, J. D. Koester, S. H. Mack, S. A. Siegelbaum, *Principles of Neural Science, Sixth Edition* (McGraw Hill Professional, 2021).
10. M. Luo, M. S. Fee, L. C. Katz, Encoding pheromonal signals in the accessory olfactory bulb of behaving mice. *Science* **299**, 1196–1201 (2003).
11. W. Lin, J. Arellano, B. Slotnick, D. Restrepo, Odors detected by mice deficient in cyclic nucleotide-gated channel subunit A2 stimulate the main olfactory system. *J Neurosci* **24**, 3703–3710 (2004).
12. V. S. Mandiyan, J. K. Coats, N. M. Shah, Deficits in sexual and aggressive behaviors in Cnga2 mutant mice *Nature Neuroscience* **8**, 1660–1662 (2005).
13. F. Xu, M. Schaefer, I. Kida, J. Schafer, N. Liu, D. L. Rothman, F. Hyder, D. Restrepo, G. M. Shepherd, Simultaneous activation of mouse main and accessory olfactory bulbs by odors or pheromones. *J Comp Neurol* **489**, 491–500 (2005).
14. Z. Wang, C. Balet Sindreu, V. Li, A. Nudelman, G. C. Chan, D. R. Storm, Pheromone detection in male mice depends on signaling through the type 3 adenylyl cyclase in the

main olfactory epithelium. *J Neurosci* **26**, 7375–7379 (2006).

15. M. Sam, S. Vora, B. Malnic, W. Ma, M. V. Novotny, L. B. Buck, Odorants may arouse instinctive behaviours *Nature* **412**, 142–142 (2001).
16. K. Trinh, D. R. Storm, Vomeronasal organ detects odorants in absence of signaling through main olfactory epithelium. *Nat Neurosci* **6**, 519–525 (2003).
17. J. F. Kaluza, F. Gussing, S. Bohm, H. Breer, J. Strotmann, Olfactory receptors in the mouse septal organ. *J Neurosci Res* **76**, 442–452 (2004).
18. H. Tian, M. Ma, Molecular organization of the olfactory septal organ. *J Neurosci* **24**, 8383–8390 (2004).
19. M. Ma, X. Grosmaitre, C. L. Iwema, H. Baker, C. A. Greer, G. M. Shepherd, Olfactory signal transduction in the mouse septal organ *Journal of Neuroscience* **23**, 317–324 (2003).
20. X. Grosmaitre, L. C. Santarelli, J. Tan, M. Luo, M. Ma, Dual functions of mammalian olfactory sensory neurons as odor detectors and mechanical sensors. *Nat Neurosci* **10**, 348–354 (2007).
21. J. Fleischer, K. Schwarzenbacher, S. Besser, N. Hass, H. Breer, Olfactory receptors and signalling elements in the Grueneberg ganglion. *J Neurochem* **98**, 543–554 (2006).
22. J. Fleischer, K. Schwarzenbacher, H. Breer, Expression of trace amine-associated receptors in the Grueneberg ganglion. *Chem Senses* **32**, 623–631 (2007).
23. J. Brechbühl, M. Klaey, M. C. Broillet, Grueneberg ganglion cells mediate alarm pheromone detection in mice. *Science* **321**, 1092–1095 (2008).
24. D. M. Juilfs, H.-J. Fülle, A. Z. Zhao, M. D. Houslay, D. L. Garbers, J. A. Beavo, A subset of olfactory neurons that selectively express cGMP-stimulated phosphodiesterase (PDE2) and guanylyl cyclase-D define a unique olfactory signal transduction pathway *Proceedings of the National Academy of Sciences* **94**, 3388–3395 (1997).
25. S. H. Fuss, M. Omura, P. Mombaerts, The Grueneberg ganglion of the mouse projects axons to glomeruli in the olfactory bulb. *Eur J Neurosci* **22**, 2649–2654 (2005).
26. D. S. Koos, S. E. Fraser, The Grueneberg ganglion projects to the olfactory bulb *Neuroreport* **16**, 1929–1932 (2005).
27. D. Roppolo, V. Ribaud, V. P. Jungo, C. Lüscher, I. Rodriguez, Projection of the Grüneberg ganglion to the mouse olfactory bulb. *Eur J Neurosci* **23**, 2887–2894 (2006).
28. T. Leinders-Zufall, R. E. Cockerham, S. Michalakis, M. Biel, D. L. Garbers, R. R. Reed, F.

Zufall, S. D. Munger, Contribution of the receptor guanylyl cyclase GC-D to chemosensory function in the olfactory epithelium *Proceedings of the National Academy of Sciences* **104**, 14507–14512 (2007).

29. A. Walz, P. Feinstein, M. Khan, P. Mombaerts, Axonal wiring of guanylate cyclase-D-expressing olfactory neurons is dependent on neuropilin 2 and semaphorin 3F. *Development* **134**, 4063–4072 (2007).
30. C. Y. Su, K. Menuz, J. R. Carlson, Olfactory perception: receptors, cells, and circuits. *Cell* **139**, 45–59 (2009).
31. B. Zapiec, P. Mombaerts, The Zonal Organization of Odorant Receptor Gene Choice in the Main Olfactory Epithelium of the Mouse. *Cell Rep* **30**, 4220–4234.e5 (2020).
32. B. Malnic, J. Hirono, T. Sato, L. B. Buck, Combinatorial receptor codes for odors. *Cell* **96**, 713–723 (1999).
33. A. Chess, I. Simon, H. Cedar, R. Axel, Allelic inactivation regulates olfactory receptor gene expression *Cell* **78**, 823–834 (1994).
34. T. Bozza, P. Feinstein, C. Zheng, P. Mombaerts, Odorant receptor expression defines functional units in the mouse olfactory system *Journal of Neuroscience* **22**, 3033–3043 (2002).
35. P. Mombaerts, F. Wang, C. Dulac, S. K. Chao, A. Nemes, M. Mendelsohn, J. Edmondson, R. Axel, Visualizing an olfactory sensory map. *Cell* **87**, 675–686 (1996).
36. L. Buck, R. Axel, A novel multigene family may encode odorant receptors: a molecular basis for odor recognition *Cell* **65**, 175–187 (1991).
37. K. Raming, J. Krieger, J. Strotmann, I. Boekhoff, S. Kubick, C. Baumstark, H. Breer, Cloning and expression of odorant receptors. *Nature* **361**, 353–356 (1993).
38. R. C. Araneda, A. D. Kini, S. Firestein, The molecular receptive range of an odorant receptor *Nature neuroscience* **3**, 1248–1255 (2000).
39. I. Gaillard, S. Rouquier, J. P. Pin, P. Mollard, S. Richard, C. Barnabé, J. Demaille, D. Giorgi, A single olfactory receptor specifically binds a set of odorant molecules. *Eur J Neurosci* **15**, 409–418 (2002).
40. X. Grosmaitre, A. Vassalli, P. Mombaerts, G. M. Shepherd, M. Ma, Odorant responses of olfactory sensory neurons expressing the odorant receptor MOR23: a patch clamp analysis in gene-targeted mice *Proceedings of the National Academy of Sciences* **103**, 1970–1975

(2006).

41. H. Saito, Q. Chi, H. Zhuang, H. Matsunami, J. D. Mainland, Odor coding by a Mammalian receptor repertoire. *Sci Signal* **2**, ra9 (2009).
42. M. Ma, G. M. Shepherd, Functional mosaic organization of mouse olfactory receptor neurons *Proceedings of the National Academy of Sciences* **97**, 12869–12874 (2000).
43. A. Dewan, Olfactory signaling via trace amine-associated receptors. *Cell Tissue Res* **383**, 395–407 (2021).
44. Y. Hashiguchi, M. Nishida, Evolution of trace amine associated receptor (TAAR) gene family in vertebrates: lineage-specific expansions and degradations of a second class of vertebrate chemosensory receptors expressed in the olfactory epithelium. *Mol Biol Evol* **24**, 2099–2107 (2007).
45. R. Pacifico, A. Dewan, D. Cawley, C. Guo, T. Bozza, An olfactory subsystem that mediates high-sensitivity detection of volatile amines. *Cell Rep* **2**, 76–88 (2012).
46. P. Shi, J. P. Bielawski, H. Yang, Y. P. Zhang, Adaptive diversification of vomeronasal receptor 1 genes in rodents. *J Mol Evol* **60**, 566–576 (2005).
47. J. M. Young, B. J. Trask, V2R gene families degenerated in primates, dog and cow, but expanded in opossum. *Trends Genet* **23**, 212–215 (2007).
48. H. Shinohara, T. Asano, K. Kato, Differential localization of G-proteins Gi and Go in the accessory olfactory bulb of the rat *Journal of Neuroscience* **12**, 1275–1279 (1992).
49. A. Berghard, L. B. Buck, Sensory transduction in vomeronasal neurons: evidence for G alpha o, G alpha i2, and adenylyl cyclase II as major components of a pheromone signaling cascade *Journal of Neuroscience* **16**, 909–918 (1996).
50. C. Jia, G. Goldman, M. Halpern, Development of vomeronasal receptor neuron subclasses and establishment of topographic projections to the accessory olfactory bulb *Developmental Brain Research* **102**, 209–216 (1997).
51. C. Dulac, A. T. Torello, Molecular detection of pheromone signals in mammals: from genes to behaviour. *Nat Rev Neurosci* **4**, 551–562 (2003).
52. S. Rivière, L. Challet, D. Fluegge, M. Spehr, I. Rodriguez, Formyl peptide receptor-like proteins are a novel family of vomeronasal chemosensors. *Nature* **459**, 574–577 (2009).
53. H. Arakawa, K. R. Kelliher, F. Zufall, S. D. Munger, The receptor guanylyl cyclase type D (GC-D) ligand uroguanylin promotes the acquisition of food preferences in mice. *Chem*

Senses **38**, 391–397 (2013).

54. S. D. Munger, T. Leinders-Zufall, L. M. McDougall, R. E. Cockerham, A. Schmid, P. Wandernoth, G. Wennemuth, M. Biel, F. Zufall, K. R. Kelliher, An olfactory subsystem that detects carbon disulfide and mediates food-related social learning. *Curr Biol* **20**, 1438–1444 (2010).
55. J. Hu, C. Zhong, C. Ding, Q. Chi, A. Walz, P. Mombaerts, H. Matsunami, M. Luo, Detection of near-atmospheric concentrations of CO2 by an olfactory subsystem in the mouse. *Science* **317**, 953–957 (2007).
56. J. Fleischer, H. Breer, J. Strotmann, Mammalian olfactory receptors. *Front Cell Neurosci* **3**, 9 (2009).
57. D. T. Moran, J. C. Rowley, B. W. Jafek, M. A. Lovell, The fine structure of the olfactory mucosa in man *Journal of neurocytology* **11**, 721–746 (1982).
58. K. Kawagishi, M. Ando, K. Yokouchi, N. Sumitomo, M. Karasawa, N. Fukushima, T. Moriizumi, Stereological quantification of olfactory receptor neurons in mice. *Neuroscience* **272**, 29–33 (2014).
59. R. C. Challis, H. Tian, J. Wang, J. He, J. Jiang, X. Chen, W. Yin, T. Connelly, L. Ma, C. R. Yu, J. L. Pluznick, D. R. Storm, L. Huang, K. Zhao, M. Ma, An Olfactory Cilia Pattern in the Mammalian Nose Ensures High Sensitivity to Odors. *Curr Biol* **25**, 2503–2512 (2015).
60. K. J. Ressler, S. L. Sullivan, L. B. Buck, A zonal organization of odorant receptor gene expression in the olfactory epithelium *Cell* **73**, 597–609 (1993).
61. R. Vassar, J. Ngai, R. Axel, Spatial segregation of odorant receptor expression in the mammalian olfactory epithelium *Cell* **74**, 309–318 (1993).
62. J. Strotmann, L. Wanner, T. Helfrich, A. Beck, H. Breer, Rostro-caudal patterning of receptor-expressing olfactory neurones in the rat nasal cavity *Cell and tissue research* **278**, 11–20 (1994).
63. J. Strotmann, I. Wanner, T. Helfrich, A. Beck, C. Meinken, S. Kubick, H. Breer, Olfactory neurones expressing distinct odorant receptor subtypes are spatially segregated in the nasal neuroepithelium *Cell and tissue research* **276**, 429–438 (1994).
64. C. M. Bate, V. M. M. Carr, P. P. C. Graziadei…, Continuous nerve cell renewal in the olfactory system *Development of sensory …* (1978).
65. C. G. Hahn, L. Y. Han, N. E. Rawson, N. Mirza…, In vivo and in vitro neurogenesis in

human olfactory epithelium *Journal of ...* (2005).

66. K. Kondo, K. Suzukawa, T. Sakamoto…, Age-related changes in cell dynamics of the postnatal mouse olfactory neuroepithelium: Cell proliferation, neuronal differentiation, and cell death *Journal of ...* (2010).
67. J. W. Hinds, P. L. Hinds, N. A. McNelly, An autoradiographic study of the mouse olfactory epithelium: evidence for long-lived receptors *The Anatomical Record* (1984).
68. A. Mackay-Sim, P. W. Kittel, On the life span of olfactory receptor neurons *European Journal of Neuroscience* (1991).
69. A. M. Holl, Survival of mature mouse olfactory sensory neurons labeled genetically perinatally *Molecular and Cellular Neuroscience* (2018).
70. V. Gaun, J. R. Martens, J. E. Schwob, Lifespan of mature olfactory sensory neurons varies with location in the mouse olfactory epithelium and age of the animal. *J Comp Neurol* **530**, 2238–2251 (2022).
71. J. E. Schwob, S. L. Youngentob, G. Ring…, Reinnervation of the rat olfactory bulb after methyl bromide-induced lesion: timing and extent of reinnervation *Journal of ...* (1999).
72. C. T. Leung, P. A. Coulombe, R. R. Reed, Contribution of olfactory neural stem cells to tissue maintenance and regeneration *Nature neuroscience* (2007).
73. S. Kikuta, T. Sakamoto, S. Nagayama…, Sensory deprivation disrupts homeostatic regeneration of newly generated olfactory sensory neurons after injury in adult mice *... of Neuroscience* (2015).
74. D. T. Jones, R. R. Reed, Golf: an olfactory neuron specific-G protein involved in odorant signal transduction. *Science* **244**, 790–795 (1989).
75. H. A. Bakalyar, R. R. Reed, Identification of a specialized adenylyl cyclase that may mediate odorant detection. *Science* **250**, 1403–1406 (1990).
76. T. Nakamura, G. H. Gold, A cyclic nucleotide-gated conductance in olfactory receptor cilia *Nature* **325**, 442–444 (1987).
77. R. S. Dhallan, K.-W. Yau, K. A. Schrader, R. R. Reed, Primary structure and functional expression of a cyclic nucleotide-activated channel from olfactory neurons *Nature* **347**, 184–187 (1990).
78. S. J. Kleene, R. C. Gesteland, Calcium-activated chloride conductance in frog olfactory cilia *Journal of Neuroscience* **11**, 3624–3629 (1991).

79. T. Kurahashi, K.-W. Yau, Co-existence of cationic and chloride components in odorant-induced current of vertebrate olfactory receptor cells *Nature* **363**, 71–74 (1993).
80. S. J. Kleene, Origin of the chloride current in olfactory transduction *Neuron* **11**, 123–132 (1993).
81. G. Lowe, G. H. Gold, Nonlinear amplification by calcium-dependent chloride channels in olfactory receptor cells *Nature* **366**, 283–286 (1993).
82. J. Reisert, P. J. Bauer, K.-W. Yau, S. Frings, The Ca-activated Cl Channel and its Control in Rat Olfactory Receptor Neurons *The Journal of General Physiology* **122**, 349–364 (2003).
83. D. Reuter, K. Zierold, W. H. Schröder, S. Frings, A depolarizing chloride current contributes to chemoelectrical transduction in olfactory sensory neurons in situ *Journal of Neuroscience* **18**, 6623–6630 (1998).
84. H. Kaneko, I. Putzier, S. Frings, U. B. Kaupp, T. Gensch, Chloride Accumulation in Mammalian Olfactory Sensory Neurons *The Journal of Neuroscience* **24**, 7931–7938 (2004).
85. J. Reisert, J. Lai, K.-W. Yau, J. Bradley, Mechanism of the Excitatory Cl− Response in Mouse Olfactory Receptor Neurons *Neuron* **45**, 553–561 (2005).
86. M. Dibattista, S. Pifferi, A. Boccaccio, A. Menini, J. Reisert, The long tale of the calcium activated Cl^- channels in olfactory transduction. *Channels (Austin)* **11**, 399–414 (2017).
87. G. Pietra, M. Dibattista, A. Menini, J. Reisert, A. Boccaccio, The Ca2+-activated Cl- channel TMEM16B regulates action potential firing and axonal targeting in olfactory sensory neurons. *J Gen Physiol* **148**, 293–311 (2016).
88. F. Neureither, N. Stowasser, S. Frings, F. Möhrlen, Tracking of unfamiliar odors is facilitated by signal amplification through anoctamin 2 chloride channels in mouse olfactory receptor neurons. *Physiol Rep* **5**, e13373 (2017).
89. J. Reisert, H. R. Matthews, Adaptation of the odour-induced response in frog olfactory receptor cells *The Journal of physiology* **519**, 801–813 (1999).
90. G. J. Murphy, L. L. Glickfeld, Z. Balsen, J. S. Isaacson, Sensory neuron signaling to the brain: properties of transmitter release from olfactory nerve terminals. *J Neurosci* **24**, 3023–3030 (2004).
91. M. R. Meyer, A. Angele, E. Kremmer, U. B. Kaupp, F. Müller, A cGMP-signaling pathway in a subset of olfactory sensory neurons *Proceedings of the National Academy of Sciences*

97, 10595–10600 (2000).

92. J. Fleischer, K. Mamasuew, H. Breer, Expression of cGMP signaling elements in the Grueneberg ganglion *Histochemistry and cell biology* **131**, 75–88 (2009).
93. C. Y. Liu, S. E. Fraser, D. S. Koos, Grueneberg ganglion olfactory subsystem employs a cGMP signaling pathway *Journal of Comparative Neurology* **516**, 36–48 (2009).
94. K. Mamasuew, N. Hofmann, V. Kretzschmann, M. Biel, R.-B. Yang, H. Breer, J. Fleischer, Chemo-and thermosensory responsiveness of Grueneberg ganglion neurons relies on cyclic guanosine monophosphate signaling elements *Neurosignals* **19**, 198–209 (2011).
95. A. Schmid, M. Pyrski, M. Biel…, Grueneberg ganglion neurons are finely tuned cold sensors *Journal of …* (2010).
96. A. D. Zimmerman, S. D. Munger, Olfactory subsystems associated with the necklace glomeruli in rodents. *Cell Tissue Res* **383**, 549–557 (2021).
97. S. Hecht, S. Shlaer, M. H. Pirenne, Energy, quanta, and vision *The Journal of general physiology* (1942).
98. K. W. Yau, Phototransduction mechanism in retinal rods and cones. The Friedenwald Lecture. *Investigative ophthalmology & visual science* (1994).
99. I. B. Leskov, V. A. Klenchin, J. W. Handy, G. G. Whitlock…, The gain of rod phototransduction: reconciliation of biochemical and electrophysiological measurements *Neuron* (2000).
100. V. Bhandawat, J. Reisert, K. W. Yau, Elementary response of olfactory receptor neurons to odorants. *Science* **308**, 1931–1934 (2005).
101. V. Bhandawat, J. Reisert, K. W. Yau, Signaling by olfactory receptor neurons near threshold. *Proc Natl Acad Sci U S A* **107**, 18682–18687 (2010).
102. Y. Ben-Chaim, M. M. Cheng, K. W. Yau, Unitary response of mouse olfactory receptor neurons. *Proc Natl Acad Sci U S A* **108**, 822–827 (2011).
103. J. P. Royet, C. Souchier, F. Jourdan, H. Ploye, Morphometric study of the glomerular population in the mouse olfactory bulb: numerical density and size distribution along the rostrocaudal axis. *J Comp Neurol* **270**, 559–568 (1988).
104. R. Vassar, S. K. Chao, R. Sitcheran, J. M. Nun, L. B. Vosshall…, Topographic organization of sensory projections to the olfactory bulb *Cell* (1994).
105. K. J. Ressler, S. L. Sullivan, L. B. Buck, Information coding in the olfactory system:

evidence for a stereotyped and highly organized epitope map in the olfactory bulb *Cell* (1994).

106. J. Strotmann, S. Conzelmann, A. Beck, P. Feinstein, H. Breer, P. Mombaerts, Local permutations in the glomerular array of the mouse olfactory bulb *Journal of Neuroscience* **20**, 6927–6938 (2000).
107. M. L. Schaefer, T. E. Finger, D. Restrepo, Variability of position of the P2 glomerulus within a map of the mouse olfactory bulb. *J Comp Neurol* **436**, 351–362 (2001).
108. E. R. Soucy, D. F. Albeanu, A. L. Fantana, V. N. Murthy, M. Meister, Precision and diversity in an odor map on the olfactory bulb. *Nat Neurosci* **12**, 210–220 (2009).
109. K. Mori, K. Kishi, H. Ojima, Distribution of dendrites of mitral, displaced mitral, tufted, and granule cells in the rabbit olfactory bulb. *J Comp Neurol* **219**, 339–355 (1983).
110. L. B. Haberly, J. L. Price, The axonal projection patterns of the mitral and tufted cells of the olfactory bulb in the rat *Brain research* **129**, 152–157 (1977).
111. E. Orona, E. C. Rainer, J. W. Scott, Dendritic and axonal organization of mitral and tufted cells in the rat olfactory bulb. *J Comp Neurol* **226**, 346–356 (1984).
112. S. Nagayama, R. Homma, F. Imamura, Neuronal organization of olfactory bulb circuits. *Front Neural Circuits* **8**, 98 (2014).
113. A. J. Pinching, T. P. Powell, The neuron types of the glomerular layer of the olfactory bulb. *J Cell Sci* **9**, 305–345 (1971).
114. K. M. Igarashi, N. Ieki, M. An, Y. Yamaguchi, S. Nagayama, K. Kobayakawa, R. Kobayakawa, M. Tanifuji, H. Sakano, W. R. Chen, K. Mori, Parallel mitral and tufted cell pathways route distinct odor information to different targets in the olfactory cortex. *J Neurosci* **32**, 7970–7985 (2012).
115. F. Imamura, A. Ito, B. J. LaFever, Subpopulations of Projection Neurons in the Olfactory Bulb. *Front Neural Circuits* **14**, 561822 (2020).
116. F. Macrides, S. P. Schneider, Laminar organization of mitral and tufted cells in the main olfactory bulb of the adult hamster. *J Comp Neurol* **208**, 419–430 (1982).
117. F. Imamura, C. A. Greer, Segregated labeling of olfactory bulb projection neurons based on their birthdates *European Journal of Neuroscience* **41**, 147–156 (2015).
118. S. Nagayama, A. Enerva, M. L. Fletcher, A. V. Masurkar, K. M. Igarashi, K. Mori, W. R. Chen, Differential axonal projection of mitral and tufted cells in the mouse main olfactory

system. *Front Neural Circuits* **4**, 120 (2010).

119. J. L. Price, T. P. Powell, The morphology of the granule cells of the olfactory bulb. *J Cell Sci* **7**, 91–123 (1970).
120. J. L. Price, T. P. Powell, The synaptology of the granule cells of the olfactory bulb. *J Cell Sci* **7**, 125–155 (1970).
121. M. D. Eyre, M. Antal, Z. Nusser, Distinct deep short-axon cell subtypes of the main olfactory bulb provide novel intrabulbar and extrabulbar GABAergic connections. *J Neurosci* **28**, 8217–8229 (2008).
122. A. Hayar, S. Karnup, M. Ennis, M. T. Shipley, External tufted cells: a major excitatory element that coordinates glomerular activity *Journal of Neuroscience* **24**, 6676–6685 (2004).
123. A. Hayar, S. Karnup, M. T. Shipley, M. Ennis, Olfactory bulb glomeruli: external tufted cells intrinsically burst at theta frequency and are entrained by patterned olfactory input *Journal of Neuroscience* **24**, 1190–1199 (2004).
124. M. Antal, M. Eyre, B. Finklea, Z. Nusser, External tufted cells in the main olfactory bulb form two distinct subpopulations *European Journal of Neuroscience* **24**, 1124–1136 (2006).
125. S. Liu, M. T. Shipley, Multiple conductances cooperatively regulate spontaneous bursting in mouse olfactory bulb external tufted cells *Journal of Neuroscience* **28**, 1625–1639 (2008).
126. T. Hirata, G. Shioi, T. Abe, H. Kiyonari, S. Kato, K. Kobayashi, K. Mori, T. Kawasaki, A novel birthdate-labeling method reveals segregated parallel projections of mitral and external tufted cells in the main olfactory system *eneuro* **6**, (2019).
127. M. Najac, D. De Saint Jan, L. Reguero, P. Grandes, S. Charpak, Monosynaptic and polysynaptic feed-forward inputs to mitral cells from olfactory sensory neurons. *J Neurosci* **31**, 8722–8729 (2011).
128. S. Parrish-Aungst, M. T. Shipley, F. Erdelyi, G. Szabo, A. C. Puche, Quantitative analysis of neuronal diversity in the mouse olfactory bulb. *J Comp Neurol* **501**, 825–836 (2007).
129. A. J. Pinching, T. P. S. Powell, The neuropil of the periglomerular region of the olfactory bulb *Journal of cell science* **9**, 379–409 (1971).
130. K. Kosaka, Y. Aika, K. Toida, T. Kosaka, Structure of intraglomerular dendritic tufts of mitral cells and their contacts with olfactory nerve terminals and calbindin-immunoreactive

type 2 periglomerular neurons. *J Comp Neurol* **440**, 219–235 (2001).

131. Z. Shao, A. C. Puche, E. Kiyokage, G. Szabo, M. T. Shipley, Two GABAergic intraglomerular circuits differentially regulate tonic and phasic presynaptic inhibition of olfactory nerve terminals. *J Neurophysiol* **101**, 1988–2001 (2009).
132. B. J. Maher, G. L. Westbrook, Co-transmission of dopamine and GABA in periglomerular cells. *J Neurophysiol* **99**, 1559–1564 (2008).
133. V. Aroniadou-Anderjaska, F. M. Zhou…, Tonic and Synaptically Evoked Presynaptic Inhibition of Sensory Input to the Rat Olfactory Bulb Via GABA_BHeteroreceptors *Journal of ...* (2000).
134. J. P. McGann, N. Pírez, M. A. Gainey, C. Muratore, A. S. Elias, M. Wachowiak, Odorant representations are modulated by intra- but not interglomerular presynaptic inhibition of olfactory sensory neurons. *Neuron* **48**, 1039–1053 (2005).
135. N. E. Schoppa, J. M. Kinzie, Y. Sahara…, Dendrodendritic inhibition in the olfactory bulb is driven by NMDA receptors *Journal of ...* (1998).
136. T. C. Smith, C. E. Jahr, Self-inhibition of olfactory bulb neurons *Nature neuroscience* (2002).
137. M. Ennis, F. M. Zhou, K. J. Ciombor…, Dopamine D2 receptor–mediated presynaptic inhibition of olfactory nerve terminals *Journal of ...* (2001).
138. S. Liu, Dopaminergic Modulation of Glomerular Circuits in the Mouse Olfactory Bulb. *Front Cell Neurosci* **14**, 172 (2020).
139. A. M. Lyons-Warren, E. K. Tantry, E. H. Moss, M. Y. Kochukov, B. D. W. Belfort, J. Ortiz-Guzman, Z. Freyberg, B. R. Arenkiel, Co-transmitting interneurons in the mouse olfactory bulb regulate olfactory detection and discrimination. *Cell Rep* **42**, 113471 (2023).
140. J. L. Aungst, P. M. Heyward, A. C. Puche, S. V. Karnup, A. Hayar, G. Szabo, M. T. Shipley, Centre–surround inhibition among olfactory bulb glomeruli *Nature* **426**, 623–629 (2003).
141. C. H. Shirley, E. J. Coddington, P. M. Heyward, All-or-none population bursts temporally constrain surround inhibition between mouse olfactory glomeruli. *Brain Res Bull* **81**, 406–415 (2010).
142. S. Liu, C. Plachez, Z. Shao, A. Puche, M. T. Shipley, Olfactory bulb short axon cell release of GABA and dopamine produces a temporally biphasic inhibition-excitation response in external tufted cells. *J Neurosci* **33**, 2916–2926 (2013).

143. S. Liu, A. C. Puche, M. T. Shipley, The Interglomerular Circuit Potently Inhibits Olfactory Bulb Output Neurons by Both Direct and Indirect Pathways. *J Neurosci* **36**, 9604–9617 (2016).

144. C. E. Vaaga, J. T. Yorgason, J. T. Williams…, Presynaptic gain control by endogenous cotransmission of dopamine and GABA in the olfactory bulb *Journal of …* (2017).

145. S. D. Burton, G. LaRocca, A. Liu, C. E. Cheetham, N. N. Urban, Olfactory Bulb Deep Short-Axon Cells Mediate Widespread Inhibition of Tufted Cell Apical Dendrites. *J Neurosci* **37**, 1117–1138 (2017).

146. J. Altman, G. D. Das, Autoradiographic and histological evidence of postnatal hippocampal neurogenesis in rats *Journal of Comparative Neurology* (1965).

147. A. Carleton, L. T. Petreanu, R. Lansford…, Becoming a new neuron in the adult olfactory bulb *Nature …* (2003).

148. A. Alvarez-Buylla, D. A. Lim, For the long run: maintaining germinal niches in the adult brain *Neuron* (2004).

149. P.-M. Lledo, M. Alonso, M. S. Grubb, Adult neurogenesis and functional plasticity in neuronal circuits. *Nat Rev Neurosci* **7**, 179–193 (2006).

150. M. C. Whitman, C. A. Greer, Adult-generated neurons exhibit diverse developmental fates *Developmental neurobiology* (2007).

151. T. Kosaka, K. Kosaka, Tyrosine hydroxylase-positive GABAergic juxtaglomerular neurons are the main source of the interglomerular connections in the mouse main olfactory bulb *Neuroscience research* (2008).

152. Y. Adam, A. Mizrahi, Circuit formation and maintenance—perspectives from the mammalian olfactory bulb *Current opinion in neurobiology* (2010).

153. E. Kiyokage, Y.-Z. Pan, Z. Shao, K. Kobayashi, G. Szabo, Y. Yanagawa, K. Obata, H. Okano, K. Toida, A. C. Puche, M. T. Shipley, Molecular identity of periglomerular and short axon cells. *J Neurosci* **30**, 1185–1196 (2010).

154. A. Alvarez-Buylla, J. M. García-Verdugo…, A unified hypothesis on the lineage of neural stem cells *Nature Reviews …* (2001).

155. L. Petreanu, A. Alvarez-Buylla, Maturation and death of adult-born olfactory bulb granule neurons: role of olfaction *Journal of Neuroscience* (2002).

156. O. Belluzzi, M. Benedusi, J. Ackman, J. J. LoTurco, Electrophysiological differentiation of

new neurons in the olfactory bulb. *J Neurosci* **23**, 10411–10418 (2003).

157. P. M. Lledo, F. T. Merkle, A. Alvarez-Buylla, Origin and function of olfactory bulb interneuron diversity *Trends in neurosciences* (2008).
158. F. Lazarini, P.-M. Lledo, Is adult neurogenesis essential for olfaction? *Trends Neurosci* **34**, 20–30 (2011).
159. M. T. Shipley, F. J. Halloran, J. de la Torre, Surprisingly rich projection from locus coeruleus to the olfactory bulb in the rat *Brain research* **329**, 294–299 (1985).
160. C. E. Jahr, R. A. Nicoll, Noradrenergic modulation of dendrodendritic inhibition in the olfactory bulb *Nature* **297**, 227–229 (1982).
161. P. Q. Trombley, G. M. Shepherd, Noradrenergic inhibition of synaptic transmission between mitral and granule cells in mammalian olfactory bulb cultures *Journal of Neuroscience* **12**, 3985–3991 (1992).
162. M. Jiang, E. R. Griff, M. Ennis, L. A. Zimmer, M. T. Shipley, Activation of locus coeruleus enhances the responses of olfactory bulb mitral cells to weak olfactory nerve input *Journal of Neuroscience* **16**, 6319–6329 (1996).
163. K. J. Ciombor, M. Ennis, M. T. Shipley, Norepinephrine increases rat mitral cell excitatory responses to weak olfactory nerve input via alpha-1 receptors in vitro *Neuroscience* **90**, 595–606 (1999).
164. A. Hayar, P. M. Heyward, T. Heinbockel, M. T. Shipley, M. Ennis, Direct excitation of mitral cells via activation of α1-noradrenergic receptors in rat olfactory bulb slices *Journal of Neurophysiology* **86**, 2173–2182 (2001).
165. W. Doucette, D. H. Gire, J. Whitesell, V. Carmean, M. T. Lucero, D. Restrepo, Associative cortex features in the first olfactory brain relay station. *Neuron* **69**, 1176–1187 (2011).
166. D. Eckmeier, S. D. Shea, Noradrenergic plasticity of olfactory sensory neuron inputs to the main olfactory bulb. *J Neurosci* **34**, 15234–15243 (2014).
167. F. Levy, R. Gervais, U. Kindermann, P. Orgeur…, Importance of! b-noradrenergic receptors in the olfactory bulb of sheep for recognition of lambs. *Behavioral …* (1990).
168. K. M. Kendrick, F. Levy, E. B. Keverne, Changes in the sensory processing of olfactory signals induced by birth in sleep *Science* (1992).
169. S. Rangel, M. Leon, Early odor preference training increases olfactory bulb norepinephrine *Developmental Brain Research* (1995).

170. R. M. Sullivan, D. A. Wilson, M. Leon, Norepinephrine and learning-induced plasticity in infant rat olfactory system *Journal of Neuroscience* (1989).

171. R. M. Sullivan, D. R. Zyzak, P. Skierkowski…, The role of olfactory bulb norepinephrine in early olfactory learning *Developmental Brain ...* (1992).

172. R. M. Sullivan, G. Stackenwalt, F. Nasr…, Association of an odor with an activation of olfactory bulb noradrenergic β-receptors or locus coeruleus stimulation is sufficient to produce learned approach … *Behavioral ...* (2000).

173. C. W. Harley, A. Darby-King, J. McCann, J. H. McLean, Beta1-adrenoceptor or alpha1-adrenoceptor activation initiates early odor preference learning in rat pups: support for the mitral cell/cAMP model of odor preference learning. *Learn Mem* **13**, 8–13 (2006).

174. P. A. Brennan, H. M. Schellinck, C. de la Riva, K. M. Kendrick, E. B. Keverne, Changes in neurotransmitter release in the main olfactory bulb following an olfactory conditioning procedure in mice. *Neuroscience* **87**, 583–590 (1998).

175. S. D. Shea, L. C. Katz, R. Mooney, Noradrenergic induction of odor-specific neural habituation and olfactory memories *Journal of Neuroscience* (2008).

176. A. Veyrac, J. Sacquet, V. Nguyen, M. Marien…, Novelty determines the effects of olfactory enrichment on memory and neurogenesis through noradrenergic mechanisms ... (2009).

177. W. Doucette, J. Milder, D. Restrepo, Adrenergic modulation of olfactory bulb circuitry affects odor discrimination *Learning & memory* (2007).

178. N. Mandairon, S. Peace, A. Karnow, J. Kim…, Noradrenergic modulation in the olfactory bulb influences spontaneous and reward-motivated discrimination, but not the formation of habituation memory *European Journal of ...* (2008).

179. O. Escanilla, A. Arrellanos, A. Karnow…, Noradrenergic modulation of behavioral odor detection and discrimination thresholds in the olfactory bulb *European journal of ...* (2010).

180. A. R. Best, D. A. Wilson, Coordinate synaptic mechanisms contributing to olfactory cortical adaptation *Journal of Neuroscience* (2004).

181. D. Guérin, S. T. Peace, A. Didier, C. Linster…, Noradrenergic neuromodulation in the olfactory bulb modulates odor habituation and spontaneous discrimination. *Behavioral ...* (2008).

182. J. J. Smith, K. Shionoya, R. M. Sullivan…, Auditory stimulation dishabituates olfactory

responses via noradrenergic cortical modulation *Neural plasticity* (2009).

183. J. H. McLean, M. T. Shipley, Serotonergic afferents to the rat olfactory bulb: I. Origins and laminar specificity of serotonergic inputs in the adult rat *Journal of Neuroscience* **7**, 3016–3028 (1987).
184. M. H. Won, T. Ohno, J. G. Suh, J. C. Lee, S. M. Jo, Y. S. Oh, T. Namikawa, J. Kitoh, Serotonergic neurons are present and innervate blood vessels in the olfactory bulb of the laboratory shrew, Suncus murinus *Neuroscience letters* **243**, 53–56 (1998).
185. R. Steinfeld, J. T. Herb, R. Sprengel, A. T. Schaefer, I. Fukunaga, Divergent innervation of the olfactory bulb by distinct raphe nuclei *Journal of Comparative Neurology* **523**, 805–813 (2015).
186. M. T. Shipley, M. Ennis, Functional organization of olfactory system. *J Neurobiol* **30**, 123–176 (1996).
187. S. Liu, J. L. Aungst, A. C. Puche, M. T. Shipley, Serotonin modulates the population activity profile of olfactory bulb external tufted cells. *J Neurophysiol* **107**, 473–483 (2012).
188. A. Hardy, B. Palouzier-Paulignan, A. Duchamp, J. P. Royet, P. Duchamp-Viret, 5-Hydroxytryptamine action in the rat olfactory bulb: in vitro electrophysiological patch-clamp recordings of juxtaglomerular and mitral cells. *Neuroscience* **131**, 717–731 (2005).
189. G. C. Petzold, A. Hagiwara, V. N. Murthy, Serotonergic modulation of odor input to the mammalian olfactory bulb. *Nat Neurosci* **12**, 784–791 (2009).
190. D. Brunert, Y. Tsuno, M. Rothermel, M. T. Shipley, M. Wachowiak, Cell-Type-Specific Modulation of Sensory Responses in Olfactory Bulb Circuits by Serotonergic Projections from the Raphe Nuclei. *J Neurosci* **36**, 6820–6835 (2016).
191. J. H. McLean, A. Darby-King, R. M. Sullivan…, Serotonergic influence on olfactory learning in the neonate rat *Behavioral and neural ...* (1993).
192. J. H. McLean, A. Darby-King, E. Hodge, 5-HT_2 receptor involvement in conditioned olfactory learning in the neonate rat pup. *Behavioral neuroscience* (1996).
193. Q. Yuan, C. W. Harley, A. Darby-King…, Early odor preference learning in the rat: bidirectional effects of cAMP response element-binding protein (CREB) and mutant CREB support a causal role for … *Journal of ...* (2003).
194. T. Moriizumi, T. Tsukatani, H. Sakashita, T. Miwa, Olfactory disturbance induced by deafferentation of serotonergic fibers in the olfactory bulb *Neuroscience* (1994).

195. S. Letty, R. Child, A. Dumuis, A. Pantaloni, J. Bockaert…, 5-HT4 receptors improve social olfactory memory in the rat ... (1997).

196. E. Marchetti, A. Dumuis, J. Bockaert…, Differential modulation of the 5-HT4 receptor agonists and antagonist on rat learning and memory ... (2000).

197. L. Zaborszky, J. Carlsen, H. R. Brashear, L. Heimer, Cholinergic and GABAergic afferents to the olfactory bulb in the rat with special emphasis on the projection neurons in the nucleus of the horizontal limb of the diagonal band *Journal of Comparative Neurology* **243**, 488–509 (1986).

198. M. C. Senut, D. Menetrey, Y. Lamour, Cholinergic and peptidergic projections from the medial septum and the nucleus of the diagonal band of Broca to dorsal hippocampus, cingulate cortex and olfactory bulb: a combined wheatgerm agglutinin-apohorseradish peroxidase-gold immunohistochemical study *Neuroscience* **30**, 385–403 (1989).

199. T. Ichikawa, Y. Hirata, Organization of choline acetyltransferase-containing structures in the forebrain of the rat *Journal of Neuroscience* **6**, 281–292 (1986).

200. H. Ojima, T. Yamasaki, H. Kojima, A. Akashi, Cholinergic innervation of the main and the accessory olfactory bulbs of the rat as revealed by a monoclonal antibody against choline acetyltransferase *Anatomy and embryology* **178**, 481–488 (1988).

201. P. E. Castillo, A. Carleton, J.-D. Vincent, P.-M. Lledo, Multiple and opposing roles of cholinergic transmission in the main olfactory bulb *Journal of Neuroscience* **19**, 9180–9191 (1999).

202. R. T. Pressler, T. Inoue, B. W. Strowbridge, Muscarinic receptor activation modulates granule cell excitability and potentiates inhibition onto mitral cells in the rat olfactory bulb. *J Neurosci* **27**, 10969–10981 (2007).

203. S. Liu, Z. Shao, A. Puche, M. Wachowiak, M. Rothermel, M. T. Shipley, Muscarinic receptors modulate dendrodendritic inhibitory synapses to sculpt glomerular output. *J Neurosci* **35**, 5680–5692 (2015).

204. R. D. D'Souza, S. Vijayaraghavan, Nicotinic receptor-mediated filtering of mitral cell responses to olfactory nerve inputs involves the α3β4 subtype *Journal of Neuroscience* **32**, 3261–3266 (2012).

205. R. S. Smith, R. Hu, A. DeSouza, C. L. Eberly, K. Krahe, W. Chan, R. C. Araneda, Differential Muscarinic Modulation in the Olfactory Bulb. *J Neurosci* **35**, 10773–10785

(2015).

206. M. Bendahmane, M. C. Ogg, M. Ennis, M. L. Fletcher, Increased olfactory bulb acetylcholine bi-directionally modulates glomerular odor sensitivity. *Sci Rep* **6**, 25808 (2016).
207. A. J. Hunter, T. K. Murray, Cholinergic mechanisms in a simple test of olfactory learning in the rat *Psychopharmacology* (1989).
208. A. Perio, J. P. Terranova, P. Worms, R. M. Bluthe…, Specific modulation of social memory in rats by cholinomimetic and nootropic drugs, by benzodiazepine inverse agonists, but not by psychostimulants ... (1989).
209. A. G. Paolini, J. S. McKenzie, Effects of lesions in the horizontal diagonal band nucleus on olfactory habituation in the rat *Neuroscience* (1993).
210. J. T. Winslow, F. Camacho, Cholinergic modulation of a decrement in social investigation following repeated contacts between mice *Psychopharmacology* (1995).
211. M. I. Miranda, F. Ortiz-Godina, D. García, Differential involvement of cholinergic and beta-adrenergic systems during acquisition, consolidation, and retrieval of long-term memory of social and neutral odors *Behavioural brain research* (2009).
212. N. Mandairon, J. Sacquet, S. Garcia, N. Ravel, F. Jourdan, A. Didier, Neurogenic correlates of an olfactory discrimination task in the adult olfactory bulb. *Eur J Neurosci* **24**, 3578–3588 (2006).
213. N. Ravel, M. Vigouroux, A. Elaagouby, R. Gervais, Scopolamine impairs delayed matching in an olfactory task in rats *Psychopharmacology* (1992).
214. F. S. Roman, I. Simonetto…, Learning and memory of odor-reward association: selective impairment following horizontal diagonal band lesions. *Behavioral ...* (1993).
215. N. Ravel, A. Elaagouby, R. Gervais, Scopolamine injection into the olfactory bulb impairs short-term olfactory memory in rats. *Behavioral neuroscience* (1994).
216. F. Lévy, P. Richard, M. Meurisse, N. Ravel, Scopolamine impairs the ability of parturient ewes to learn to recognise their lambs *Psychopharmacology* (1997).
217. E. D. Rosa, M. E. Hasselmo, Muscarinic cholinergic neuromodulation reduces proactive interference between stored odor memories during associative learning in rats. *Behavioral neuroscience* (2000).
218. E. D. Rosa, M. E. Hasselmo, M. G. Baxter, Contribution of the cholinergic basal forebrain

to proactive interference from stored odor memories during associative learning in rats. *Behavioral neuroscience* (2001).

219. D. Saar, Y. Grossman, E. Barkai, Long-lasting cholinergic modulation underlies rule learning in rats *Journal of Neuroscience* (2001).
220. J. A. V. Kroon, A. P. Carobrez, Olfactory fear conditioning paradigm in rats: effects of midazolam, propranolol or scopolamine *Neurobiology of learning and memory* (2009).
221. C. Linster, P. A. Garcia, M. E. Hasselmo…, Selective loss of cholinergic neurons projecting to the olfactory system increases perceptual generalization between similar, but not dissimilar, odorants. *Behavioral ...* (2001).
222. M. L. Fletcher, D. A. Wilson, Experience modifies olfactory acuity: acetylcholine-dependent learning decreases behavioral generalization between similar odorants *The Journal of neuroscience* (2002).
223. N. Mandairon, C. J. Ferretti, C. M. Stack…, Cholinergic modulation in the olfactory bulb influences spontaneous olfactory discrimination in adult rats *European Journal of ...* (2006).
224. J. L. Price, T. P. Powell, An experimental study of the origin and the course of the centrifugal fibres to the olfactory bulb in the rat. *Journal of anatomy* (1970).
225. B. J. Davis, F. Macrides, W. M. Youngs, S. P. Schneider, D. L. Rosene, Efferents and centrifugal afferents of the main and accessory olfactory bulbs in the hamster. *Brain Res Bull* **3**, 59–72 (1978).
226. J. D. Olmos, H. Hardy, L. Heimer, The afferent connections of the main and the accessory olfactory bulb formations in the rat: An experimental HRP-study *Journal of Comparative ...* (1978).
227. L. B. Haberly, J. L. Price, Association and commissural fiber systems of the olfactory cortex of the rat. I. Systems originating in the piriform cortex and adjacent areas *Journal of Comparative Neurology* (1978).
228. B. J. Davis, F. Macrides, The organization of centrifugal projections from the anterior olfactory nucleus, ventral hippocampal rudiment, and piriform cortex to the main olfactory bulb in the … *Journal of Comparative Neurology* (1981).
229. C. K. H. Reyher, W. K. Schwerdtfeger, H. G. Baumgarten, Interbulbar axonal collateralization and morphology of anterior olfactory nucleus neurons in the rat *Brain*

research bulletin (1988).

230. J. A. D. Carlos, L. López-Mascaraque…, Connections of the olfactory bulb and nucleus olfactorius anterior in the hedgehog (Erinaceus europaeus): Fluorescent tracers and HRP study *Journal of* ... (1989).
231. G. M. Shepherd, Synaptic organization of the mammalian olfactory bulb *Physiological reviews* (1972).
232. G. H. Otazu, H. Chae, M. B. Davis, D. F. Albeanu, Cortical Feedback Decorrelates Olfactory Bulb Output in Awake Mice. *Neuron* **86**, 1461–1477 (2015).
233. M. Sassoé-Pognetto, J. K. Utvik, P. Camoletto, M. Watanabe, F. A. Stephenson, D. S. Bredt, O. P. Ottersen, Organization of postsynaptic density proteins and glutamate receptors in axodendritic and dendrodendritic synapses of the rat olfactory bulb. *J Comp Neurol* **463**, 237–248 (2003).
234. R. Balu, R. T. Pressler, B. W. Strowbridge, Multiple modes of synaptic excitation of olfactory bulb granule cells. *J Neurosci* **27**, 5621–5632 (2007).
235. S. Matsutani, Trajectory and terminal distribution of single centrifugal axons from olfactory cortical areas in the rat olfactory bulb. *Neuroscience* **169**, 436–448 (2010).
236. F. Markopoulos, D. Rokni, D. H. Gire, V. N. Murthy, Functional properties of cortical feedback projections to the olfactory bulb. *Neuron* **76**, 1175–1188 (2012).
237. A. M. Boyd, J. F. Sturgill, C. Poo, J. S. Isaacson, Cortical feedback control of olfactory bulb circuits. *Neuron* **76**, 1161–1174 (2012).
238. C. Mazo, G. Lepousez, A. Nissant, M. T. Valley, P. M. Lledo, GABAB Receptors Tune Cortical Feedback to the Olfactory Bulb. *J Neurosci* **36**, 8289–8304 (2016).
239. A. J. Aqrabawi, C. J. Browne, Z. Dargaei, D. Garand, C. S. Khademullah, M. A. Woodin, J. C. Kim, Top-down modulation of olfactory-guided behaviours by the anterior olfactory nucleus pars medialis and ventral hippocampus. *Nat Commun* **7**, 13721 (2016).
240. Z. Chen, K. Padmanabhan, Top-down feedback enables flexible coding strategies in the olfactory cortex. *Cell Rep* **38**, 110545 (2022).
241. D. Krone, M. Mannel, E. Pauli, T. Hummel, Qualitative and quantitative olfactometric evaluation of different concentrations of ethanol peppermint oil solutions. *Phytother Res* **15**, 135–138 (2001).
242. N. Uchida, Z. F. Mainen, Odor concentration invariance by chemical ratio coding. *Front*

Syst Neurosci **1**, 3 (2007).

243. T. A. Cleland, S. Y. Chen, K. W. Hozer, H. N. Ukatu, K. J. Wong, F. Zheng, Sequential mechanisms underlying concentration invariance in biological olfaction. *Front Neuroeng* **4**, 21 (2011).
244. Y. Niimura, A. Matsui, K. Touhara, Extreme expansion of the olfactory receptor gene repertoire in African elephants and evolutionary dynamics of orthologous gene groups in 13 placental mammals. *Genome Res* **24**, 1485–1496 (2014).
245. G. Sicard, Receptor cell responses to odorants: similarities and differences among odorants *Brain research* (1984).
246. S. Firestein, C. Picco, A. Menini, The relation between stimulus and response in olfactory receptor cells of the tiger salamander. *The Journal of Physiology* (1993).
247. T. Sato, J. Hirono, M. Tonoike…, Tuning specificities to aliphatic odorants in mouse olfactory receptor neurons and their local distribution *Journal of ...* (1994).
248. K. Nara, L. R. Saraiva, X. Ye, L. B. Buck, A large-scale analysis of odor coding in the olfactory epithelium. *J Neurosci* **31**, 9179–9191 (2011).
249. P. Duchamp-Viret, M. A. Chaput, A. Duchamp, Odor response properties of rat olfactory receptor neurons. *Science* **284**, 2171–2174 (1999).
250. K. Kajiya, K. Inaki, M. Tanaka, T. Haga…, Molecular bases of odor discrimination: reconstitution of olfactory receptors that recognize overlapping sets of odorants *Journal of ...* (2001).
251. H. Hamana, J. Hirono, M. Kizumi, T. Sato, Sensitivity-dependent hierarchical receptor codes for odors *Chemical senses* (2003).
252. R. C. Araneda, Z. Peterlin, X. Zhang…, A pharmacological profile of the aldehyde receptor repertoire in rat olfactory epithelium *The Journal of ...* (2004).
253. Y. Oka, A. Nakamura, H. Watanabe…, An odorant derivative as an antagonist for an olfactory receptor *Chemical senses* (2004).
254. Y. Oka, M. Omura, H. Kataoka, K. Touhara, Olfactory receptor antagonism between odorants *The EMBO journal* (2004).
255. T. S. McClintock, K. Adipietro, W. B. Titlow…, In vivo identification of eugenol-responsive and muscone-responsive mouse odorant receptors *Journal of ...* (2014).
256. D. C. Gonzalez-Kristeller, J. B. P. D. Nascimento…, Identification of agonists for a group

of human odorant receptors *Frontiers in* ... (2015).

257. Y. Jiang, N. N. Gong, X. S. Hu, M. J. Ni, R. Pasi…, Molecular profiling of activated olfactory neurons identifies odorant receptors for odors <i>in vivo</i *Nature* ... (2015).
258. B. von der Weid, D. Rossier, M. Lindup, J. Tuberosa, A. Widmer, J. D. Col, C. Kan, A. Carleton, I. Rodriguez, Large-scale transcriptional profiling of chemosensory neurons identifies receptor-ligand pairs in vivo. *Nat Neurosci* **18**, 1455–1463 (2015).
259. N. Sato-Akuhara, N. Horio, A. Kato-Namba…, Ligand specificity and evolution of mammalian musk odor receptors: effect of single receptor deletion on odor detection *Journal of* ... (2016).
260. X. S. Hu, K. Ikegami, A. Vihani, K. W. Zhu, M. Zapata…, Concentration-dependent recruitment of mammalian odorant receptors *eneuro* (2020).
261. B. D. Rubin, L. C. Katz, Optical imaging of odorant representations in the mammalian olfactory bulb. *Neuron* **23**, 499–511 (1999).
262. N. Uchida, Y. K. Takahashi, M. Tanifuji, K. Mori, Odor maps in the mammalian olfactory bulb: domain organization and odorant structural features. *Nat Neurosci* **3**, 1035–1043 (2000).
263. M. Meister, T. Bonhoeffer, Tuning and topography in an odor map on the rat olfactory bulb *Journal of Neuroscience* **21**, 1351–1360 (2001).
264. T. Bozza, J. P. McGann, P. Mombaerts, M. Wachowiak, In vivo imaging of neuronal activity by targeted expression of a genetically encoded probe in the mouse. *Neuron* **42**, 9–21 (2004).
265. H. Spors, M. Wachowiak, L. B. Cohen, R. W. Friedrich, Temporal dynamics and latency patterns of receptor neuron input to the olfactory bulb. *J Neurosci* **26**, 1247–1259 (2006).
266. C. A. de March, W. B. Titlow, T. Sengoku, P. Breheny, H. Matsunami, T. S. McClintock, Modulation of the combinatorial code of odorant receptor response patterns in odorant mixtures. *Mol Cell Neurosci* **104**, 103469 (2020).
267. S. Inagaki, R. Iwata, M. Iwamoto, T. Imai, Widespread Inhibition, Antagonism, and Synergy in Mouse Olfactory Sensory Neurons In Vivo. *Cell Rep* **31**, 107814 (2020).
268. T. S. McClintock, Q. Wang, T. Sengoku, W. B. Titlow, P. Breheny, Mixture and concentration effects on odorant receptor response patterns in vivo. *Chem Senses* bjaa032 (2020).

269. P. Pfister, B. C. Smith, B. J. Evans, J. H. Brann, C. Trimmer, M. Sheikh, R. Arroyave, G. Reddy, H. Y. Jeong, D. A. Raps, Z. Peterlin, M. Vergassola, M. E. Rogers, Odorant Receptor Inhibition Is Fundamental to Odor Encoding. *Curr Biol* **30**, 2574–2587.e6 (2020).
270. L. Xu, W. Li, V. Voleti, D. J. Zou, E. M. C. Hillman, S. Firestein, Widespread receptor-driven modulation in peripheral olfactory coding. *Science* **368**, eaaz5390 (2020).
271. J. D. Zak, G. Reddy, M. Vergassola, V. N. Murthy, Antagonistic odor interactions in olfactory sensory neurons are widespread in freely breathing mice. *Nat Commun* **11**, 3350 (2020).
272. G. Reddy, J. D. Zak, M. Vergassola, V. N. Murthy, Antagonism in olfactory receptor neurons and its implications for the perception of odor mixtures. *Elife* **7**, e34958 (2018).
273. K. J. Gregory, P. M. Sexton…, Allosteric modulation of muscarinic acetylcholine receptors *Current …* (2007).
274. N. T. Burford, M. J. Clark, T. S. Wehrman…, Discovery of positive allosteric modulators and silent allosteric modulators of the μ-opioid receptor *Proceedings of the …* (2013).
275. J. Garcia-Carceles, J. M. Decara…, A Positive Allosteric Modulator of the Serotonin 5-HT_{2C} Receptor for Obesity *Journal of Medicinal …* (2017).
276. S. Ahn, B. Pani, A. W. Kahsai, E. K. Olsen, G. Husemoen…, Small-molecule positive allosteric modulators of the β2-adrenoceptor isolated from DNA-encoded libraries *Molecular …* (2018).
277. M. A. Stanczyk, K. E. Livingston, L. Chang…, The δ-opioid receptor positive allosteric modulator BMS 986187 is a G-protein-biased allosteric agonist *British Journal of …* (2019).
278. E. A. Wold, J. Chen, K. A. Cunningham, J. Zhou, Allosteric Modulation of Class A GPCRs: Targets, Agents, and Emerging Concepts *Journal of Medicinal Chemistry* **62**, 88–127 (2019).
279. W. S. Cain, Odor intensity: mixtures and masking *Chemical senses* (1975).
280. D. G. Laing, H. Panhuber, M. E. Willcox, E. A. Pittman, Quality and intensity of binary odor mixtures *Physiology & behavior* (1984).
281. L. M. Kay, T. Crk, J. Thorngate, A redefinition of odor mixture quality. *Behavioral neuroscience* (2005).
282. S. Firestein, A code in the nose *Science's STKE* (2004).

283. G. Buzsaki, A. Draguhn, Neuronal oscillations in cortical networks *science* (2004).

284. S. Panzeri, N. Brunel, N. K. Logothetis, C. Kayser, Sensory neural codes using multiplexed temporal scales. *Trends Neurosci* **33**, 111–120 (2010).

285. D. Kleinfeld, M. Deschênes, F. Wang, J. D. Moore, More than a rhythm of life: breathing as a binder of orofacial sensation. *Nat Neurosci* **17**, 647–651 (2014).

286. R. Iwata, H. Kiyonari, T. Imai, Mechanosensory-Based Phase Coding of Odor Identity in the Olfactory Bulb. *Neuron* **96**, 1139–1152.e7 (2017).

287. R. M. Carey, J. V. Verhagen, D. W. Wesson, N. Pírez, M. Wachowiak, Temporal structure of receptor neuron input to the olfactory bulb imaged in behaving rats. *J Neurophysiol* **101**, 1073–1088 (2009).

288. T. Connelly, Y. Yu, X. Grosmaitre, J. Wang, L. C. Santarelli, A. Savigner, X. Qiao, Z. Wang, D. R. Storm, M. Ma, G protein-coupled odorant receptors underlie mechanosensitivity in mammalian olfactory sensory neurons. *Proc Natl Acad Sci U S A* **112**, 590–595 (2015).

289. N. E. Schoppa, G. L. Westbrook, Glomerulus-specific synchronization of mitral cells in the olfactory bulb. *Neuron* **31**, 639–651 (2001).

290. A. Hayar, M. T. Shipley, M. Ennis, Olfactory bulb external tufted cells are synchronized by multiple intraglomerular mechanisms. *J Neurosci* **25**, 8197–8208 (2005).

291. N. E. Schoppa, Synchronization of olfactory bulb mitral cells by precisely timed inhibitory inputs. *Neuron* **49**, 271–283 (2006).

292. F. Macrides, S. L. Chorover, Olfactory bulb units: activity correlated with inhalation cycles and odor quality. *Science* **175**, 84–87 (1972).

293. H. Spors, A. Grinvald, Spatio-temporal dynamics of odor representations in the mammalian olfactory bulb. *Neuron* **34**, 301–315 (2002).

294. B. Bathellier, D. L. Buhl, R. Accolla, A. Carleton, Dynamic ensemble odor coding in the mammalian olfactory bulb: sensory information at different timescales. *Neuron* **57**, 586–598 (2008).

295. K. M. Cury, N. Uchida, Robust odor coding via inhalation-coupled transient activity in the mammalian olfactory bulb. *Neuron* **68**, 570–585 (2010).

296. I. Fukunaga, M. Berning, M. Kollo, A. Schmaltz, A. Schaefer, Two Distinct Channels of Olfactory Bulb Output *Neuron* **75**, 320–329 (2012).

297. H. Matsumoto, H. Kashiwadani, H. Nagao, A. Aiba, K. Mori, Odor-Induced Persistent Discharge of Mitral Cells in the Mouse Olfactory Bulb *Journal of Neurophysiology* **101**, 1890–1900 (2009).

298. M. A. Patterson, S. Lagier, A. Carleton, Odor representations in the olfactory bulb evolve after the first breath and persist as an odor afterimage *Proceedings of the National Academy of Sciences* **110**, (2013).

299. M. Smear, A. Resulaj, J. Zhang, T. Bozza, D. Rinberg, Multiple perceptible signals from a single olfactory glomerulus. *Nat Neurosci* **16**, 1687–1691 (2013).

300. N. Uchida, Z. F. Mainen, Speed and accuracy of olfactory discrimination in the rat. *Nat Neurosci* **6**, 1224–1229 (2003).

301. N. M. Abraham, H. Spors, A. Carleton, T. W. Margrie, T. Kuner, A. T. Schaefer, Maintaining accuracy at the expense of speed: stimulus similarity defines odor discrimination time in mice *neuron* **44**, 865–876 (2004).

302. D. Rinberg, A. Koulakov, A. Gelperin, Speed-accuracy tradeoff in olfaction. *Neuron* **51**, 351–358 (2006).

303. J. J. Hopfield, Pattern recognition computation using action potential timing for stimulus representation. *Nature* **376**, 33–36 (1995).

304. T. W. Margrie, A. T. Schaefer, Theta oscillation coupled spike latencies yield computational vigour in a mammalian sensory system *The Journal of physiology* (2003).

305. A. T. Schaefer, K. Angelo, H. Spors, T. W. Margrie, Neuronal oscillations enhance stimulus discrimination by ensuring action potential precision. *PLoS Biol* **4**, e163 (2006).

306. I. Fukunaga, J. T. Herb, M. Kollo, E. S. Boyden, A. T. Schaefer, Independent control of gamma and theta activity by distinct interneuron networks in the olfactory bulb. *Nat Neurosci* **17**, 1208–1216 (2014).

307. J. Niessing, R. W. Friedrich, Olfactory pattern classification by discrete neuronal network states. *Nature* **465**, 47–52 (2010).

308. C. D. Wilson, G. O. Serrano, A. A. Koulakov, D. Rinberg, A primacy code for odor identity. *Nat Commun* **8**, 1477 (2017).

309. D. W. Wesson, R. M. Carey, J. V. Verhagen…, Rapid encoding and perception of novel odors in the rat *PLoS biology* (2008).

310. E. Chong, M. Moroni, C. Wilson, S. Shoham, S. Panzeri, D. Rinberg, Manipulating

synthetic optogenetic odors reveals the coding logic of olfactory perception. *Science* **368**, eaba2357 (2020).

311. V. Bhandawat, G. Maimon, M. H. Dickinson, R. I. Wilson, Olfactory modulation of flight in Drosophila is sensitive, selective and rapid *Journal of Experimental Biology* **213**, 4313–4313 (2010).
312. A. T. Schaefer, T. W. Margrie, Spatiotemporal representations in the olfactory system. *Trends Neurosci* **30**, 92–100 (2007).
313. S. Junek, E. Kludt, F. Wolf, D. Schild, Olfactory coding with patterns of response latencies. *Neuron* **67**, 872–884 (2010).
314. H. B. Barlow, Possible principles underlying the transformation of sensory messages *Sensory communication* (1961).
315. H. Ohguro, J. P. V. Hooser, A. H. Milam…, Rhodopsin phosphorylation and dephosphorylation in vivo∗ *Journal of Biological …* (1995).
316. K. B. Lee, J. A. Ptasienski, M. Bünemann…, Acidic amino acids flanking phosphorylation sites in the M2 muscarinic receptor regulate receptor phosphorylation, internalization, and interaction with arrestins *Journal of Biological …* (2000).
317. S. B. Liggett, Update on current concepts of the molecular basis of β2-adrenergic receptor signaling *Journal of allergy and clinical immunology* (2002).
318. J. A. Pitcher, N. J. Freedman, R. J. Lefkowitz, G protein-coupled receptor kinases. *Annu Rev Biochem* **67**, 653–692 (1998).
319. S. S. G. Ferguson, Evolving concepts in G protein-coupled receptor endocytosis: the role in receptor desensitization and signaling *Pharmacological reviews* (2001).
320. J. M. Willets, R. A. J. Challiss, S. R. Nahorski, Non-visual GRKs: are we seeing the whole picture *Trends in pharmacological …* (2003).
321. J. L. Benovic, H. Kühn, I. Weyand, J. Codina, M. G. Caron, R. J. Lefkowitz, Functional desensitization of the isolated beta-adrenergic receptor by the beta-adrenergic receptor kinase: potential role of an analog of the retinal protein arrestin (48-kDa protein). *Proc Natl Acad Sci U S A* **84**, 8879–8882 (1987).
322. M. J. Lohse, J. L. Benovic, J. Codina, M. G. Caron, R. J. Lefkowitz, beta-Arrestin: a protein that regulates beta-adrenergic receptor function. *Science* **248**, 1547–1550 (1990).
323. W. P. Hausdorff, M. Bouvier, B. F. O'Dowd, G. P. Irons, M. G. Caron, R. J. Lefkowitz,

Phosphorylation sites on two domains of the beta 2-adrenergic receptor are involved in distinct pathways of receptor desensitization. *J Biol Chem* **264**, 12657–12665 (1989).

324. T. M. Dawson, J. L. Arriza, D. E. Jaworsky, F. F. Borisy, H. Attramadal, R. J. Lefkowitz, G. V. Ronnett, Beta-adrenergic receptor kinase-2 and beta-arrestin-2 as mediators of odorant-induced desensitization. *Science* **259**, 825–829 (1993).
325. I. Boekhoff, J. Inglese, S. Schleicher, W. J. Koch, R. J. Lefkowitz, H. Breer, Olfactory desensitization requires membrane targeting of receptor kinase mediated by beta gamma-subunits of heterotrimeric G proteins. *J Biol Chem* **269**, 37–40 (1994).
326. K. Peppel, I. Boekhoff, P. McDonald, H. Breer, M. G. Caron, R. J. Lefkowitz, G protein-coupled receptor kinase 3 (GRK3) gene disruption leads to loss of odorant receptor desensitization. *J Biol Chem* **272**, 25425–25428 (1997).
327. A. Kato, J. Reisert, S. Ihara, K. Yoshikawa…, Evaluation of the role of g protein-coupled receptor kinase 3 in desensitization of mouse odorant receptors in a Mammalian cell line and in olfactory sensory neurons *Chemical ...* (2014).
328. G. Antunes, A. M. Sebastião, F. M. Simoes de Souza, Mechanisms of Regulation of Olfactory Transduction and Adaptation in the Olfactory Cilium *PLoS ONE* **9**, e105531 (2014).
329. S. S. G. Ferguson, J. Zhang, L. S. Barak, M. G. Caron, Pleiotropic role for GRKs and b-arrestins in receptor regulation *Physiology* (1997).
330. S. J. Royle, The cellular functions of clathrin. *Cell Mol Life Sci* **63**, 1823–1832 (2006).
331. H. Tsuga, K. Kameyama, T. Haga, T. Honma, J. Lameh, W. Sadée, Internalization and down-regulation of human muscarinic acetylcholine receptor m2 subtypes. Role of third intracellular m2 loop and G protein-coupled receptor kinase 2. *J Biol Chem* **273**, 5323–5330 (1998).
332. A. L. Matharu, S. J. Mundell, J. L. Benovic, E. Kelly, Rapid agonist-induced desensitization and internalization of the A(2B) adenosine receptor is mediated by a serine residue close to the COOH terminus. *J Biol Chem* **276**, 30199–30207 (2001).
333. M. L. Rankin, R. S. Alvania, E. L. Gleason, R. C. Bruch, Internalization of G protein-coupled receptors in single olfactory receptor neurons. *J Neurochem* **72**, 541–548 (1999).
334. A. Mashukova, M. Spehr, H. Hatt, E. M. Neuhaus, Beta-arrestin2-mediated internalization of mammalian odorant receptors. *J Neurosci* **26**, 9902–9912 (2006).

335. W. P. Hausdorff, J. Sung, M. G. Caron…, [C] Recent molecular analyses of β-adrenergic receptor phosphorylation, sequestration and down regulation *Asia pacific journal of ...* (1992).

336. L. F. Horgue, A. Assens, L. Fodoulian, L. Marconi, J. Tuberosa, A. Haider, M. Boillat, A. Carleton, I. Rodriguez, Transcriptional adaptation of olfactory sensory neurons to GPCR identity and activity. *Nat Commun* **13**, 2929 (2022).

337. J. Bradley, D. Reuter, S. Frings, Facilitation of calmodulin-mediated odor adaptation by cAMP-gated channel subunits *Science* (2001).

338. T. Y. Chen, K. W. Yau, Direct modulation by Ca(2+)-calmodulin of cyclic nucleotide-activated channel of rat olfactory receptor neurons. *Nature* **368**, 545–548 (1994).

339. T. Kurahashi, T. Shibuya, Ca2+-dependent adaptive properties in the solitary olfactory receptor cell of the newt *Brain research* (1990).

340. F. Zufall, G. M. Shepherd, S. Firestein, Inhibition of the olfactory cyclic nucleotide gated ion channel by intracellular calcium. *Proc Biol Sci* **246**, 225–230 (1991).

341. A. Boccaccio, L. Lagostena, V. Hagen, A. Menini, Fast adaptation in mouse olfactory sensory neurons does not require the activity of phosphodiesterase. *J Gen Physiol* **128**, 171–184 (2006).

342. W. Bönigk, J. Bradley, F. Müller, F. Sesti, I. Boekhoff, G. V. Ronnett, U. B. Kaupp, S. Frings, The native rat olfactory cyclic nucleotide-gated channel is composed of three distinct subunits. *J Neurosci* **19**, 5332–5347 (1999).

343. U. B. Kaupp, R. Seifert, Cyclic nucleotide-gated ion channels. *Physiol Rev* **82**, 769–824 (2002).

344. J. Zheng, W. N. Zagotta, Stoichiometry and assembly of olfactory cyclic nucleotide-gated channels. *Neuron* **42**, 411–421 (2004).

345. M. Liu, T. Y. Chen, B. Ahamed, J. Li, K. W. Yau, Calcium-calmodulin modulation of the olfactory cyclic nucleotide-gated cation channel *Science* (1994).

346. J. Bradley, W. Bönigk, K. W. Yau, S. Frings, Calmodulin permanently associates with rat olfactory CNG channels under native conditions *Nature neuroscience* (2004).

347. D. Weitz, M. Zoche, F. Müller, M. Beyermann, H. G. Körschen, U. B. Kaupp, K. W. Koch, Calmodulin controls the rod photoreceptor CNG channel through an unconventional binding site in the N-terminus of the beta-subunit. *EMBO J* **17**, 2273–2284 (1998).

348. M. E. Grunwald, W. P. Yu, H. H. Yu, K. W. Yau, Identification of a domain on the beta-subunit of the rod cGMP-gated cation channel that mediates inhibition by calcium-calmodulin. *J Biol Chem* **273**, 9148–9157 (1998).

349. M. C. Trudeau, W. N. Zagotta, Mechanism of calcium/calmodulin inhibition of rod cyclic nucleotide-gated channels. *Proc Natl Acad Sci U S A* **99**, 8424–8429 (2002).

350. Y. Song, K. D. Cygnar, B. Sagdullaev, M. Valley, S. Hirsh, A. Stephan, J. Reisert, H. Zhao, Olfactory CNG channel desensitization by Ca2+/CaM via the B1b subunit affects response termination but not sensitivity to recurring stimulation. *Neuron* **58**, 374–386 (2008).

351. G. A. Wayman, S. Impey, D. R. Storm, Ca2+ inhibition of type III adenylyl cyclase in vivo. *J Biol Chem* **270**, 21480–21486 (1995).

352. J. Wei, G. Wayman, D. R. Storm, Phosphorylation and inhibition of type III adenylyl cyclase by calmodulin-dependent protein kinase II in vivo. *J Biol Chem* **271**, 24231–24235 (1996).

353. J. Wei, A. Z. Zhao, G. C. Chan, L. P. Baker, S. Impey, J. A. Beavo, D. R. Storm, Phosphorylation and inhibition of olfactory adenylyl cyclase by CaM kinase II in Neurons: a mechanism for attenuation of olfactory signals. *Neuron* **21**, 495–504 (1998).

354. T. Leinders-Zufall, M. Ma, F. Zufall, Impaired odor adaptation in olfactory receptor neurons after inhibition of Ca2+/calmodulin kinase II. *J Neurosci* **19**, RC19 (1999).

355. J. Reisert, H. Zhao, Perspectives on: information and coding in mammalian sensory physiology: response kinetics of olfactory receptor neurons and the implications in olfactory coding. *J Gen Physiol* **138**, 303–310 (2011).

356. F. F. Borisy, G. V. Ronnett, A. M. Cunningham…, Calcium/calmodulin-activated phosphodiesterase expressed in olfactory receptor neurons ... *of Neuroscience* (1992).

357. J. A. Cherry, R. L. Davis, A mouse homolog of dunce, a gene important for learning and memory in drosophila, is preferentially expressed in olfactory receptor neurons *Journal of neurobiology* (1995).

358. D. M. Juilfs, H. J. Fülle, A. Z. Zhao…, A subset of olfactory neurons that selectively express cGMP-stimulated phosphodiesterase (PDE2) and guanylyl cyclase-D define a unique olfactory signal … *Proceedings of the* ... (1997).

359. K. D. Cygnar, H. Zhao, Phosphodiesterase 1C is dispensable for rapid response termination of olfactory sensory neurons. *Nat Neurosci* **12**, 454–462 (2009).

360. C. Chen, T. Nakamura, Y. Koutalos, Cyclic AMP diffusion coefficient in frog olfactory cilia *Biophysical journal* (1999).

361. R. J. Flannery, D. A. French, S. J. Kleene, Clustering of cyclic-nucleotide-gated channels in olfactory cilia *Biophysical journal* (2006).

362. B. P. Menco, Ciliated and microvillous structures of rat olfactory and nasal respiratory epithelia. A study using ultra-rapid cryo-fixation followed by freeze-substitution or freeze-etching. *Cell Tissue Res* **235**, 225–241 (1984).

363. M. Pyrski, J. H. Koo, S. K. Polumuri, A. M. Ruknudin, J. W. Margolis, D. H. Schulze, F. L. Margolis, Sodium/calcium exchanger expression in the mouse and rat olfactory systems. *J Comp Neurol* **501**, 944–958 (2007).

364. S. J. Kleene, The electrochemical basis of odor transduction in vertebrate olfactory cilia. *Chem Senses* **33**, 839–859 (2008).

365. J. Reisert, H. R. Matthews, Response properties of isolated mouse olfactory receptor cells *The Journal of physiology* **530**, 113–122 (2001).

366. S. Antolin, H. R. Matthews, The effect of external sodium concentration on sodium-calcium exchange in frog olfactory receptor cells. *J Physiol* **581**, 495–503 (2007).

367. A. B. Stephan, E. Y. Shum, S. Hirsh, K. D. Cygnar, J. Reisert, H. Zhao, ANO2 is the cilial calcium-activated chloride channel that may mediate olfactory amplification. *Proc Natl Acad Sci U S A* **106**, 11776–11781 (2009).

368. A. B. Stephan, S. Tobochnik, M. Dibattista, C. M. Wall, J. Reisert, H. Zhao, The Na(+)/Ca(2+) exchanger NCKX4 governs termination and adaptation of the mammalian olfactory response. *Nat Neurosci* **15**, 131–137 (2011).

369. C. Martelli, D. A. Storace, Stimulus Driven Functional Transformations in the Early Olfactory System. *Front Cell Neurosci* **15**, 684742 (2021).

370. J. P. Rospars, P. Lansky, M. Chaput, P. Duchamp-Viret, Competitive and noncompetitive odorant interactions in the early neural coding of odorant mixtures. *J Neurosci* **28**, 2659–2666 (2008).

371. T. Shibuya, S. Shibuya, Olfactory epithelium: unitary responses in the tortoise *Science* (1963).

372. R. C. Gesteland, C. D. Sigwart, [C] Olfactory receptor units—a mammalian preparation *Brain research* (1977).

373. J. Reisert, K. W. Yau, F. L. Margolis, Olfactory marker protein modulates the cAMP kinetics of the odour-induced response in cilia of mouse olfactory receptor neurons. *J Physiol* **585**, 731–740 (2007).
374. J. Reisert, H. R. Matthews, Adaptation of the odour-induced response in frog olfactory receptor cells *The Journal of physiology* **519**, 801–813 (1999).
375. D. Trotier, Intensity coding in olfactory receptor cells. *Semin Cell Biol* **5**, 47–54 (1994).
376. F. Kawai, T. Kurahashi, A. Kaneko, Quantitative analysis of Na+ and Ca2+ current contributions on spike initiation in the newt olfactory receptor cell. *Jpn J Physiol* **47**, 367–376 (1997).
377. T. Kurahashi, A. Menini, Mechanism of odorant adaptation in the olfactory receptor cell. *Nature* **385**, 725–729 (1997).
378. T. Leinders-Zufall, C. A. Greer, G. M. Shepherd, F. Zufall, Imaging odor-induced calcium transients in single olfactory cilia: specificity of activation and role in transduction. *J Neurosci* **18**, 5630–5639 (1998).
379. M. Ma, W. R. Chen, G. M. Shepherd, Electrophysiological characterization of rat and mouse olfactory receptor neurons from an intact epithelial preparation. *J Neurosci Methods* **92**, 31–40 (1999).
380. A. S. Ghatpande, J. Reisert, Olfactory receptor neuron responses coding for rapid odour sampling. *J Physiol* **589**, 2261–2273 (2011).
381. J. V. Verhagen, D. W. Wesson, T. I. Netoff, J. A. White, M. Wachowiak, Sniffing controls an adaptive filter of sensory input to the olfactory bulb. *Nat Neurosci* **10**, 631–639 (2007).
382. R. M. Carey, M. Wachowiak, Effect of sniffing on the temporal structure of mitral/tufted cell output from the olfactory bulb. *J Neurosci* **31**, 10615–10626 (2011).
383. T. Kurahashi, A. Menini, Mechanism of odorant adaptation in the olfactory receptor cell. *Nature* **385**, 725–729 (1997).
384. F. Zufall, T. Leinders-Zufall, The cellular and molecular basis of odor adaptation. *Chem Senses* **25**, 473–481 (2000).
385. M. Wachowiak, J. P. McGann, P. M. Heyward, Z. Shao, A. C. Puche, M. T. Shipley, Inhibition [corrected] of olfactory receptor neuron input to olfactory bulb glomeruli mediated by suppression of presynaptic calcium influx. *J Neurophysiol* **94**, 2700–2712 (2005).

386. G. J. Murphy, J. S. Isaacson, Presynaptic cyclic nucleotide-gated ion channels modulate neurotransmission in the mammalian olfactory bulb. *Neuron* **37**, 639–647 (2003).

387. N. Pírez, M. Wachowiak, In vivo modulation of sensory input to the olfactory bulb by tonic and activity-dependent presynaptic inhibition of receptor neurons. *J Neurosci* **28**, 6360–6371 (2008).

388. H. Kazama, R. I. Wilson, Homeostatic matching and nonlinear amplification at identified central synapses. *Neuron* **58**, 401–413 (2008).

389. N. Mandairon, C. Stack, C. Linster, Olfactory enrichment improves the recognition of individual components in mixtures. *Physiol Behav* **89**, 379–384 (2006).

390. N. Mandairon, C. Stack, C. Kiselycznyk, C. Linster, Broad activation of the olfactory bulb produces long-lasting changes in odor perception. *Proc Natl Acad Sci U S A* **103**, 13543–13548 (2006).

391. O. Escanilla, N. Mandairon, C. Linster, Odor-reward learning and enrichment have similar effects on odor perception. *Physiol Behav* **94**, 621–626 (2008).

392. N. Mandairon, A. Didier, C. Linster, Odor enrichment increases interneurons responsiveness in spatially defined regions of the olfactory bulb correlated with perception. *Neurobiol Learn Mem* **90**, 178–184 (2008).

393. M. D. Rabin, Experience facilitates olfactory quality discrimination. *Percept Psychophys* **44**, 532–540 (1988).

394. C. Jehl, J. P. Royet, A. Holley, Odor discrimination and recognition memory as a *Perception & psychophysics* (1995).

395. C. E. J. Cheetham, U. Park, L. Belluscio, Rapid and continuous activity-dependent plasticity of olfactory sensory input. *Nat Commun* **7**, 10729 (2016).

396. T. Tsukahara, D. H. Brann, S. L. Pashkovski, G. Guitchounts, T. Bozza, S. R. Datta, A transcriptional rheostat couples past activity to future sensory responses. *Cell* **184**, 6326–6343.e32 (2021).

397. H. W. Wang, C. J. Wysocki, G. H. Gold, Induction of olfactory receptor sensitivity in mice. *Science* **260**, 998–1000 (1993).

398. E. Fitzwater, D. M. Coppola, Olfactory Deprivation and Enrichment: An Identity of Opposites? *Chem Senses* **46**, bjaa071 (2021).

399. H. K. Kato, M. W. Chu, J. S. Isaacson, T. Komiyama, Dynamic sensory representations in

the olfactory bulb: modulation by wakefulness and experience. *Neuron* **76**, 962–975 (2012).

400. N. Buonviso, R. Gervais, M. Chalansonnet, M. Chaput, Short-lasting exposure to one odour decreases general reactivity in the olfactory bulb of adult rats. *Eur J Neurosci* **10**, 2472–2475 (1998).
401. N. Buonviso, M. Chaput, Olfactory experience decreases responsiveness of the olfactory bulb in the adult rat *Neuroscience* (1999).
402. M. W. Chu, W. L. Li, T. Komiyama, Balancing the Robustness and Efficiency of Odor Representations during Learning. *Neuron* **92**, 174–186 (2016).
403. Y. Yamada, K. Bhaukaurally, T. J. Madarász, A. Pouget, I. Rodriguez, A. Carleton, Context- and Output Layer-Dependent Long-Term Ensemble Plasticity in a Sensory Circuit. *Neuron* **93**, 1198–1212.e5 (2017).
404. Z. V. Gugel, E. G. Maurais, E. J. Hong, Chronic exposure to odors at naturally occurring concentrations triggers limited plasticity in early stages of Drosophila olfactory processing. *Elife* **12**, e85443 (2023).
405. O. Gschwend, N. M. Abraham, S. Lagier, F. Begnaud, I. Rodriguez, A. Carleton, Neuronal pattern separation in the olfactory bulb improves odor discrimination learning. *Nat Neurosci* **18**, 1474–1482 (2015).
406. N. M. Abraham, V. Egger, D. R. Shimshek, R. Renden, I. Fukunaga, R. Sprengel, P. H. Seeburg, M. Klugmann, T. W. Margrie, A. T. Schaefer, T. Kuner, Synaptic inhibition in the olfactory bulb accelerates odor discrimination in mice. *Neuron* **65**, 399–411 (2010).
407. M. M. Moreno, K. Bath, N. Kuczewski, J. Sacquet, A. Didier, N. Mandairon, Action of the noradrenergic system on adult-born cells is required for olfactory learning in mice. *J Neurosci* **32**, 3748–3758 (2012).
408. K. A. Sailor, M. T. Valley, M. T. Wiechert, H. Riecke, G. J. Sun, W. Adams, J. C. Dennis, S. Sharafi, G. L. Ming, H. Song, P. M. Lledo, Persistent Structural Plasticity Optimizes Sensory Information Processing in the Olfactory Bulb. *Neuron* **91**, 384–396 (2016).
409. Y. Livneh, A. Mizrahi, Experience-dependent plasticity of mature adult-born neurons. *Nat Neurosci* **15**, 26–28 (2011).
410. N. Mandairon, N. Kuczewski, F. Kermen, J. Forest…, Opposite regulation of inhibition by adult-born granule cells during implicit versus explicit olfactory learning *Elife* (2018).

411. J. Forest, L. Chalençon, M. Midroit, C. Terrier, I. Caillé, J. Sacquet, C. Benetollo, K. Martin, M. Richard, A. Didier, N. Mandairon, Role of Adult-Born Versus Preexisting Neurons Born at P0 in Olfactory Perception in a Complex Olfactory Environment in Mice. *Cereb Cortex* **30**, 534–549 (2020).
412. Y. Livneh, Y. Adam, A. Mizrahi, Odor processing by adult-born neurons. *Neuron* **81**, 1097–1110 (2014).
413. W. J. Tyler, G. C. Petzold, S. K. Pal, V. N. Murthy, Experience-dependent modification of primary sensory synapses in the mammalian olfactory bulb. *J Neurosci* **27**, 9427–9438 (2007).
414. K. M. Guthrie, D. A. Wilson, M. Leon, Early unilateral deprivation modifies olfactory bulb function. *J Neurosci* **10**, 3402–3412 (1990).
415. D. A. Wilson, R. M. Sullivan, The D2 antagonist spiperone mimics the effects of olfactory deprivation on mitral/tufted cell odor response patterns. *J Neurosci* **15**, 5574–5581 (1995).
416. C. G. Lau, V. N. Murthy, Activity-dependent regulation of inhibition via GAD67. *J Neurosci* **32**, 8521–8531 (2012).
417. B. D. Grier, L. Belluscio, C. E. J. Cheetham, Olfactory Sensory Activity Modulates Microglial-Neuronal Interactions during Dopaminergic Cell Loss in the Olfactory Bulb *Frontiers in Cellular Neuroscience* **10**, 22 (2016).
418. M. Sawada, N. Kaneko, H. Inada, H. Wake…, Sensory input regulates spatial and subtype-specific patterns of neuronal turnover in the adult olfactory bulb *Journal of …* (2011).
419. E. Galliano, C. Hahn, L. P. Browne, P. R Villamayor, C. Tufo, A. Crespo, M. S. Grubb, Brief Sensory Deprivation Triggers Cell Type-Specific Structural and Functional Plasticity in Olfactory Bulb Neurons. *J Neurosci* **41**, 2135–2151 (2021).
420. B. P. Bean, The action potential in mammalian central neurons. *Nat Rev Neurosci* **8**, 451–465 (2007).
421. M. H. P. Kole, J. J. Letzkus, G. J. Stuart, Axon initial segment Kv1 channels control axonal action potential waveform and synaptic efficacy *Neuron* (2007).
422. D. M. Cummings, L. Belluscio, Continuous neural plasticity in the olfactory intrabulbar circuitry. *J Neurosci* **30**, 9172–9180 (2010).
423. K. B. Quast, K. Ung, E. Froudarakis, L. Huang, I. Herman, A. P. Addison, J. Ortiz-Guzman, K. Cordiner, P. Saggau, A. S. Tolias, B. R. Arenkiel, Developmental broadening of

inhibitory sensory maps. *Nat Neurosci* **20**, 189–199 (2017).

424. W. Kelsch, C.-W. Lin, C. P. Mosley, C. Lois, A critical period for activity-dependent synaptic development during olfactory bulb adult neurogenesis. *J Neurosci* **29**, 11852–11858 (2009).
425. D. A. Wilson, M. Leon, Spatial patterns of olfactory bulb single-unit responses to learned olfactory cues in young rats. *J Neurophysiol* **59**, 1770–1782 (1988).
426. R. M. Sullivan, D. A. Wilson, M. Leon, Associative Processes in Early Olfactory Preference Acquisition: Neural and Behavioral Consequences. *Psychobiology (Austin, Tex)* **17**, 29–33 (1989).
427. M. Bouslama, E. Durand, L. Chauvière, O. Van den Bergh, J. Gallego, Olfactory classical conditioning in newborn mice. *Behav Brain Res* **161**, 102–106 (2005).
428. R. M. Sullivan, D. R. Zyzak, P. Skierkowski, D. A. Wilson, The role of olfactory bulb norepinephrine in early olfactory learning. *Brain Res Dev Brain Res* **70**, 279–282 (1992).
429. R. M. Sullivan, D. A. Wilson, C. Lemon, G. A. Gerhardt, Bilateral 6-OHDA lesions of the locus coeruleus impair associative olfactory learning in newborn rats. *Brain Res* **643**, 306–309 (1994).
430. R. M. Sullivan, G. Stackenwalt, F. Nasr…, Association of an odor with an activation of olfactory bulb noradrenergic β-receptors or locus coeruleus stimulation is sufficient to produce learned approach … *Behavioral ...* (2000).
431. G. U. Busto, I. Cervantes-Sandoval, R. L. Davis, Olfactory learning in Drosophila. *Physiology (Bethesda)* **25**, 338–346 (2010).
432. H. M. Schellinck, C. A. Forestell, V. M. LoLordo, A simple and reliable test of olfactory learning and memory in mice *Chemical Senses* (2001).
433. C. Linster, B. A. Johnson, A. Morse, E. Yue, M. Leon, Spontaneous versus reinforced olfactory discriminations. *J Neurosci* **22**, 6842–6845 (2002).
434. I. Imayoshi, M. Sakamoto, T. Ohtsuka, K. Takao…, Roles of continuous neurogenesis in the structural and functional integrity of the adult forebrain *Nature ...* (2008).
435. V. Breton-Provencher, M. Lemasson…, Interneurons produced in adulthood are required for the normal functioning of the olfactory bulb network and for the execution of selected olfactory behaviors *Journal of ...* (2009).
436. N. Mandairon, S. Sultan, M. Nouvian, J. Sacquet, A. Didier, Involvement of newborn

neurons in olfactory associative learning? The operant or non-operant component of the task makes all the difference. *J Neurosci* **31**, 12455–12460 (2011).

437. C. Linster, B. A. Johnson, E. Yue, A. Morse, Z. Xu, E. E. Hingco, Y. Choi, M. Choi, A. Messiha, M. Leon, Perceptual correlates of neural representations evoked by odorant enantiomers. *J Neurosci* **21**, 9837–9843 (2001).
438. S. V. Jones, D. C. Choi, M. Davis, K. J. Ressler, Learning-dependent structural plasticity in the adult olfactory pathway. *J Neurosci* **28**, 13106–13111 (2008).
439. M. D. Kass, M. C. Rosenthal, J. Pottackal, J. P. McGann, Fear learning enhances neural responses to threat-predictive sensory stimuli. *Science* **342**, 1389–1392 (2013).
440. J. P. Bhattarai, M. Schreck, A. H. Moberly, W. Luo, M. Ma, Aversive Learning Increases Release Probability of Olfactory Sensory Neurons. *Curr Biol* **30**, 31–41.e3 (2020).
441. B. G. Dias, K. J. Ressler, Parental olfactory experience influences behavior and neural structure in subsequent generations. *Nat Neurosci* **17**, 89–96 (2014).
442. F. G. Morrison, B. G. Dias, K. J. Ressler, Extinction reverses olfactory fear-conditioned increases in neuron number and glomerular size. *Proc Natl Acad Sci U S A* **112**, 12846–12851 (2015).
443. N. M. Abraham, R. Vincis, S. Lagier, I. Rodriguez, A. Carleton, Long term functional plasticity of sensory inputs mediated by olfactory learning. *Elife* **3**, e02109 (2014).
444. M. W. Chu, W. L. Li, T. Komiyama, Lack of Pattern Separation in Sensory Inputs to the Olfactory Bulb during Perceptual Learning. *eNeuro* **4**, ENEURO.0287–17.2017 (2017).
445. M. Alonso, C. Viollet, M. M. Gabellec, V. Meas-Yedid, J. C. Olivo-Marin, P. M. Lledo, Olfactory discrimination learning increases the survival of adult-born neurons in the olfactory bulb. *J Neurosci* **26**, 10508–10513 (2006).
446. A. Mouret, G. Gheusi, M. M. Gabellec, F. de Chaumont, J. C. Olivo-Marin, P. M. Lledo, Learning and survival of newly generated neurons: when time matters. *J Neurosci* **28**, 11511–11516 (2008).
447. S. Sultan, N. Mandairon, F. Kermen, S. Garcia, J. Sacquet, A. Didier, Learning-dependent neurogenesis in the olfactory bulb determines long-term olfactory memory. *FASEB J* **24**, 2355–2363 (2010).
448. T. W. Chen, T. J. Wardill, Y. Sun, S. R. Pulver, S. L. Renninger, A. Baohan, E. R. Schreiter, R. A. Kerr, M. B. Orger, V. Jayaraman, L. L. Looger, K. Svoboda, D. S. Kim, Ultrasensitive

fluorescent proteins for imaging neuronal activity. *Nature* **499**, 295–300 (2013).

449. J. Li, T. Ishii, P. Feinstein, P. Mombaerts, Odorant receptor gene choice is reset by nuclear transfer from mouse olfactory sensory neurons. *Nature* **428**, 393–399 (2004).
450. S. Hasegawa, S. Hamada, Y. Kumode, S. Esumi, S. Katori, E. Fukuda, Y. Uchiyama, T. Hirabayashi, P. Mombaerts, T. Yagi, The protocadherin-α family is involved in axonal coalescence of olfactory sensory neurons into glomeruli of the olfactory bulb in mouse *Molecular and Cellular Neuroscience* **38**, 66–79 (2008).
451. Y. Nagai, H. Sano, M. Yokoi, Transgenic expression of Cre recombinase in mitral/tufted cells of the olfactory bulb. *Genesis* **43**, 12–16 (2005).
452. Q. Qiu, A. Scott, H. Scheerer, N. Sapkota, D. K. Lee, L. Ma, C. R. Yu, Automated analyses of innate olfactory behaviors in rodents. *PLoS One* **9**, e93468 (2014).
453. T. A. Pologruto, B. L. Sabatini, K. Svoboda, ScanImage: flexible software for operating laser scanning microscopes. *Biomed Eng Online* **2**, 13 (2003).
454. J. Jackson, M. M. Karnani, B. V. Zemelman, D. Burdakov…, Inhibitory control of prefrontal cortex by the claustrum *Neuron* (2018).
455. G. Lopes, N. Bonacchi, J. Frazão, J. P. Neto, B. V. Atallah, S. Soares, L. Moreira, S. Matias, P. M. Itskov, P. A. Correia, R. E. Medina, L. Calcaterra, E. Dreosti, J. J. Paton, A. R. Kampff, Bonsai: an event-based framework for processing and controlling data streams. *Front Neuroinform* **9**, 7 (2015).
456. A. Mathis, P. Mamidanna, K. M. Cury, T. Abe, V. N. Murthy, M. W. Mathis, M. Bethge, DeepLabCut: markerless pose estimation of user-defined body parts with deep learning. *Nat Neurosci* **21**, 1281–1289 (2018).
457. M. Pachitariu, C. Stringer, M. Dipoppa, S. Schröder, L. F. Rossi, H. Dalgleish, M. Carandini, K. D. Harris, Suite2p: beyond 10,000 neurons with standard two-photon microscopy *bioRxiv* (2016).
458. J. Schindelin, I. Arganda-Carreras, E. Frise, V. Kaynig, M. Longair, T. Pietzsch, S. Preibisch, C. Rueden, S. Saalfeld, B. Schmid, J. Y. Tinevez, D. J. White, V. Hartenstein, K. Eliceiri, P. Tomancak, A. Cardona, Fiji: an open-source platform for biological-image analysis. *Nat Methods* **9**, 676–682 (2012).
459. M. L. Hines, N. T. Carnevale, NEURON: a tool for neuroscientists. *Neuroscientist* **7**, 123–135 (2001).

460. M. L. Hines, A. P. Davison, E. Muller, NEURON and Python. *Front Neuroinform* **3**, 1 (2009).

461. C. T. Frenz, A. Hansen, N. D. Dupuis, N. Shultz, S. R. Levinson, T. E. Finger, V. E. Dionne, NaV1.5 sodium channel window currents contribute to spontaneous firing in olfactory sensory neurons. *J Neurophysiol* **112**, 1091–1104 (2014).

462. G. Lowe, G. H. Gold, Nonlinear amplification by calcium-dependent chloride channels in olfactory receptor cells. *Nature* **366**, 283–286 (1993).

463. H. Spors, D. F. Albeanu, V. N. Murthy, D. Rinberg, N. Uchida, M. Wachowiak, R. W. Friedrich, Illuminating Vertebrate Olfactory Processing. *J Neurosci* **32**, 14102–14108 (2012).

464. B. Jemiolo, F. Andreolini, T. M. Xie, D. Wiesler, M. Novotny, Puberty-affecting synthetic analogs of urinary chemosignals in the house mouse, Mus domesticus. *Physiol Behav* **46**, 293–298 (1989).

465. C. Boschat, C. Pélofi, O. Randin, D. Roppolo, C. Lüscher, M.-C. Broillet, I. Rodriguez, Pheromone detection mediated by a V1r vomeronasal receptor. *Nat Neurosci* **5**, 1261–1262 (2002).

466. N. Subramanian, D. A. Storace, Brief odor stimulation evokes short-term adaptation in mitral/tufted glomeruli in the mouse olfactory bulb *Program No. 293.09. 2022 Neuroscience Meeting Planner. San Diego, CA.: Society for Neuroscience, 2022. Online.* (2022).

467. D. W. Wesson, T. N. Donahou, M. O. Johnson, M. Wachowiak, Sniffing behavior of mice during performance in odor-guided tasks. *Chem Senses* **33**, 581–596 (2008).

468. D. A. Wilson, C. Linster, Neurobiology of a simple memory. *J Neurophysiol* **100**, 2–7 (2008).

469. D. W. Wesson, E. Levy, R. A. Nixon, D. A. Wilson, Olfactory dysfunction correlates with amyloid-beta burden in an Alzheimer's disease mouse model. *J Neurosci* **30**, 505–514 (2010).

470. A. Nunez-Parra, R. K. Maurer, K. Krahe, R. S. Smith, R. C. Araneda, Disruption of centrifugal inhibition to olfactory bulb granule cells impairs olfactory discrimination. *Proc Natl Acad Sci U S A* **110**, 14777–14782 (2013).

471. J. Zou, W. Wang, Y. W. Pan, S. Lu, Z. Xia, Methods to measure olfactory behavior in mice.

Curr Protoc Toxicol **63**, 11.18.1–11.18.21 (2015).

472. K. R. Gamble, D. W. Smith, Discrimination of "odorless" mineral oils alone and as diluents by behaviorally trained mice. *Chem Senses* **34**, 559–563 (2009).
473. L. R. Saraiva, K. Kondoh, X. Ye, K. H. Yoon, M. Hernandez, L. B. Buck, Combinatorial effects of odorants on mouse behavior. *Proc Natl Acad Sci U S A* **113**, E3300–6 (2016).
474. J. Jackson, M. M. Karnani, B. V. Zemelman, D. Burdakov, A. K. Lee, Inhibitory Control of Prefrontal Cortex by the Claustrum. *Neuron* **99**, 1029–1039.e4 (2018).
475. T. Nath, A. Mathis, A. C. Chen, A. Patel, M. Bethge, M. W. Mathis, Using DeepLabCut for 3D markerless pose estimation across species and behaviors. *Nat Protoc* **14**, 2152–2176 (2019).
476. M. R. Nassar, K. M. Rumsey, R. C. Wilson, K. Parikh, B. Heasly, J. I. Gold, Rational regulation of learning dynamics by pupil-linked arousal systems. *Nat Neurosci* **15**, 1040–1046 (2012).
477. M. Naber, K. Nakayama, Pupil responses to high-level image content. *J Vis* **13**, 7 (2013).
478. H. I. Liao, S. Kidani, M. Yoneya, M. Kashino, S. Furukawa, Correspondences among pupillary dilation response, subjective salience of sounds, and loudness. *Psychon Bull Rev* **23**, 412–425 (2016).
479. D. A. Ganea, A. Bexter, M. Günther, P. M. Gardères, B. M. Kampa, F. Haiss, Pupillary Dilations of Mice Performing a Vibrotactile Discrimination Task Reflect Task Engagement and Response Confidence. *Front Behav Neurosci* **14**, 159 (2020).
480. P. Montes-Lourido, M. Kar, I. Kumbam, S. Sadagopan, Pupillometry as a reliable metric of auditory detection and discrimination across diverse stimulus paradigms in animal models. *Sci Rep* **11**, 3108 (2021).
481. K. Mori, M. C. Nowycky, G. M. Shepherd, Impulse activity in presynaptic dendrites: analysis of mitral cells in the isolated turtle olfactory bulb. *J Neurosci* **2**, 497–502 (1982).
482. J. Johnston, K. Delaney, Synaptic activation of T-type Ca2+ channels via mGluR activation in the primary dendrite of mitral cells. *J Neurophysiol* **103**, 2557–2569 (2010).
483. W. R. Chen, J. Midtgaard, G. M. Shepherd, Forward and backward propagation of dendritic impulses and their synaptic control in mitral cells *Science* (1997).
484. M. Djurisic, S. Antic, W. R. Chen…, Voltage imaging from dendrites of mitral cells: EPSP attenuation and spike trigger zones *Journal of …* (2004).

485. M. Djurisić, D. Zecević, Imaging of spiking and subthreshold activity of mitral cells with voltage-sensitive dyes. *Ann N Y Acad Sci* **1048**, 92–102 (2005).

486. S. Charpak, J. Mertz, E. Beaurepaire…, Odor-evoked calcium signals in dendrites of rat mitral cells *Proceedings of the …* (2001).

487. M. N. Economo, K. R. Hansen, M. Wachowiak, Control of Mitral/Tufted Cell Output by Selective Inhibition among Olfactory Bulb Glomeruli. *Neuron* **91**, 397–411 (2016).

488. T. P. Eiting, M. Wachowiak, Differential impacts of repeated sampling on odor representations by genetically-defined mitral and tufted cell subpopulations in the mouse olfactory bulb *Journal of Neuroscience* (2020).

489. S. D. Burton, A. Brown, T. P. Eiting, I. A. Youngstrom, T. C. Rust, M. Schmuker, M. Wachowiak, Mapping odorant sensitivities reveals a sparse but structured representation of olfactory chemical space by sensory input to the mouse olfactory bulb. *Elife* **11**, e80470 (2022).

490. Y. Oka, Y. Takai, K. Touhara, Nasal airflow rate affects the sensitivity and pattern of glomerular odorant responses in the mouse olfactory bulb. *J Neurosci* **29**, 12070–12078 (2009).

491. J. Johnston, L. Lagnado, General features of the retinal connectome determine the computation of motion anticipation. *Elife* **4**, e06250 (2015).

492. J. Johnston, S. H. Seibel, L. S. A. Darnet, S. Renninger, M. Orger, L. Lagnado, A Retinal Circuit Generating a Dynamic Predictive Code for Oriented Features. *Neuron* **102**, 1211–1222.e3 (2019).

493. S. O. Ögren, H. K. Hall, C. Köhler, O. Magnusson, S.-E. Sjöstrand, The selective dopamine D 2 receptor antagonist raclopride discriminates between dopamine-mediated motor functions *Psychopharmacology* **90**, 287–294 (1986).

494. F. Brugger, U. Wicki, H.-R. Olpe, W. Froestl, S. Mickel, The action of new potent GABAB receptor antagonists in the hemisected spinal cord preparation of the rat *European journal of pharmacology* **235**, 153–155 (1993).

495. P. Mombaerts, F. Wang, C. Dulac, S. K. Chao, A. Nemes, M. Mendelsohn, J. Edmondson, R. Axel, Visualizing an olfactory sensory map. *Cell* **87**, 675–686 (1996).

496. J. Reisert, J. Lai, K. W. Yau, J. Bradley, Mechanism of the excitatory Cl- response in mouse olfactory receptor neurons. *Neuron* **45**, 553–561 (2005).

497. B. G. Sanganahalli, K. L. Baker, G. J. Thompson, P. Herman, G. M. Shepherd, J. V. Verhagen, F. Hyder, Orthonasal versus retronasal glomerular activity in rat olfactory bulb by fMRI. *Neuroimage* **212**, 116664 (2020).

498. B. von der Weid, D. Rossier, M. Lindup, J. Tuberosa, A. Widmer, J. D. Col, C. Kan, A. Carleton, I. Rodriguez, Large-scale transcriptional profiling of chemosensory neurons identifies receptor-ligand pairs in vivo. *Nat Neurosci* **18**, 1455–1463 (2015).

499. J. S. Huang, T. Kunkhyen, A. N. Rangel, T. R. Brechbill, J. D. Gregory, E. D. Winson-Bushby, B. Liu, J. T. Avon, R. J. Muggleton, C. E. J. Cheetham, Immature olfactory sensory neurons provide behaviourally relevant sensory input to the olfactory bulb. *Nat Commun* **13**, 6194 (2022).

500. R. Gross-Isseroff, D. Lancet, Concentration-dependent changes of perceived odor quality *Chemical senses* **13**, 191–204 (1988).

501. D. G. Laing, P. K. Legha, A. L. Jinks, I. Hutchinson, Relationship between molecular structure, concentration and odor qualities of oxygenated aliphatic molecules *Chemical senses* **28**, 57–69 (2003).

502. W. Fischler-Ruiz, D. G. Clark, N. R. Joshi, V. Devi-Chou, L. Kitch, M. Schnitzer, L. F. Abbott, R. Axel, Olfactory landmarks and path integration converge to form a cognitive spatial map. *Neuron* **109**, 4036–4049.e5 (2021).

503. J. L. McClelland, T. T. Rogers, The parallel distributed processing approach to semantic cognition. *Nat Rev Neurosci* **4**, 310–322 (2003).

504. D. Y. Lin, S. D. Shea, L. C. Katz, Representation of natural stimuli in the rodent main olfactory bulb. *Neuron* **50**, 937–949 (2006).

505. R. C. Li, C. C. Lin, X. Ren, J. S. Wu, L. L. Molday, R. S. Molday, K. W. Yau, Ca^{2+}-activated Cl current predominates in threshold response of mouse olfactory receptor neurons. *Proc Natl Acad Sci U S A* **115**, 5570–5575 (2018).

506. T. Faber, J. Joerges, R. Menzel, Associative learning modifies neural representations of odors in the insect brain. *Nat Neurosci* **2**, 74–78 (1999).

507. S. W. Santoro, C. Dulac, The activity-dependent histone variant H2BE modulates the life span of olfactory neurons. *Elife* **1**, e00070 (2012).

508. S. Zhao, H. Tian, L. Ma, Y. Yuan, C. R. Yu, M. Ma, Activity-dependent modulation of odorant receptor gene expression in the mouse olfactory epithelium. *PLoS One* **8**, e69862

(2013).

509. X. Ibarra-Soria, T. S. Nakahara, J. Lilue, Y. Jiang, C. Trimmer, M. A. Souza, P. H. Netto, K. Ikegami, N. R. Murphy, M. Kusma, A. Kirton, L. R. Saraiva, T. M. Keane, H. Matsunami, J. Mainland, F. Papes, D. W. Logan, Variation in olfactory neuron repertoires is genetically controlled and environmentally modulated. *Elife* **6**, e21476 (2017).

510. D. Tadres, P. H. Wong, T. To, J. Moehlis, M. Louis, Depolarization block in olfactory sensory neurons expands the dimensionality of odor encoding. *Sci Adv* **8**, eade7209 (2022).